THE UNIVERSITY
of EDINBURGH

Investigating the Role of Wnt/Planar Cell Polarity (PCP) in Neuromesodermal Progenitors (NMPs)

THE UNIVERSITY
of EDINBURGH

Julia Alice Watson

A thesis submitted in fulfilment of requirements for the degree of

Doctor of Philosophy

Institute for Stem Cell Research, MRC Centre for Regenerative Medicine

School of Biological Sciences, University of Edinburgh

September 2017

Declaration

I declare that the work presented here in this thesis is my own, unless otherwise stated. The work described in this thesis has not been submitted for any other degree or professional qualification

Julia Alice Watson

The little girl just could not sleep because her thoughts were way too deep, her mind had gone out for a stroll and fallen down a rabbit hole…

-Alice in Wonderland

Acknowledgements

First, I would like to thank my supervisors, Prof. Val Wilson and Dr. Guillaume Blin, for giving me the opportunity to do this research. Without your advice and enthusiasm this thesis would not be what it is today. I would also like to thank the other members of my committee, Dr. Steven Pollard, and Dr. Sally Lowell, who have guided me at crucial moments. I am also appreciative to the Medical Research Council (MRC) for providing the scholarship.

I have had the privilege of spending the past 4 years with some of the friendliest people around, which make up the special community that is SCRM. Special mentions for imaging 'dream team' Dr. Eoghan O'Duibhir and Dr. Bertrand Verney for helping me through a plethora of imaging curses over the years. Additionally, this work would not be possible without Dr. Claire Cryer and Dr. Fiona Rossi for all their help with flow cytometry. Another duo I must mention are Helen and Marilyn, who were always able to cheer me up even on the worst tissue culture days. Also, I need to thank Anne Wiblin (Abcam) for her generous help with finding Wnt/PCP specific antibodies.

Of course, thanks go to my two lab families, Wilson and Lowell, who have supported me throughout my time and created the perfect niche for a successful PhD. It is impossible to thank everyone from these labs over the years, but each one has been important for this work. A particular appreciation to Ron Wilkie who had a solution to any lab problems at the back of his drawer. To my family duo Eleni and Filip, you cannot even begin to imagine how sad I will be when you both depart on your new adventures, though I am sure the 'lab fam' chat will be filled with GIFs for a lifetime. Thanks for all the pep talks, laughs and quotable phrases, I honestly wouldn't have got through this without you both. To my fellow half-scandi Karolina, huge thanks for all the Operetta advice that stopped me from losing it towards the end. Matt, thank you for the invaluable advice on all aspects of lab life, as well as encouraging me to get out and break some bones every now and again - buffalo style! And not forgetting my Portuguese lucky charm Catarina de Cunha e Silva Martins Costa who came at the most perfect time to see me through to the end, the lab will not be the same without you, and neither will my Graphpad or Inkscape skills.

Finally, I owe my biggest appreciation to my external support crew, the Watson and Mathews family.

Over my lifetime, the Watson clan have provided a stable environment for me to achieve goals I never even thought would be possible. Not only financial support but also unrelenting emotional support whenever I have needed it, even tolerating frequent late night teary unintelligible phone calls. The reason I am even doing this is because of you. You instilled a thirst for knowledge from a young age, and taught me to not fear the unknown but embrace it as an exciting challenge. To John, sorry that I have set the bar particularly high this time, good luck trying to top this one.

David Mathews words cannot express how grateful I am to you, your support for me has been unfaltering. This wouldn't be possible without the sacrifices you personally made, and you are fully within your right to claim a bit of this as your own. Thanks for keeping me sane, watering and feeding me, dragging me out of bed, repeatedly picking me up when I didn't think I could carry on, you were the source of light in the darker moments and I hope that one day I can return the favour if it is ever needed. Thanks also go to your extended family whose words of encouragement kept me going to the end.

Abstract

Neuromesodermal progenitors (NMPs) are bipotent progenitors, located at the caudal end of the embryo and are essential for axis formation. These stem cell-like progenitors possess the ability to self-renew and differentiate to both mesodermal and neural lineages, such as skeletal muscle and spinal cord derivatives. These progenitors arise at E8.5 and are localised in the caudal lateral epiblast (CLE), a posterior region of the embryo near the primitive streak. Later in development, they reside in the tail bud until cessation of axial elongation at E13.5. Throughout these stages NMPs are characteristically marked by co-expression of *T(Bra)* (Brachyury) and *Sox2*. This characteristic is also present in *in vitro* NMPs, which can be derived from Epiblast Stem Cells (EpiSCs) through treatment with Wnt/β-catenin signalling agonists and Fgf2, which simulates their *in vivo* environment.

Protein and mRNA profiling of NMPs and mutant phenotypes *in vivo* supports the hypothesis that a non-canonical Wnt pathway, the Wnt/Planar Cell Polarity pathway (PCP) could be involved in NMP fate decision and/or maintenance. This thesis focuses on understanding more about the role of PCP by aiming to identify the spatio-temporal profile of Wnt/PCP pathway components in NMP regions during axial elongation, as well as determining its role in NMP behaviour through manipulation of this pathway via *in vivo* and *in vitro* assays

Employing in situ hybridisation and immunohistochemistry techniques, key Wnt/PCP components, including Pk1, Vangl2 and Ptk7, were confirmed to be present in in vivo and in vitro NMPs, thus, providing strong evidence that Wnt/PCP may be involved regulating NMP behaviour.

Disruption of Wnt/PCP signalling through overexpression of Wnt/PCP components was tested in refined *in vivo* and *in vitro* assays. Overexpression of Vangl2 and Ptk7, but not Pk1 in NMPs regions *in vivo* resulted in loss of contribution to neural lineages, as well as lower contribution to NMP regions themselves. Similarly, Wnt/PCP components were disrupted *in vitro* through generation of dox-inducible overexpression cells lines for Wnt/PCP components. These lines were used to generate NMPs from an optimised novel alternative source Epiblast-Like Cells (EpiLCs), however no clear affect to lineage was observed.

Overall this work has successfully advanced our knowledge of Wnt/PCP mediated control of NMP differentiation and maintenance, and provided a finer grained description of the relationships between them.

Contents

List of Tables

List of Figures

List of Abbreviations

AB	Antibody
AVE	Anterior Visceral Endoderm
BABB	1 Benzyl Alcohol: 2 Benzyl Benzonate
BM	Basement Membrane
CE	Convergence and Extension
CHIR	CHIR99021
CLE	Caudal Lateral Epiblast
CNH	Chordoneural Hinge
CRM	Centre for Regenerative Medicine
DAPI	4’ , 6-diamidino-2-phenylindole
DMSO	Dimethylsulphoxide
Dox	Doxycycline
DVE	Distal Visceral Endoderm
E	Embryonic Day
EMT	Epithelial to Mesenchymal Transition
EpiLC	Epiblast-Like Cells
EpiSC	Epiblast-derived Stem Cells
ESCs	Embryonic Stem Cells
EXE	Extraembryonic Ectoderm
Fig.	Figure
FCS	Foetal Calf Serum
GFP	Green Fluorescent Protein
GOI	Gene of Interest
hf	head fold
HF	High Fidelity

ICE	Inducible Cassette Exchange Locus
ICM	Inner Cell Mass
IHC	Immunohistochemistry
ISH	In Situ Hybridisation
KSR	Knock out Serum Replacement
L	Lateral
LIF	Leukemia Inhibitory Factor
LM	Lateral Mesoderm
LUT	Look Up Table
MEF	Mouse Embryonic Fibroblasts
MRC	Medical Research Council
NEAA	Non-essential Amino Acids
NMP	Neuromesodermal Progenitor
NSB	Node-Streak Border
OD	Optic Density
PBS	Phosphate-buffered saline
PCP	Planar Cell Polarity
PCR	Polymerase Chain Reaction
PD03	PD0325901
PE	Primitive Endoderm
Pen/Strep	Penicillin/Streptomycin
PFA	Paraformaldehyde
PS	Primitive Streak
PXM	Paraxial Mesoderm
RFP	Red Fluorescent Protein
RT°C	Room Temperature
S	Supplementary

SEM	Standard Error of the Mean
T(Bra)	T(Brachyury)
T2A	Thosea Asigna virus 2A
TC	Tissue Culture
TCA	Trichloroacetic Acid
TE	Trophectoderm
VE	Visceral Endoderm
vs	Versus
WT	Wildtype

Chapter 1: Introduction

1.1 General Introduction

This chapter will include a general introduction to early Mouse *(Mus musculus)* embryo development, the process of gastrulation and axial elongation. Followed by the evidence for the existence of Neuromesodermal Progenitors (NMPs), the bipotent progenitor responsible for neural and mesodermal (paraxial and tail bud mesoderm) lineage production during axial elongation. I will discuss where they are found, important signalling pathways for their maintenance and differentiation, before describing their generation *in vitro* from multiple embryonic stem cell (ESC) sources. Therein I will introduce Wnt/Planar Cell Polarity (PCP) Signalling as a potential candidate for regulating NMP behaviour. I will provide a review of the literature, considering where its components have been reported to be expressed, Wnt/PCP mutant phenotypes as well as applicable functional roles. Finally, I will briefly discuss new methods of investigating its role in mammalian systems.

1.2 Early Mouse embryo development - pluripotency and lineage segregation

1.2.1 Pre-implantation

Mammalian embryo development begins after fertilisation with the generation of a single cell totipotent cell (zygote), which possesses the ability to give rise to all embryonic and extraembryonic lineages. This ability remains following subsequent symmetric divisions which produce progressively smaller but identical cells, called blastomeres (Tarkowski and Wróblewska, 1967). Upon asymmetrical cell division at the morula stage (16-32 cells, embryonic day (E) 2.5) two visibly distinct populations exist, polarised cells at the outer edge and inner cells at the core of the developing morula. Following cavitation (E3.5)(Smith and McLaren, 1977), the blastocyst is formed, in which previously polarised cells contribute to cells of the trophectoderm (TE), and inner cells contribute to form the inner cell mass (ICM). This is the first point during development when lineage contribution potential segregates between cells, with cells of the ICM retaining totipotent potential, and cells of the trophectoderm limited to cells of extra-embryonic lineages only (reviewed in Saiz and Plusa, 2013). Further lineage segregation follows at E4.0 when the embryo hatches

from surrounding zona pellucida membrane, and cells of the ICM form the pre-implantation epiblast and primitive endoderm (PE) lineages (reviewed in Gardner, 1998). Cells of the TE and PE go on to form extra-embryonic tissues which support the developing embryo. Cells of the pre-implantation epiblast however remain pluripotent, meaning they have the capacity to become derivatives of all three embryonic germ layers to form the embryo proper (reviewed in Arnold and Robertson, 2009; Stower and Srinivas, 2014).

1.2.2 Post-implantation, establishment of the anterior/posterior axis

Around E5.0 implantation occurs, and the morphology of the embryo changes to form the 'egg cylinder', named due to its shape. The embryo at this stage is elongated along the proximal-distal axis, and a cavity has formed within the centre of the epiblast cells. The epiblast is surrounded by extraembryonic tissues, above lies the extraembryonic ectoderm (EXE) derived from the TE, and enveloping both, the visceral endoderm (VE) derived from the PE. Anterior and posterior identities are determined by interactions between secreted factors from these different tissues, including Wnts, Nodal and bone morphogenic protein (BMP). Ultimately a specialised signalling centre is specified in the distal VE (DVE) (reviewed in Arnold and Robertson, 2009). The DVE expresses factors which antagonize TGF-beta and Wnt signalling activity, including *left-right determination factor 1* (Lefty1) and *Cerberus* (*Cer1*). From E5.5 onwards the cells of the DVE expressing these factors migrate anteriorly and are replaced by new cells expressing *Cer1* and *Lefty1* which form the anterior VE (AVE) (reviewed in Arkell and Tam, 2012; Stower and Srinivas, 2014) .

1.2.3 Gastrulation and the primitive streak

At around E6.5, gastrulation initiates, marking inception of the three germ layers, ectoderm, mesoderm and definitive endoderm (Arkell and Tam, 2012). The primitive streak, appears as cells converge to what is now the posterior of the embryo, at the opposite side to the AVE (reviewed in Beddington and Robertson, 1999; Arnold and Robertson, 2009). Cells of the epiblast that were initially a cup shaped epithelium undergo epithelial to mesenchymal transition (EMT) characterised by loss of apical-basal polarity and breakdown of basement membranes and cell-cell contacts (reviewed

in Nakaya and Sheng, 2008). This allows the cells to delaminate and migrate through the streak emerging to form cells of nascent mesoderm and definitive endoderm between the epiblast and the VE. During gastrulation BMP4, Nodal and Wnt3 reinforce each other's expression (Ben-Haim et al., 2006), and are essential for this process, highlighted by defects in gastrulation and mesoderm formation when components are mutated ;*Wnt3* (Liu et al., 1999), *Nodal* (Conlon et al., 1994), *BMP4* (Winnier et al., 1995). Moreover correct EMT of cells is dependent on *Fibroblast growth factor receptor (Fgfr1)* and *Fibroblast growth factor 8 (Fgf8*) which is expressed in the primitive streak (Crossley and Martin, 1995). *Fgf8-/-* mutants are characterised by an accumulation of cells in the primitive streak, which ingress but fail to leave (Sun et al., 1999). This accumulation is also present in *Fgfr1-/-* mutants which also exhibit aberrant mesodermal patterning as well as reduction of *Snail*, a key factor in normal EMT (Ciruna and Rossant, 2001; Deng et al., 1994; Yamaguchi et al., 1994).

1.2.4 Cell fate during gastrulation

Between E6.5-E7.5 the primitive streak elongates distally from the posterior pole until it reaches the distal tip of the embryo. Cells to the anterior of the primitive streak form a specialised structure, the node, the Mouse equivalent to the Spemann's organiser (*Xenopus*) or Hensen's node (Chick, *Gallus domesticus*). Extensive lineage tracing and grafting experiments have been conducted and reviewed to create detailed fate maps of cells during gastrulation (Beddington, 1994; Kinder et al., 1999, 2001; Lawson, 1999; Lawson et al., 1991; Lu et al., 2001; Tam and Behringer, 1997; Wilson and Beddington, 1996). The fate of cells emerging from the primitive streak is dependent on the timing and anterior-posterior site of their ingression. The first cells ingressing at the posterior streak, closest to high BMP4 signalling from ExE, are fated to form extraembryonic tissues (Winnier et al., 1995). Mesoderm emerging later from the intermediate and anterior streak, give rise to lateral plate, paraxial and cardiac mesoderm. Whilst cells ingressing closest to the anterior tip of the primitive streak, form mid-line axial mesendoderm tissue, including cells of the node, notochord, prechordal plate, and definitive endoderm (DE) (reviewed in Arnold and Robertson, 2009). Cells that do not travel through the streak but remain in the epiblast form ectoderm, giving rise to surface ectoderm and neural tissues.

During this time, key genes associated with subsequent cell fate are upregulated in somewhat overlapping regions of the embryo. These include several mesoderm markers; *T(Brachyury*) or *T(Bra)*, is expressed broadly throughout the primitive streak, node and notochord; *Eomesodermin* (*Eomes*) expressed in the anterior streak; *Caudal-type homeobox protein 2* (*Cdx2*) expressed broadly in the primitive streak; *MIX1 homeobox-like 1* (*Mixl1*) expressed in the intermediate primitive streak; and *Mesoderm posterior 1* (*Mesp1)* a cardiac progenitor marker is expressed in streak and more anterior tissues. *Forkhead box protein A2* (*Foxa2*) is expressed in the most anterior streak, and labels anterior mesendoderm (bipotent mesodermal and endodermal lineages), as well as the prechordal plate and anterior midline endoderm (Arnold and Robertson, 2009). Anterior neuroectoderm is marked by *orthodenticle homeobox 2 (Otx2)* expression (reviewed in Arnold and Robertson, 2009).

Despite this apparent regionalisation of cell fate associated with differential expression of key genes, this does not truly reflect the developmental potential of these cells. In experiments where anterior or posterior pieces of the E7.5 epiblast were grafted to the testis capsule, no differences were detected in terms of their potential to contribute to all germ layers (Beddington, 1983). Thus, although the fate of epiblast stem cells is determined by their positioning in the epiblast their potential remains adaptable.

As gastrulation progresses the node and primitive streak remain localised at the distal and posterior of the embryo respectively. The production of presomitic mesoderm by the streak drives somitogenesis, the process by which somites are made. Pluripotency disappears at the onset of somitogenesis reflecting at least in part the loss of pluripotency gene *Oct4* (Osorno et al., 2012). Tissue is added along the axis sequentially from the rostral to the caudal end by cells derived from the primitive streak and adjacent epiblast, in a process termed axial elongation. As the axis extends the primitive streak remains at the most caudal end. Subsequently the primitive streak becomes enclosed by the posterior neuropore which is the temporarily open region of the neural plate that forms anterior to the primitive streak.

forming the posterior neuropore, until E10.5 when it closes to form the tail bud. From this point the tailbud is the source of cells for continuing body axis elongation until E13.5 when axial elongation arrests (reviewed in Wilson et al., 2009).

1.3 Neuromesodermal Progenitors (NMPs)

1.3.1 Evidence for bipotent progenitors during axial elongation

Fate mapping and retrospective clonal analysis experiments have indicated the presence of progenitors in vertebrate throughout axial elongation which have the capability to persist, as well as differentiating to generate both mesodermal (paraxial and tail bud mesoderm) and neural tissue (reviewed in Wilson et al., 2009).

Evidence supporting this idea came from fate maps generated based on cell tracing studies in cultured embryos. In chick, single cells labelled within Hensen's node, the chick equivalent to the Mouse node, were found to contribute to more than one tissue (somite and notochord or notochord and ventral neural tube), and thus had dual fates (Selleck and Stern, 1991). Moreover, these initial findings were supported by similar cell labelling experiments performed in Mouse embryos. Cells labelled within the epiblast at the prospective organiser region were able to contribute descendants to multiple tissue lineages, as well as contributing to cells remaining in the node region (Lawson et al., 1991). Labelling of the node in late streak and headfold (hf) stage embryos also provided evidence of similar multipotent cells, with labelled cells forming clones consisting of both mesodermal and neural lineages. Furthermore, labelling of cells more anterior to the node, did not have the same result, with only contribution to neuroectodermal tissues (Forlani et al., 2003). Thus together, these studies in chick and Mouse suggested the presence of cells with the ability to persist and additionally contribute to multiple lineages.

Experiments using retrospective clonal analysis were key in understanding more about these stem-like cells, specifically their persistence throughout axial elongation. These clonal analysis studies exploit a non-functional modified form of the *lacZ* gene, *laacZ* which spontaneously repairs, leading to the expression of β-gal in the revertant cell, and all its descendants (Bonnerot et al., 1987). Initially, use of this *laacZ* reporter driven by myotome (muscle progenitor of the somite), or neural specific promotors, and subsequent retrospective clonal lineage analysis identified the presence of stem cells in both myotome and nervous system formation (Mathis and Nicolas, 2000; Nicolas et al., 1996). Both systems reported clones, spanning large areas of the axis. Characteristics of these clones suggested that a pool of self-renewing cells with the

ability to differentiate and contribute to tissues throughout axial elongation existed for both mesodermal and neural lineages.

Furthermore, the presence of bipotent cells was finally confirmed using the insertion of *laacZ* driven by the ubiquitously expressed *Rosa26* locus, which was not restricted to report a specific lineage. Retrospective clonal analysis of this line finally verified the presence of bipotent axial progenitors during axial elongation, termed Neuromesodermal Progenitors (NMPs), which can contribute to both neuroectodermal and mesodermal tissues (Tzouanacou et al., 2009). Clones from E8.5 and E10.5 embryos suggested that these progenitors were present in a single progenitor pool continually throughout elongation, peaking in size between gastrulation to early organogenesis, and then decreasing during tail bud stage. These experiments confirmed the presence of NMPs during axial elongation and provided insight in to where these progenitors were located, nevertheless they did not confirm the exact location of NMPs.

1.3.2 Location of NMPS

1.3.2.1 Node- Streak border (NSB) and Caudal Lateral Epiblast (CLE)

The location of neuromesodermal progenitors was revealed using a combination of multiple and single cell lineage tracing and transplantation experiments, in which tissue from a labelled donor was grafted to a host to establish what tissue types it could give rise to.

As mentioned above, multipotent cells were first identified in the node region in chick (Selleck and Stern, 1991) and in Mouse (Beddington, 1994; Lawson et al., 1991) located at the most anterior primitive streak (Fig. 1.1A). The morphology of the node is initially a rosette of cells at the distal tip of the egg cylinder, which evolves to form a distinctive morphology with a ‘pit’ of ciliated cells surrounded by radially arranged ‘crown’ cells in a horseshoe which disappear around the 7 somite stage (Bellomo et al., 1996; Jurand, 1974; Sulik et al., 1994).

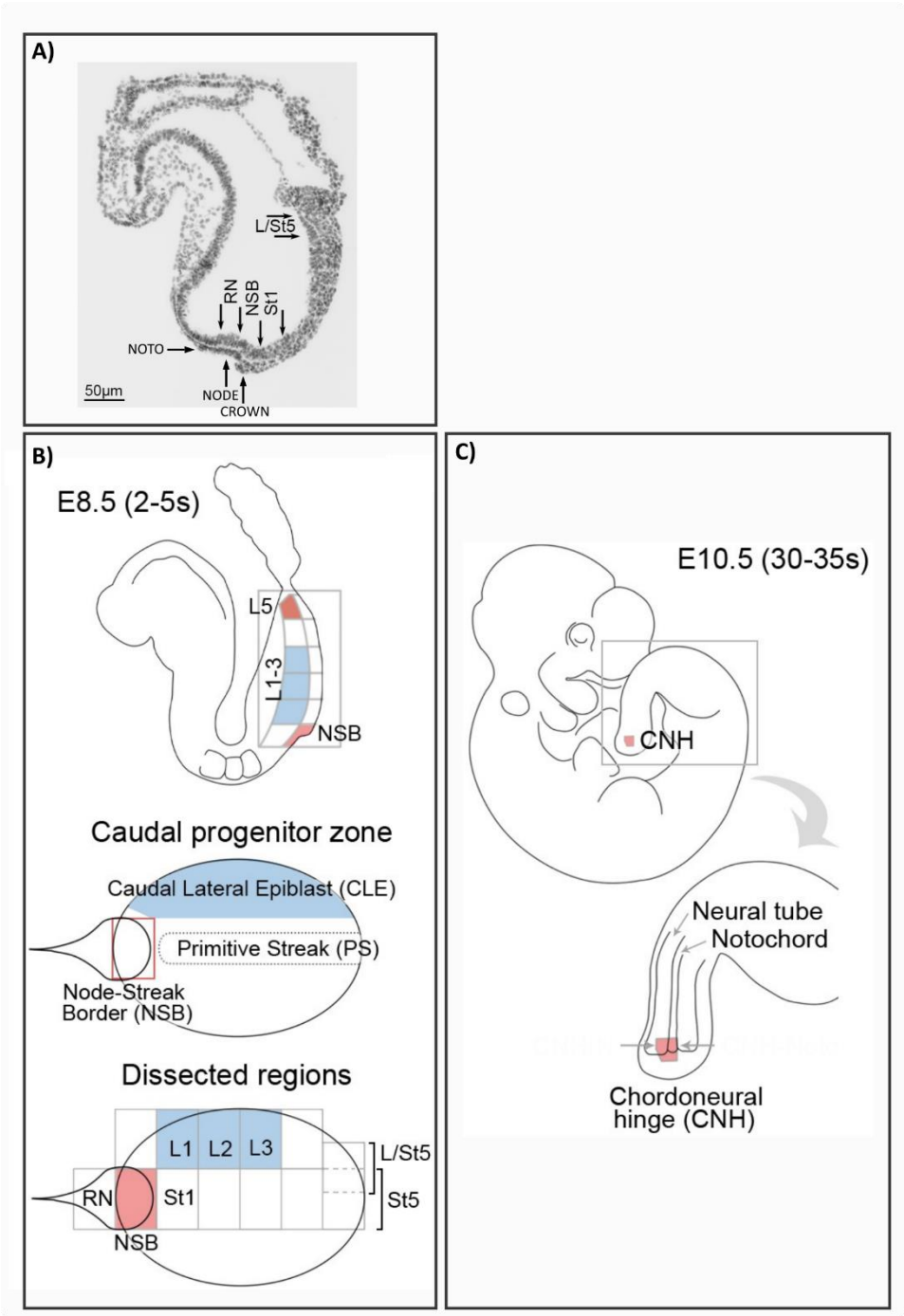

Figure 1.1 Location of Neuromesodermal Progenitors (NMPs)

(A) DAPI stained sagittal section at E8.5 (2-5 somite embryo) illustrates position of the notochord (noto), node, crown of the node, rostral node (RN), and the node-streak border (NSB) which contains NMPs. **(B)** Schematic of E8.5 (2-5 somite) embryo illustrates the position of the Caudal Lateral Epiblast (CLE), in which NMPs additionally reside (L1-L3). The CLE is adjacent to the primitive streak (PS). **(C)** Following neuropore closure at E9.5, NMPs are found in the tail bud, here shown for E10.5, until axial cessation at E13.5. During this time NMPs reside in the chordoneural hinge, which constitutes the caudalmost region of the ventral neural tube in contact with the notochord. Images modified from (Wymeersch et al., 2016). s- somite, L - lateral, St-Streak.

The node consists of two layers, namely the dorsal layer (dorsal node), a highly proliferative layer which is contiguous with the epiblast, and the ventral layer (ventral node) which is adjacent to the primitive streak and relatively quiescent. The ventral layer and the streak appear to be separated by basement membrane except for the extreme anterior end of the streak, however cell mixing between these layers is not thought to be extensive (Bellomo et al., 1996).

Following epiblast fate map experiments by Lawson et al., (1991), the fate of cells in the node and primitive streak at E8.25-E8.5, early somitogenesis, was examined in Mouse through DiI labelling of cells in specific locations (Wilson and Beddington, 1996). Ventral node showed predominantly notochordal fate, although additional hindgut labelling was also present, perhaps due to unintended labelling of adjacent endoderm cells. Moreover, as labelled cells also remain in the node following culture, this suggests notochord progenitors reside in the ventral node. Labelling the dorsal node in addition to the ventral node showed additional labelling of neurectoderm and paraxial mesoderm, showing distinct fates for these two node layers. Additionally, distinctions were found between labelled regions of the streak, with rostral streak fated for paraxial mesoderm, and caudal for lateral mesoderm (Smith et al., 1994; Wilson and Beddington, 1996).

Further detailed fate maps were constructed using homotopic grafts of GFP-expressing cells from the node and streak regions (Cambray and Wilson, 2007). In line with previous reports, cells of the streak gave rise to paraxial mesoderm (rostral most four-fifths of the streak), or lateral mesoderm (most caudal fifth of the streak), and cells of the ventral node contributed to notochord cells only. However cells at the junction between the caudal most node, and the rostral most part of the primitive streak, termed the node-streak border (NSB), were the only cells that could give rise to multiple lineages, namely notochord, neural tube (ventral), and paraxial and tailbud mesoderm along the length of the axis (Cambray and Wilson, 2007). The fate of cells in the epiblast lateral (L) to the primitive streak, termed the caudal lateral epiblast (CLE), was also investigated. Two distinct regions were found, the most rostral three-fifths (L1-L3) contributed to paraxial mesoderm and neural tube, whilst the caudal fifth (L5) showed lateral mesoderm contribution with negligible contribution to neural lineages

(Cambray and Wilson, 2007). NSB and CLE cell are also biased in their contribution to lineages, with NMPs residing in the NSB and CLE giving rise to more ventral and dorsal neural tube respectively (Cambray and Wilson, 2007).

Altogether this work established a fate map of cells located in the posterior of the Mouse embryo at early somitogenesis. In summary, cells residing in the NSB and CLE can contribute to both neural and mesodermal lineages during axial elongation confirming these regions as the only possible location for neuromesodermal progenitors (Fig. 1.1A-B). Further heterotopic grafts undertaken revealed a pattern within the CLE, whereby posterior and medial cells were more likely to contribute to mesoderm, while anterior and lateral cells tended to adopt neural fates. However NMPs in all locations showed extensive plasticity: their eventual fate as neurectoderm or mesoderm was determined by their environment (Wymeersch et al., 2016).

1.3.2.2 Chordoneural Hinge (CNH)

In homotopic grafts of the NSB, and to a lesser extent, the CLE resulted in labelled cells residing in a specific area of the tail bud, termed the chordoneural hinge (CNH), which constitutes the caudalmost region of the ventral neural tube in contact with the widened notochordal plate (Cambray and Wilson, 2002, 2007) (Fig. 1.1C). These experiments supported the idea that there is a cellular continuity between the primitive streak and the CNH. Grafting of CNH regions derived from E10.5-E12.5 embryos into E8.5 NSB resulted in contribution to both neural and mesodermal tissue, as well the CNH itself (Cambray and Wilson, 2002). Importantly this was not possible using tissue from other regions of the tailbud, including adjacent tail bud mesoderm (TBM) (McGrew et al., 2008). Moreover, serially passaging through consecutive CNH to NSB was possible, with continuous contribution to axis and CNH, indicating that the CNH of E10.5- E12.5 embryos and the NSB are equivalent (Cambray and Wilson, 2002). Supporting the idea that NSB and CNH are a continuum through development, orientation of key gene expression domains, are mirrored between the node/primitive streak regions and tailbud (Cambray and Wilson, 2002). Despite differences between species morphology the presence of bipotent stem cells contributing to neural and mesodermal lineages have also been identified in chick, with comparable organisation within the axis (reviewed in Wilson, Olivera-Martinez and Storey, 2009).

In conclusion, despite limitations of individual experiments, together these fate map, retrospective clonal analysis, homotopic and serially grafting experiments demonstrate the presence of a pool of bipotent progenitors during axial elongation, residing initially in the NSB and CLE of E8.5 embryos and then in CNH region of the tail bud. The potency of these cells to form only neural and mesodermal lineages has since been verified using kidney capsule grafts, confirming these cells not pluripotent (Wymeersch et al., 2016).

1.3.3 Cessation of axial elongation

Axial elongation terminates at E13.5, although the mechanism by which this occurs is not fully understood. Many mutant mice with short tails have been described, with premature axial termination thought to reflect disruption of NMP behaviour. Indeed at least some of these mutants are known to affect NMP behaviour directly. Conversely axial elongation has been associated retinoic acid induced apoptosis (Shum et al., 1999), as well as a loss of important NMP maintenance factors which decrease gradually before disappearing by E13.5 (Cambray and Wilson, 2007). Additionally, mice with homozygous mutations in homeoboxb13 (Hoxb13) exhibit longer tails, suggesting a role for this gene in axial cessation (Economides et al., 2003).

1.3.4 T(Bra) and Sox2 co-expression marks NMPs

As mentioned above, areas in which NMPs reside during axial elongation exhibit similar spatial expression of important regulatory genes. These including, *Wnt3a, Fgf8, T(Bra), Caudal Type Homeobox 2* (*Cdx2), Even-skipped homeobox 1 (Evx1)* and *NKX1 homeobox 2 gene* (*Nkx1.2, also Sax1)*. The expression of these genes however is never restricted solely to NMP residing areas (Cambray and Wilson, 2007)cam, and despite extensive investigations currently no single gene marker which uniquely identifies NMPs has been reported. Instead, in several vertebrate species regions containing NMPs are hallmarked by the co-expression of neural marker *SRY-box2 (Sox2)* and primitive streak/nascent mesoderm marker *T(Bra)*(Martin and Kimelman, 2012; Olivera-Martinez et al., 2012). T(Bra) and Sox2 co-expressing cells are consistently found in the Mouse NSB/CLE and CNH throughout axial elongation (Wymeersch et al., 2016). Furthermore, in Mouse, Sox2 and T(Bra) co-expressing cells reach their maximum numbers during mid-trunk formation, coinciding with an

inferred peak in NMP numbers based on retrospective clonal analysis (Tzouanacou et al., 2009; Wymeersch et al., 2016). Moreover T(Bra) and Sox2 co-expression is lost at E13.5 coinciding with cessation of axial elongation. However it should be noted that co-expression of these two factors may not be exclusive to NMPs, as mesoderm-committed midline streak also contains some cells expressing both components (Wymeersch et al., 2016).

1.3.4.1 T(Brachyury) - T(Bra)

T(Bra) is a T-box transcription factor, whose expression is one of the earliest hallmarks of streak formation, and is essential for gastrulation (Beddington et al., 1992; Rivera-Perez and Magnuson, 2005; Thomas and Beddington, 1996; Wilson and Beddington, 1997; Wilson et al., 1995). *T(Bra)* is a direct target of Wnt3a signalling and at late gastrulation *T(Bra)* is expressed in the node, the notochord, and newly formed mesoderm (Wilkinson, Bhatt and Herrmann, 1990; Yamaguchi *et al.*, 1999; Cambray and Wilson, 2007). Expression of *T(Bra)* persists in the tail bud, labelling the notochord, CNH and tail bud mesoderm (Cambray and Wilson, 2007). Homozygous mutations for *T(Bra)* have relatively normal gastrulation but later truncations are present in caudal regions, with loss of notochord and mesoderm, which ultimately leads death around E10.5 (Beddington et al., 1992; Rashbass et al., 1994; Wilkinson et al., 1990). This phenotype is shared but less severe for heterozygous mutations, with evidence suggesting abnormalities are due to defects in cell movements which cause accumulation of cells in the primitive streak (Wilson and Beddington, 1997; Yanagisawa et al., 1981). As previously mentioned *T(Bra)* is a target of Wnt signalling, but also is reported to target components of both Fgf and Wnt signalling pathways (Casey et al., 1998; Evans et al., 2012; Yamaguchi et al., 1999a).

1.3.4.2 Sox2

Sox2 is one of a large family of transcription factors, which share homology within their HMG-box DNA binding domain (Schepers et al., 2002). *Sox2* and other members of the subfamily group B are mostly associated with high expression in the nervous system including in adult tissue, but they are also expressed in early embryogenesis (Pevny et al., 1998; Sarkar and Hochedlinger, 2013; She and Yang, 2015; Wood and Episkopou, 1999). *Sox2* expression initiates at the pre-implantation stage, and is

restricted to the ICM of blastocysts. Following implantation, it is expressed throughout the epiblast before becoming restricted to more anterior regions by E7. From the onset of somitogenesis *Sox2* is expressed highest in neurectoderm but also found in endoderm as well as the developing germ cells (Avilion et al., 2003; Wood and Episkopou, 1999). Homozygous mutants of *Sox2* are embryonic lethal, and die around implantation, reflecting its importance in blastocyst stage embryos (Avilion et al., 2003). *Sox2* has been shown to have a specific enhancer (N1), controlling its expression in streak and CLE regions during development (Yoshida et al., 2014). Activation of this enhancer was shown to be dependent on dual action of Wnt3 (Wnt/β-catenin) and Fgf8 signalling (Takemoto et al., 2005). Interestingly, it has recently been shown that T(Bra) and Sox2 mutually repress each other's expression such that NMPs exist in a Sox2-low, T(Bra)-low state (Koch et al., 2017).

In summary, unique T(Bra) and Sox2 expression generally represents cells of mesoderm and neural fate, respectively, whereas co-expression labels bipotent NMPs. Maintenance of their co-expression and overall NMPs numbers appears to be highly regulated by feedback at the transcriptional level, and between mutually-reinforcing Fgf and Wnt/β-catenin signalling. Various essential components of these feedback mechanism include *(Nkx1.2)* (Delfino-Machin et al., 2005; Schubert et al., 1995), and *Caudal-related homeobox (Cdx)* genes (Chawengsaksophak et al., 2004; Savory et al., 2009).

1.3.5 *In vitro* derivation of NMPs

Neuromesodermal progenitors have also recently been generated *in vitro* from diverse sources, namely Mouse embryonic stem cells (ESCs), Epiblast stem cells (EpiSCs), as well as human ESCs (Gouti et al., 2014; Tsakiridis et al., 2014; Turner et al., 2014). These *in vitro* NMPs display a similar phenotype to *in vivo* NMPs, including co-expression of *T(Bra)* and *Sox2*, and other markers characteristic of NMP identity. In clonal assays, single cells can produce both neural and mesoderm cell types, providing further evidence that these cells are equivalent to their *in vivo* counterparts (Tsakiridis and Wilson, 2015). Functionally similarity to *in vivo* NMPs was further demonstrated when they were grafted into NSB regions of Mouse embryos, and contributed to both mesodermal and neural lineages (Gouti et al., 2014). In all cases NMPs have been

derived through dual activation of Fgf signalling, using Fgf ligands and Wnt/β-catenin signalling, using CHIRON99021 (CHIR) a potent agonist of this signalling pathway, or recombinant Wnt3a (N2B27/CHIR/FGF) (reviewed in Henrique *et al.*, 2015)(Gouti et al., 2014). These *in vitro* derived NMPs are a transient population, which following prolonged culture over a few days will terminally differentiate.

1.3.5.1 Source cells for NMPs *in vitro*

As mentioned above NMPs have been generated *in vitro* from Mouse ESCs and EpiSCs through treatment with Fgf and Wnt agonists. These two source populations are both stem cells, in that they can self-renew, by dividing to give rise to exact copies of themselves, permitting them to be propagated indefinitely, and additionally can differentiate, shown by multilineage differentiation *in vitro* and teratoma formation when grafted to adult mice (Tesar et al., 2007). However these cell types are very different in terms of behaviour, morphology culture requirements, transcriptional and epigenetic profiles and differentiation potential (reviewed in Morgani, Nichols and Hadjantonakis, 2017).

1.3.5.2 Pre-implantation ESCs - LIF/FCS and 2i/LIF ESCs

ESCs can be derived from the ICM of preimplantation E4.5 embryos (Evans and Kaufman, 1981; Martin, 1981). They were initially grown in the presence of foetal calf serum (FCS) on Mouse embryonic fibroblasts (MEFs), termed feeders, which promote self-renewal of ESCs through the productions of Leukaemia Inhibitory Factor (LIF)(Smith et al., 1988). MEFs can be replaced by addition of recombinant LIF and coating of plates with a gelatine substrate (LIF/FCS). ESCs are considered equivalent to the 'naïve' preimplantation epiblast, and if placed under the environment of host embryo, exhibit all attributes of epiblast identity and potency (reviewed in Nichols and Smith, 2009).

However, ESCs cultured in LIF/FCS are not homogeneous: individual cells exhibit differences in transcriptome, self-renewal probabilities and developmental potentials (reviewed in Morgani, Nichols and Hadjantonakis, 2017). ESCs are primed for lineage specification/differentiation through Oct4/Sox2 driven FGF4 activation of the ERK pathway (reviewed in Silva and Smith, 2008). In LIF/FCS conditions this activation of differentiation is inhibited by factors within the FCS, however since serum is

undefined this can be variable, as too can directed differentiation from these cultures which commonly contain a minority of ~~cells~~ spontaneous differentiation (Morgani et al., 2017; Ying and Smith, 2003). As an alternative ESCs can be cultured with LIF in defined culture conditions (N2B27) where the addition of two inhibitors (2i), PD0325901 (PD03) (MEK/Erk pathway inhibitor) and CHIR (GSK3β inhibitor and Wnt/β-catenin agonist) which serve to neutralise inductive differentiation stimuli, together termed 2i/LIF (Silva and Smith, 2008; Silva et al., 2008). Cells cultured in 2i/LIF conditions are much more homogeneous, with reduced expression of lineage markers and significantly less spontaneous differentiation. Thus this condition is referred to as the 'ground' or 'naïve' state pluripotency (Marks et al., 2012; Morgani et al., 2017; Nichols and Smith, 2009; Silva and Smith, 2008).

In summary, despite similarities in pluripotency between ESCs in LIF/FSC and 2i/LIF culture, due to the homogeneity of cells in 2i/LIF culture it is considered more advantageous as a starting population for cell differentiation.

1.3.5.3 Post-implantation - EpiSCs and EpiLCs

Mouse EpiSC lines have been derived from post implantation Mouse epiblasts from E5.5 to E8 (Brons et al., 2007; Osorno et al., 2012; Tesar et al., 2007). The culture requirements for EpiSC are distinct from ESCs, with propagation promoted by serum-free culture (N2B27) with the addition of Fgf and Activin (N2B27/FGF/Activin) on fibronectin substrate (Brons et al., 2007; Tesar et al., 2007). EpiSC cells can also be generated *in vitro* directly from ESCs cell lines by long term culture of ESCs in EpiSC conditions, a process involving extensive cell death and differentiation (Turco et al., 2012). Reversion to the ESC state from EpiSCs, however, is extremely inefficient (Guo et al., 2009; Zhang et al., 2016).

The distinct functionality of ESC and EpiSCs is demonstrated by the efficient integration of ES cells in pre-implantation but not post-implantation embryos (Evans and Kaufman, 1981; Huang et al., 2012; Martin, 1981), and EpiSCs in post-implantation embryos but not preimplantation ones (Huang et al., 2012; Tesar et al., 2007). Like ESCs, EpiSCs express the core pluripotency factors *Oct4*, *Sox2* and *Nanog*, but lack the expression of naive pluripotency markers such as Esrrb and Nr5a2 (Guo et al., 2009; Tesar et al., 2007). Instead, EpiSCs express many post-implantation

embryo markers including *Fgf5*, *Otx2* and *Lefty*, and are thought to be *'primed'* for differentiation (primed state).

Initially EpiSCs were thought to correspond to early post-implantation embryos (E5-E6) (Tesar et al., 2007) however a comparison of the transcriptome of multiple EpiSC lines with carefully staged embryos throughout gastrulation revealed that they do not resemble any one postimplantation stage, instead having a distinct EpiSC identity (Kojima et al., 2014a). Furthermore, their expression of lineage markers including mesoderm markers *T(Bra)*, *Eomes*, *Mixl1*, endoderm markers *Foxa2*, *Sox17*, suggests that at least subpopulations of these cells are similar to early primitive streak cells (Kojima et al., 2014b). Generally, EpiSCs cultures are very heterogenous and vulnerable to spontaneous differentiation. In accordance, sub-populations relating to early (pluripotent) and later lineages (differentiation) have been described (Han *et al.*, 2010). Adding to the complexity of EpiSC, comparison of multiple EpiSC lines indicated significant variation between lines in terms of the levels of key gastrulation markers including *T(Bra)* and overall differentiation potential (Bernemann *et al.*, 2011). The cause of this variation is still not understood but was not correlated to how these EpiSCs were derived (Bernemann *et al.*, 2011).

A third state akin to the post-implantation epiblast, epiblast-like cells (EpiLCs), has also been described. 2i/LIF cultures, treated with Activin and Fgf in defined media with the addition of knock out replacement serum (KSR) (N2B27/Activin/Fgf/KSR) pass through a transient EpiLC state with cells being transcriptionally dynamic over 3 days of culture, characterised by a wave of cell death upon day 3 (Hayashi and Saitou, 2013; Hayashi et al., 2011, 2012). This EpiLC state is termed 'formative', and thought to be representative of E5.5-6.25 embryo stages, transcriptionally reflecting a mid-point between 'naïve' (ESCs) and 'primed' (EpiSC) states. At 48 hours EpiLCs are transcriptionally reflective of E5.75 embryos, with levels of both pluripotent and differentiation markers, lower than those for ESCs and EpiSCs respectively. They form a near-homogenous population of cells exhibiting minimal spontaneous differentiation (Hayashi et al., 2011). Despite the identification of this advantageous starting population for differentiation protocols, exploration of its functional abilities have been limited to the derivation of primordial germ cells, a lineage whose

differentiation is not possible with EpiSC. So far there has been no publication using EpiLCs as a starting population for generation of *in vitro* NMPs.

In summary, distinct stages of epiblast development are reproducible *in vitro*; stable 'naïve' (ESCs) and 'primed' (EpiSCs) states, and transient 'formative' (EpiLCs) and NMPs. They represent a developmental continuum which we can exploit to further our understanding of developmental mechanisms. However, many questions remain unanswered in terms of the robustness or reliability of some of these cells lines, including EpiSCs which contain lots of variance between and within cell lines. Additionally, it remains unclear if EpiLCs could be a utilised as an alternative to EpiSCs especially as a starting population to generate NMPs from.

1.3.6 Important signalling pathways for NMPs

The activity of several signalling pathways has been implicated in the maintenance and fate choice of NMPs during axial elongation, these include Wnt/β-catenin and FGF signalling.

1.3.6.1 Fgf

The Fgf signalling pathway consists of a family of extracellular ligands, receptors and intracellular signalling components (reviewed in Dorey and Amaya, 2010). Fgfs are characterised by a shared core of 140 amino acids and affinity for heparan sulphates. Many Fgf ligand family members are expressed in the streak and tail bud during axial elongation, and of particular interest are *Fgf8* and *Fgf4* (Cambray and Wilson, 2007; Crossley and Martin, 1995). Loss of both Fgf4 and Fgf8 signalling in early gastrulation results in embryonic lethality, with mutants showing axial truncations, which are phenotypes that could include disruptions in NMP behaviour (Naiche et al., 2011). Only when double conditional mutants were generated was a reduction in paraxial mesoderm identified, which appeared to be due to reductions in paraxial precursors rather than problems with EMT (Boulet and Capecchi, 2012). Moreover as previously mentioned Fgf8-/- and Fgfr1-/- mutants have problems in gastrulation with cells failing to undergo correct EMT (Sun et al., 1999). These conditional mutants also appeared to have ectopic neural tubes, suggesting NMPs may have shifted their fate from mesoderm to neural lineages in the absence of Fgf signalling (Boulet and Capecchi, 2012). Furthermore Fgf is essential for the derivation of *in vitro* NMPs, and has

additionally been associated with inhibition of neural commitment from EpiSC cultures (Gouti et al., 2014; Greber et al., 2010).

In summary, in both *in vitro* and *in vivo* systems, Fgf is crucial for regulating NMP behaviour.

1.3.6.2 Canonical Wnt/β-catenin Signalling

Like the Fgf signalling pathway, Wnt signalling pathways are highly evolutionarily conserved pathways involved in the regulation of many crucial aspects of development. All Wnt pathways consist of secreted Wnt glycoproteins which signal through Frizzled (Fzd) family of receptors and additional co-receptors (reviewed in Komiya and Habas, 2008). Wnt signalling can be dependent on β-catenin stabilisation (canonical) or alternatively β-catenin independent (non-canonical). Much of the investigation into the role of Wnt signalling in NMP maintenance and fate choice has focused on specifically canonical Wnt/β-catenin signalling, which requires recruitment of β-catenin to activate downstream targets.

Wnt3a secreted glycoprotein is key to activation of this pathway, and is upstream of many mesoderm associated gene targets including *T(Bra), T-Box protein6 (Tbx6)* and *Mesogenin1 (Msgn1)*(Yamaguchi *et al.*, 1999; Nowotschin *et al.*, 2012). Mutations of *Wnt3a* or its targets show strikingly similar phenotypes, with reduction in presomitic mesoderm as well as formation of ectopic neural tube (Chapman and Papaioannou, 1998; Nowotschin et al., 2012; Yoshikawa et al., 1997). These phenotypes highlight the importance of canonical Wnt/β-catenin signalling for mesoderm differentiation, and suggest that when absent NMPs revert to neural fate. In accordance overexpression of Wnt3a specifically in caudal regions (under Cdx2 enhancer) prevents the formation of neural tissues, however axial defects are still present (Jurberg et al., 2014). Direct interference with β-catenin levels has influenced similar fate decisions. NMPs in mesodermal fated regions of the CLE could be diverted to neural differentiation when β-catenin was conditionally downregulated (Wymeersch et al., 2016).

Evidence has also supported the idea that Wnt/β-catenin signalling may also be important for maintenance of the NMP progenitor pool. When β-catenin levels were reduced during axial elongation NMPs numbers were simultaneously reduced

(Wymeersch et al., 2016). In addition the activation of Wnt/β-catenin signalling is essential for the generation of NMPs from EpiSCs *in vitro* (Gouti et al., 2014).

This apparent paradox between the need for Wnt/β-catenin signalling for both differentiation and maintenance can be partly resolved by the seemingly dose-dependent action of *Wnt3a* and *T(Bra)*. Experiments utilising chimeric embryos with varying cell levels of T(Bra) showed that cells lacking T(Bra) were biased towards neural differentiation compared to those expressing high T(Bra) which formed mesoderm precociously (Wilson and Beddington, 1997). Moreover, Wnt3a hypomorph mutants show a graded phenotype, with increasing levels of Wnt3a necessary for increasingly more posterior mesoderm (Greco et al., 1996). Thus distinct levels of Wnt/β-catenin appear to be required for regulating the behaviour of NMPs toward different lineages and continuation of axial elongation.

In summary, both canonical Wnt signalling and Fgf play an important role in the balance between maintenance of NMPs and their differentiation towards mesodermal and neural fates *in vivo* and *in vitro*. However, it remains unresolved whether the balance of canonical Wnt/β-catenin and Fgf signalling is all that is needed to determine neural fate, or whether additional pathways play a critical role in this balance?

1.4 Planar Cell Polarity (PCP)

1.4.1 Wnt/Planar Cell Polarity (PCP) as a candidate for NMP regulation

NMPs are bipotent, giving rise to tissue of both mesodermal and neural lineages. NMP derivatives include; pre-somitic mesoderm which forms somites (paraxial mesoderm) that give rise to future muscle and bone; and neural tissues that form the neural tube and give rise to future spinal cord.

Phenotypically mutants of components that are important for NMP regulation are characterised by abnormalities in overall body axis, including shortening or curvature of the anterior-posterior (AP) axis, and loss or gain of NMP derivatives. With alterations in the balance of maintenance and differentiation of NMPs leading to premature termination or, alternatively, the overproduction of neurectoderm or mesoderm leading to inappropriate morphology. Individual mutations of components

of the noncanonical Wnt/Planar Cell Polarity (PCP) signalling pathway result in shortened anterior-posterior axis phenotypes (reviewed in Table 1.1). It is not clear if this shortening is due to an axial truncation, however this phenotype may suggest that these components have a role in regulating NMP behaviour. Furthermore, many of these components have been reported to be expressed in NMP-containing regions during axial elongation, supporting the idea they may be involved (reviewed in Table 1.1).

As mentioned previously, non-canonical (β-catenin independent) signalling pathways downstream of Wnt signalling via Fzd receptors are known to play important roles in development. One of these, the Wnt/Planar Cell Polarity (PCP) is pivotal for establishing planar cell polarity which is critical for coordinating morphogenetic behaviours of individual cells and cell populations (reviewed in Gray, Roszko and Solnica-Krezel, 2011).

Cell polarity refers to an intrinsic bias in internal cell organisation. Planar cell polarity is perpendicular to apicobasal polarity, and thus internal cellular components are localised asymmetrically over the plane of the tissue, usually towards an external structural landmark or signal, known as tissue polarity (Fig. 1.2) (reviewed in Strutt and Strutt, 2009). Wnt/PCP exists on two levels, at a cellular level and at a tissue level. Wnt/PCP components are initially uniformly expressed within an individual cell (Fig. 1.2A) until Wnt/PCP activity is established through intercellular and intracellular interactions (Fig. 1.2C). This promotes the characteristic asymmetric localisation of cellular organelles including Golgi and cytoskeleton (Carvajal-Gonzalez et al., 2016; Sepich et al., 2011), as well as core Wnt/PCP components, associated with Wnt/PCP activity (Fig. 1.2B) (reviewed in Bornens, 2008).

Research has provided evidence of two systems that contribute to PCP, namely, the Fat/Dachsous (Ft/Ds) system and the core Wnt/PCP system, with the interactions between the two unclear even in well studied *Drosophila* models (Reviewed in Lawrence, Struhl and Casal, 2007). Mutants of the Ft/Ds pathway Ft4-/- and Ds1-/- show minor axial defects with shorter axes and curly tails, however they are mostly characterised by substantial kidney defects (Mao et al., 2011; Saburi et al., 2008, 2012). Due to the more severe axial defect phenotypes exhibited by mutations of the

core Wnt/PCP pathway, as well as the reported expression of core Wnt/PCP genes in NMP regions this thesis will focus on their role in NMP behaviour.

1.4.2 Roles of Wnt/PCP in embryonic development

The importance of core Wnt/PCP components were first described in *Drosophila* over 30 years ago, with Wnt/PCP mutants having visually striking defects in the orientation of the hairs and bristles in *Drosophila* wing (Gubb and Garcia-Bellido, 1982). Components of the Wnt/PCP pathway are highly evolutionarily conserved and are crucial for important vertebrate developmental processes. In vertebrates, the most documented role has been in convergence and extension (CE), the process by which the body axis narrows (converges) and elongates (extends) along the anterior-posterior axis during early development (reviewed in Mlodzik, 2002; Roszko, Sawada and Solnica-Krezel, 2009). In Zebrafish, Wnt/PCP has been shown to additionally regulate the plane of cell division during this process (Gong et al., 2004; Quesada-Hernández et al., 2010). Neural tube closure is also a common defect in Wnt/PCP vertebrate mutants, including those of *Vangl2* and *Celsr1*, due to CE defects (Doudney and Stanier, 2005). In addition to CE defects Wnt/PCP mutants also characterised by disruption in orientation of sensory hair cells of the inner ear, hair follicles, cilia in node cells and airway epithelium, axon guidance and limb elongation (Antic et al., 2010; Borovina et al., 2010; Curtin et al., 2003; Gao et al., 2011; Goodrich, 2008; Gros et al., 2010; Guo et al., 2004; Montcouquiol et al., 2003; Song et al., 2010; Tatin et al., 2013).

Parallels of *Drosophila* asymmetric distribution of core components have been identified in many of these vertebrate Wnt/PCP systems, and thus considered evolutionarily conserved. PCP is most often described in flat epithelial layers but it is also known to be important for more three dimensional (3D) mesenchymal tissues including the heart, however in these systems the asymmetric distribution of core Wnt/PCP proteins is not well understood (Le Garrec et al., 2013; Pop et al., 2013). Furthermore, it remains possible that Wnt/PCP components are required for processes that are not related to Wnt/PCP.

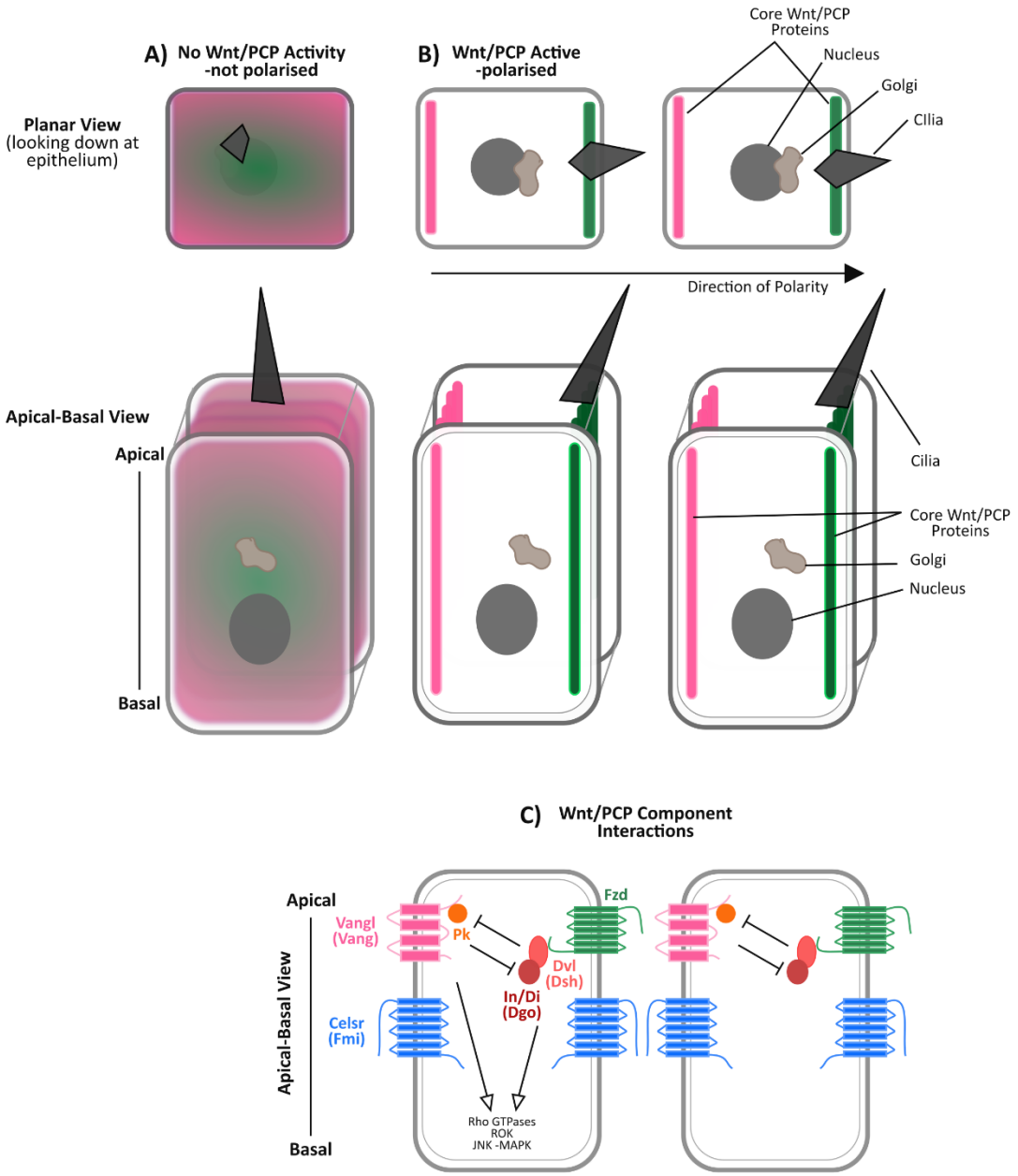

Figure 1.2 Wnt/PCP signalling and tissue polarity.
Schematic depiction of the establishment and propagation of epithelial tissue polarity through interactions between core Wnt/PCP components. **(A)** Core Wnt/PCP components are initially universally expressed in the cell, and organelles (i.e Cilia and Golgi) are randomly localised. **(B)** When cells become polarised (tissue polarity), Wnt/PCP components and organelles (i.e Cilia and Golgi) are polarised within individual cells and across neighbours in a unified direction. **(C)** Planar polarity is established through intercellular and intracellular interactions between core Wnt/PCP components. These interactions resolve to two complexes at opposing sides of the cell, these are Vangl-Celsr-Pk and Fzd-Celsr-Dvl-In/Di. Downstream pathways of Wnt/PCP activation active on Rho GTPases, Rho-associated kinase (ROK) and JNK-type mitogen activated protein kinase (MAPK) cascade. Names in brackets are *Drosophila*. Inspired and adapted from (Yang and Mlodzik, 2015).

1.4.3 Mechanism of core Wnt/PCP pathway action

Much of the research on the mechanism of Wnt/PCP initiation and propagation through tissues has been done with *Drosophila*. This model has been pivotal in uncovering interactions between different components. I will first discuss some of the findings using *Drosophila*, before discussing recent findings in vertebrate systems.

1.4.3.1 Core Wnt/PCP components and their interactions

Classically this pathway is composed of six proteins. Three of the components are transmembrane; ***Frizzled* (*Fzd*)** receptors ; ***Van gogh like* (*Vangl*)** -*van gogh (vang)/strabismus* in *Drosophila* ; ***Celsr*** (also *starry night)* - *flamingo (fmi)* in *Drosophila*; and three are cytoplasmic; ***Prickle* (*Pk*)**; ***Dishevelled* (*Dvl*)** ;and ***Inversin/Diversin (In/Di)***- *Diego (Dgo)* in *Drosophila* (reviewed in Yang and Mlodzik, 2015).

Through interactions between components, these separate into two complexes at opposing sides of the cell, which provide the basis for planar polarisation (Fig. 1.2B). These interactions which occur intercellularly and intracellularly, result in the formation of a ***Fzd-Celsr-Dvl-In/Di*** (*Fzd-Fmi-Dvl-Dgo*) protein complex on one side and a ***Vangl-Celsr-Pk*** (*Vang-Fmi-Pk*) complex on the opposite side of the same cell.

Interactions between the complexes are generally thought to be inhibitory intracellularly, which serve to localise complexes to mutually exclusive regions (Fig. 1.2C). This is mediated by *Pk* which inhibits *Fzd-Dvl* formation by binding to *Dvl*. Moreover the distinct localisation of these complexes is amplified by *Vangl (vang)* which recruits *Pk* to the membrane (Bastock, 2003; Das et al., 2004; Jenny et al., 2003; Tree et al., 2002). *Dgo* however antagonises this effect on *Dvl* and serves to protect the *Fzd/Dvl* complex.

In contrast intercellular interactions mutually reinforce and stabilise PCP across a field of cells (reviewed in Yang and Mlodzik, 2015). It has been suggested that because *Celsr* (*fmi*) co-localises to both *Fzd* and *Vangl (vang)*, it may function through homophilic adhesion to facilitate interaction between the two complexes on the cell surface of neighbouring cells (Chen et al., 2008; Lawrence et al., 2008; Struhl et al.,

2012; Strutt and Strutt, 2008; Wu and Mlodzik, 2008). This intercellular bridging is thought to be key to the establishment and propagation of PCP across tissues.

1.4.3.2 Disruption of Wnt/PCP

In *Drosophila* the tight regulation of Wnt/PCP can be disrupted by either loss or gain (overexpression) of core Wnt/PCP genes, which leads to random distribution of other core factors and mis-orientation of hair cells (Seifert and Mlodzik, 2007; Yang and Mlodzik, 2015).

The propagation of planar polarity between cells is demonstrated by the finding that disruption of planar polarity is not limited to cells with altered levels of components, but can also affect the orientation of wildtype neighbours (Wu and Mlodzik, 2008). *Fzd-Vang* interactions through *Celsr* (*fmi*)-promoted intercellular bridge formation is thought to be key to this process, with *Fzd* acting as a provider of cues and *Vangl* (*vang*) as a receiver (Struhl et al., 2012; Wu and Mlodzik, 2008, 2009). Conversely disruption in levels of cytoplasmic components, including *Pk* and *Dvl* do not have effects on neighbouring cells suggesting their primary involvement in intracellular rather than intercellular polarity signalling (Strutt and Strutt, 2007; Veeman et al., 2003; Wu and Mlodzik, 2009).

1.4.3.3 Wnt/PCP Downstream Signalling

Despite extensive research the exact mechanisms by which these six core components activate downstream signalling, these remain elusive. Interaction between *Fzd* and *Dvl*, and subsequent juxtamembrane subcellular localisation of *Dvl* appears to be important in activating downstream signalling but it is unclear exactly how this is mediated (Axelrod, 2001; Wong et al., 2003). This complex has been associated with a multitude of downstream targets including, Rho GTPases, Rho-associated kinase (ROK) and the JNK-type mitogen-activated protein kinase (MAPK) cascade (Fig. 1.2C) (reviewed in Mlodzik, 2002; Veeman, Axelrod and Moon, 2003; Yang and Mlodzik, 2015). These downstream pathways generally converge on cytoskeletal regulation which is essential for coordinating dynamic movements intracellularly (organelles) and intercellularly (coordinating movement of cells themselves) (reviewed in Strutt and Strutt, 2009; Wallingford, 2012). The contribution of these

downstream effectors appears very context dependent, and it is unknown if activation of these pathways is dependent on asymmetric localisation of components.

1.4.4 Core Wnt/PCP in vertebrates

As mentioned, *Drosophila* has provided a sophisticated genetic model in which interactions between components could be investigated. Much less is known about how Wnt/PCP operates in mammalian species. This is due in part to the presence of multiple homologs for each component, between which there is redundancy in function. In Mouse, there are two *Vangl*, four *Pk*, ten *Fzd* receptors, three *Celsr* and three *Dvl* homologs. Despite high conservation of sequences between *Drosophila* and vertebrate species there still may be some differences in how the components function in Wnt/PCP signalling. In addition, the readout of cell orientation in *Drosophila* epithelia is simplified by the presence of obvious phenotypes such as aberrant wing hair cell orientation.

To combat this complication, investigations on Wnt/PCP mechanisms in vertebrates have utilised simple systems in which cell orientation is obvious. One of the most firmly established Mouse Wnt/PCP models is the mammalian auditory epithelium (Montcouquiol et al., 2003). In Mouse the inner ear consists of mechanosensory hair cell bundles which each have a bundle of actin-based stereocilia arranged in a crescent shape. In wildtype mice, the orientation of these cells are highly regulated, as seen with the tissue wide coordination of stereocilia orientation across cells in the tissue. However, in Wnt/PCP mutants the orientation of these stereocilia bundles are disrupted, and appear random, with complete loss of tissue polarity. Use of this system as a read out of Wnt/PCP signalling functionality has aided the more recent identification of other components that are involved in Wnt/PCP signalling in vertebrates. These include two families of tyrosine kinase Wnt/PCP co-receptors, Ror and Protein tyrosine kinase 7 (Ptk7).

1.4.4.1 Tyrosine-protein kinase receptor Ror (*Ror1 and Ror2*)

Tyrosine-protein kinase receptor Ror1 and 2 (*Ror1, Ror2*) encode transmembrane proteins which serve as Wnt co-receptors. Binding between Wnt5a and Ror2 has been identified in *in vitro* systems, and the downstream effects examined (Mikels and Nusse, 2006; Oishi et al., 2003). Moreover Ror2 has thus been identified as an

important modulator of several Wnt5 induced non-canonical responses including activation of JNK, inhibition of Wnt/β-catenin signalling, and phosphorylation of Dvl proteins (Gao et al., 2011; Ho et al., 2012; Mikels and Nusse, 2006; Nishita et al., 2010; Nomachi et al., 2008). During limb development Wnt5a and Ror2 interactions are important for establishing Wnt/PCP through phosphorylation of Vangl2 which appears to mediate its activity (Gao et al., 2011).

1.4.4.2 Protein tyrosine kinase 7 (*Ptk7*)

Protein tyrosine kinase 7 (Ptk7), also known as Colon carcinoma kinase-4 (CCK-4) due to its discovery in colon carcinoma cells, encodes an evolutionarily conserved transmembrane protein with tyrosine homology (Lu et al., 2004; Mossie et al., 1995). Ptk7 was first identified as a potential Wnt/PCP component after inner ear polarity defects were found in mutants (Lu et al., 2004). Additionally, like many components of Wnt/PCP signalling, mutations in Ptk7 have been implicated in many human neural tube defects (Wang et al., 2015). Further investigations in multiple vertebrates have now shown roles for Ptk7 in CE, gastrulation, neurulation and Wolffian duct elongation (Caddy et al., 2010; Lu et al., 2004; Paudyal et al., 2010; Williams et al., 2014; Xu et al., 2016; Yen et al., 2009). Yet despite these investigations many questions regarding its signalling function remain unanswered.

Xenopus has been the most utilised model in dissecting these interactions but species differences make it hard to determine if they are conserved in Mouse. Ptk7 consists of seven immunoglobulin(Ig) domains, a transmembrane domain and a catalytically inactive tyrosine kinase intracellular domain (Kroiher et al., 2001). Despite being catalytically inactive this intracellular domain has been shown to have interactions in *Xenopus* with β-catenin (perhaps antagonistically) and Dsh, which is thought to be the route through which Ptk7 elicits Wnt/PCP signalling (Puppo et al., 2011; Shnitsar and Borchers, 2008). Correspondingly the transmembrane and extracellular domain has been implicated in interacting with extracellular components of Wnt signalling, including Wnt ligands, Fzd receptors, and co-receptors in *Xenopus* models. These interactions include components of both Wnt/β-catenin; Wnt3a and LRP6 (Wnt/β-catenin co-receptor) and Wnt/PCP; Wnt5a and Ror2 (Bin-Nun et al., 2014; Martinez

et al., 2015; Peradziryi et al., 2011; Podleschny et al., 2015; Puppo et al., 2011; Shnitsar and Borchers, 2008).

Although, the role of Ptk7 in activating Wnt/PCP is firmly established, its role in Wnt/β-catenin signalling is debated. This is due to contradicting evidence supporting and refuting its role in this pathway, suggesting its role is highly context dependent (reviewed in Peradziryi, Tolwinski and Borchers, 2012). Recently experiments on Zebrafish even provided evidence that in some contexts Ptk7 can promote Wnt/PCP whilst inhibiting Wnt/β-catenin signalling, suggesting a role in modulating the pathway choice following Wnt activation (Hayes et al., 2013).

Adding to the complexity of Ptk7, it has also been identified as a target of membrane type-1 matrix metalloproteinase (MT1-MMP/MMP14) (Golubkov and Strongin, 2012; Golubkov et al., 2010, 2011). Ptk7 is cleaved by MMP14 in its extracellular Ig domain close to the transmembrane domain, producing a secreted extracellular fragment. A novel Ptk7 *chuzhoi* mutant, in which an additional cleavage site is present, exhibits neural tube defects typical of Wnt/PCP disruption, suggesting excessive extracellular proteolysis causes the defects seen in Ptk7 mutants (Golubkov et al., 2011; Paudyal et al., 2010). Recent evidence has also implicated Vangl2 in the trafficking of MMP14 within the cell (Williams et al., 2012).

In summary Ptk7 has been identified as an important regulator of Wnt/PCP pathway. As well as interacting with Wnt/PCP specific components Ptk7 has also been identified to interact with Wnt/β-catenin specific components though its role in this pathway remain controversial. Furthermore, in Zebrafish systems Ptk7 has been shown to activate Wnt/PCP whilst attenuating Wnt/β-catenin signalling, suggesting a role in switching between Wnt pathways. Overall Ptk7s actions are somewhat context-dependent and many unknowns remain in terms of its function, specifically in Mouse models were investigations have been limited.

The idea that a co-receptor for Wnt signalling may be involved in choosing between Wnt/PCP and Wnt/β-catenin pathways is especially interesting in the context of NMP regulation, where the balance between maintenance and differentiation depends on unknown factors regulating Wnt/β-catenin signalling.

1.4.5 Wnt/PCP & Fate choice

Most investigations into the role of Wnt/PCP have focused on how Wnt/PCP modulates cytoskeleton to influence cell movement or morphology rather than cell fates. However, there is some evidence that components of Wnt/PCP are important for cell fate decision. For example, in *Drosophila* some components are essential for the asymmetric cell division which underlies the development of the sensory organ precursors (Gho and Schweisguth, 1998). Examples of this in vertebrate are limited but are of increasing interest. To establish the potential role of the core Wnt/PCP pathway in NMP behaviour below I will examine the literature for each component in terms of its described mRNA and protein expression during axial elongation, mutant phenotypes and functions potentially relevant for NMP behaviour. Findings are summarised in (Table. 1.1); note that for many of the components gene expression and mutant phenotype data was collated from research focused on neuroectodermal development in which caudal structures were not fully described.

1.4.5.1 Wnt ligands - *Wnt5a, Wnt5b, Wnt11*

The specific Wnt signalling pathway that is activated, either non-canonical (including Wnt/PCP signalling) or canonical (β-catenin dependent), is partially dependent on which Wnt ligand binds to surface receptors. As previously discussed, Wnt3a is the key Wnt ligand involved in Wnt/β-catenin signalling, Wnt5a and Wnt11 however are thought to be primarily responsible for activating Wnt/PCP signalling, across vertebrate species (Andre et al., 2015; Gros et al., 2010; Heisenberg et al., 2000; Tada and Smith, 2000)(reviewed in Logan and Nusse, 2004; Kikuchi *et al.*, 2012). As mentioned previously, interactions between Wnt5a and co-receptor Ror2 resulting in downstream activation of Wnt/PCP have been reported *in vitro* and *in vivo* models. In the limb bud Ror2 is imperative for sensing Wnt5a dosages across the tissue, suggesting a dose-dependent activation of Wnt/PCP signalling is important (Gao et al., 2011).

Wnt5a is expressed in the primitive streak and in the tail bud during axial elongation. *Wnt5a* appears as a gradient in the primitive streak, which is localised to caudal regions when compared to *Wnt3a* which extends more anteriorly. In the tailbud *Wnt5a* is broadly expressed and is present in presomitic mesoderm and endoderm

Table 1.1 Summary of Wnt/PCP component expression during axial elongation and mutant phenotypes.

	E7.5- E8.5			E8.5	E9.5	E10.5	E11.5	E12.5	E13.5	References	Truncation Phenotype	References	Cell Localisation
	PS	NSB/node	CLE	TB	TB	TB	TB	TB	TB				
Celsr1	xx	xx	x	x	xx	xx	n/d	n/d	n/d	(Shima *et al.* , 2002; Crompton, Du Roure and Rodriguez, 2007)	n/d	(Zhou *et al.* , 2008; Tissir *et al.* , 2010)	Not Asymmetric
Celsr2	x	xx	xx	x	x	x	n/d	n/d	n/d	(Shima *et al.* , 2002; Crompton, Du Roure and Rodriguez, 2007)	xx	(Curtin *et al.* , 2003)	Not Asymmetric
Celsr3	x	x	xx	x	n/d	n/d	n/d	n/d	n/d	(Shima *et al.* , 2002; Crompton, Du Roure and Rodriguez, 2007)	n/d	(Zhou *et al.* , 2008; Tissir *et al.* , 2010)	Not Asymmetric
Dvl1	x	x	n/s	x	x	x	n/d	n/d	n/d	(Bois *et al.* , 1996)	-	(Lijam *et al.* , 1997)	Asymmetric
Dvl2	n/d	n/d	n/d	n/d	n/d	x	n/d	n/d	n/d	(Tissir and Goffinet, 2006)	x	(Hamblet, 2002)	Asymmetric
Dvl3	n/d	n/d	n/d	n/d	n/d	x	n/d	n/d	n/d	(Tissir and Goffinet, 2006)	-	(Etheridge *et al.* , 2008)	Asymmetric
Fzd1	n/d	n/d	n/d	x	x	x	n/d	n/d	n/d	(Borello *et al.* , 1999)	-	(Yu *et al.* , 2010, 2012)	n/d
Fzd2	n/d	n/d	n/d	n/d	n/d	n/d	n/d	n/d	n/d	(Borello *et al.* , 1999)	-	(Yu *et al.* , 2010, 2012)	n/d
Fzd3	n/d	n/d	n/d	x	x	xx	n/d	n/d	n/d	(Borello *et al.* , 1999)	xx	(Wang, Guo and Nathans, 2006)	Asymmetric
Fzd6	n/d	n/d	n/d	x	x	x	n/d	n/d	n/d	(Borello *et al.* , 1999)	xx	(Wang, Guo and Nathans, 2006)	Asymmetric
Fzd7	n/d	n/d	n/d	-	-	-	n/d	n/d	n/d	(Borello *et al.* , 1999)	x	(Yu *et al.* , 2012)	n/d
Pk1	xx	xx	xx	xx	xx	n/d	n/d	n/d	n/d	(Bekman and Henrique, 2002; Crompton, Du Roure and Rodriguez, 2007)	x	(Yang, Bassuk and Fritzsch, 2013)	Asymmetric
Pk2	-	x	-	n/d	n/d	n/d	n/d	n/d	n/d	(Crompton, Du Roure and Rodriguez, 2007)	n/d		n/d
Ptk7	n/d	n/d	n/d	xx	xx	n/d	n/d	n/d	n/d	(Paudyal *et al.* , 2010)	xx	(Yen *et al.* , 2009; Paudyal *et al.* , 2010)	Not Asymmetric
Ror1	-	-	-	-	n/d	n/d	n/d	n/d	n/d	(Matsuda *et al.* , 2001)	-	(Takeuchi *et al.* , 2000)	Not Asymmetric
Ror2	xx	xx	n/s	xx	xx	xx	xx	n/d	n/d	(Matsuda *et al.* , 2001; Verhey van Wijk *et al.* , 2009)	x	(DeChiara *et al.* , 2000; Takeuchi *et al.* , 2000; Nomi *et al.* , 2001)	Not Asymmetric
Vangl1	n/d	n/d	n/d	x	x	x	x	x	x	(Torban *et al.* , 2008; Pryor *et al.* , 2014)	xx	(Torban *et al.* , 2008; Antic *et al.* , 2010)	Asymmetric
Vangl2	x	x	n/s	x	x	x	n/d	n/d	n/d	((Kibar et al., 2001; Murdoch et al., 2001 ; Pryor et al., 2014)	xx	(Murdoch *et al.* , 2001; Yin *et al.* , 2012)	Asymmetric
Wnt11	x	xx	n/s	xx	x	x	n/d	n/d	n/d	(Kispert *et al.* , 1996)	n/d	(Andre *et al.* , 2015)	Secreted
Wnt5a	xx	x	n/s	xx	xx	n/d	n/d	n/d	n/d	(Takada *et al.* , 1994; Yamaguchi *et al.* , 1999)	xx	(Yamaguchi *et al.* , 1999)	Secreted

Summary of gene expression data based on published in situ hybridisation reports, and axial truncation phenotypes based mutant reports in the literature. 'xx' (dark green) - highly expressed in region, 'x' (light green) - expressed in the region, '-' (red) - not expressed in the region, 'n/d' - no data , 'n/s' no sections to confirm CLE expression. Axial truncations graded 'xx' (dark green) - severe when no tail or extremely short tail was exhibited, 'x' (light green) - curly or kinked tail, '-' (red) no axial truncation phenotype, and 'n/d' no data. Additionally, reported cellular localisation of these proteins is indicated. PS - primitive streak, NSB- Node streak border, CLE - caudal lateral epiblast, TB - tail bud

(Takada et al., 1994a). *Wnt11* is expressed in a punctate pattern from E6.75 at the posterior of the embryo. Expression then splits into two distinct expression domains, the node and the most caudal primitive streak, including extraembryonic mesoderm. At E8 expression in the node disappears but expression in the caudal end of the embryo persists, strongest in rostral somites and the tail tip, until at least E11.5 (Andre et al., 2015; Kispert et al., 1996).

Wnt5a-/- mutants exhibit caudal truncation, with loss of tail and significant shortening of the anterior-posterior (A-P) axis (Yamaguchi et al., 1999b). Despite this caudal defect, expression of many genes implicated in axial elongation, including, *Fgf8*, *T(Bra)*, *Evx1* are maintained in these mutants. Defects in cell proliferation have been identified, suggesting a role for Wnt/PCP in this process (Yamaguchi et al., 1999b). Axial defects in *Wnt11*-/- mutants have not been described in detail, however these mutants die before birth due to severe defects in kidney development (Majumdar et al., 2003). *Wnt11*-/- and *Wnt5a*-/- double mutants show an exacerbation of axial shortening suggesting redundancy between the two (Andre et al., 2015). These mutants have disruptions in CE which results in abnormal notochord development and patterning of the axis. They also exhibit defects in EMT with ectopic expression of adhesion markers and accumulation of NMPs in the tail bud. Additionally, upregulation of Sox2 and down regulation of T(Bra) protein is present in the tail bud of these mutants as well as disruption in somite formation suggesting that *Wnt5a* and *Wnt11* may have a role in NMP behaviour. In these mutants expression of Vangl1, in the notochord is decreased, suggesting interactions between *Wnt11/Wnt5a* with Wnt/PCP signalling (Andre et al., 2015). Overall it is unclear if the disruption to NMPs and their derivatives are a direct consequence of loss of Wnt/PCP signalling in *Wnt5*-/-;*Wnt11*-/- mutants or an indirect consequence of abnormal notochord formation due to defects in convergence and extension. These mutants also exhibit shortening of the *Wnt3a* expression domain in the tail bud, raising the possibility that Wnt5a/Wnt11 may interact with Wnt/β-catenin pathway activation through regulation of Wnt3a. This potential interaction has been reported in several contexts before including Mouse limb development, in which Wnt5a promotes β-catenin degradation (Topol et al., 2003). However this regulation is not well understood, and in other contexts and species

Wnt5a has also been shown to have agonistic effects on this pathway (reviewed in Logan and Nusse, 2004; Kikuchi *et al.*, 2012).

In summary, *Wnt5a* and *Wnt11* are known regulators of the Wnt/PCP pathway and are expressed in the caudal regions of the embryo, in which NMPs reside during axial elongation. *Wnt5a-/-* mutants exhibit a more severe axial truncation than Wnt11-/- mutants, however axial disruption is enhanced in double knock outs, providing further evidence that they may have role in regulating NMP behaviour. These *Wnt5a-/-*; *Wnt11-/-* mutants also exhibit increased levels of Sox2, decreased levels of T(Bra) protein and reduced mesoderm formation, suggesting again that NMPs are not properly regulated in these mutants. However, determining whether these observations are due to direct disruption of NMPs remains elusive due to severe disruptions in CE which cause major disruption to tissues adjacent to NMPs, including adjacent notochord. Vertebrate models have also shown Wnt5a-Ror complexes are important for dose-dependent activation of Wnt/PCP across tissues, which is potentially interesting in terms of NMPs which also require Wnt/β-catenin signalling in a dose-dependent manner. Additionally, the reported inhibition of Wnt3a and downstream β-catenin signalling by Wnt5a also raises the possibility that this could also be happening in NMP areas, and could be a potential mechanism by which Wnt/β-catenin levels could be regulated.

1.4.5.2 *Fzd 1, 3, 6, 7*

In total, there are 10 different Fzd family members in mammals, with some evidence supporting the involvement of Fzd1,3,6 and 7 in Wnt/PCP signalling. Deciphering their role in Wnt/PCP is complicated due to functional redundancy between different family members. The details of Wnt-Fzd specificity are still relatively unknown, with many interactions between family members and co-receptors yet to be discovered.

In general Mouse mutants for Fzd family members are less severe than for other core Wnt/PCP components. *Fzd1-/-* show no apparent phenotype, whilst *Fzd2-/-* mutants are associated with cleft palate defects (Yu et al., 2010, 2012). Only a small proportion of *Fzd7-/-* mutant display cardiac abnormalities, with the majority exhibiting no phenotype except for a kinked tail. More severe phenotypes are produced with double knockouts, with *Fzd2-/-;Fzd7-/-* exhibiting severe defects in CE and open neural tube,

phenotypes associated with Wnt/PCP mutants (Wang et al., 2016; Yu et al., 2012). Genetic interactions were observed when *Fzd1, Fzd2* and *Fzd7* were crossed with non-functional *Vangl2* (*looptail*) mutant, as double mutants had enhanced frequency of neural tube defects; however, it is still not clear if this interaction is specifically through Wnt/PCP signalling. Additionally *Fzd7-/-* kinked shorted tail phenotype is enhanced in *Fzd7-/-;Wnt5a-/+* double mutants which have a significantly higher tail truncation (Yu et al., 2012).

Unlike Fzd1,2 and 7 whose roles in Wnt/PCP are still relatively unknown, Fzd3 and Fzd6 are more established as Wnt/PCP signalling activating receptors. Fzd6 was first identified to have a role in Wnt/PCP when hair follicles in Fzd6-/- mutant were found to be orientated aberrantly in random orientations (Guo et al., 2004; Wang et al., 2006). Fzd3 also appears to signal through Wnt/PCP, and is important in axon growth and guidance in the forebrain (Hua et al., 2014). Fzd3-/-;Fzd6-/- double mutants show disrupted inner ear sensory hair cell orientation and neural tube closure defects akin to those of *Vangl2-/-* (looptail mutants), and additionally shortening of the axis with an apparent curly tail (Wang et al., 2006).

In the literature, the expression for *Fzd1,3,6,7* has been reported between E8.5 and E10.5 on wholemount embryos (Borello et al., 1999). *Fzd1* expression is found in many mesoderm structures, and is initially expressed strongly in the intermediate mesoderm and rostral edge of newly formed somites, with some weak expression in the presomitic mesoderm. From the reported *in situ* hybridisations *Fzd1* in the tail bud is unclear, but does look to be expressed to a weaker extent than that described previously for mesodermal structures. During somitogenesis *Fzd3* is expressed strongly in the dorsal neural tube, but is additionally present in somites. Its expression is particularly strong in the neural folds of E8.5 embryos, but is also present in more posterior regions, including the tail bud. This expression in the tail bud is reported up to E10.5, with expression in the CNH never verified. At E8.5 *Fzd6* is expressed along the entire length of the notochord and underlying endoderm. Additionally, it is present at the rostro-lateral edge of newly formed somites from E9.5 (Borello et al., 1999). From the reported data *Fzd6* appears to be expressed in the tail bud however it is not clear exactly where it is localised due to lack of transverse sections. *Fzd7* is expressed

along the ventro-lateral borders of newly formed somites (akin to *Fzd1*), as well as expression in distinct areas of presomitic mesoderm at low levels. It is also expressed in the ventromedial neural tube (Borello et al., 1999). In the reported expression patterns *Fzd7* does not appear to be expressed in the tailbud for any stage.

In summary *Fzd1, 3, 6, 7* are expressed in overlapping but distinct areas in embryonic development. Many appear to be expressed in mesoderm and mesodermal derivatives, however they are additionally expressed in neural tissues. Overall the extent and tissue specificity of expression in the tail bud for each family member is unclear due to minimal descriptive data in these areas. However, it does appear that of all Wnt/PCP Fzd family members, *Fzd3* and *Fzd6*, mutants of which have the more severe truncations, are more highly expressed in caudal regions from E8.5 to E10.5.

Reports of Fzd1,3,6,7 protein expression are limited. Fzd3 and Fzd6 has been identified in the inner ear, where these components are known to control the orientation of hair cells through Wnt/PCP. In this tissue Fzd3 and Fzd6 protein is asymmetrically distributed within cells. This profile in the inner ear is lost in non-functional Vangl2-/- (*looptail*) mutants in which normal levels of Fzd3 and Fzd6 protein are present but not asymmetrically localised (Wang et al., 2006). Asymmetric localisation of Fzd6 has also been reported in cells of the epidermis; similarly this asymmetry is lost in non-functional *Vangl2-/- (looptail)* or *Celsr1-/- (crsh)* mutants (Devenport and Fuchs, 2008).

In summary, of all the Wnt/PCP Fzd family members, *Fzd3* and *Fzd6* represent the best candidates for potential regulation of NMP behaviour. Despite limitations in published *in situ* data they appear to be expressed in the tail bud during axial elongation, meaning they are in the right place at the right time to have an influence on NMP behaviour. Additionally, their mutants exhibit severe axial truncations, which could be due to abnormal regulation of NMP maintenance or differentiation, though it is not clear from the described data if there is a biased loss of one tissue type, or if all are affected equally.

1.4.5.3 *Dvl1,2,3*

There are three mammalian *Dvl* family members which, as previously mentioned, have functions in both Wnt/β-catenin and Wnt/PCP pathways through interactions with Fzd receptors (Mlodzik, 2016). Dvl proteins share three highly conserved domains; N-terminal DIX domain, which activates Wnt/β-catenin targets including *Axin*; PDZ domain, which mediates interactions with Fzd receptors; and C-terminal DEP domain, which has been linked to Wnt/PCP function of *Dvl* (Axelrod et al., 1998; Wong et al., 2003) (reviewed in Wallingford and Habas, 2005; Mlodzik, 2016). Cytoplasmic localisation of Dvl is important for Wnt/β-catenin signalling. In contrast, Wnt/PCP signalling requires membrane translocation of Dvl protein (Wu, Klein and Mlodzik, 2004; Wallingford and Habas, 2005). Limiting levels of Dvl has been proposed as an explanation to why activation of one pathway may downregulate another (Wallingford and Habas, 2005). Additional proteins may also be involved in regulating Dvl downstream activation of pathways. These include Naked Cuticle (Nkd) family members which have been shown to interact with the PDZ domain of Dvl and appear to antagonise Wnt/β-catenin signalling. However more investigation in to its function in Mouse is needed to understand its role in regulating of signalling pathway balance (Rousset et al., 2001; Wharton et al., 2001; Yan et al., 2001). As previously mentioned Wnt5a-Ror2 interactions are also known to phosphorylate Dvl proteins, however the function of this phosphorylation is not completely understood (Ho et al., 2012).

Expression data for *Dvl* family members is lacking in the literature, with only few embryo stages described. In one report, *Dvl3* is described from E7.5 to E9. *Dvl3* is initially expressed highly in the neural fold and neural plate, as well as the primitive streak. Later at E8.5 highest levels are found in the somites and developing CNS, before being expressed in almost all other tissues of the embryo at low levels at E9 (Bois et al., 1996). Similar descriptions are reported for *Dvl1* and *Dvl2*, with high levels in the developing CNS and somites, and all other tissue expressing low levels at E10.5 (Tissir and Goffinet, 2006). Thus, all Dvl family members are expressed to some extent in all tissues, probably a reflection of their role in both Wnt pathways.

Dvl2-/- mutants have a low survival rate and display many cardiac abnormalities, neural tube defects and skeletal malformation. Of those that survive, approximately a

quarter have a kinked tail phenotype (Hamblet, 2002). *Dvl3-/-* mutants also exhibit cardiac defects, however no skeletal or truncation defects are reported (Etheridge et al., 2008). *Dvl1-/-* mutants are associated with abnormalities in social interaction, and display wildtype tails (Lijam et al., 1997). *Dvl1-/-;Dvl2-/-* mutants have more severe skeletal malformations which are not limited to caudal tissues, and they frequently display tightly curled tails (Hamblet, 2002). Similar phenotypes are described for *Dvl2+/-;Dvl3-/-* mutants which appear to have a shortened axis with absence or truncated kinked tails (Etheridge et al., 2008).

In mammalian systems reports of the localisation of Dvl proteins in Wnt/PCP contexts are limited to the inner ear. In the inner ear Dvl1, 2 and 3 proteins are all found to be asymmetrically localised (Etheridge et al., 2008; Lee et al., 2012; Wang et al., 2005). This asymmetry is not as prominent versus other asymmetrically localised proteins. In *Vangl2-/-* (*looptail*) mutants this asymmetric juxtamembrane location of Dvl2 is lost (Wang et al., 2005).

In summary, *Dvl2* represents the best candidate to have function in regulating Wnt/PCP in NMPs. Loss of this protein results in kinked tail phenotype, suggesting mis-regulation of NMP populations. In addition, *Dvl2*, as with all *Dvl* family members, is expressed throughout the developing embryo including the tailbud region, providing support for the idea that these may play a role in NMP behaviour. Its role in both signalling pathways also offers a potential mechanism by which Wnt signalling may be modulated during axial elongation.

1.4.5.4 *Vangl and Pk*

There are two mammalian *Vangl* family members, *Vangl1* and *Vangl2*. As previously mentioned these family members form a complex with *Pk* which is important in establishing Wnt/PCP. There are four Prickle homologs in the Mouse genome, *Pk1* and *Pk2* are the two most closely related to that of *Drosophila*, with *Pk3* and *Pk4* being more distinct with unknown functions in Wnt/PCP signalling.

Vangl2 mutant *looptail* (Lp) was one of the first mutants used to demonstrate the functional significance of Wnt/PCP in mammalian systems (Murdoch *et al.*, 2001). Lp mutants have a missense mutation in cytoplasmic domain of Vangl2 protein which

results in a dominant mutant phenotype. Since its discovery, additional *Vangl2* mutants have been generated, all of which exhibit disruptions in hair cell orientations, severe neural tube defects, as well as iconic looped tails (Yin et al., 2012). Knockouts of *Vangl1* have neural tube closure defects but do not appear to have truncations of the body axis or looped tail phenotype (Antic et al., 2010; Torban et al., 2008). Human mutations of VANGL1 and VANGL2 are both associated with several neural tube defects including spina bifida (Kibar et al., 2010; Lei et al., 2010). In Mouse, embryos with mutations in both *Vangl1* and *Vangl2* show a greater proportion of Wnt/PCP defects, showing redundancy between the two family members (Torban et al., 2008). These mutants also exhibit an accumulation of cells at the primitive streak which is akin to those exhibited by *Wnt5a-/-;Wnt11-/-* mutants (Andre et al., 2015). Double mutations of Vangl2 and *Wnt5a*, *Celsr1* (*crsh*), *Dvl* family members, *Ptk7*, *Ror2* or *Scribble*, a key regulator of apicobasal polarity, exhibit enhanced severity in Wnt/PCP disruption phenotypes, highlighting the importance of Vangl2 in regulating Wnt/PCP (Etheridge et al., 2008; Gao et al., 2011; Lu et al., 2004; Murdoch et al., 2014; Qian et al., 2007). *Pk1* and *Pk2* are essential for apicobasal polarity during early development resulting in embryonic lethality in full knock outs prior to gastrulation (Tao et al., 2012). Alternative mutants with partial disruption of the Pk1 protein have been generated, and show skeletal abnormalities including a truncated tail (Liu et al., 2014; Yang et al., 2013). The expression of other genes, including *Fgf8*, *Vangl2* and *Wnt5a* are also disrupted in the limb bud of these mutants. Axial defects in Pk2 mutants have not been reported.

Vangl1 and *Vangl2* expression during embryo development has not been fully described in the literature although some publications do exist examining its expression in relation to neural tube defects. *Vangl1* is expressed at E8 in the floor plate and notochord throughout the anterior-posterior body axis (Pryor et al., 2014; Torban et al., 2008). Additionally, *Vangl1* appears to be present in the caudal regions of the embryo including the primitive streak, although the exact location of its expression was not examined in the tail bud. Throughout the timepoints examined E8-E13.5 *Vangl1* expression remains high in the notochord. At E9.5 it appears that *Vangl1* may be additionally expressed in the tail bud. *Vangl2* expression is reported from E7 to E10. Its expression is closely associated with neuroectodermal tissues throughout

this time but also appears to be expressed in other non-neural tissues, including caudal mesoderm and hindgut. Additionally *Vangl2* appears to be expressed in the streak and in the tail bud, though the exact localisation remains elusive due to lack of sections for these regions (Kibar et al., 2001; Pryor et al., 2014). *Pk1* and *Pk2* expression patterns have been described between E5.5 to E9 (Bekman and Henrique, 2002; Crompton et al., 2007). At E5.5 *Pk1* is restricted to the posterior epiblast, whilst *Pk2* expression in limited to the node. At gastrulation in situ hybridisation on sections reveal that *Pk1* expression is highest in the CLE and streak, which continues to headfold stage. *Pk1* expression is additionally found in the node, paraxial mesoderm and the neural folds. At E9.5 *Pk1* expression is high in the tail bud however lack of sections make it impossible to determine any tissue specific localisation of this expression pattern (Bekman and Henrique, 2002; Crompton et al., 2007).

Due to its key role in Wnt/PCP signalling, the localisation of Vangl proteins has been described in an array of Mouse tissues, including neuroectoderm, node, notochord, oviduct, inner ear, limb bud (Andre et al., 2015; Antic et al., 2010; Gao et al., 2011; Montcouquiol, 2006; Torban et al., 2007, 2008; vandenBerg and Sassoon, 2009). In these tissues, Vangl family members are typically reported as asymmetrically distributed within cells, a hallmark of Wnt/PCP activity, and co-localised with Pk family members. This asymmetry of Vangl2 is lost in Wnt/PCP mutants which exhibit diffuse expression of Vangl2 on all membranes (Gao et al., 2011; Qian et al., 2007). This diffuse Vangl localisation is also reported in wildtype limb buds in locations where Wnt/PCP is inactive (Gao et al., 2011). Reports of Pk protein are far fewer, but include asymmetric localisation in cells of the ventral node, inner ear, and limb bud (Antic et al., 2010; Deans et al., 2007; Gao et al., 2011). In Vangl2 mutants Pk localisation is disrupted (Yin et al., 2012).

In summary both *Vangl1* and *Vangl2* are expressed predominantly in neurectoderm and notochord, but also in more caudal structures including the tail bud, suggesting they could be involved in regulation of NMP behaviour. In line with this, Pk1 which forms a complex with Vangl is well described in the literature and is highly expressed in NMPs of the CLE, and the tail bud during axial elongation. Mutations of these components all cause truncation phenotypes characteristic of mis-regulated NMP

behaviour. Together these findings provide strong evidence for the involvement of *Vangl* and *Pk* complexes in regulating NMP behaviour during axial elongation.

1.4.5.5 *Celsr*

Celsr1, *Celsr2* and *Celsr3* are the mammalian homologs to the *Drosophila Fmi* gene. They have redundancy between them, with upregulation of other family members when one is knocked out (Cortijo et al., 2012).

In situ hybridisations for *Celsr* family members have been described in detail from E5.5 to E8, including embryo sections showing expression in the CLE, where NMPs reside (Crompton et al., 2007; Formstone and Little, 2001; Hadjantonakis et al., 1998, 1997; Shima et al., 2002). All *Celsr* family members are first detected throughout the E5.5 epiblast. At E7.5 *Celsr1* is highest in the streak and the node but is also found elsewhere. *Celsr2* and *Celsr3* are also expressed in the primitive streak at E7.5 but higher levels are found in the prospective anterior neuroectoderm. At headfold stage (E8) expression of all family members is widespread but highest in the neural folds. Additionally, the streak and the adjacent CLE, were NMPs reside, are positive for all members. Later stages are described in less detail, making it unclear to what extent CNH regions express *Celsr* family members (Shima et al., 2002). From E9.5, broad but distinct expression in neuroepithelium is present for each family member. Additionally, these members appear to be expressed in the tailbud, highest and more broadly for *Celsr1* than the other family members.

In the literature, there are very few reports of the protein distribution of Celsr family proteins in mammalian species. In *Drosophila* wing, Celsr is found at proximal and distal cell edges. In *Fzd* mutants its localisation is more fragmented at the boundary (Usui et al., 1999). Celsr2 protein has been examined in E18 Mouse whisker and neurons, and Celsr1 in oviduct epithelium (Shima et al., 2002). In these tissues Celsr proteins are localised to opposing membranes within in the same cell in accordance to the localisation of Celsr described in *Drosophila* (Shi et al., 2014).

Two mutants for *Celsr1* have been identified from mutagenesis screens, namely spin *cycle* (*scy*) and crsh (Curtin et al., 2003). Like other members of the core Wnt/PCP pathway these mutant exhibit severe neural tube defects. Although their axial

phenotype is not thoroughly described in the literature their AP axis appears severely truncated (Curtin et al., 2003). Additionally, these mutants exhibit mis-orientation of hair cells from the earliest stage that hair bundle orientation is detectable. Mutants of *Celsr2* and *Celsr3* have been generated, but their phenotype has only been described in terms of forebrain development, thus it remains unclear if they also exhibit axial defects (Tissir et al., 2010; Zhou et al., 2008). Mutants of *Celsr2* and *Celsr3* have also shown Celsr family members to be critical for Wnt/PCP dependent differentiation of apicobasal polarised pancreas progenitors (Cortijo et al., 2012).

In summary, all members of the *Celsr* family are expressed in the CLE regions where the NMPs reside during embryonic development, and this expression continues to later in axial elongation where they are expressed in the tail bud. Mutants of *Celsr1* also have severe truncations in caudal structures akin to those described for *Vangl2* mutants. Altogether this data suggest that Celsr family members could be involved in regulation of NMPs during axis elongation.

1.4.5.6 *Ror*

The expression profiles for *Ror* family members has been described from E7.5 to E8.5 (*Ror1*) and E7.5 to E11.5 (*Ror2*) (Matsuda et al., 2001; Verhey van Wijk et al., 2009). *Ror1* expression is restricted to anterior neuroectodermal tissue from E7.5 to E8.5. Conversely, *Ror2* is expressed at E7.5 in the primitive streak. At E8.5 *Ror2* is expressed highly in the neuroepithelium but is also expressed to high levels in neural and non-neural tissues in more posterior regions. At E9.5 *Ror2* is expressed highly at the caudal end of the embryo including in presomitic mesoderm (Takeuchi et al., 2000). This high expression in the tailbud continues to E11.5 (Verhey van Wijk et al., 2009). Ror2 protein has been described in the literature in endoderm development, during which it is not asymmetrically localised (Yamada et al., 2010).

Ror2-/- mutants exhibit dwarfism, with short limbs and truncated tail (Nomi et al., 2001; Takeuchi et al., 2000). In *Ror2*-/- mutants the expression domain but not the intensity levels of *T(Bra)* were reduced, reflecting smaller presomitic mesoderm found in these mutants which also have smaller somites. (DeChiara et al., 2000; Schwabe et al., 2004). *Ror1* does not exhibit a truncated body axis phenotype (Takeuchi et al., 2000).

In summary, due to its restricted expression in anterior tissues and its lack of truncation phenotype Ror1 is unlikely to have a role in influencing NMP behaviour during axial elongation. Ror2 on the other hand represents a strong candidate, being expressed in caudal regions of the embryo from E7.5 to E11.5 and with knock out mice exhibiting tail shortening, phenotypic of NMP mis-regulation. Additionally, the smaller presomitic mesoderm and somites in these mutants may reflect its importance in specification of mesodermal fate.

1.4.5.7 *Ptk7*

Ptk7 expression during Mouse embryo development has been described in the literature but not in much detail especially in NMP regions. *Ptk7* is first described in head fold stage embryos, in which levels of *Ptk7* are highest in caudal regions of the embryo, and lower levels in the neuroepithelium and somites. This pattern of high level of *Ptk7* in caudal embryo regions continues later into development to E9.5 (Paudyal et al., 2010).

Mutants for *Ptk7*, exhibit truncation and kinking of the body axis and severe neural tube defects (Paudyal et al., 2010; Yen et al., 2009). *Ptk7*-/- mutants are morphologically normal prior to early somite stages, however by 5-somite stage, the axis of these embryos are shorter and wider than even *Ptk7*-/+ littermates (Lu et al., 2004; Yen et al., 2009). The nodes of these mutants are also significantly wider, the presomitic mesoderm thinner and the somites shorter (A-P), a product of CE defects identified in these regions (Yen et al., 2009). Conversely *T(Bra)* conditional *Ptk7* knockouts do not exhibit the same severity of CE associated neural tube defects but still exhibit coiled tails (Xu et al., 2016).

In the literature Ptk7 protein has always been reported to be localised to the cell membrane (Lu et al., 2004; Paudyal et al., 2010). Unlike core Wnt/PCP components Ptk7 protein is not associated with asymmetrical localisation, and localisation remains unchanged when *Vangl2 (looptail)* or *Celsr1* are mutated (Lu et al., 2004; Paudyal et al., 2010). Additionally no change in *Vangl2* or *Celsr1* was identified in *Ptk7* mutants (Paudyal et al., 2010).

In summary, due to its high expression in caudal regions during embryonic development and the axial truncations exhibited by *Ptk7* mutants, *Ptk7* represents a potential candidate for NMP regulation.

Altogether the literature has provided some useful information and insight to which Wnt/PCP components represent the best candidates to investigate in terms of NMP behaviour regulation. Overall many of the components are expressed in the node/streak and later tailbud regions during axial elongation. All *Celsr* family members and *Pk1* were confirmed to be specifically expressed in the CLE, but unfortunately the literature could not provide this specificity for the other Wnt/PCP components, or for any gene expression specifically in the CNH. Furthermore, due to the lack of gene expression in NMP regions, *Fzd7* and *Ror1* are unlikely to have roles in NMP behaviour. However at least one family member of each gene was found to be expressed in node/streak or tailbud supporting the idea that this signalling pathway may be active in NMP regions during axial elongation.

Overall axial defects were most severe for *Celsr2*, *Fzd3*, *Fzd6*, *Ptk7*, *Vangl1*, *Vangl2* and *Wnt5a* mutants, which all exhibited truncation of the axis. This provides strong evidence that the Wnt/PCP pathway is important for correct axial elongation, further supporting the idea that this pathway regulates NMP behaviour. In the most severe cases neural tube closure was the most predominant defect, however disruption to a variety of mesodermal structures (presomitic mesoderm, somites and skeletal defects) were additionally reported in *Wnt5a*, *Ptk7* and *Ror2* mutants. Together this suggests that disruption of Wnt/PCP may bias NMP differentiation.

Moreover, the dual role of *Ror2*, *Ptk7* and *Dvl* in both Wnt/PCP and Wnt/β-catenin signalling pathways provides a potential mechanism by which Wnt/β-catenin signalling could be modulated in NMPs .

1.4.6 New avenues of investigation

To date investigation into the role of Wnt/PCP in Mouse development has been limited to the use of non-functional or full mutant knock outs. These mutants show severe disruptions in the axis from gastrulation onwards and this precludes the interpretation of roles for Wnt/PCP in developmental processes that follow this initial disruption.

Furthermore, this is particularly evident when considering the role of Wnt/PCP in NMP behaviour. Defects in CE coincide with the start of axial elongation, making it impossible to determine if axial defects are due to impaired CE alone or to true alterations in NMP behaviour. In other animal models including *Zebrafish* or *Xenopus*, tools are available to conditionally disrupt Wnt/PCP in a spatial and time dependent manner. This has ultimately resulted in a greater understanding of the role of Wnt/PCP in tissues beyond these early developmental disruptions (reviewed in Gray, Roszko and Solnica-Krezel, 2011).

In Mouse systems tools to conditionally disrupt Wnt/PCP are limited but available. One option is electroporation which permits the introduction of DNA in a time and spatial dependent manner. Despite the advantages, it has not been fully exploited and only a few investigations reporting its use. One report uses electroporation to disrupt Wnt/PCP via introduction of non-functional *Vangl2* constructs in ciliated cells of Mouse brain ventricles (Guirao et al., 2010). However recent work on spinal cord regeneration showed that simply overexpressing wildtype *Pk1* or *Vangl2* constructs is enough to perturb Wnt/PCP signalling, and alter cell division planes (Albors et al., 2015). Experiments introducing exogenous *Vangl2* in clusters of Mouse inner ear cells via retrovirus, showed that disruption in cell orientation is not only limited to cells with Wnt/PCP disruption but also but also in their neighbours (Sienknecht et al., 2011). This work aligns with current understanding of Wnt/PCP signalling, where under/overexpression of single components is considered enough to overwhelm the delicately balanced system and disrupt its function. Despite the evidence supporting the use of overexpressing wildtype Wnt/PCP components to disrupt its signalling and the advantages of electroporation, to date this system has not been utilised further.

Another alternative, but underutilised system to investigate Wnt/PCP is examination of cell polarity based on the positioning of organelles. As mentioned previously, cell polarity is characterised by the asymmetric organisation of components within a cell, which includes the aforementioned Wnt/PCP component proteins (Vangl, Pk etc.), but additionally includes organelles within the cell (Bornens, 2008). In the literature both Golgi, and more recently Centrosomes have been used as indicators of individual cell polarity (Boehm et al., 2010; Carvajal-Gonzalez et al., 2016). Studies analysing cell

polarity and division dynamics were first conducted on simple epithelia with either planar (flat) geometry or simple axes to work with (Blankenship et al., 2006; Concha and Adams, 1998). However following gastrulation embryo development in vertebrate becomes complicated quickly with dynamic cell movements in all three dimensions which cannot be analysed using simple 2D systems. Advances in technology have been made to try and overcome this problem and quantitatively analyse 3D polarity information. One of the first was examination of the embryonic Mouse heart, a highly complex structure with 3D looping of tissue (Le Garrec et al., 2013; Pop et al., 2013). This study pioneered simple analysis of polarity based on nuclear elongation and organelle positioning within the cell. This analysis would be particularly interesting in NMP regions where the presence of Wnt/PCP/tissue polarity has not yet been investigated. Of increasing interest is the CLE region, a curved epithelia of T(Bra) and Sox2 co-expressing cells whose fate appear to be determined by their location and not by the expression of any specific gene.

1.5 Scope of the Thesis

Taken together the in-depth review of Wnt/PCP mutant phenotypes and the expression profile of Wnt/PCP components in NMP regions outlined above, hold support for the idea that Wnt/PCP signalling may be important for NMP regulation during axial elongation. However, many unknowns remain. Despite the reported expression of mRNA the presence of Wnt/PCP proteins have yet to be investigated specifically in NMP regions. Additionally, a refined investigation is essential to affirm a role for Wnt/PCP signalling in the regulation of NMPs, and furthermore specifically what this role is in terms of maintenance and/or differentiation of these bipotent progenitors.

In this thesis I aim to provide answers to some of these unknowns. In Chapter 3 I investigate expression patterns of Wnt/PCP component mRNA and protein specifically in NMP regions. Complementarily to this, the polarity of cells within NMP regions throughout axial elongation are investigated by examining the positioning of individual cell organelles. In Chapter 4 I investigate the ability to derive NMPs from an alternative *in vitro* stem cell population, subsequently characterise this population, and examine the presence of Wnt/PCP proteins in these cultures, as well as those previously described. Finally, in Chapter 5, I describe the generation of tools to disrupt

Wnt/PCP signalling *in vivo* and *in vitro*, and their implementation to investigate and unlock the true role of Wnt/PCP in NMPs maintenance and differentiation.

Chapter 2: Materials and Methods

2.1 Materials

2.1.1 General Reagents

Table 2.1	Details of General Reagents	
Product	**Vendor**	**Catalogue Number**
0.25% Trypsin EDTA, Phenol red	Gibco	25200-056
10 mM dNTP Mix	Invitrogen	18427-013
100mm x 20mm TC-Treated Culture Dish	Corning	430167
1Kb and 100bp Ladder	NEB	N3232L, N3231L
35 x 10mm Tissue Culture Dish	Falcon	35-3001
3 M Sodium Acetate	Thermofisher Scientific	R1181
5’ T5 exonuclease	NEB	M0363
50 mM 2-Betamercaptoethanol	Gibco	31350-010
Accutase ® Solution	Sigma	A6964
Agarose, ultra pure	Invitrogen	16500-500
Amaxa P3 Primary Cell 4-D nucleofector X Kit L	Lonza	V4XP-3012
Ammonium Chloride	Acros Organics	423285000
Ampicillin	Calbiochem	171254
Anti-digoxigenin (DIG)-AP	Roche	11093274910
Aquatex	Merck Millipore	108562
B27	Gibco	17504-044
Bacto™ Agar	BD	214010
Benzyl Alcohol	Sigma Aldrich	8421

Benzyl Benzoate	Sigma Aldrich	B6630
Bovine Fibronectin	Sigma Aldrich	F1141
Bovine Serum Albumin	Sigma	A8412
CellCarrier-96 Black, Optically Clear Bottom, Tissue Culture Treated, Sterile, 96-Well with Lid	PerkinElmer	6005550
CHIR 99021 (CHIR)	Axon	1386
Chloroform	Fisher Scientific	67-66-3
Costar ® 10 ml Stripette ®	Corning Incorporated	4101
Costar ® 12 well clear TC-treated multiple well plates, individually wrapped, sterile	Corning	3513
Costar ® 24 well clear TC-treated multiple well plates, individually wrapped, sterile	Corning	3524
Costar ® 25ml Stripette ®	Corning Incorporated	4251
Costar ® 48 well clear TC-treated multiple well plates, individually wrapped, sterile	Corning	3584
Costar ® 50ml Stripette ®	Corning Incorporated	4501
Costar ® 5ml Stripette ®	Corning Incorporated	4051
Costar ® 6 well clear TC-treated multiple well plates, individually wrapped, sterile	Corning	3516
Costar ® 96 well clear flat bottom TC-treated microplate	Corning	3595
Coverglasses/Menzel-Glaser	Agar Scientific	L4338-1
CryoTube ™ Vial	Thermo Scientific	377224

DAPI	Biotium	40043
DAPI (flow cytometry)	Molecular Probes	D1306
Dimethyl Sulfoxide (DMSO)	VWR Chemicals	23500.26
DMEM/F-12	Gibco	12634-010
Donkey Serum	Sigma/Abcam	D9663/Ab166643
Doxycycline Hyclate (Doxycycline/Dox)	Sigma	D9891
Dulbecco's Phosphate Buffered Saline	Sigma	D8537
Ethanol Absolute AnalaR NORMAPUR®	VWR	101074F
Facs Cell Strainer Tube	Falcon	352235
Fast-Read 102 Cell Counter	Biosigma S.r.l	BVS100
FGF basic (bFGF)	R&D	233-FB-025/CF
Fibronectin from bovine plasma	Sigma	F1141
Filter Tip Bevelled 10 µl	StarLab	S1121-3810
Filter Tip Bevelled 50 µl	StarLab	S1120-2810
Filter Tip Universal 1000 µl	Greiner Bio-one	740288
Foetal Calf Serum (FSC)	Gibco	10270
G418 Sulphate	PAA	P27-011
Gelatine (Embedding)	Sigma Aldrich	48722
Gelatine (TC)	Sigma	G1890
Glasgow Minimum Essential Medium (GMEM)	Sigma	G5154
Glycine	Sigma	G8898-500G
High Vaccum Silicone Grease	VWR Chemicals	331353N
HiSpeed Plasmid Maxi Kit	Qiagen	12662

HyPure™ Molecular Biology Grade Water	GE	SH30538.02
Human Acitivin A	PeproTech	120-14E
Isoamyl Alcohol	Fisher Scientific	A393
Isopropanol, 99.5%, for molecular biology, DNAse RNAse and Protease free	Acros Organics	327272500
Kanamycin	Calbiochem	420311
KnockOut ™ Serum Replacement (KSR)	Gibco	10828-028
L- Glutamine 200 mM	ThermoFisher	25030-024
Labelling Tape	Anachem	SL9355
Laminin (from Engelbreth-Holm-Swarm murine sarcoma basement membrane)	Sigma	L2020 1mg/ml
LB Broth, Miller (Luria-Bertani)	BD	244620
Lightcycler® Multiwell Plate 384, White	Roche	4729749001
Lightcycler® Probes Master	Roche	4887301001
M13 Forward and Reverse Primers	Invitrogen	N52002/ N53002
M2 Medium	Sigma	M7167-100ml
MEM non-essential amino acids (NEAA)	Gibco	11140-035
Methanol AnalaR Normapur ®	VWR	20847.24
Microtube 1.5ml	Sarstedt	72.692.005
Millex®-GP syringe filter unit, 0.22 µm, diameter 33 mm, gamma sterilized	Millipore	SLGP033RS
Millex®-GP syringe filter unit, 0.45 µm, diameter 33 mm, gamma sterilized	Millipore	SLHP033RS

Molecular Biology Grade Water	Hyclone	SH30538
M-MLV Reverse Transcriptase	Invitrogen	28025-013
N2	Gibco	17502-048
Neurobasal ® Medium	Gibco	21103-049
Paraformaldehyde (PFA)	Sigma Aldrich	P6148
PCR Tubes - 8-Strip	Sarstedt	72.991.002
PD0325901 (PD03)	Axon	1408
Penicillin-Streptomycin (10000 U/ml)	Gibco	15140-122
Phenol	Fisher Scientific	A9311
Phosphate Buffered Saline (PBS) Tablet	Sigma	P4417
Phosphate Buffered Saline (PBS)	Sigma	D8537
Phusion DNA Polymerase	NEB	M0530
Plain Stubs	Agar Scientific	G307
Poly-L-Orthinine Solution	Sigma	P4957
Polysine™ Microscope Slides	VWR	631-0107
Prolong ® Gold Antifade Reagent	Life Technologies	P36930
Random Primers	Invitrogen	48190-011
Recombinant Human Fgf Basic (146aa)	R&D	233-fb-025
Recombinant human/rat/Mouse Activin A	Peprotech	120-14E
Recombinant mWnt-3a	R&D	1324-WN/CF
RNAse-free ddH_2O	Roche	
Rnase H	New England Biolabs	M0297L
RNase-free Eppendorf tubes	Ambion Invitrogen	AM12400

RNaseOut™ Recombinant Ribonuclease Inhibitor	Invitrogen	1077-019
Safe-Lock® Tubes	Eppendorf	T9661
Snap-cap Tube	Falcon	352059
Sodium Acetate	Fisher Scientific	R1181
Sodium Azide (NaN_3)	Sigma Aldrich	S2002
SP6/T7 Transcription Kit	Roche	10999644001
Standard Petri Dishes 90 mm, Single Vent	Sigma	101R20
Stop Solution	Promega	M199A
Subcloning Efficiency ™ DH5α ™ Competent Cells	Invitrogen	18265-017
Sucrose	Sigma	S0389
SYBR® Safe DNA Gel Stain	Invitrogen	S33102
T4 DNA ligase	NEB	M0202L
Taq DNA Polymerase Kit	Qiagen	201203
Transfer Pippettes	Sarstedt	86.1172.010
Trichloroacetic Acid	Sigma Aldrich	T6399
Tris Base	Fisher	BP152-1
Triton™ X-100	Sigma	T8532
UltraPure ™ Agarose	Invitrogen	16500100
UltraPure ™ Dnase/Rnase-Free Distilled Water	Gibco	10977
Universal Tube	Sterilin	128/FS
Universal (rolling culture)	NUNC	
Universal Container Flow Seal Cap	Thermo Scientific	128A/FS
Vectashield Non-Hardening Medium	Vector Labs	H-1200

Xgal	Promega	V394A

2.1.2 Instruments/Equipment

Table 2.2	Instrument/Equipment Details
Equipment	**Company**
4D- nucleofector ™ System Core Unit/X Unit	Lonza
Attoflour ™ Cell chamber	Life Technologies
Blue Light Transilluminator	Sygene
BTX Electro Square Porator ECM 830	BTX, San Diego, CA, USA
Centrifuge 5702	Eppendorf
Cool LED Illumination unit - pE-300	CoolLED
DNA Engine thermal cycler, PTC-200	BioRad
Forceps for embryo dissection	Dumostar
Gel Tanks	Engineering & Design Plastics Ltd.
‘Genetrode’ electrode	BTX Model 516
Glass Coplin Staining Jar, cat 107	Thermo Fisher
ImmEdge Hydrophobic PAP Pen, H4000	Vector
IncuShaker, 10 L H1010 BR13-00	Benchmark Scientific
Leica Cryostat, CM1900	Leica Microscopes systems
LightCycler® 480 Instrument II	Roche
LSR Fortessa	BD
Nanodrop ND1000 Spectrophotometer	Thermofisher Scientific
NanoVue Plus Spectophotometer	GE healthcare
Olympus BX-61	Olympus

Olympus Cat SZH-121, dissection microscope	Olympus
Olympus IX51 Microscope (TC)	Olympus
Operetta High-Content Imaging System	Perkin Elmer
ORCA-R2 monochrome camera	Hamamatsu
Retiga 2000R Scientific Camera	QImaging
Roller Bottle Aparatus	BTC engineering
Sanyo CO2 incubator	Sanyo
Slides and Coverslips	Scientific Lab Supplies
SP8 Inverted Confocal Microscope system	Leica Microscopes systems
StereoZoom SMZ-U dissection microscope	Nikon
SUB Aqua 18 Plus Waterbath	Grant
Thermomixer compact	Eppendorf
TProfessional Standard Thermocycler	Biometra
UV Transilluminator - G:BOX F3	Syngene

2.1.3 Antibodies

Before use in immunohistochemistry all primary and secondary antibodies diluted in blocking solution were spun at 13000rpm in eppendorf tubes for 5 minutes at RT°C (room temperature), care was then taken not to aspirate the liquid at the very tip to minimise use of aggregated antibody.

2.1.3.1 Primary Antibodies

Table 2.3	**Primary Antibodies**				
Target	**Supplier**	**Catalogue Number**	**Raised in**	**Clonal type**	**Dilution**
Celsr1	Abcam	Ab196600	Rabbit	Polyclonal	1:100
Celsr2	Abcam	Ab90817	Rabbit	Polyclonal	1:100
Celsr2	Protein Tech	19940-1-AP	Rabbit	Unknown	1:100
Celsr2	(Shima et al., 2002)	n/a	Mouse	Monoclonal	100% serum
Celsr3	Protein Tech	19939-1-AP	Rabbit	Unknown	1:100
Collagen IV	Abcam	Ab19808	Rabbit	Polyclonal	1:200
Dvl1	Protein Tech	14314-1-AP	Rabbit	Unknown	1:100
Dvl2	NEB	3224	Rabbit	Monoclonal	1:100
Dvl2	NEB	3216	Rabbit	Polyclonal	1:100
Fzd 3	Abcam	Ab75233	Rabbit	Polyclonal	1:200
Fzd 3	Abcam	Ab102965	Rabbit	Polyclonal	1:200
Fzd 6	Abcam	Ab98180	Rabbit	Polyclonal	1:100
Fzd 6	Abcam	Ab128916	Rabbit	Monoclonal	1:200
Fzd 6	Protein Tech	13982-1-AP	Rabbit	Unknown	1:100

Fzd 6	R&D	AF1526	Goat	Polyclonal	1:15
γ-Tubulin	Abcam	Ab11316	Mouse	Monoclonal	1:250
GM130	BD Transduction	610823	Mouse	Monoclonal	1:400
LaminB1	Abcam	Ab16048	Rabbit	Polyclonal	1:1000 /1:500
Nkd2	Abcam	Ab170804	Rabbit	Polyclonal	1:100
Pericentrin	Abcam	Ab4448	Rabbit	Polyclonal	1:2000
Prickle2	Abcam	Ab65964	Rabbit	Polyclonal	1:100
Prickle2	Abcam	Ab183652	Rabbit	Polyclonal	1:100
Ptk7	Protein Tech	17799-1-AP	Rabbit	Unknown	1:100
Ptk7	Abcam	Ab62073	Rabbit	Polyclonal	1:50
Ptk7	Abcam	Ab62074	Rabbit	Polyclonal	1:50
Ror2	Santa Cruz	A17-SC 83034	Goat	Polyclonal	1:50
Sox2	Abcam	Ab92494	Rabbit	Monoclonal	1:200
T(Brachyury)	R&D	AF2085	Goat	Polyclonal	1:200
Vangl1	Abcam	Ab176575	Rabbit	Monoclonal	1:200
Vangl1	Abcam	Ab80055	Rabbit	Polyclonal	1:100
Vangl2	Abcam	Ab76174	Rabbit	Polyclonal	1:100
Vangl2	Abcam	Ab60172	Goat	Polyclonal	1:200
Vangl2	Merck Millipore	ABN373	Rabbit	Polyclonal	1:500
Wnt11	Abcam	Ab31962	Rabbit	Polyclonal	1:100
Wnt11	Abcam	Ab96730	Rabbit	Polyclonal	1:100
Wnt11	Abcam	Ab176910	Rabbit	Polyclonal	1:100

Wnt5a	Abcam	Ab174100	Rabbit	Polyclonal	1:100
Wnt5a	R&D	AF645	Goat	Polyclonal	1:60
ZO-1	Invitrogen	33-9100	Rabbit	Monoclonal	1:400

2.1.3.2 Secondary Antibodies

Table 2.4	**Secondary Antibodies**			
Target Species	**Species Raised in**	**Fluorophore**	**Company**	**Catalogue Number**
Goat	Donkey	488	Molecular Probes	Alexa Flour ® A-11055
Goat	Donkey	555	Molecular Probes	Alexa Flour ® A-21432
Goat	Donkey	568	Molecular Probes	Alexa Flour ® A11057
Goat	Donkey	647	Molecular Probes	Alexa Flour ® A21447
Mouse	Donkey	488	Molecular Probes	Alexa Flour ® A21202
Mouse	Donkey	555	Molecular Probes	Alexa Flour ® A-31570
Mouse	Donkey	568	Molecular Probes	Alexa Flour ® A10037
Mouse	Donkey	647	Molecular Probes	Alexa Flour ® A31571
Rabbit	Donkey	488	Molecular Probes	Alexa Flour ® A21206
Rabbit	Donkey	555	Molecular Probes	Alexa Flour ® A-31572
Rabbit	Donkey	568	Molecular Probes	Alexa Flour ® A10042

Rabbit	Donkey	647	Molecular Probes	Alexa Flour ® A-31573
Rabbit	Donkey	405	BioLegend DyLight	406409

2.1.4 Solutions Prepared

Standard molecular biology solutions were prepared according to (Sambrook and W Russell, 2001). Frequent solutions included:

- 4% (w/v) PFA: PFA dissolved in PBS (pH 7.4)
- DNA loading dye: Orange G (Sigma) 0.25%, glycerol (Fisher) 30%, in water.
- PBS (not for cell culture): 5 PBS tablets/L water
- TBE: Tris Base (Fisher) 22.5 mM, orthoboric acid (Fisher) 22.5 mM, EDTA 500 µM pH 8.0, in water.
- 15% sucrose (w/v) solution: sucrose dissolved in PBS (pH 7.4)
- 15% sucrose (w/v) 7% gelatin solution: gelatin dissolved in 15% sucrose solution at 37;
- 50% Rat serum culture medium: 50% heat inactivated Rat serum and filtered 50% DMEM supplemented with 0.1% Non-essential Amino Acids (NEAA) and 2 mM L-glutamine (using a 0.45 µm filter). After mixing, 1µL/mL of penicillin-streptomycin was added.
- PBS-T: PBS with 0.1% Triton X-100
- Blocking buffer: 5% Donkey serum and 0.01% sodium azide in PBS
- Antibiotic stock
  Ampicillin 1000x: 100 mg ampicillin powder in 1 mL DNase/RNase-free H_2O
  Kanamycin 1000x: 50 mg kanamycin powder in 1 mL DNase/RNase-free H_2O
  Following filtration through a 0.22 µm filter, stocks were kept at -20°C for long term storage, and once thawed were stored at 4°C for no longer than 2 weeks.

2.1.5 Primers

2.1.5.1 PCR Primer Sequences

Table 2.5	**PCR Primer Sequences**		
Target	**Forward**	**Reverse**	**Use in thesis**
Pk1	GATCCAGAGACTCTCGCAGG	GTGATGTTGGACAACGC	ISH probe generation

M13 (Invitrogen)	GTAAAACGACG GCCAG	CAGGAAACA GCTATGAC	TOPO Sequencing
p2lox sequencing primers	GCTGTTCTCCT CTTCCTCATCTC	TCCCCCTGAA CCTGAAACAT	p2lox sequencing

PCR primers used for Gibson assembly and conventional cloning found in section 2.2.5.7.

2.1.5.2 RT-qPCR Primers

These were designed using web-based Roche Universal Probe Library (UPL) System Assay Design. UPL probes are 165 short dual-labelled hydrolysis probes which are choosen specifically to match the gene of interest, and ensure amplification detected in RT-qPCR reactions is specific to this gene of interest.

Table 2.6	**RT-qPCR Primers Details**		
Target	**Forward Primer**	**Reverse Primer**	**UPL Probe**
Oct4	GTTGGAGAAGGTGG AACCAA	CTCCTTCTGCAGG GCTTTC	95
Fgf8	CAGGTCCTGGCCAA CAAG	GGTCTCCACAATG AGCTTCG	29
Foxa2	AAGTAGCCACCACA CTTCAGG	TGGCCCATCTATT TAGGGAC	32
Cdx2	CACCATCAGGAGGA AAAGTGA	CTGCGGTTCTGAA ACCAAAT	34
Evx1	CAGGGAGAACTACG TTTCAAGAC	GCCGGTTCTGAAA CCACA	66
Nkx1.2	CCAATCGGGTCACA GGAG	CGCATCCTCAGCT TCCTC	13
Ptk7	AGGCTGAGCCCCAC TACAT	GGAAATCCTCAGG AACTGTTTG	67
Tbx6	CCGAGAAAATGGCA GAAACT	GTGTATCCCCACT CCCACAG	21

Wnt3a	AATGGTCTCTCGGGAGTTTG	CTTGAGGTGCATGTGACTGG	53
Pax6	GTTCCCTGTCCTGTGGACTC	ACCGCCCTTGGTTAAAGTCT	78
Sox1	GTGACATCTGCCCCCATC	GAGGCCAGTCTGGTGTCAG	60
Sox2	GTGTTTGCAAAAAGGGAAAAGT	TCTTTCTCCCAGCCCTAGTCT	34
Mesp1	ACCCATCGTTCCAGTACGC	AGCATGTCGCTGCTGAAGA	89
T(Bra)	CAGCCCACCTACTGGCTCTA	GAGCCTGGGGTGATGGTA	100
Sox17	CACAACGCAGAGCTAAGCAA	CGCTTCTCTGCCAAGGTC	97
HoxA6	CCCTGTTTACCCCTGGATG	GGTAGCGGTTGAAGTGGAAT	47
HoxA4	TCCTCGTCCTCGTTACTGCT	TCCAATCCTGGCAAAGTTGT	62
HoxD13	GGAACAGCCAGGTGTACTGTG	GGCTGGTTTAAAGCCACATC	5
TBP (housekeeping)	GGGGAGCTGTGATGTGAAGT	CCAGGAAATAATTCTGGCTCA	97
SDHA (housekeeping)	CAGTTCCACCCCACAGGTA	TCTCCACGACACCCTTCTGT	71

2.1.6 Kits Used

Table 2.7	**Details of Kits**	
Product	**Vendor**	**Catalogue Number**
Absolutely RNA Miniprep Kit	Agilent Technologies	400800
DNA Clean & Concentrator™-5	Zymo Research Corp	D4003
Lonza Amaxa P3 Primary Cell 4-D nucleofector x L+Kit L (12RCT)	Lonzo	V4XP-3012 F-10984

Plasmid Maxi Kit	Qiagen	12162
Platinum PFX	Thermofisher	11708-013
Q5 High Fidelity DNA polymerase	NEB	M0491S
QIAprep Spin Miniprep Kit	Qiagen	27104
QIAquick Gel Extraction Kit	Qiagen	28704
rAPid Alkaline Phosphatase	Roche, Sigma Aldrich	4898133001
Zero blunt ™ PCR cloning kit with pCR™-bluntII-TOPO vector	Invitrogen	K280002/450245

2.2 Methods

2.2.1 Embryology

2.2.1.1 Animal Husbandry/ Maintenance of mice

Wildtype (WT) MF1 (outbred) Mouse strain was housed and bred in the Animal Unit of the Medical Research Council (MRC) Centre for Regenerative Medicine (CRM) according to the provisions of the provisions of the Animals (Scientific Procedures) Act (1986).

All mice were maintained in a stabilized environment on a 10 hours light, 14 hours dark cycle. Embryos at specific developmental stages were obtained by setting up timed matings overnight and inspecting the presence of vaginal plugs the following morning. Embryonic day (E)0.5 was designated to the day at noon when plugs were observed, assuming copulation occurred at midnight.

2.2.1.2 Embryo and adult tissue collection and dissection

Pregnant females were culled by cervical dislocation by Animal Unit staff. The uterus was extracted from the abdominal cavity, the decidua then placed in M2 Medium (Sigma) at room temperature. Adult tissue was removed at the same time and placed in M2 medium (Sigma) at room temperature (RT°C). Using forceps, the decidua and Reichert's membrane were removed from the embryo, and when necessary adult tissue further dissected in M2 medium under a zoom stereo microscope (Olympus, Nikon).

Special care was taken for embryos for *ex vivo* culture for which the yolk sac, amnion and the ectoplacental cone were kept intact. Samples for immunohistochemistry were fixed as described in 2.2.2.1.

2.2.1.3 Grafting cells from *in vitro* culture into embryos

Grafting was performed under a dissecting stereomicroscope using a hand pulled micropipette. Cells were cultured in 6-well plates and then scraped from the plate using a 20-200 µl pipette tip. The resulting cell sheets were placed close to the embryos and drawn into the micropipette by gentle suction using a mouth pipette. The cells were gently blown out, and a small cell clump containing 10-20 cells was sucked into the mircropipette again and placed close to the opening of the micropipette. The embryo was held loosely in place with forceps while the micropipette was inserted in the region of interest to create an opening. Cells were then gently expelled as the micropipette was drawn out of the embryo, leaving a short string of cells lodged in the epiblast (Huang et al., 2012).

2.2.1.4 Electroporation of embryos

Electroporation was performed by Catarina Martins Costa and Dr Filip Wymeersch.

Electroporation was performed as described in (Huang et al., 2015). Briefly, embryos with 2-6 somites (E8.5) were dissected and transferred to PBS. A DNA solution containing 1.2 µg/µL (or 3 µg/ml, in independent experiments) of circular expression plasmid in 1xPBS with 0.01% Fast Green dye was prepared. This was microinjected into the amniotic cavity using a mouth pipette and a fine glass injection needle, prepared from a glass capillary (1.5mm outside diameter) using a micropuller equipped with a heating element.

Immediately after microinjection, embryos were placed in PBS, between a pair of parallel 0.5 mm diameter, 1 mm long, L-shaped, gold tipped 'Genetrode' electrodes (BTX Model 516), set 5 mm apart, and electroporated by using a BTX Electro Square Porator ECM 830 (BTX, San Diego, CA, USA). Embryos were positioned with their node/anterior streak pointing towards the positive pole; the targeted area of electroporation was the caudal end of the embryo, including the NSB and CLE, within which NMPs are found. Electroporation conditions were optimised to minimise

embryo damage and maximise DNA uptake. Several conditions were tested, and the ideal settings were defined as follows: 30 V in 3 pulses of 30 ms duration each, with a 1s interval between pulses. Following electroporation, embryos were transferred to M2 to recover for a few seconds and then placed in culture for rolling 24 hours as described below 2.2.1.5.

To evaluate the success and record the zone of electroporation, after 2hr each individual embryo was taken out of culture briefly imaged, in brightfield, red fluorescence and green fluorescence (to assess auto fluorescence). This allowed the cells to incorporate the electroporated plasmid and express the encoded proteins. Embryos with damage to extraembryonic tissues, or those not successfully electroporated, were discarded and the remaining were imaged again. Another selection took place, in which embryos that had not developed well were discarded; a beating heart, closed headfolds and embryonic turning were the three main features considered to represent normal development.

2.2.1.5 Rolling culture of embryos

Embryos were cultured according to Huang *et al.*, 2012. Briefly up to three embryos were cultured in rotating bottles containing 1ml/embryo pre-warmed, pre-gassed 50% Rat serum:50% culture medium. Each bottle was connected to a gas drum continually providing 5%CO_2:5%O_2 balanced N_2 (BTC Engineering) inside a 37°C incubator. Heat-inactivated Rat serum was prepared according to (Hogan et al., 1994; Martin and Cockroft, 2008). Animal bleeding was performed in house by Valerie Wilson, Filip Wymeersch and myself.

2.2.2 Histology

2.2.2.1 Sample Fixation

2.2.2.1.1 Tissue for sectioning

Dissected embryos for embedding and sectioning were fixed with 4% (w/v) PFA in PBS at 4°C overnight unless stated otherwise.

Alternative fixation was used to optimise immunohistochemistry performance for specific antibodies, the details are outlined in the Table 2.8 below

Table 2.8	Fixation Protocols
Fixation Type	**Fixation Length/Temperature**
3.7% (w/v) PFA in 0.1% PBS-T	Overnight at 4°C
10% (w/v) Trichloroacetic Acid (TCA) in ddH_2O (Ice cold)	1 hour at 4°C
Methanol	-20°C for 1 hour

Following fixation samples were washed with PBS for three 5 minute washes before being processed for embedding.

2.2.2.1.2 Tissue for wholemount immunohistochemistry

Dissected embryos for wholemount immunohistochemistry were fixed for 2 hours at 4°C with either 4% (w/v) PFA in PBS or on occasion 3.7% (w/v) PFA in PBS for specific protocols. Embryos were then washed in 0.1% (v/v) Triton in PBS.

2.2.2.1.3 Cultured cells

Following at least one quick wash with PBS, cultured cells were fixed with fresh 4% (w/v) PFA in PBS at RT°C for 10 minutes. PFA was removed and fixed cells were washed for at least 2 minutes gently with PBS three times.

2.2.2.1.4 Embryos for In Situ Hybridisation

Embryos for use in in situ hybridisation were transferred to 4% (w/v) PFA in PBS (pH7.4) and fixed overnight at 4°C. The following day the samples were rinsed three times with DEPC-treated PBS and dehydrated through a series of methanol (VWR) concentrations (25%, 50%,75% and 100% (v/v) methanol in DEPC-treated PBS). Embryos were stored in 100% methanol at -20°C in Safe-Lock ® tubes (Eppendorf).

2.2.2.2 Preparation of cryostat sections

Following washes fixed samples for embedding were transferred into a bijou vials with 15% (w/v) sucrose solution, for between 2 hours and overnight at 4°C depending on sample size. The sucrose solution was then replaced with melted 15% (w/v) sucrose, 7% gelatin (Sigma-Aldrich) solution. Samples were kept at 37°C and allowed to sink to the bottom of the vial. The samples were transferred and orientated in a metal based

mould underneath a dissecting microscope using pointed dentist tools. Once in position the sucrose/gelatin solution was placed carefully on ice to set. Samples were frozen by holding the metal base of the mould close to the surface of liquid nitrogen. Blocks were stored at -80°C, and allowed to equilibrate for at least a few hours in the chamber of the cryostat (Leica CM1900, Leica Microsystems). Samples were sectioned at 7µm thickness and were stored at -80°C until required.

2.2.3 Immunofluorescence

2.2.3.1 Immunofluorescent staining on Mouse cryosections

Slides containing cryostat sections were thawed at RT°C for 10 minutes. To remove the gelatin, slides were then placed into a coplin staining jar (ThermoFisher) containing preheated PBS and left in a water bath at 50°C. Sections were carefully circled with a PAP pen (Vector) to keep reagents localized on tissue specimens. All steps were conducted by adding small droplets onto outlined sections in a humidified box in the dark at RT°C.

Sections were permeabilised with 0.5% (v/v) Triton-X100 in PBS for at least 15 minutes. Excess fixative was quenched with either 0.5 M Glycine pH7.5 in PBS or 50 mM NH_4Cl (Acros Organics) in PBS for at least 15 minutes. Non-specific antigens were blocked with a blocking buffer, consisting of 5% Donkey serum (v/v) in PBS with 0.1% NaN_3 for at least 1 hour. Primary antibodies (Table 2.3) were diluted in blocking solution according to manufacturers' suggested or optimised concentrations, and added to the sections for at least 1 hour, but more commonly overnight at 4°C. Sections were washed with PBS three times for 5 minutes. Secondary antibodies (Table 2.4) were diluted 1:1000 in blocking solution and added to the sections for 1 hour at RT°C. The sections were then washed with PBS three times for 5 minutes, the last of which contained DAPI (1:1000) (Biotium). Upon completion of staining the slides were mounted using either Prolong® Gold Antifade Reagent (Molecular Probes) or Vectasheild non-hardening medium (Vecta Labs) with a coverslip. Mounted sections were stored at 4°C until imaging.

When use of this protocol did not result in clear and strong fluorescence signal, antigen retrieval was sometimes performed prior to staining. Following 10 minutes of cryosection thawing at room temperature, the slides were placed in a plastic slide

holder and submerged in a plastic lidded box containing 10 mM sodium citrate pH 6.0. Antigen retrieval was performed in a standard microwave for a total of 10 minutes, ensuring the temperature never reached boiling point and topping up with ddH_2O when necessary to ensure constant molarity of solutions. Slides were then cooled before further processing as described above without the need to remove the gelatin.

When two or more primary antibodies raised in different host species were used for multicolour immunofluorescent detection, the primary antibodies would be incubated together. When primary antibodies had the same host species they would be stained sequentially.

Positive controls based on EST gene profile concentrations, and negative controls sections for which the primary antibody incubation was left out were run alongside each immunohistochemistry.

2.2.3.2 Immunofluorescent staining on Mouse wholemount embryos

Following fixation embryos were permeabilised with 0.1% (v/v) Triton™ in PBS for at least 1 hour. Excess fixation was then quenched using 0.5M Glycine pH7.5 in PBS or 50mM NH_4Cl (Acros Organics) in PBS for at least 1 hour at room temperature. Embryos were washed for 15 minutes 3 times with 0.1% (v/v) Triton™ PBS. Embryos were then placed in blocking solution, 5% Donkey serum (v/v) in PBS with 0.1% NaN_3, overnight at 4°C.

Primary antibodies (Table 2.3) diluted in blocking solution were left to incubate at RT°C, unless stated otherwise, on shaker for at least 2 overnights depending on the success of staining. After washing for 15 minutes three times with 0.1% (v/v) Triton™ in PBS, the secondary antibody diluted 1:1000 in blocking solution was added to the embryos again for 2 overnights in the dark at RT°C unless stated otherwise. After washing for 15 minutes three times with 0.1% Triton™ in PBS, if applicable DAPI diluted 1:1000 was incubated for 5 minutes, before performing another wash.

In preparation for imaging with clearing agent, 1 Benzyl Alcohol: 2 Benzyl Benzonate (BABB) (Becker et al., 2013), embryos were serially dehydrated into methanol. First in 50% methanol 50% (v/v) 0.1% Triton™ in PBS for 10 minutes, then 80% methanol

20% (v/v) 0.1% Triton™ in PBS for 10 minutes and finally in 100% methanol which was refreshed once. Embryos were then stored in methanol until imaging. In preparation for imaging embryos were placed individually in a Attoflour ™ Cell Chamber and then BABB solution for clearing was added on top and mixed carefully with a transfer pipette. Following imaging, embryos were placed back in methanol and stored at 4°C if re-imaging was necessary.

When using two or more primary antibodies for multicolour immunofluorescent detection, the antibodies were stained sequentially. Except for the use of T(Bra) antibody (R&D) which was used alongside any other primary antibody.

2.2.3.3 Immunofluorescent staining on cultured cells

Following fixation cells were permeabilised with 0.5% (v/v) Triton™ in PBS for at least 15 minutes at room temperature. Fixative was quenched using either 0.5M Glycine pH7.5 or 50mM NH_4Cl (Acros Organics) for 15 minutes at room temperature. Cells were washed gently 3 times with PBS, before incubating in blocking solution 5% Donkey serum (v/v) in PBS with 0.1% NaN_3 for at least 1 hour.

Primary antibodies were diluted in blocking serum and incubated for 1 hour at RT°C. The cells were then washed three times for 5 minutes in PBS. Secondary antibodies diluted 1:1000, unless stated otherwise, in blocking solution were added to the cell for 1 hour at RT°C in the dark. Cells were washed with PBS for 5 minutes three times, with the final wash containing DAPI 1:1000 (Biotium) if necessary. In some instances, cells only had 2 washes between stages to prevent cell loss.

When two or more primary antibodies raised in different host species were used for multicolour immunofluorescent detection, the primary antibodies would be incubated together. When primary antibodies had the same host species they would be stained sequentially.

2.2.4 Imaging

2.2.4.1 Immunohistochemistry on cryosections

Mounted sections were imaged using an upright fluorescence stereomicroscope, Olympus BX-61 fluorescence compound microscope (Olympus), with an ORCA-R2 monochrome camera (Hamamatsu) driven by Volocity software.

2.2.4.2 Immunohistochemistry on wholemount embryos

Wholemount immunohistochemistry embryos were imaged using Leica SP8 Inverted confocal microscope with LAS X Software (Leica). Images were processed for figures using ImageJ (FIJI).

Images of wholemount embryos from grafting experiments were acquired with digital camera (QimaginG) attached to a Nikon AZ100.

2.2.4.3 Immunohistochemistry on *in vitro* cultured embryos

Cultured cells were imaged using an Olympus IX51 inverted microscope, with Retiga-2000R Fast camera (QImaging). Cells following immunohistochemistry were imaged in the Operetta High-Content Imaging System (Perkin Elmer), using the Harmony Content Analysis Software (Perkin Elmer), linked to Columbus software (Perkin Elmer). Images of 96 well plates were acquired with 10x (whole well acquired) or 20x (quarter well acquired) objectives.

2.2.4.4 Image Analysis

2.2.4.4.1 PickCells/NESSY

- **Conversion of files**

Large embryo image '.TIF' files, greater than 5GB were converted to '.ICS' format, using ImageJ plug-in 'Bio-Format Exporter', before importing to PickCells for analysis. All other *in vitro* files were imported to PickCells as '.TIF' format.

- **Segmentation**

Segmentation of nuclei for PickCells analysis was conducted with Nessy (Nuclear Envelope Segmentation System) Software created by Dr Guillaume Blin (Lowell Lab, University of Edinburgh). All segmentation settings for *in vitro* samples were optimised on reference images containing a high number of overlapping cells which

are the most challenging to segment. For embryo segmentation, regions of interest (NMP regions) were used to optimise settings. Multiple segmentation attempts were performed to optimise settings for all samples. The same segmentation settings were applied to all samples in a single experiment. Specific settings for all stages of segmentation using Nessy are outlined below.

1) Pre-processing

Pre-processing of images was performed to enhance edges of cells to aid their identification and maxima were identified which are the starting points of nuclear outer edge tracing (Table 2.9).

Table 2.9	**Pre-processing Settings PickCells**
***In vitro* samples**	***In vivo* samples**
Scale:2.5 Maxima:2.5	Scale:2 Maxima:2

2) Single z-stack segmentation

Settings were optimised to aid creation of cell edge traces based on the maxima calculated previously. Then for each sample type a classifier was trained by selecting valid and in valid shapes, and applied to the initial cell traces to improve cell recognition (Table 2.10).

Table 2.10	**Single z-slice Segmentation Settings (PickCells)**
***In vitro* samples**	***In vivo* samples**
Search Radius: 3 Delta: 0.1 Min Radius: 12 Max Radius: 36 Shape Selection: tailored classifier	Search Radius: 3 Delta: 0.11 Min Radius: 6 Max Radius: 35 Shape Selection: tailored classifier

3) 2D to final 3D segmentation

2D single z-stack segmentation slices were combined to create a final 3D segmentation result by choosing settings, including expected final 3D volume and overlap of 2D z-stack slices. (Table 2.11).

Table 2.11	**2D to 3D Segmentation Settings (PickCells)**
***In vitro* samples**	***In vivo* samples**
Min Volume: 2500 Max Volume: 25000 Search Radius: 43.2 Min Overlap: 0.7 Allowed Slice Jumps: 2 Split Tolerance: 4 Other: Finalisation & Deletion of Flat structures	Min Volume: 1500 Max Volume: 4750 Search Radius: 25 Min Overlap: 0.75 Allowed Slice Jumps: 2 Split Tolerance: 4 Other: Finalisation & Deletion of Flat structures

4) Editing incorrect segmentation

Despite optimisation of settings some cells remained incorrectly segmented. Common mis-segmentations, including segmentation of gaps between cells, missing cells and oversegmentation, were corrected using NESSY segmentation editor. Note that segmentation of cells at the edge of images in *in vitro* samples was not possible.

5) Centriole Detection

Identification of Centrosomes with PickCells spot detector was conducted using the following settings, Radius - 0.5, Sigma - 0.1 and minimum intensity -50.

2.2.4.4.2 Using Columbus on Operetta acquired images

Acquired images using the Operetta were processed using Columbus Image Data Storage and Analysis system. Optimised segmentation settings are outlined below. Average intensities of Sox2 and T(Bra) were exported for each cell in each well.

Minimum thresholds for T(Bra) and Sox2 positivity were defined for each experiment by judgment of cell negativity.

Table 2.12	**'Replated' Conditions- Columbus Analysis Parameters**
Nuclei Method	C (common threshold: 0.3. Area: 30microns)
Select Populations	Area (>80,<400), DAPI Intensity (>200, <4000), Roundness (>0.5)
Sox2 Positive	>60
T(Bra) Positive	>50

Table 2.13	**'Not Replated' Conditions- Columbus Analysis Parameters**
Nuclei Method	C (common threshold: 0.3. Area: 30microns)
Select Populations	Area (>70,<300), DAPI Intensity (>200, <2000), Roundness (>0.7)
Sox2 Positive	>60
T(Bra) Positive	>50

Table 2.14	**Inducible Cell Line Columbus Analysis Parameters**
Nuclei Method	C (common threshold: 0.4/0.5. Area: 30microns)
Select Populations	Area (>50,<650), DAPI Intensity (>150, <11000), Roundness (>0.7)
Sox2 Positive	>150
T(Bra) Positive	>100

2.2.4.4.3 Using ImageJ on Immunohistochemisry sections

2.2.4.4.3.1 Details of the Rainbow RGB Look up table

ImageJ was used to process images. Look up tables were applied to expression data. Details of LUT 'Rainbow RGB' below.

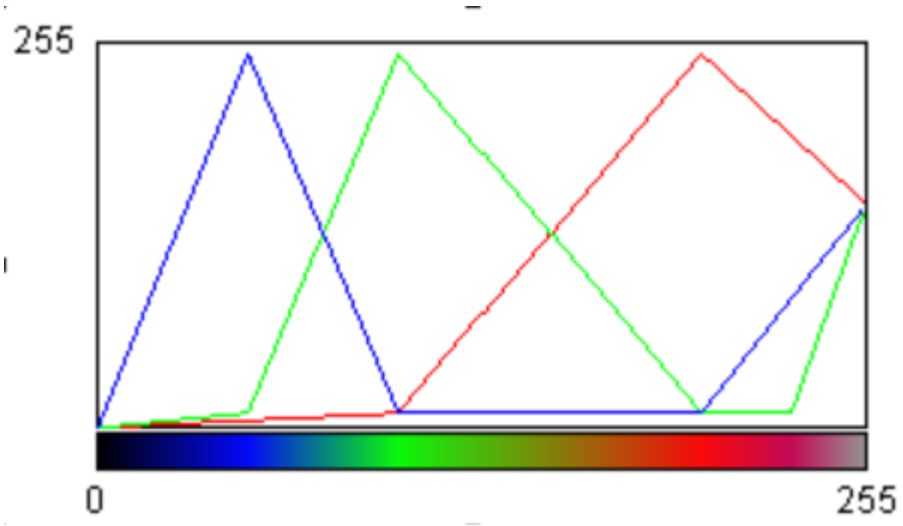

2.2.4.4.3.2 Creating red blood cell autofluorescence overlay

Red blood cell overlay was created by capturing autofluorescence of red blood cells using an unused channel. This was converted to a layer on Inkscape or traced, coloured yellow, and overlaid on corresponding images.

2.2.5 DNA Cloning Methods

2.2.5.1 Restriction Enzyme Digestions

DNA digestions typically were incubation of 1-10µg of DNA with 5-100 units of the appropriate restriction enzymes, in excess, in the appropriate buffers and conditions as recommended by the manufactures. (NEB). Digestions were generally performed for 1 hour, or 2 if sequential enzyme digestion was necessary, followed by 20-minutes of heat inactivation if appropriate. Incubations were performed in a DNA Engine thermal cycler (BioRad) or TProfessional Standard Thermocycler (Biometra).

Table 2.15	Restriction Enzymes Details	
Product	**Vendor**	**Cat #**
EcoRI-HF	NEB	R3101S
XhoI	NEB	R0146S
BamHI	NEB	R0136S
NotI-HF	NEB	R3189S
SmaI	NEB	R0141S
AscI	NEB	R0558S
AgeI -HF	NEB	R3552S
BstBI	NEB	R0519S
KasI	NEB	R0544S

2.2.5.2 Agarose Gels

To generate electrophoretic gels, UltraPure ™ Agarose (Invitrogen) was mixed with TBE and heated with a microwave until the agarose powder was fully melted. The solution was allowed to cool but not solidify, and SYBR® Safe DNA Gel Stain (Invitrogen) was added at 1:1000 dilution to allow the visualisation of nucleic acids. The solution was mixed, and poured into a gel mould and allowed to set at RT°C. The concentration of agarose mixed with TBE varied from 1-2% (weight/volume) depending on the size of the DNA fragment to be visualised.

2.2.5.3 Gel Electroporesis

The samples to be analysed were mixed with DNA loading dye (dye added at 1:6 dilution), loaded into a well of the prepared electrophoresis gel submerged in TBE, and subject to electrophoresis at 70V-100V for 30-90 minutes, depending on the size of the DNA to be visualised. A DNA ladder was loaded next to the samples for size comparison, 1kb DNA ladder or 100bp DNA Ladder (NEB). After completion of the run, the gel was imaged under an ultraviolet transilluminator (G:BOX F3, Syngene) to verify the correct size of the DNA fragment.

2.2.5.4 DNA purification

2.2.5.4.1 Using gel purification kits

When DNA was separated in agarose gels by electrophoresis (2.2.5.3), a gel slice containing the desired band was excised using a clean scalpel on a Blue Light Transilluminator (Syngene) and transferred to an Eppendorf tube. The excised band was then purified using QIAquick Gel Extraction Kit (Qiagen) following manufacturer's instructions. Note that some PCR product for use in cloning were also purified usingQIAquick Gel Extraction Kit (Qiagen) without gel electrophoresis following manufacturers guidelines. PCR products for further use in in situ probe production were purified using DNA Clean & Concentrator ™ columns (Zymo Research Corp).

2.2.5.4.2 Using ethanol precipitation

Ethanol precipitation was also used to purify DNA further. Briefly 0.1volume 3M sodium acetate/H_2O pH5.2 solution to 1 volume of DNA sample was added with 2x volumes of -20°C 100% ethanol. This was vortexed for 10 seconds, and placed in -20°c for 1 hour. DNA was pelleted by centrifuging at 14,000 g for 30 minutes at RT°C. Supernatent was removed and pellet was washed and centrifuged with 200µl of fresh 70% ethanol/H_2O solution at 4°C. Purified DNA was obtained by air drying the pellet and resuspended in appropriate volume DNase/RNase free H_2O (Gibco).

2.2.5.5 Quantification of DNA concentration

The concentration of DNA in solution was measured using a NanoVue Plus Spectophotometer (GE Healthcare) or Nanodrop, ND-1000 (ThermoFisherScientific) according to the manufacturer's instructions.

2.2.5.6 Dephosphorylation of linear DNA ends

rApid Alkaline Phosphatase (Roche, Sigma Alrich) was used according to manufacturer's instructions to prevent self-ligation of DNA fragments by removing the 5' phosphoryl termini and thus reduce vector background in ligase reactions. Briefly linear DNA was incubated with 1xrAPid Alkaline Phosphotase (Table 2.16) for 10 minutes at 37°C, then the enzyme was heat inactivated by incubating at 75°C for 2 minutes.

Table 2.16	Alkaline Phosphatase Reaction
Reagent	**Amount**
Linearised DNA	up to 1µg
Buffer	2µl
Alkaline Phosphatase	1µl

2.2.5.7 Generating Wnt/PCP plasmids using DNA fragment ligation

Pk1 plasmid sequence was generated based on *Mus musculus* prickle planar cell polarity protein 1 sequence (NM_001033217.4 -NCBI), chosen due to homology to *Pk1* sequence previously used to disrupt Wnt/PCP signalling in *Axolotl* neural regeneration (Albors et al., 2015). *Vangl2* plasmid sequence was generated based on NM_033509.4 sequence (NCBI). Wildtype *Ptk7* sequence was generated based on *Mus musculus* protein tyrosine kinase 7 sequence (NM_175168.4 -NCBI).

Plasmids were created by subcloning amplified inserts into backbones using either Gibson assembly (Gibson, 2011) (*Ptk7* & *Vangl2*) or conventional cloning (*Pk1*). For Gibson Assembly subcloning, gene inserts were created by designing gene specific primers to predicted sequences on NCBI database, and amplifying sequences from plasmids (Ptk7 based constructs) or embryonic cDNA (*Pk1* and *Vangl2* constructs).

T2A fragments, encoding a 'self-cleaving' 2A peptide (Kim et al., 2011), were made either by amplification from plasmid, or by annealing of primer pairs. These peptides are thought to 'self-cleave' through the action of ribosome skipping during the synthesis of a peptide bond close to its C-terminus (Kim et al., 2011). These inserts were subcloned in to a backbone containing CAG and RFP. Overall efficiency of Gibson Assembly was low, but successful for generation of *Ptk7* and *Vangl2* constructs. Despite further optimisation including, purification of insert, adjustment of ligation ratios, and de-phosphorylation of the backbone, ultimately attempts to create a CAG-Pk1-T2A-RFP plasmid using Gibson Assembly were unsuccessful. Instead this plasmid was created using conventional cloning techniques, through a 4-way ligation of amplified inserts and a CAG backbone.

2.2.5.7.1 Using Gibson Assembly

2.2.5.7.1.1 Home-made Gibson assembly mastermix

Mastermix (Table 2.17) was prepared on ice, 10µl aliquots were made and stored at -20°C.

Table 2.17	**Gibson Assembly master mix**	
Reagent	**Volume (2x)**	**Final conc (1x)**
1M Tris-HCl	40µl	100mM
1M $MgCl_2$	4µl	10mM
dNTPs (100mM)	3.1µl	0.2mM each
Phusion DNA polymerase (2U/µl)	5µl	0.5U/reaction (25U/ml)
5' T5 exonuclease (10U/µl)	0.32µl	0.16 U/reaction (8U/ml)
dH_2O	147.48µl	

2.2.5.7.1.2 Creating fragments for Gibson assembly

Fragments were designed and created for use in Gibson assembly based on the NEB Gibson Assembly ® cloning kit instruction manual. Briefly primers were designed to amplify fragments with appropriate overlaps. These primers were used with PFX Platinum or high-fidelity Q5 polymerase (as described below) in PCR reactions to create all fragments needed. Note that fragments that were too small to amplify by PCR were created by annealing primers by heating primer mix to 95°c and allowing to cool. Backbone was also cut with appropriate restriction digestion enzymes. All fragments and backbone were gel purified.

Note that RFP originates from commercially available ptagRFP-N (Evrogen).

Table 2.18	**Fragment Amplification and Backbone Restriction for TetO-Ptk7-T2A-GFP**		
Plasmid	**Insert**	**Forward Primer**	**Reverse Primer**
TetO-Ptk7-T2A-GFP	1-Kosak-Ptk7 (plasmid)	ATCCAGCCTCCGGGCCGGCCGGCGCGCCACGCCACCATGGGAGCCCGCCCGCTG	ACCACCAGATTGAAAATACAAATTTTCACCCTGCTTGCTGTCTGCAGGGCTG
	2- GFP (plasmid)	GGTGAAAATTTGTATTTTCAATCTGGTGGTGGCTCCGGAGAGGGCAGAGG	GAATTCGATATCAAGCTTATCGAGCTTACTTGTACAGCTCGTCCATGCCGAG
		Name	**Restriction Digestion Enzyme**
	Backbone	PGK -TetO-	AscI

Table 2.19	**Fragment Amplification and Backbone Restriction Digest for CAG-Ptk-T2A-RFP**		
Plasmid	**Insert**	**Forward Primer**	**Reverse Primer**
CAG-Ptk7-T2A-RFP	1-Kosak-Ptk7 (TetO-Ptk7-GFP plasmid) 3299bp	CGGTACCGCGGGCCCGGGCCGGCCGGCGCCACGCCACCA	CGACCGGTGGATCCCGTGGGCCAGGATTCTCCTCGACGTC
		Name	**Restriction Digestion Enzyme**
	Backbone	CAG-RFP	SmaI

Table 2.20	**Fragment Amplification and Backbone Restriction Digest for CAG-Ptk7ΔICM-T2A-RFP**		
Plasmid	**Insert**	**Forward Primer**	**Reverse Primer**

CAG-Ptk7ΔICM-T2A-RFP	1- Ptk7 (plasmid) 2084bp	CGGTACCGCGGGCCCGGGCCGGCCGGCGCCACGCCACCA	ATACAAATTTTCACCCTGGATCATCTTGTATGGGGGAGGG
	2- t2a (plasmid) 124bp	TACAAGATGATCCAGGGTGAAAATTTGTATTTTCAATCTG	CGACCGGTGGATCCCGTGGGCCAGGATTCTCCTCGACGTC
		Name	**Restriction Digestion Enzyme**
	Backbone	CAG-RFP	SmaI

Table 2.21	**Fragment Amplification and Backbone Restriction Digest for CAG-sPtk7-T2A-RFP**		
Plasmid	**Insert**	**Forward Primer**	**Reverse Primer**
CAG-sPtk7-T2A-RFP	1- Kosak ATG (primer annealing) 40bp	GATCCAGCCTCCGGGCCGGCCGGCGCCACGCCACCATGGGAGCCCGCCCGCTG	CAGCGGGCGGGCTCCCATGGTGGCGTGGCGCGCCGGCCGGCCCGGAGGCTGGATC
	2- Ptk7 (plasmid) 600bp	GCCACGCCACCATGGAAAAACTCAAGTTCACGCCACCAC C	ATACAAATTTTCACCCTGGATCATCTTGTATGGGGGAGGG
	3- t2a (plasmid) 124bp	TACAAGATGATCCAGGGTGAAAATTTGTATTTTCAATCTG	CGACCGGTGGATCCCGTGGGCCAGGATTCTCCTCGACGTC
		Name	**Restriction Digestion Enzyme**
	Backbone	CAG-RFP	SmaI

Table 2.22	Fragment Amplification and Backbone Restriction for CAG-Vangl2-T2A-RFP		
Plasmid	**Insert**	**Forward Primer**	**Reverse Primer**
CAG-Vangl2-T2A-RFP	1- Kosak-Vangl2 (plasmid) 1586bp	AATTCCTCGAGCTCAAGCTTGCCGCCACCATGGACACCGAGTCCCAGTACTCGG	CCTCTGCCCTCTCCGGAGCCCACAGAGGTCTCCGACTGCAGCCGC
	2- t2a (primer annealing) 103bps	TGCAGTCGGAGACCTCTGTGGGCTCCGGAGAGGGCAGAGGAAGTCTGCTAACATGCGGTGACGTCGAGGAGAATCCTGGCCCAGTCGCCACCATGGTGTCTAAG	CTTAGACACCATGGTGGCGACTGGGCCAGGATTCTCCTCGACGTCACCGCATGTTAGCAGACTTCCTCTGCCCTCTCCGGAGCCCACAGAGGTCTCCGACTGCA
		Name	**Restriction Digestion Enzyme**
	Backbone	CAG-RFP	BstBI, AgeI

2.2.5.7.1.3 Gibson assembly protocol

Mastermix described above was defrosted on ice, and components added to the mix (Table 2.23). This reaction was incubated for 50°C for at least 15 minutes up to maximum of 60 minutes if 2 or more fragments were to be inserted. 2µl of reaction was then transformed in bacteria. The remainder was stored at -20°C to be transformed in future if needed. Control reactions containing backbone only were also carried out and transformed to check for self-ligation of the backbone.

Table 2.23	Gibson Assembly Reaction
Reagent	**Volume/Concentration**
Mastermix	10µl (x1)
Backbone	50ng

Insert fragment(s)	1:3, 1:5 molar ratio (vector:insert) (50-250ng)
Water	up to10µl

2.2.5.7.2 Using Conventional cloning and T4 ligase

2.2.5.7.2.1 Designing primers to create fragments for conventional cloning

Conventional cloning was used to create CAG-Pk1-RFP. For this, primers were designed to amplify fragments with appropriate restriction sites at their ends. Fragments were created using High Fidelity Q5 Polymerase. They then underwent digestion with fragment specific restriction enzyme (Table 2.24), gel purified and then used in T4 ligase reaction as described below Table 2.25.

Table 2.24	**Fragment Amplification and Backbone Restriction for CAG-Pk1-T2A-RFP**				
Plasmid	**Insert**	**Forward Primer**		**Reverse Primer**	
		Sequence	Restriction site	Sequence	Restriction site
CAG-Pk1-T2A-RFP	Kosak-Prickle	CTAGCTCGAGGCCGCCACCATGCCTTTGGAGATGGAACC	XhoI	CTGCTCCACTCTGGCTTTC	EcoRI
	Prickle-T2A	GAGCAGGTTTCGCTAACGAG	EcoRI	CATGGGCGCCTGGGCCAGGATTCTCCTCGACGTCACCGCATGTTAGCAGACTTCCTCTGCCCTCTCCGGAGCCAGAAATGATACAGTTTTTGC	KasI
	RFP	CTAGGGCGCCATGGTGTCTAAG	KasI	CATGGCGGCCGCTCAATTAAGTTTGTGCCCCA	NotI

		GGCGAAGA			
		Name	**Restriction Digestion Enzyme**		
	Backbone	CAG	XhoI & NotI		

2.2.5.7.2.2 Ligation of conventional cloning fragments using T4 Ligase

Linear fragments created using conventional cloning techniques were ligated using T4 ligase (NEB) according to manufacturer's instructions Briefly, a 20µl reaction was carried out (Table 2.25) and left at 16°C overnight. Both 1:3 and 1:5 vector to insert molar ratio was used. The reaction was then heat inactivated by incubating for 10 minutes at 65°C.

Table 2.25	**T4 DNA Ligase Reaction**
Component	**Amount**
T4 Ligase Buffer (x10)	2µl
Vector DNA	40 – 75ng
Insert DNA(s)	1:3, 1:5 molar ratio (vector:insert)
Nuclease-free water	up to 20µl
T4 Ligase	1µl

2.2.5.7.3 Preparation of gene specific p2lox plasmids

To generate Wnt/PCP specific inducible cell lines, A2lox.Cre ES cells needed to be targeted via nucleofection with gene specific p2Lox plasmids (Iacovino et al., 2011, 2014). To generate Wnt/PCP p2lox plasmids, the Wnt/PCP genes of interest (GOI) were subcloned into a p2Lox plasmid. P2lox plasmids and Wnt/PCP plasmids (Fig. 2.1), underwent double digestion with either EcoRI (*Ptk7* inserts) or XhoI and NotI (*Pk1* and *Vangl2*). This allowed the excision of excess EGFP from the p2Lox plasmid,

and creation of gene of interest (GOI)-T2A-RFP insert from the Wnt/PCP plasmids. These pieces underwent gel electrophoresis and subsequent gel extraction and purification of the correct DNA fragments. P2lox plasmid backbone, and individual GOI fragments were ligated with T4 ligase. Correct ligation was confirmed by restriction digest and sequencing using forward and reverse primers. Note that RFP alone plasmid was cloned by Matt Malaguti (Lowell Lab, MRC Centre for Regenerative Medicine).

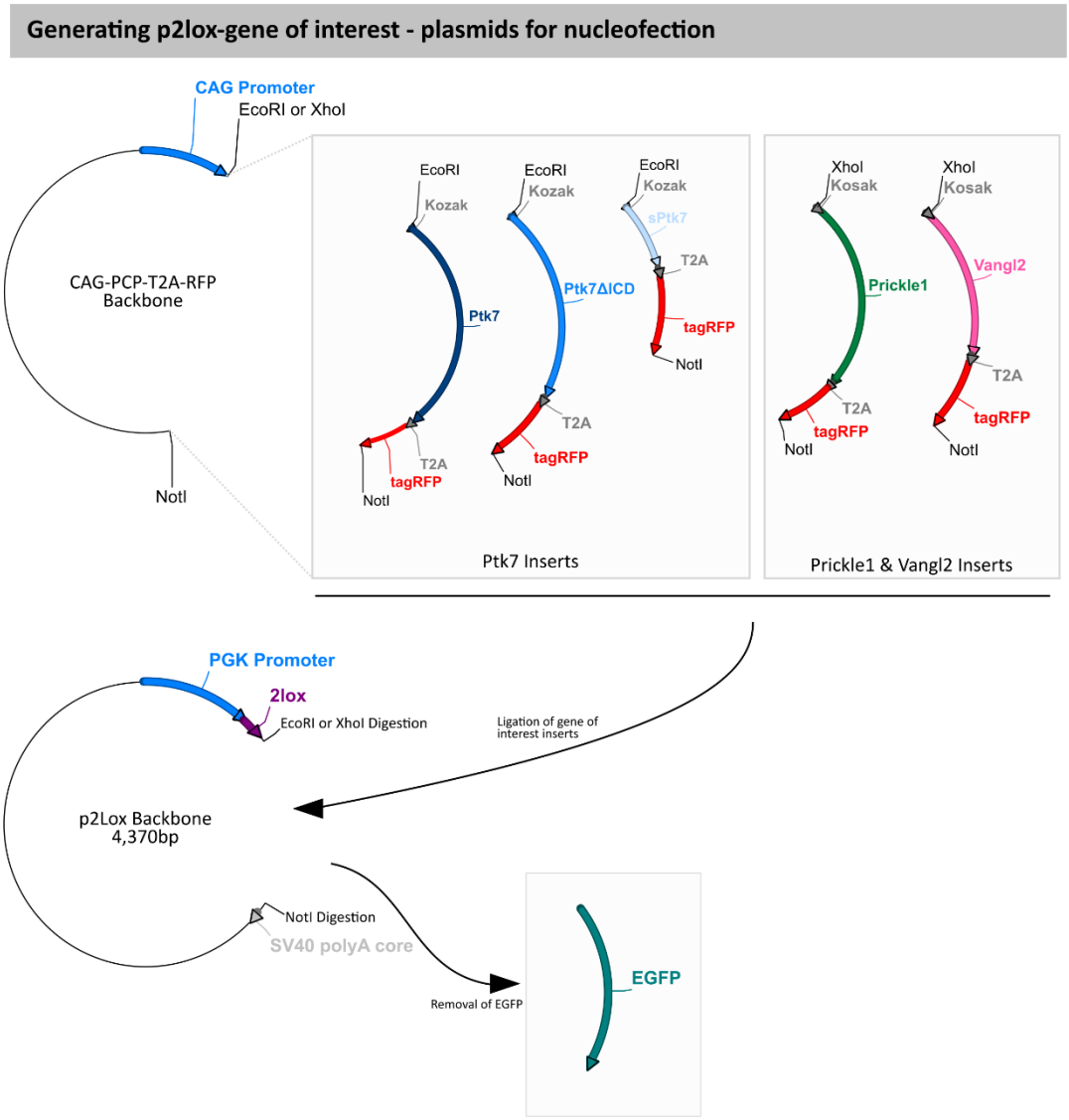

Figure 2.1 - Conversion of electroporation plasmids to generate p2lox inducible cell line plasmids. Wnt/PCP inducible cell lines were created by generating p2lox plasmids specific for each Wnt/PCP component. Wnt/PCP plasmids created for electroporation experiments (2.2.5.7), and p2lox backbone were digested with either EcoRI or XhoI and NotI, then underwent ligation to create final p2lox.Wnt/PCP plasmids for use in nucleofection to create Wnt/PCP cells lines.

2.2.5.8 pCR™-BluntII-TOPO plasmid

DNA fragments were ligated to pCR™-bluntII-TOPO vector using Zero Blunt ™ PCR cloning kit (Invitrogen) according to manufacturer's instructions. Briefly 4µl of purified PCR products were incubated with 1µl salt solution and 1µl pCR™-bluntII-TOPO vector for 30 minutes at RT°C. The solution was then plated with the addition of 10µl of Xgal on Kanamycin selection agar plates.

2.2.5.9 Preparation of selective bacterial plates

LB-agar was prepared by the Wash Staff at the MRC CRM, by dissolving 1.5% Bacto™ Agar (BD) in LB. LB-agar was melted by microwaving the mixture and allowing it to cool but not set. The appropriate antibiotic was added at 1:100 dilution, and approximately 10mls of the mixture were poured into 90mm standard Petri Dishes (Sterilin). The LB-agar was left to solidify at RT°C before use. Plates were stored at 4 °C for no longer than 2 weeks.

Ampicillin 1000x stocks were prepared by dissolving 100mg ampicillin powder (Calbiochem) in 1ml DNase/RNase-free water (Gibco) and filtering the solution through a 0.22µm filter (Millipore). Kanamycin 1000X stocks were prepared by dissolving 50mg kanamycin powder (Calbiochem) in 1ml DNase/RNase-free water (Gibco) and filtering the solution through a 0.22µm filter (Millipore). Antibiotic stock aliquots were kept at -20°C, and upon thawing an aliquot was kept at 4°C for no longer than 3 weeks.

2.2.5.10 Preparation of chemically competent bacteria

A 3ml overnight culture was diluted into 200 ml of LB medium and incubated at 37°C with rotation at 180rpm until its optical density at a wavelength of 600nm $(OD)_{600}$ reached 0.6 absorption units. The bacteria were collected in 50ml sterile falcon tubes and centrifuged for 10 minutes at 4300rpm at 4°C. The pellet was re-suspended at 25mls of ice cold 0.1M $CaCl_2$, incubated for 25 minutes on ice and centrifuged as described above. The pellet was resuspended in 10ml of ice cold 0.1M $CaCl_2$ and kept at 4°C overnight without rotation. 2ml of 80% glycerol were added and mixed gently with the bacterial solution, which was then divided into 200µl aliquots, snap frozen in liquid nitrogen and stored at -80°C.

2.2.5.11 Plasmid transformation into DH5α bacteria

Plasmids were transformed into chemically competent DH5α *Escherichia coli (*Invitrogen) according to the manufacturer's instructions. Fewer than 200ng of DNA, in a solution of 10µl or less, were added to an Eppendorf containing 50µl of DH5α bacteria thawed on ice, and gently mixed. The mixture was incubated on ice for 20 minutes before being heated to 42°C for 50 seconds in a water bath, then placed on ice for a further minute. 100µl liquid LB was added to each reaction, and incubated at 37°C in a thermoshaker for at least 45 minutes. The mixture was then plated on to selective preheated LB plates overnight at 37°C.

2.2.5.12 Plasmid purification from bacteria

To purify plasmid DNA from bacteria, clones of transformed bacteria were picked and inoculated in 5ml of LB medium supplemented with relevant antibiotic drug selection using 14ml Round Bottom Snap Cap tubes (Falcon). Bacteria were cultured in an incubated shaker (Incu-Shaker, Benchmark Scientific) set a 37°C/ 200rpm overnight. Bacterial cells propagating the plasmid DNA of interest were collected by centrifugation of the culture at 13000rpm for 10 minutes. Plasmid DNA was purified from the pellet using QIAprep Spin Miniprep Kit (Qiagen) or Qiagen Plasmid Maxi Kit (Qiagen).

Quantity and purity of the purified DNA were determined and diagnostic restriction digestion and subsequent sequencing was performed.

2.2.5.13 Plasmid sequencing

Sequencing of plasmids was performed by GenePool service at the University of Edinburgh, making use of the BigDye ® Terminator Cycle Sequencing technology (Invitrogen). 6µl solution samples sent to the service consisted of 300-500ng plasmid DNA and 1µl of 3.2µM primer solution. Sequencing reads were analysed using ApE software. SNPs were checked using online databases.

2.2.5.14 Polymerase Chain Reaction (PCR)

2.2.5.14.1 Platinum™ PFX PCR

Platinum ™ PFX DNA Polymerase (ThermoFisher) was used to amplify DNA when high fidelity of amplification was needed. PCR using PFX was performed according to manufacturer's instructions, reaction as follows,

Table 2.26	**PFX Reaction**	
Reagent	**Volume**	**Final Concentration**
10x PFX amplification buffer	5µl	1x
50mM $MgSO_4$	0.5 – 2µl	0.5 -2mM
dNTP mix (10mM each)	1.5µl	300µM each
Forward Primer (10µM)	1.5µl	300nM
Reverse Primer (10µM)	1.5µl	300nM
Platinum ® Pfx DNA Polymerase	0.4µl	1unit/reaction
10x PCR_x Enhancer Solution (for optimisation)	0-15µl	Variable depending on optimisation
Autoclaved, distilled water	To 50µl	Variable

Note that in cases where amplification was poor, 10x PCR_x Enhancer Solution was used to enhance amplification.

Thermal cycling was performed using a DNA Engine thermal cycler (BioRad) or TProfessional Standard Thermocycler (Biometra). The cycle conditions were,

Table 2.27	**Thermocycling PFX**		
Step	**Temperature**	**Duration (mins:sec)**	**Repeats**
Initial Denaturation	94°C	05:00	
Denaturation	94°C	00:15	<34 cycles

Annealing	57-72°C	00:30	
Extension	68°C	00:30+ (1:00 per kb)	
Final Extension	68°C	5:00	

Annealing temperatures were based on manufacturers' instructions and optimisation using NEB Tm Calculator online resource.

2.2.5.14.2 Q5 PCR

Thermal cycling was performed using Q5® High-Fidelity DNA Polymerase (NEB) in cases where PFX did not amplify the sequence efficiently due to limited primer within Gibson assembly protocols.

PCR using Q5 was performed according to manufacturer's instructions, reaction as follows,

Table 2.28	**Q5 Reaction**	
Component	**Volume**	**Final Concentration**
5x Q5 Reaction Buffer	10µl	1x
10mM dNTPs	1µl	200µM
10µM Forward Primer	2.5µl	0.5µM
10µM Reverse Primer	2.5µl	0.5µM
Template DNA	Variable	<1000ng
Q5 High-Fidelity DNA Polymerase	0.5µl	0.02U/µl
5x Q5 High GC Enhancer (for optimisation)	0-10µl	Variable
Nuclease-Free Water	Up to 50µl	Variable

Note that in cases where amplification was poor and contained GC-rich targets (>65%), 5x Q5 High GC Enhancer Solution was used to optimise melting temperature (Tm) and improve specificity and/or yield of Q5 reactions.

Thermal cycling was performed using a DNA Engine thermal cycler (BioRad) or TProfessional Standard Thermocycler (Biometra). The cycle conditions were,

Table 2.29	**Thermocycling for Q5 Reactions**		
Step	**Temperature**	**Duration (mins:sec)**	**Repeats**
Initial Denaturation	98°C	00:30	
Denaturation	98°C	00:10	> x34
Annealing	58-72°C	00:30	
Extension	72°C	00:30 per kb	
Final Extension	72°C	02:00	

2.2.5.14.3 Quantitative real time PCR (qRT-PCR)

Quantitative real-time PCR was performed using the Roche LightCycler ® 480 Real-Time PCR System, alongside the Universal ProbeLibrary (UPL) system, in which short nucleic acid probe coupled to a fluorophore and a quencher that specifically binds the DNA region to be amplified. Primers were tested on a cDNA sample and verifying the presence of a single amplicon on an electrophoretic gel. Serial dilution was run beside analysed samples. These serial dilutions consisted of diluted amplified amplicon or diluted cDNA samples. qRT-PCR experiments were carried out in 384-well plates, using an 8µl reaction volume. This consisted of 4µl (1x) LightCycler ® 480 Probes Master, 1.2µl of Water, 0.36µl of forward and reverse primers (10µM, 450nM final), 0.08µl UPL probe (100nM final), and 2µl template cDNA. Cycling conditions according to manufactures instructions (45 cycles).

To normalise expression values for each gene of interest for each biological sample, the average expression value of the gene of interest in 3 replicate reactions was divided by the average expression value of house-keeping genes (geomean of TBP and SDHA). Error bars were created by calculating the standard error of the mean between normalised replicates. All sample levels shown relative to 2i/LIF samples.

2.2.6 RNA Methods

2.2.6.1 Total RNA isolation

Total RNA was extracted from cultured cells using the Absolutely RNA Miniprep Kit (Agilent Technologies), following manufacturer's instructions. The concentration of the isolated RNA was measure using NanoVue Plus Spectrophotometer (GE Healthcare) or Nanodrop (ThermoScientific).

2.2.6.2 cDNA synthesis

First-strand cDNA synthesis was performed using M-MLV Reverse Transcriptase (Invitrogen) following manufacturer's instructions. To digest the RNA template, 1µl (5U) RNase H (NEB), which specifically hydrolyses RNA which is hybridised to DNA was used according to manufacturer's instructions. All samples were generated from the same predicted concentraton of RNA, and were diluted separately in the same volume water

2.2.6.3 In situ hybridisation on whole mount embryos

In situs were performed by Catarina Martins Costa and Filip Wymeersch.

In situ hybridisation for Pk1 were conducted as described in (Cambray and Wilson, 2007). Briefly to produce probes, gene specific primers for Pk1 NM_001028389 from (Okuda et al., 2007) were dissolved to 100µM and used in 50µl PCR reaction with Q5 polymerase to pick up the amplicon from a pool of cDNA, prepared from RNA isolated from different embryonic Mouse tissues. The choice of cDNA was made on the relative abundance of the transcript in various tissues, reported in online databases (Unigene, NCBI).

A small proportion of the PCR sample was electrophoresed on an agarose gel to check the presence of the amplicon. The remaining PCR sample was cleaned up using DNA Clean & Concentrator ™ columns (Zymo Research Corp), eluted and concentrated

into 6µl ddH_2O. The concentration was quantified and maximum volume 3µl was used to clone the amplicon into pCR®II-TOPO® (Invitrogen), transformed in DH5α bacterial cells and plated on Kanamycin selection plates. Bacterial clones were picked and screened for the incorporation of the amplicon by extracting DNA and performing a diagnostic enzymatic digestion. The sequence and orientation of the amplicon was checked by DNA sequencing using M13 (-20) Forward and M13 Reverse (Invitrogen) sequencing primers.

2.2.7 Cell Culture

2.2.7.1 Cell lines

2.2.7.1.2 Wild-type embryonic stem cell lines

E14JU09 ES cells are a clonal line derived by the Transgenic Unit in our Institute from ES cells obtained from chimeric embryos generated with E14tg2a ES cells. They have a 129/Ola genetic background and are hypoxanthine phosphoribosyl transferase deficient. They have a high propensity for germline colonisation (observation made by the Transgenic Unit staff).

2.2.7.1.3 Transgenic lines

Ubiquitously expressing GFP cells used for grafting were, C2 (Guo et al., 2009) and A-EGFP (Gilchrist et al., 2003). A2.Lox cells used to make Wnt/PCP inducible cell lines were donated from Lesley Foresters (MRC Centre for Regenerative Medicine) which originated from (Iacovino et al., 2011, 2014).

2.2.7.2 Incubation

All cultures were incubated 37°C with 5% CO_2. Cell lines were routinely checked for mycroplasma by PCR analysis (performed by Tissue Culture Staff). A Fastread haemocytometer (Kisker Biotech) was used to count cell numbers when required.

2.2.7.3 LIF/FCS Culture

Composition of undefined ES cell culture media hereinafter termed LIF/FCS are outlined in Table 2.30.

Table 2.30	LIF/FCS Media Composition		
Component	**Volume**	**Components/Stock Concentration**	**Final Concentration**
Glasgow Minimum Essential Medium (GMEM, Sigma)	500mls		
Foetal Calf Serum (FCS, Gibco)	51ml		10%
L-Glutamine/ pyruvate solution	11ml	5.5ml- 100mM sodium pyruvate (Invitrogen) 5.5ml – 200mM L-glutamine (Invitrogen)	Sodium pyruvate 1mM L-Glutamine 2mM
Non-Essential Amino Acids (NEAA, Gibco)	5.5mls		1x
0.1M 2-mecaptoethanol	1.1ml		
LIF supplement (TC facility)	570µl	100,000U/ml (1000x)	100U/ml (1x)

Cells passaged in LIF/FCS were passaged when they reached approximately 80% confluency. To passage ES cells cultured in LIF/FCS, 9cm treated cell culture dishes were coated with 0.1% (w/v) gelatine (Sigma) in PBS for 15 minutes prior to cell passaging. The medium was aspirated from the cells, and the cells were washed twice with sterile PBS (Sigma). 0.05% solution of trypsin EDTA (1:5 dilution of 0.25% Trypsin EDTA, Gibco in PBS) was added to the culture, and moved to 37°C until cell detachment (usually 2 minutes). 10 volumes of LIF/FCS was then added to the cells to quench the trypsin EDTA. The cells were broken by pipetting up and down, transferred to universal tube(Sterilin) and spun at 300g for 3 minutes. The medium was aspirated and the cell re-suspended in fresh LIF/FCS medium and plated at the desired density on the prepared gelatinised dish, after aspiration of the gelatine solution. Cells were split between 1:8 and 1:15 at each passage depending on the cell line.

2.2.7.4 Culturing ESCs on irradiated MEFs in LIF/FCS

Donated MEFs were isolated and irradiated by Dr Aida Costa (Lowell Lab). The day before ES cells were to be added MEFs were defrosted and re-suspended in LIF/FCS media and plated on untreated 10cm tissue culture plates. The following day media was aspirated before ESC cells were added on top suspended in LIF/FCS media. Media was changed everyday, and cells passaged when cells became confluent.

2.2.7.5 N2B27 Medium

Components of chemically defined medium hereinafter termed N2B27 are outlined in Table 2.31.

Table 2.31	**N2B27 Media Composition**
Component	**Volume**
DMEM/F12 (Gibco)	25ml
Neurobasal (Gibco)	25ml
L-Glutamine (Invitrogen)	500µl
2 -mercaptoethanol	100µl
Non Essential Amino Acids (NEAAs)(Invitrogen)	500µl
N2 (Gibco)	250µl
B27 (Gibco)	500µl

2.2.7.6 2i/LIF Culture

The composition 2i/LIF culture media is similar to the composition of N2B27 as described above except for the exclusion of NEAA, and with addition of 2 inhibitors, 1µM PD0325901 (Axon) and 3µM CHIR99021 (Axon), and 100U/ml LIF (Table 2.32). This media is herein termed 2i/LIF.

Table 2.32	2i/LIF Media Composition

Component	Volume
DMEM/F12 (Gibco)	25ml
Neurobasal (Gibco)	25ml
L-Glutamine (Invitrogen)	500µl
2 -mercaptoethanol	100µl
N2 (Gibco)	250µl
B27 (Gibco)	500µl
LIF	50µl
PD0325901/PD03 (Axon)	5µl
CHIR99021/CHIR (Axon)	15µl

To passage ES cells cultured in 2i/LIF, plates were coated in poly-L-ornithine (Sigma) (re-used) for at least 2 hours at 4°C. The poly-L-ornithine coating was removed and replaced with 5µg/ml laminin (Sigma) (v/v) in PBS for at least 2 hours at 4°C. The medium was aspirated from the cells, the cells washed with sterile PBS (Sigma) and Accutase (Sigma) was added to the cells. Cells were incubated in accutase at 37°C for no longer than 2 minutes, then this was quenched with 5 volumes of 2i/LIF media. Cells were detached by pipetting up and down until the majority of cells were detached, and then transferred to a universal (Sterilin) and pelleted at 400g for 3 minutes. The medium was aspirated and the cells re-suspended in fresh 2i/LIF medium and plated at the desired density on the prepared poly/laminin coated plates, after aspiration of the laminin solution. Generally, cells cultured in 2i/LIF were seeded at a density of 100,000 cells/cm^2 and passaged after 3 days or at a density of 50,000 cells/cm^2 and passaged after 4 days, and routinely plated on 6 well plates.

2.2.7.7 EpiSC Culture

The composition of EpiSC culture media, herein termed N2B27/Activin/FGF is the same as the composition of N2B27 as described above except that it is supplemented with fresh,

- 20ng/ml (final) –Recombinant human/rat/Mouse activin A (Peprotech)
- 10ng/ml (final) –Recombinant human Fgf Basic (R&D systems)

To passage EpiSC, plates were coated with 7.5µg/ml bovine fibronectin (Sigma-Aldrich) and were left at RT°C for at least 5 minutes. EpiSCs were passaged when they reached 60-80% confluency. Medium was aspirated from the cells, the cells washed with sterile PBS (Sigma) and 200µl of accutase (Sigma) was added. Cells were incubated at 37°C for about 1 minute, and then tapped carefully against the bench in order to detach and break cells into small clumps of about 4-8 cells. Accutase was quenched through the addition of un-supplemented N2B27 media. The desired density was then transferred to a universal (Sterilin) containing more N2B27 media. Cells were then pelleted through centrifugation at 300g for 3 minutes, the excess media aspirated and the cell re-suspended in Activin/FGF/N2B27, and plated on to the prepared fibronectin covered plates after aspiration of the fibronectin solution. EpiSC were routinely passaged in 6well plates at a density of 1:8 to 1:15 every other day depending on the cell line.

2.2.7.8 Cryopreservation

2.2.7.8.1 Cell Freezing

To cryopreserve cells, they were subject to trypsinisation/accutase treatment and pelleting following standard passaging routines described above. Once the supernatant was aspirated off, the cells were re-suspended in FCS+10% dimethylsulphoxide (DMSO) for FCS based cultures, or in knockout serum replacement (KSR)(Gibco) +10% DMSO. 1ml of FCS/KSR +DMSO solution was used for each aliquot frozen (usually cells from a single 6 well plate well per aliquot). The resuspended cell solution was then aliquoted to a cryovial and immediately placed on dry ice. These were then transferred to -80°C for short-term storage or to liquid nitrogen tanks for long-term storage.

2.2.7.8.2 Cell Defrosting

To defrost cells, prewarmed media appropriate to cell type was placed into a universal. The frozen aliquot of cells was thawed in a water bath at 37°C and immediately added to the aliquoted media. Cells were then pelleted and supernatant aspirated. The cells were re-suspended in the appropriate culture medium and plated on to pre-coated plates.

2.7.7.9 Flow Cytometry

2.7.7.9.1 Sample preparation

Cell samples were prepared for flow cytometry by generating single-cell suspensions with standard passaging methods and following pelleting, the cells were re-suspended in a FACS buffer consisting of 4-10% FCS (v/v) in PBS. Cells were passed through a cell strainer into a 5ml tube (Falcon) and kept on ice. To distinguish live and dead cells, final concentration of 0.1µg/ml DAPI (Molecular probes) was added to each sample (dead cells being positive for DAPI). Flow analysis was performed on the LSR Fortessa (BD). The lasers used to excite each fluorophore, and the optical filters used to detect emissions are shown in Table 2.33.

Table 2.33	**Excitation and Emission Wavelengths of Fluorophores**	
Fluorophore	**Laser**	**Optical Filter (Fortessa)**
GFP	488nm	B525/50
RFP	561nm	YG582/15
DAPi	405nm	V450/50

2.7.7.9.2 Sample analysis

Flow cytometry experiments were performed as recommended by the manufacturers equipment. The software used on the machines was FACSDiva. 10,000 cells were analysed for each sample, and E14Ju09 ES cells with and without DAPI staining were used as negative controls. Further negative controls are outlined with each experiment.

2.7.7.9.3 Data Analysis

Data generated by the analysers was exported as '.fcs' files. Analysis was performed with the FlowJo software. Debris was excluded by gating using forward scatter and side scatter. Comparison of the amplitude and height of the side scatter signal was used to exclude doublets. Dead cells were then excluded by gating for DAPI-negative cells. Gating to calculate percentages of positive and negative cells was performed using E14JU09 fluorescently negative cells unless stated otherwise.

2.7.7.10 2i/LIF to EpiLCs Differentiation

Similar to the protocol described in (Hayashi et al., 2011). 2i/LIF cells were LIFted as for passaging, counted and plated at specified density on plates pre-coated with 7.5µg/ml bovine fibronectin (Sigma-Aldrich). Cells cultured in EpiLC media, a N2B27 based media, herein named N2B27/Activin/FGF/KSR, Table 2.34, supplemented with,

- 20ng/ml (final) –Recombinant human/rat/Mouse activin A (Peprotech)
- 10ng/ml (final) –Recombinant human Fgf Basic (R&D systems)

Table 2.34	**EpiLC Media Composition**
Component	**Volume**
DMEM/F12 (Gibco)	25ml
Neurobasal (Gibco)	25ml
L-Glutamine (Invitrogen)	500µl
2 -mercaptoethanol	100µl
Knock Out Serum Replacement	500µl
N2 (Gibco)	250µl
B27 (Gibco)	500µl

2.7.7.11 *In vitro* derivation of Neuromesodermal Progenitors (NMPs) from Mouse EpiSCs

The generation of *in vitro* neuromesodermal progenitors (NMPs) was performed as described in (Gouti et al., 2014). Briefly, following accutase treatment and spinning as

per normal passaging, EpiSCs were re-suspended, counted and plated at 2105cells/cm^2 in N2B27 media supplemented with

- 3μM (final) CHIR99021 Wnt agonist (Axon)
- 20ng/ml (final) –Recombinant human Fgf Basic (R&D systems)

Herein termed N2B27/CHIR/Fgf EpiSCs were cultured in these conditions for 48-72 hours, with media change when appropriate.

2.7.7.12 Generation of transgenic inducible overexpressing ES cells (2i/LIF)

Inducible overexpressing ES cells were generated using an inducible cassette exchange rapid recombination system described by (Iacovino et al., 2011, 2014). Briefly this system allows for rapid generation of conditional inducible murine ES cells by targeting genes into an Inducible Cassette Exchange (ICE) locus, a locus encoding a doxycycline-inducible floxed cre within the HPRT locus, which replaces itself with an incoming floxed gene of interest. This is achieved by generating p2lox plasmids of the gene of interest inserts (described in 2.2.5.7.3 and Fig. 2.1) and nucleofecting into A2lox.Cre Mouse ES cells. Cells lines to overexpress *Ptk7*, two *Ptk7* dominant negative, *Vangl2*, *Pk1* and *RFP* alone (control) were generated using this system.

2.7.7.12.1 Removing A2lox.Cre mES cells from Mouse Embryonic Fibroblasts (MEFs).

A2lox.cre Mouse ES cells were donated by Lesley Forrester's lab (MRC, CRM) and were originally cultured in LIF/FCS conditions on irradiated MEFs. In order to remove irradiated MEFs from the culture the ESCs were treated with trypsin for 2 minutes, re-suspended in ESC media, spun to remove trypsin and re-suspended in ESC media. To minimise MEF number in the culture this cell/media mix was then placed on an untreated 9cm dish for 45 minutes to an hour to allow MEFs but not ESCs to attach, then the supernatant containing ESCs was removed, cells counted and moved to LIF/FCS (29,090 cells/cm^2 on gelatine) or 2i/LIF (10,526 cells/cm^2 on pre-treated poly/laminin) culture conditions. Cells were then passaged as described in 2.2.7.3 (LIF/FCS) and 2.2.7.6 (2i/LIF) until no MEFs were present in the culture. Numbers of MEFs remaining in LIF/FCS culture conditions decreased with increasing passaging,

however cells were prone to differentiation. Contrastingly in 2i/LIF conditions, MEF numbers were already negligible in early passages. Typically, by passage 3 no MEFs were present in the culture, and cells formed normal 2i/LIF cell colonies with minimal differentiation of cells. Due to the minimal differentiation of cells in 2i/LIF conditions, as well as low MEF numbers, this condition was chosen for nucleofection with generated p2Lox.Wnt/PCP plasmids.

2.7.7.12.2 G148 Kill curve for 2i/LIF cell culture

Upon nucleofection, the neomycin gene, downstream from gene of interest site, is repaired in cells correctly targeted, which allowed the use of G418 selection to screen for correctly targeted clones. As 2i/LIF does not contain serum, which may enhance G418 action, a titration of G418 was done using wildtype 2i/LIF ES cells to ensure that similar concentrations to (Iacovino et al., 2011, 2014) would not damage correctly targeted cells. A kill curve was performed in 2i/LIF conditions using 0-200µg/ml of G148. Following 5 days of treatment with G148 all cells in 200µg/ml treatment well had died, thus this concentration, which is the same as that for culture with serum, was used to check positively targeted cell lines following nucleofection.

2.7.7.12.3 Recombination of p2lox plasmids in 2i/LIF Culture using nucleofection

The day before harvesting A2lox cells for recombination, Cre expression was induced by treatment with doxycycline (dox) 1µl/ml, or left in culture without dox (-dox control). Poly-l-ornithine was added to 9cm treated dishes, one for each cell line plus control, which was left to incubate overnight in the fridge. The following day this was replaced with laminin and left for 2 hours in the fridge, until being replaced by 2i/LIF medium and prewarmed to reduce cell death by placing in the incubator.

Dox was refreshed 2 hours before (except for the -dox control). The nucleofection kit used was the Lonza Amaxa P3 Primary Cell 4D nucleofector x L + Kit L (Lonza). Cells were accutased as normal and 500,000 cells were spun down for each construct, and resuspended in 82µl P3 4D nucleofector x solution and 18µl supplement. 4mg (or 10µl maximum) miniprep DNA was added to each and mixed gently (Table 2.35). CAG-RFP plasmid was used as a positive control with -dox cells to get an idea of nucleofection efficiency. The plasmid/solution mix was transferred into the cuvettes

and gently tapped to ensure no bubbles were present between electrodes. Using a 4D Nucleofector ™ System, programme CG-104 for Mouse embryonic stem cells was applied to each cuvette. Contents of each cuvette was removed and added to pre-heated poly/laminin coated plate.

Table 2.35	**Concentration of P2Lox Plasmids Used for Nucleofection**		
Plasmid	**DNA Conc**	**Volume**	**Final Conc**
p2lox:CAG-Ptk7-T2A-RFP	240ng/µl	10µl	2.40µg
p2lox:CAG-Ptk7ΔICM -T2A-RFP	275ng/µl	10µl	2.75µg
p2lox:CAG-sPtk7-T2A-RFP	257ng/µl	10µl	2.57µg
p2lox:CAG-Vangl2-T2A-RFP	213ng/µl	10µl	2.13µg
p2lox:CAG-Pk1-T2A-RFP	417ng/µl	6µl	2.50µg
p2lox:RFP (control)	543ng/µl	4.7µl	2.55µg

2.7.7.12.4 Selection and expansion of single dox-inducible clones

Nucleofection efficiency was checked after 2 days by examination of RFP expression in -dox control plate, and 200ng/µl of G418 selection in fresh media was added to each plate including this control. Once all the colonies in the -dox control were dead, usually 7 days, single colonies from nucleofected plates for each construct were transferred to pre-coated wells of a 96 well plate, and pipetted up and down to make into single cells. These cells continued to be passaged once they reached confluency into subsequently bigger wells until they reached 6 well plate. The induction of each clone was tested by flow cytometry and clones with high induction were then frozen until needed.

2.7.7.12.5 Recombination to generate cell lines

Pk1 clone picking and induction efficiency analysis was carried out by MSc Student Catarina Martins Costa

Recombination via nucleofection of A2lox.Cre cell lines with PCP p2Lox plasmids was conducted for all plasmids to create individual cells lines. Control RFP only cell line was also generated using P2Lox-RFP plasmid created by Mattias Malaguti (Lowell Lab). Overall targeting efficiency was high, and following G148 selection, at least 100 colonies survived for each cell line from the initial 50,000 cells that were nucleofected. Individual cell colonies were picked, passaged through gradually bigger wells, and the induction efficiency tested.

Chapter 3: Examining polarity in NMP regions during axial elongation

1.1 Introduction & Aims

From the comprehensive review of published *in situ* hybridisations and functional data for Wnt/PCP components, several questions remain concerning the full spatial and temporal profile of these components and tissue polarity, specifically in NMP regions. This information is key to understanding the role of Wnt/PCP signalling in the regulation of NMP behaviour and as such makes the three specific aims of this chapter, outlined below,

(1) Despite published *in situ* hybridisation data for many Wnt/PCP components it remains unknown if many of these components are expressed in NMP regions during axial elongation. I aim to provide a more fine-grained description of their role in NMP regions by performing *in situ* hybridisations of Wnt/PCP components, and comprehensively examine the NMP regions, NSB, CLE and CNH during axial elongation.

(2) Establishment of Wnt/PCP in individual cells and propagation of tissue polarity to neighbouring cells is reliant on asymmetric distribution of many core Wnt/PCP components, including Vangl and Pk. When Wnt/PCP is not active these core components are uniformly distributed. Thus, examination of mRNA alone cannot provide conclusive evidence that Wnt/PCP is active. For Wnt/PCP activity to be determined the localisation of Wnt/PCP component proteins needs to be examined. I aim to examine the profiles of Wnt/PCP components at a protein level to decisively determine if Wnt/PCP is active in NMP regions.

(3) An alternative but underutilised system to investigate cell polarity is through the examination of organelle positioning within the cell. This strategy has been exploited primarily in flat epithelial systems to understand Wnt/PCP polarity, but has also been used in early embryo development to understand cell polarity and cell movements during gastrulation. So far NMP regions have not been examined, and therefore for the final objective I aim to use a similar strategy to understand more about polarity of NMPs and cell movements that occur in NMP regions.

3.2 NMP regions across axial elongation express *Pk1*

In situ hybridisations were performed and images assembled by MSc Student Catarina Martins Costa

Despite previous documentation of Wnt/PCP component expression profiles using in situ hybridisation these were not focused on NMP-containing areas, and thus their localisation in these areas remained unclear. Therefore, in situ hybridisation probes were cloned and transcribed for Pk1, results documented in Figure 3.1. *Pk1* mRNA was present at all examined stages, from E7.5 to E10.5. At E7.5 and E8.5 *Pk1* detection was broadly expressed in the embryo, including posterior tissues: node, primitive streak and adjacent CLE (Fig. 3.1A-B). This is in alignment with previous reports which describe its expression in these areas (Crompton et al., 2007). At E9.5 and E10.5 *Pk1* mRNA was found along the full length of the embryo (anterior and posterior tissue) (Fig. 3.1C-D). Examining tail bud sections confirmed expression of *Pk1* in the mesoderm (somites and tail bud), neural tube, gut and the CNH.

Note that intense localised labelling was present along the amniotic cavity at E7.5 and the gut at E9.5. As this was limited to the edges of cavities which are prone to probe trapping, and because asymmetric distribution of *Pk1* mRNA has not been previously reported it was assumed to be an artefact of probe trapping.

In summary *Pk1* mRNA was found to be broadly expressed in early stages of embryonic development (E7.5-E10.5) including NMP containing regions (NSB and CLE and CNH).

3.3 Examining localisation of Wnt/PCP component protein distribution in NMPs

In the absence of comprehensive information on the protein localisation of Wnt/PCP components in NMP regions, antibodies for these were sourced and trialled. Antibody performance was assessed by similarity to published protein distribution either at the cellular level (location within the cell), or tissue level. Where possible positive controls were used alongside samples, and chosen based on information from published data as well as online resources (Unigene, NCBI). In total 32 antibodies were tested, details of which are outlined in Table 3.1.

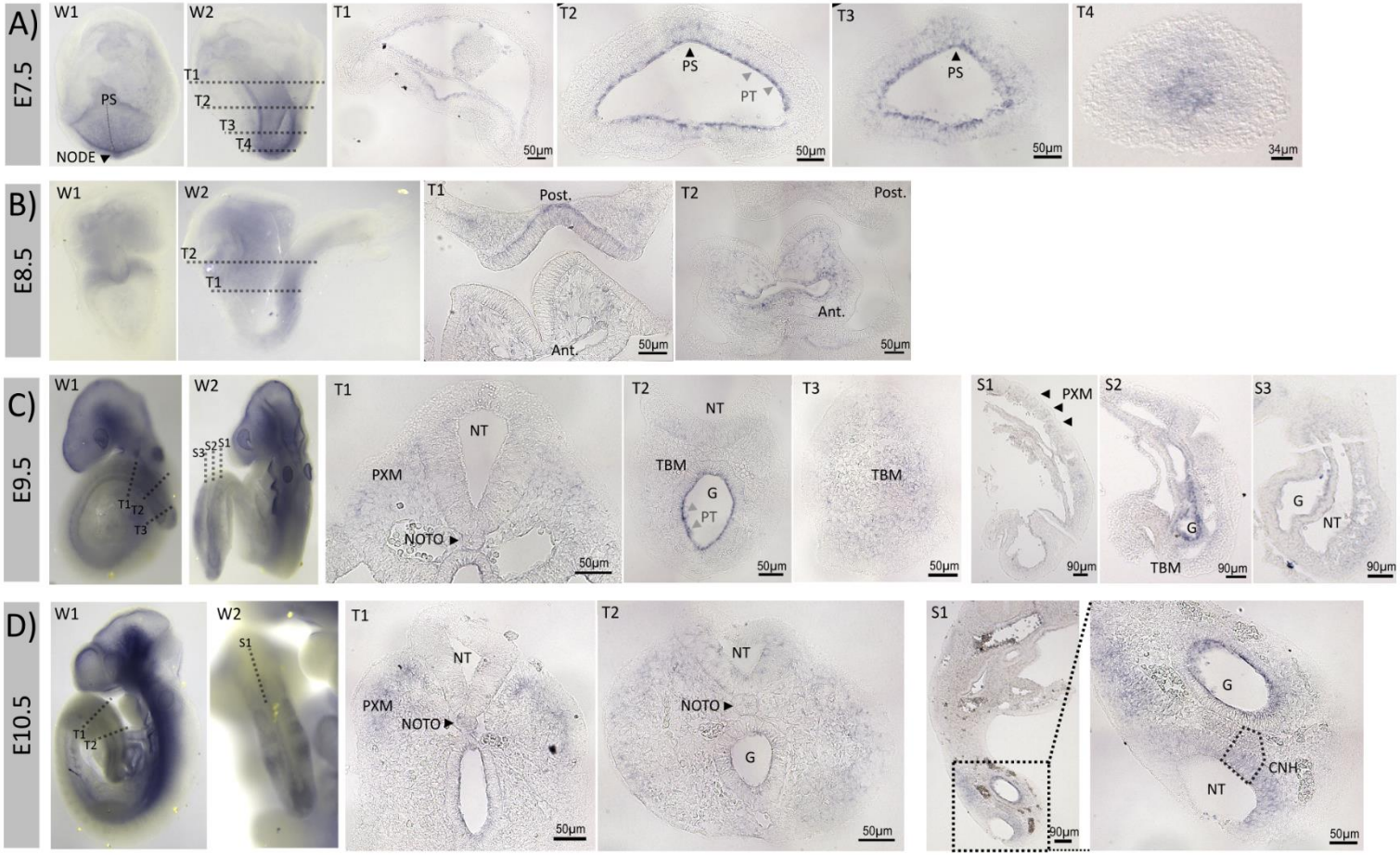

Figure 3.1: In situ hybridisation for *Pk1*. Figure shows wholemount in situ hybridisation to detect *Pk1* in **(A)** E7.5, **(B)** E8.5, **(C)** E9.5 and **(D)** E10.5 wholemount (W) embryos, and corresponding transverse (T) and sagittal (S) sections. PS- primitive streak, PT- probe trapping, Post - posterior, Ant - Anterior, PXM - paraxial mesoderm, NOTO- notochord, TBM - tail bud mesoderm, G-Gut, NT- neural tube, CNH chordoneural hinge. Tiled microscopic acquisitions were stitched using FIJI software (Preibisch et al., 2009).

Four antibodies were adequate for reliable protein visualisation following optimisation**.** These were: anti-Ptk7 17799-1-AP (Proteintech), anti-Ptk7 ab62074 (Abcam), anti-Fzd6 AF1526 (R&D) and anti-Vangl2 ABN373 (Merck Millipore). These were utilised to further examine protein distribution in NMP-containing areas during axial elongation.

3.3.1 NMPs express Ptk7 protein during axial elongation (early headfold to E13.5)

All three antibodies recognising Ptk7 protein showed specific and strong staining. Ptk7 Abcam 62073 will not be discussed further as the other antibodies showed superior staining. Ptk7 had been only briefly described in the literature, with mRNA reported to be predominantly found in caudal regions from headfold stage to E9.5 (Paudyal et al., 2010). Additionally its protein had been described as non-asymmetrically localised to the cell membrane using commercially unavailable transgenic reporter lines and generated antibodies (Lu et al., 2004; Paudyal et al., 2010; Yen et al., 2009). Immunohistochemistry using Ptk7 Abcam-62074 antibody was performed on transverse sections for E9.5, E10.5 and E12.5 (Fig. 3.2, Fig. 3.3). Throughout these examined stages Ptk7 protein was always localised to the cell membrane and levels in anterior sections were very low, in keeping with published reports of Ptk7 localisation.

In E9.5 anterior tail bud sections, Ptk7 expression was highest in the neuroectoderm and flanking paraxial mesoderm, but was also present in the notochord, and the dorsal gut (Fig. 3.2A). Strikingly more ventral regions of the gut, the intermediate and ventral mesoderm appeared to have relatively lower levels of Ptk7. In more posterior sections Ptk7 was expressed in all tissues to some level (Fig. 3.2B). Expression was highest in all mesoderm and neuroectoderm, including dividing cells, characterised by rounded morphology, condensed chromosomes and location on the ventricular surface of the emerging neuroectoderm (Fig. 3.2C) as noted previously (Noctor et al., 2001). In these sections Ptk7 protein expression was lowest in the notochord and gut. Overall Ptk7 expression at E9.5 was generally broad, with specific levels of expression dependent on specific tissue type.

Antibody	Source	Catalogue #	Species	Type	Reference	Tissue Tested	Fixation	Control Tissue	Dilution	Performance	Figure
Celsr1	Abcam	Ab196600	Rabbit	Polyclonal	-	E9.5	PFA	Ovary/Oviduct	1:100, 1:500	-	-
Celsr2	Abcam	Ab90817	Rabbit	Polyclonal	-	E9.5, E10.5	PFA, PFA-T, TCA, Methanol	Ovary/Oviduct	1:100, 1:250	-	-
Celsr2	ProteinTech	19940-1-AP	Rabbit	Polyclonal	-	E9.5	PFA	Ovary/Oviduct	1:100, 1:250	-	-
Celsr2	Tadashi Uemura	n/a	Mouse	Monoclonal	Shima et al.,2002	E8.5, E9.5	PFA	Ovary, Adrenal Gland	100% serum	-	-
Celsr3	ProteinTech	19939-1-AP	Rabbit	Polyclonal	-	E9.5	PFA	Ovary/Oviduct	1:100, 1:250	-	-
Dvl1	ProteinTech	14314-1-AP	Rabbit	Polyclonal	-	E9.5	PFA	Ovary/Oviduct	1:100, 1:250	-	-
Dvl2	NEB	3224	Rabbit	Monoclonal	Lee et al.,2012	E9.5, E10.5 & EpiSC	PFA	-	1:100, 1:200, 1:300	-	-
Dvl2	NEB	3216	Rabbit	Polyclonal	-	E9.5, E10.5 & EpiSC	PFA	-	1:100, 1:200	-	-
Fzd3	Abcam	Ab75233	Rabbit	Polyclonal	-	E9.5	PFA, TCA control	Ovary/Oviduct	1:200, 1:1000	-	-
Fzd3	Abcam	Ab102965	Rabbit	Polyclonal	-	E9.5	PFA, TCA control	Ovary/Oviduct	1:200, 1:500	-	-
Fzd6	Abcam	Ab98180	Rabbit	Polyclonal	-	E9.5	PFA, TCA control	Ovary/Oviduct	1:100, 1:500	-	-
Fzd6	Abcam	Ab128916	Rabbit	Monoclonal	-	E9.5	PFA, TCA control	Ovary/Oviduct	1:200, 1:500	-	-
Fzd6	ProteinTech	13982-1-AP	Rabbit	Polyclonal	-	E9.5	PFA	Ovary/Oviduct	1:100, 1:250	-	-
Fzd6	R&D	AF1526	Goat	Polyclonal	Chang et al., 2016	All NMP stages	PFA	Adrenal Gland	1:15	***	Fig. 3.9 & 3.10
Nkd1	Abcam	Ab133650	Rabbit	Monoclonal	-	E10.5	PFA	Ovary/Oviduct	1:100, 1:200, 1:500	-	-
Prickle2	Abcam	Ab65964	Rabbit	Polyclonal	-	E9.5	PFA	Ovary/Oviduct	1:100, 1:500	-	-
Prickle2	Abcam	Ab183652	Rabbit	Polyclonal	-	E9.5	PFA	Ovary/Oviduct	1:100, 1:500	-	-
Ptk7	ProteinTech	17799-1-AP	Rabbit	Polyclonal	-	All NMP stages	PFA	Ovary/Oviduct	1:100, 1:250	***	Fig. 3.4-3.8
Ptk7	Abcam	Ab62073	Rabbit	Polyclonal	-	E9.5, EpiSC	PFA	Ovary/Oviduct	1:50, 1:200, 1:500	*	-
Ptk7	Abcam	Ab62074	Rabbit	Polyclonal	-	E9.5, EpiSC	PFA	Ovary/Oviduct	1:50, 1:200, 1:500	**	Fig. 3.2-3.4
Ror2	Santa Cruz	A17-SC 83034	Goat	Polyclonal	-	E10.5, 9.5	PFA	Connective Tissue	1:50	-	-
Vangl1	Abcam	Ab176575	Rabbit	Monoclonal	-	E9.5, E10.5	PFA, PFA-T, TCA, Methanol	Ovary/Oviduct	1:200, 1:500	-	-
Vangl1	Abcam	Ab80055	Rabbit	Polyclonal	-	E9.5, E10.5	PFA, PFA-T, TCA, Methanol	Ovary/Oviduct	1:100, 1:250	-	-
Vangl1	Atlas	HPA 025235	Rabbit	Polyclonal	-	E10.5	PFA	Ovary/Oviduct	1:100, 1:200, 1:500	-	-
Vangl2	Abcam	Ab76174	Rabbit	Polyclonal	-	E9.5, E10.5	PFA, PFA-T, TCA, Methanol	Ovary/Oviduct	1:100, 1:250	-	-
Vangl2	Abcam	Ab60172	Goat	Polyclonal	-	E9.5, E10.5	PFA, PFA-T, TCA, Methanol	Ovary/Oviduct	1:200, 1:500	-	-
Vangl2	Merck Millipore	ABN373	Rabbit	Polyclonal	-	All NMP stages	PFA	Ovary/Oviduct	1:500	***	Fig. 3.11-3.13
Wnt11	Abcam	Ab31962	Rabbit	Polyclonal	-	E9.5	PFA	Conn.Tissue, Ovary/Oviduct	1:100	-	-
Wnt11	Abcam	Ab96730	Rabbit	Polyclonal	-	E9.5	PFA	Conn.Tissue, Ovary/Oviduct	1:100	-	-
Wnt11	Abcam	Ab176910	Rabbit	Polyclonal	-	E9.5	PFA	Conn.Tissue, Ovary/Oviduct	1:100	-	-
Wnt5a	Abcam	Ab174100	Rabbit	Polyclonal	-	E9.5	PFA	Adrenal Gland, Conn. Tissue	1:100	-	-
Wnt5a	R&D	AF645	Goat	Polyclonal	-	E9.5, E10.5	PFA	Adrenal Gland	1:60	-	-

Table 3.1: Details of trialled Wnt/PCP component antibodies.

Table documents all antibodies trialled to detect Wnt/PCP component proteins. Outlined are general antibody details, including source, catalogue number, species the antibody was produced in, clonal type and any associated publications using the antibody are outlined. Additional details of histological protocol used in the trial are outlined, including tissue fixation type, embryo stage of tissue, positive control tissues and the dilutions trialled. Finally details of antibody performance, rated from '-' were no adequate staining was observed to '***' when antibody performance was the best. PFA – Paraformaldehyde, PFA-T - Paraformaldehyde with triton, TCA – Trichloroacetic Acid, Conn. Tissue – Connective Tissue.

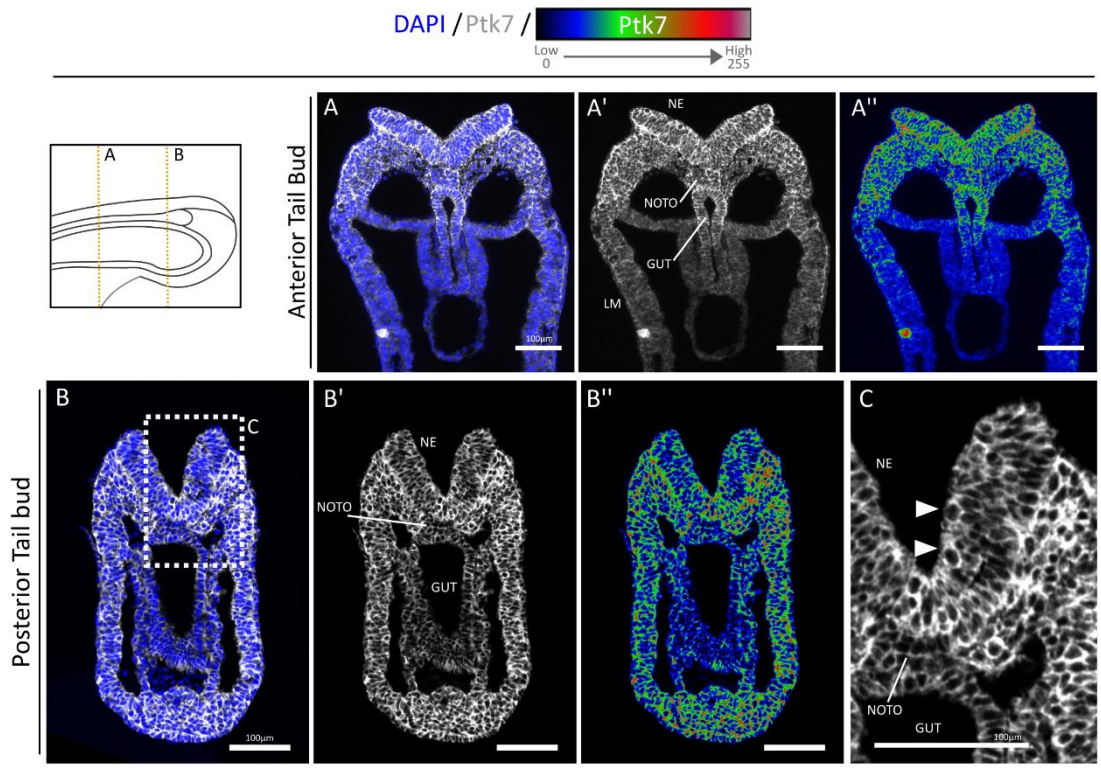

Figure 3.2 Ptk7 protein profile in E9.5 tail bud sections, using Abcam-Ab62074.
Figure details immunohistochemistry of Ptk7 protein performed using Abcam 62074, on E9.5 Mouse transverse tailbud sections. Schematic shows approximate anterior to posterior positioning of **(A)** anterior tailbud and **(B)** posterior tailbud sections. Ptk7 protein is membrane bound and expressed highest in neuroectoderm (NE), notochord (NOTO) and dorsal gut, and low in lateral mesoderm (LM) in anterior sections (A). In posterior tail bud sections Ptk7 is expressed highest in NE (including dividing cells, arrowhead in (C)), NOTO and lowly in the gut. RainbowRGB look up table (LUT)/ colourmap applied to Ptk7 expression level in A'' and B''. Captured image intensity values from 0 (low) to 255 (high) were transformed to a specific colour along the LUT/colour map spectrum detailed above images.

At later stages, E10.5, E12.5, (Fig. 3.3A-C), Ptk7 protein was present at some level in all tail bud tissue, but highest in the mesoderm. Akin to observations at E9.5 stages, the gut and the notochord had relatively low level of expression. However, unlike at E9.5 the neuroectoderm, which at this stage has closed to form the neural tube, it was relatively much lower, and similar to that of notochord, gut and surface ectoderm. Additionally, at these stages Ptk7 appeared to be apically localised within the posterior neural tube.

Overall Ptk7 protein recognised by this antibody had a broad expression pattern in the tail bud during axial elongation. Generally, Ptk7 levels in the tail bud were highest in

the open neuroectoderm and mesoderm, and relatively low in the notochord, gut, surface ectoderm and closed neural tube.

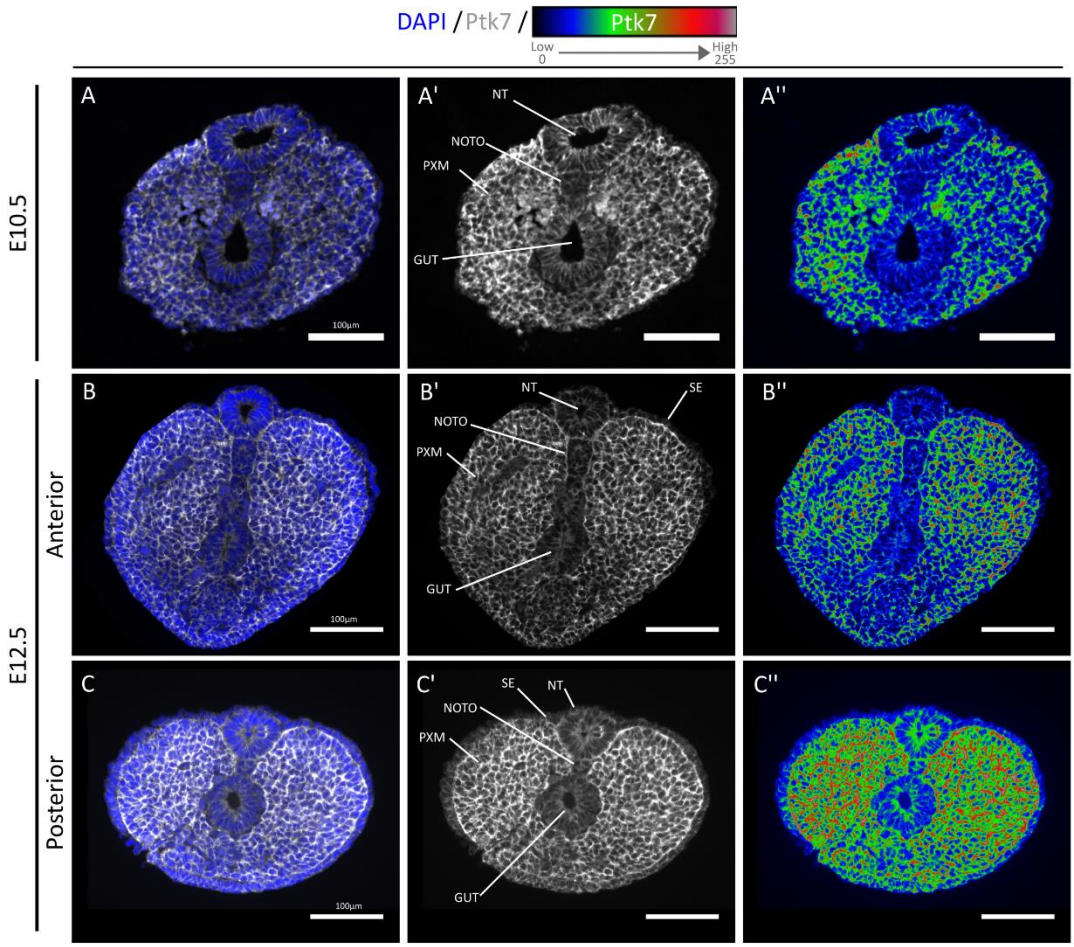

Figure 3.3 Ptk7 protein profile in E10.5 and E12.5 tail bud sections, using Abcam-Ab62074.
Figure details immunohistochemistry of Ptk7 protein performed using Abcam Ab62074, on **(A)** E10.5 and E12.5 Mouse transverse **(B)** anterior and **(C)** posterior tail bud sections. Ptk7 protein is membrane bound and expressed highest in the mesoderm, including paraxial mesoderm (PXM). Ptk7 is lowest in surface ectoderm (SE), notochord (NOTO), neural tube (NT) and gut. RainbowRGB look up table (LUT) applied to Ptk7 expression level in A'',B'' and C'', LUT details above images.

Immunohistochemistry was also performed using Ptk7 antibody from Proteintech-17799-1, which was a more sensitive antibody than the one previously described from Abcam. The performance of the antibody afforded the opportunity to do wholemount staining on early embryos in addition to those performed on sections. During wholemount immunohistochemistry the amniotic membranes of the embryo was pierced to allow the antibody to access the epiblast.

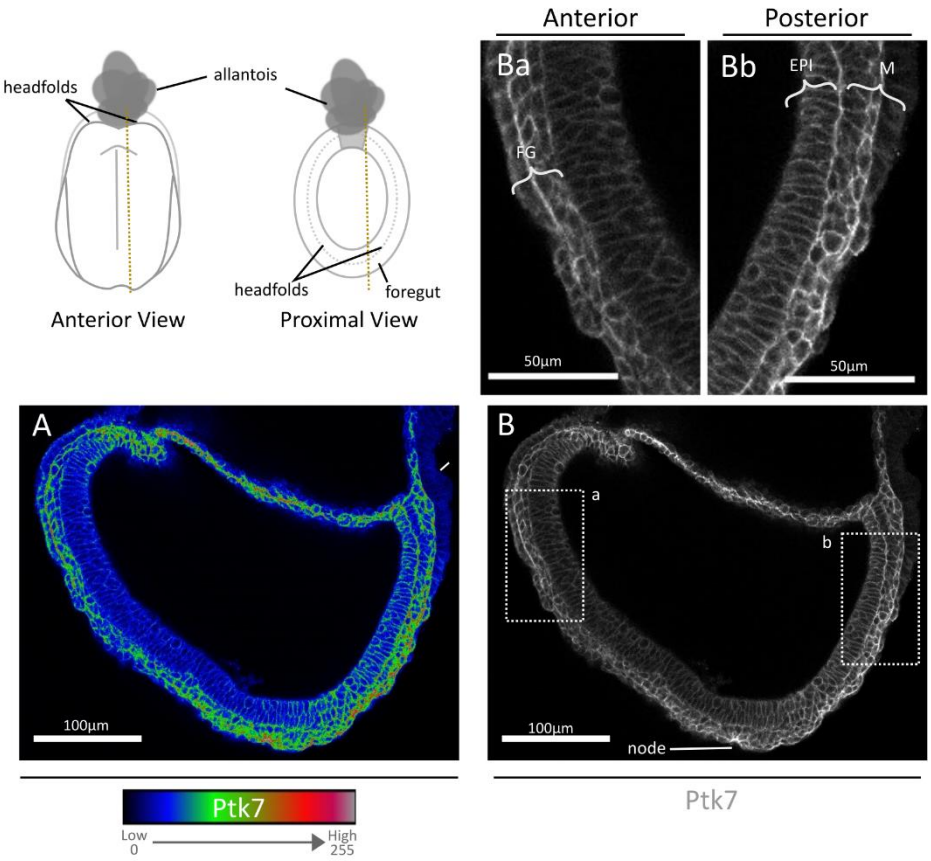

Figure 3.4 – Ptk7 protein profile at early headfold stage, using Proteintech 17799-1.
Immunohistochemistry of Ptk7 protein using Proteintech 17799-1 on wholemount embryos at early headfold. Yellow dashed line on schematic indicates approximate parasagittal z-slice shown in **(A)** and **(B)**. Ptk7 is high in the node. In anterior tissue **(Ba)** Ptk7 is expressed highly in developing foregut (FG). In posterior regions **(Bb)**, Ptk7 is expressed in cells of the epiblast (EPI) and adjacent mesoderm (M). Ptk7 – Grayscale or Rainbow LUT, details of which are detailed below the image. Posterior to right-hand side in A-B.

In wholemount early headfold embryos, Ptk7 was expressed highest in cells at the distal and posterior regions of the embryo, most notably the mesoderm cells flanking the primitive streak (Fig. 3.4Bb) and the edge of the node (Fig. 3.4A-B). Adjacent cells of the epiblast also expressed Ptk7 but at a lower level, and extraembryonic cells were negative. In the anterior of the embryo cells of the foregut also express Ptk7 (Fig. 3.4Ba).

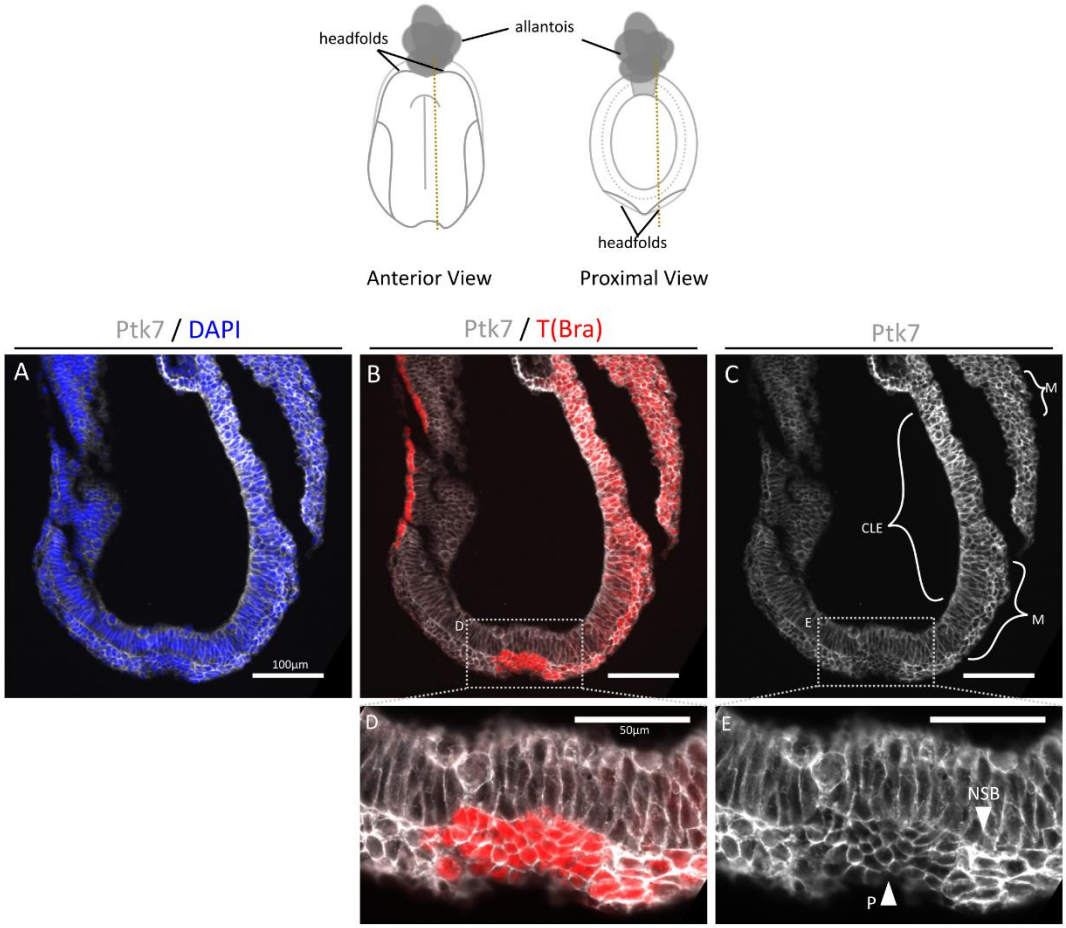

Figure 3.5 – Ptk7 protein profile at late headfold stage, using Proteintech 17799-1.
Immunohistochemistry of Ptk7 protein using Proteintech 17799-1 on a parasagittal section from head fold stage embryo. Yellow dashed line on schematic indicates approximate medial-lateral position of section shown in (A-C). Ptk7 expression is high cells of the node (P-Pit cells) and node-streak border (NSB) (arrows, D-E). Additionally, Ptk7 is expressed in NMPs of the caudal lateral epiblast (CLE), and adjacent mesoderm (M). Anterior (left), Posterior (right).

In late head fold stage para-sagittal sections Ptk7 protein was highly expressed in the posterior of the embryo compared to the anterior (Fig. 3.5A-C). Ptk7 appeared to be lower in the cells of the node pit, labelled by high brachyury expression however surrounding cells, including cells at the node streak border expressed high levels of Ptk7 (Fig. 3.5D-E) as did mesoderm cells and adjacent caudal lateral epiblast (CLE) (previously epiblast).

Wholemount immunohistochemistry was additionally performed on embryos undergoing somitogenesis, and embryos imaged with confocal microscopy. Comparable Ptk7 protein profiles were found to that described for headfold stages. Looking transversely, cells in the anterior head folds show minimal levels of Ptk7

protein when compared to cells in the posterior of the embryo (Fig. 3.6A). Cells of the primitive streak and newly formed mesoderm, had the highest level of Ptk7 protein, whilst adjacent NMPs in the CLE showed a medium level of Ptk7 expression which was the most intense in dividing cells on the apical surface (Fig. 3.6Bc). Panning through z-slices confirmed the intensity of Ptk7 protein was consistent in NMPs throughout all distal to proximal levels of the CLE (Fig. 3.6Ba-f). Cells of the ventral node and NSB had high levels of expression akin to that for newly formed mesoderm, whilst cells of the dorsal node had similar levels to cells of CLE.

Immunohistochemistry on E9.5 transverse tissue showed differential staining to the alternative Ptk7 Abcam-62074 antibody. Unlike the previous antibody, the notochord and gut were positive for Ptk7, as confirmed with T(Bra) double staining (Fig. 3.7A-C). Opposing previous observations, the same level of Ptk7 was seen throughout the whole transverse section and not just in cells of the mesoderm and neuroectoderm which had been reported before. Akin to previous stages, dividing cells in the neural tube had intense Ptk7 staining (Fig. 3.7B).

To investigate Ptk7 protein profile across tissues in more detail, immunohistochemistry was performed on sagittal sections. This also afforded the examination of the CNH, were the NMPs reside. Sagittal sections confirmed a consistent level of Ptk7 protein in the gut, neural tube and notochord (Fig. 3.7D-I). Overall Ptk7 protein expression was highest in the neuroectodermal folds and tail bud mesoderm., and lower in the ventral gut and underlying lateral mesoderm. Additionally, there was a general decrease of Ptk7 protein from posterior to anterior tissue, in line with observations using the other antibody. Double staining of T(Bra) and Ptk7 allowed close examination of the CNH, where the NMPs reside (Fig. 3.7E-I). Ptk7 was present within the CNH at the same level as surrounding notochord, neural tube, gut and tail bud mesoderm.

To examine whether this pattern in the tail bud persisted into later embryonic stages, Ptk7 immunohistochemistry was performed on sagittal sections from E10.5 -E13.5 tail bud (Fig. 3.8A-D). At all stages a gradient of Ptk7, high in posterior, low in anterior tissue was observed. Ptk7 protein was broadly expressed throughout the tail bud.

Unlike the previous antibody no reduction of Ptk7 in the neural tube was found from E10.5 – E13.5.

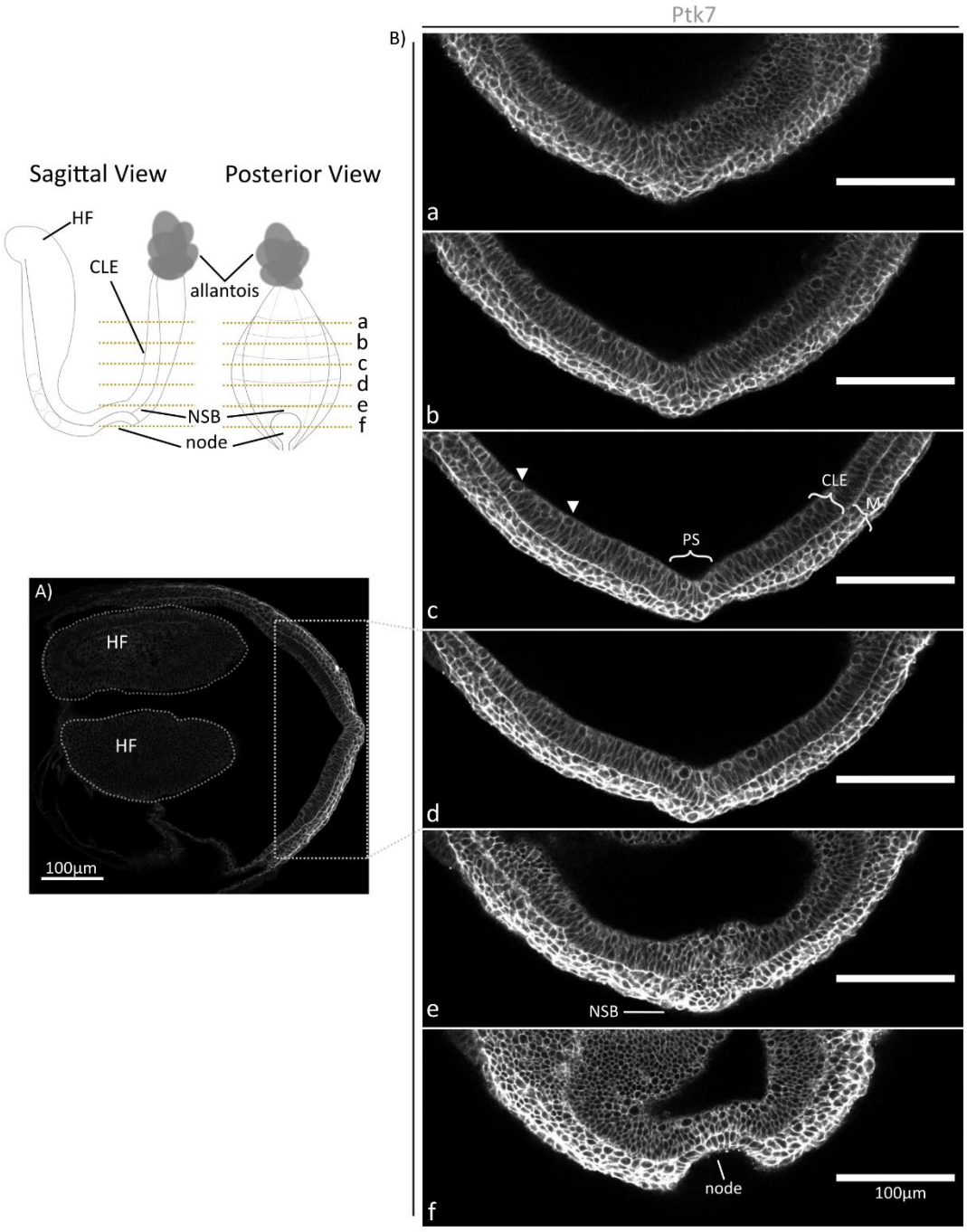

Figure 3.6 – Ptk7 protein profile at early somitogenesis, using Proteintech 17799-1.
Immunohistochemistry of Ptk7 protein using Proteintech 17799-1 on a wholemount early somitogenesis embryo. (A) Single transverse z-slice, Ptk7 is low in headfolds (HF), high in the caudal embryo (right). Yellow dashed lines on schematic indicates approximate transverse z-slices of magnified caudal embryo shown in (Ba-f). Ptk7 is consistently expressed in NMPs of the caudal lateral epiblast (CLE) including those dividing (Bc, arrowheads), cells of the mesoderm (M) and primitive streak (PS), node-streak border (NSB, Be) and node (f).

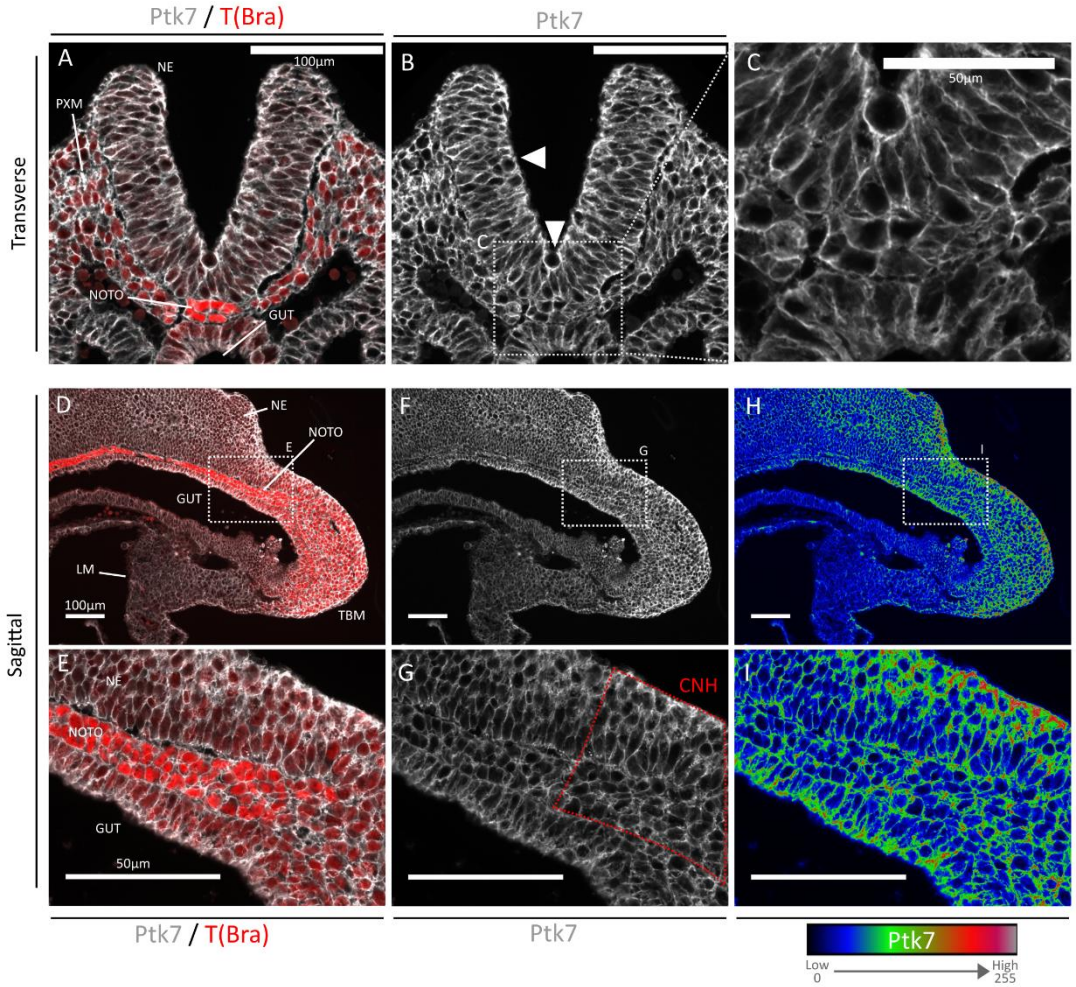

Figure 3.7 – Ptk7 protein profile in E9.5 tail bud, Proteintech 17799-1.
Immunohistochemistry of Ptk7 protein using Proteintech 17799-1, on E9.5 Mouse transverse (A-C) and sagittal sections from E9.5 (D-I). T(Bra)-red, marks mesoderm including notochord. In transverse sections (A-C) Ptk7 is expressed in all tissue types, including neuroectoderm (NE) including dividing cells (arrowhead), notochord (NOTO), gut and paraxial mesoderm (PXM). Sagittal sections (D-H), and magnification (E-I). Ptk7 is expressed highly in posterior tissues, including chordoneural hinge (CNH)-red dashed box, Ptk7 expression is lowest in lateral mesoderm (LM). Anterior to left, posterior to right for sagittal sections. Ptk7 – Grayscale or Rainbow LUT(detailed below the image).

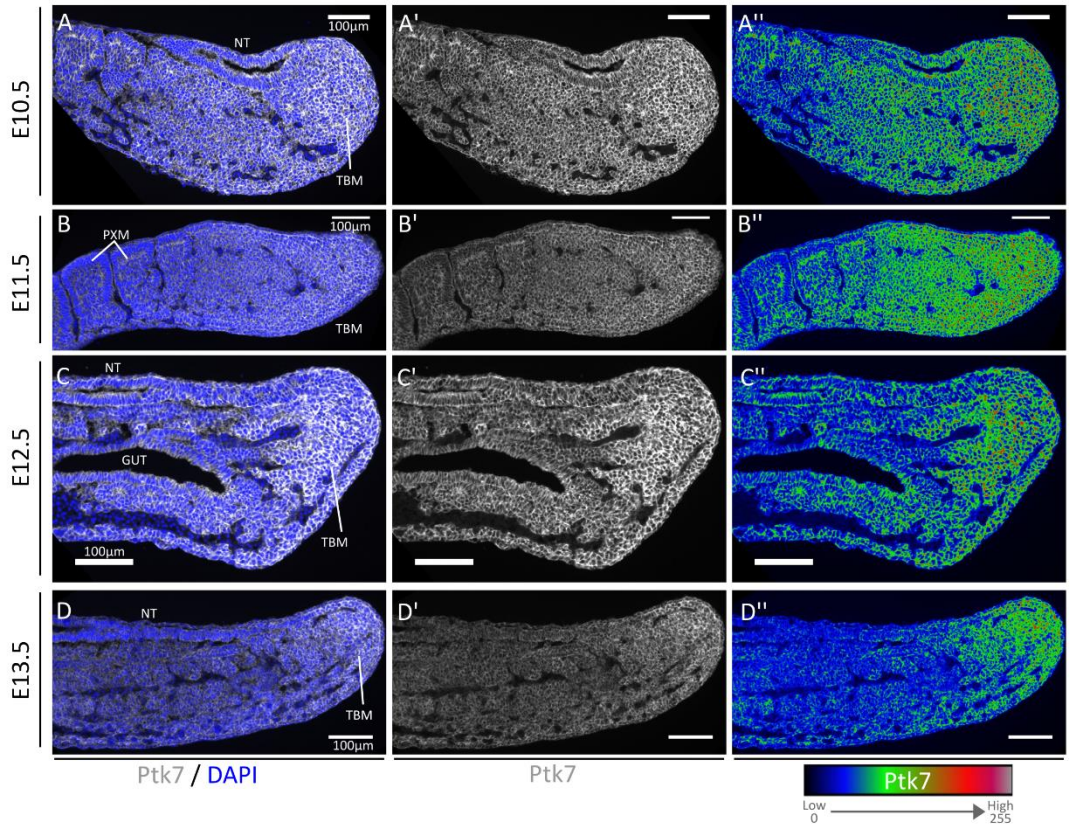

Figure 3.8 – Ptk7 protein profile in E10.5 - 13.5 tail bud, Proteintech 17799-1.
Immunohistochemistry of Ptk7 protein using Proteintech 17799-1, Mouse **(A)** E9.5, **(B)** E11.5, **(C)** E12.5 and **(D)** E13.5 sagittal sections. Ptk7 is highest in the posterior tail bud but is generally expressed in all tissue types, including tail bud mesoderm (TBM), paraxial mesoderm (PXM), neural tube (NT), and gut. Ptk7 – Grayscale or Rainbow LUT (detailed below images). DAPI- Blue.

In summary both antibodies performed well and reported membrane bound Ptk7 protein highly expressed in the posterior tissues as reported previously in the literature via in situ hybridisation (Lu et al., 2004; Paudyal et al., 2010; Yen et al., 2009). Both antibodies showed Ptk7 immunofluorescence in cells located in the posterior portion of the embryo from the streak stage right up until the end of axial elongation at E13.5.

However notable differences in Ptk7 protein localisation were found between two Ptk7 antibodies. The second antibody from Proteintech detected Ptk7 broadly in all tissues of the tail bud at all stages, however the first antibody from Abcam did not detect Ptk7 protein in the closed neural tube, notochord and gut. This is likely to reflect the detection of different Ptk7 epitopes by the two antibodies. The first antibody, Abcam 62074, recognises a 15 amino acid peptide towards the N-terminus of Ptk7 protein found in the extracellular domain. The second antibody, Proteintech 17799-1-AP, conversely recognises a peptide sequence towards the C-terminal of Ptk7 protein, in

the cytoplasmic domain. Between these two antibody recognition sites lies the region at which Ptk7 can be cleaved by MMP14, which results in the production of a N-terminal soluble fragment and membrane bound C-terminal (Golubkov et al., 2010). Thus observed differences in Ptk7 protein localisation between these antibodies is likely to reflect the differences in Ptk7 protein state, with the first (Abcam 62074) detecting non-cleaved Ptk7 absent for the notochord, gut and neural tube, and the second (Proteintech 17799-1-AP) detecting both cleaved and uncleaved Ptk7 protein throughout the tail bud.

3.3.2 Notochord and anterior NSB/CNH cells express Fzd6 protein during axial elongation (late headfold - E13.5)

Previously Fzd6 had only been briefly described in the literature, in which mRNA was reported to be expressed along the entire length of the notochord and underlying endoderm from E8.5 to E9.5. However posterior limits of this expression at these stages were not shown in detail and expression patterns at other timepoints remain unknown (Borello et al., 1999). Similarly little had been reported on Fzd6 protein in posterior tissue during development, although it had been reported as asymmetrically localised within cells of the inner ear and in the Mouse epidermis (Devenport and Fuchs, 2008; Wang et al., 2006). To examine some of these unknowns, successful immunohistochemistry staining for Fzd6 protein was obtained using Fzd6-AF1526 (R&D) on Mouse embryo sections from late headfold to E13.5 (Fig. 3.9).

At late headfold Fzd6 protein, was localised to the cell membrane, and was restricted to cells in the distal region of the embryo specifically those of the notochord, ventral node, crown of the node and node streak border (NSB) (Fig. 3.9A). Fzd6 was highest in the ventral node, and was flanked by two areas of lower expression, the notochord, and the node streak border (NSB) (Fig. 3.9B). In these cells Fzd6 does not appear to be asymmetrically localised. Cells of the dorsal node (DN) and the primitive streak were negative.

In E9.5 transverse tail bud sections, Fzd6 protein was expressed highly in the notochord, and at relatively lower levels in gut, highest in cells adjacent to the notochord (Fig. 3.9C-D). Additionally, expression was found in the surface ectoderm (SE) including the ventral ectodermal ridge of the tail bud (Fig. 3.9C) aligning with

previous reports of Fzd6 in Mouse epidermis (Devenport and Fuchs, 2008). All other cells including those of the neural tube were negative for Fzd6 protein. Sagittal sections showed that this pattern was not limited to posterior tissue, but was also found in anterior regions of the notochord (Fig. 3.9E). In CNH regions, Fzd6 was predominantly expressed in cells of the notochord, including those cells in the CNH (Fig. 3.9F).

This expression of Fzd6 protein along the length of the notochord, and underlying gut continues from E11.5 to E13.5 (Fig. 3.10A-F). Throughout this time the notochord exhibited high level of Frizzled protein, with adjacent underlying gut also expressing Fzd6 protein but to relatively lower levels. Fzd6 was also detected at low levels in the surface ectoderm. In all regions were Fzd6 was found to be expressed it was predominantly localised to the cell surface but did not appear asymmetrically localised within individual cells.

Consistent with this data, previously *Fzd6* mRNA had been reported in the notochord and the gut between E8.5-E10.5 (Borello et al., 1999). Thus, Fzd6 is expressed most highly in the notochord, including cells immediately underlying NMP-containing areas in NSB and CNH, and additionally in the gut and surface ectoderm throughout axial elongation. In these areas Fzd6 did not appear to be asymmetrically localised in individual cells, unlike the previously reported distribution of Fzd6 in the inner ear and Mouse epidermis (Devenport and Fuchs, 2008; Wang et al., 2006).

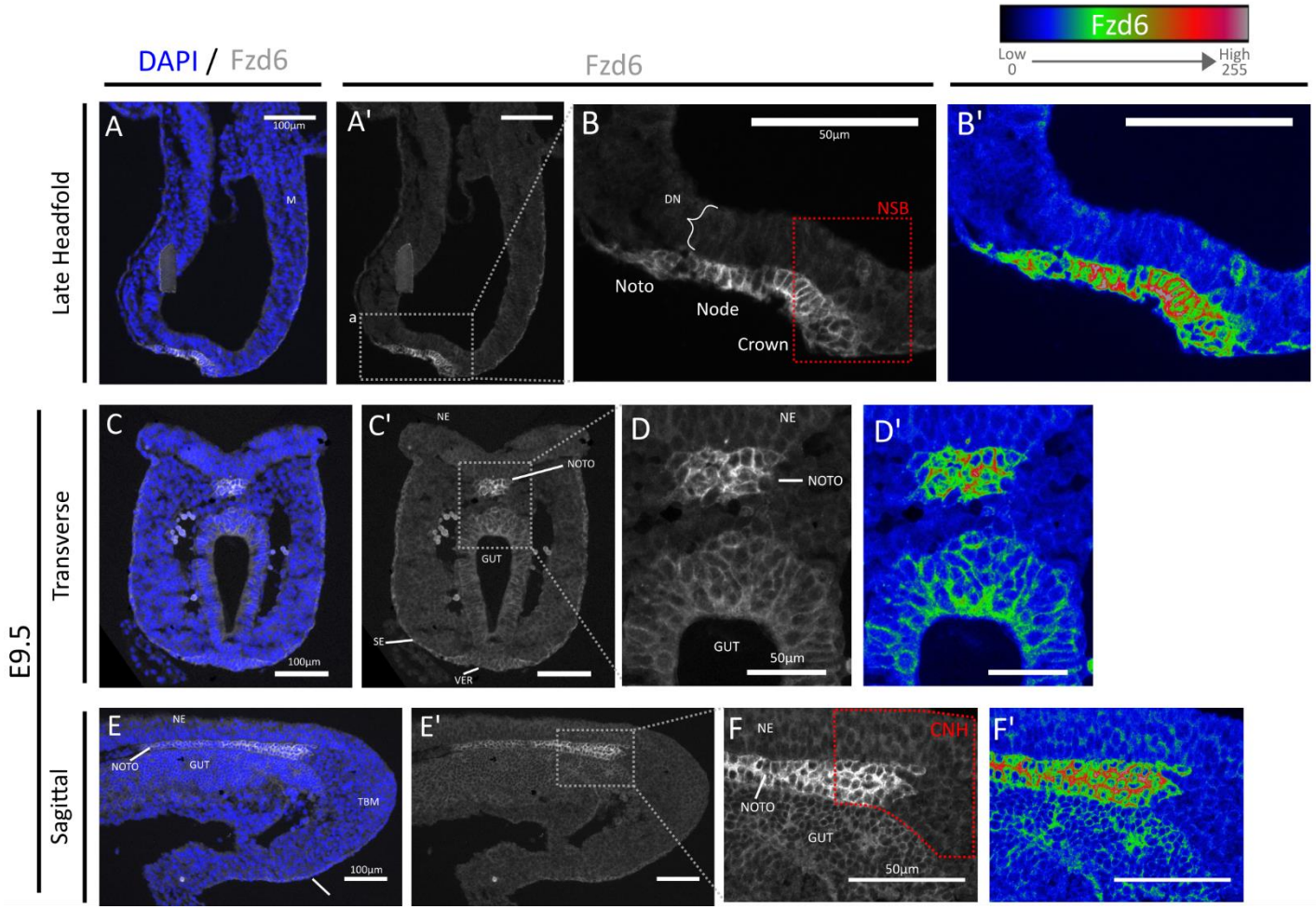

Figure 3.9– Fzd6 protein profile from late headfold to E9.5 tailbud.

Immunohistochemistry of Fzd6 protein on sagittal and transverse mouse tail bud sections from **(A-B)** late headfold, **(C-D)** E9.5 transverse **(E-F)** E9.5 sagittal embryos. Fzd6 is expressed in cells of the notochord (noto), node, crown and most anterior node-streak border (NSB). Fzd6 protein is expressed throughout the notochord, including chordoneural hinge (CNH), underlying endoderm and surface ectoderm at E9.5.

Notochord (NOTO), surface ectoderm (SE), tail bud mesoderm (TBM), neuroectoderm (NE), paraxial mesoderm (PXM), ventral ectodermal ridge (VER). Fzd6 – Grayscale or Rainbow LUT (detailed above images). DAPI-Blue. Auto-fluorescent red blood cells are labelled yellow with overlay.

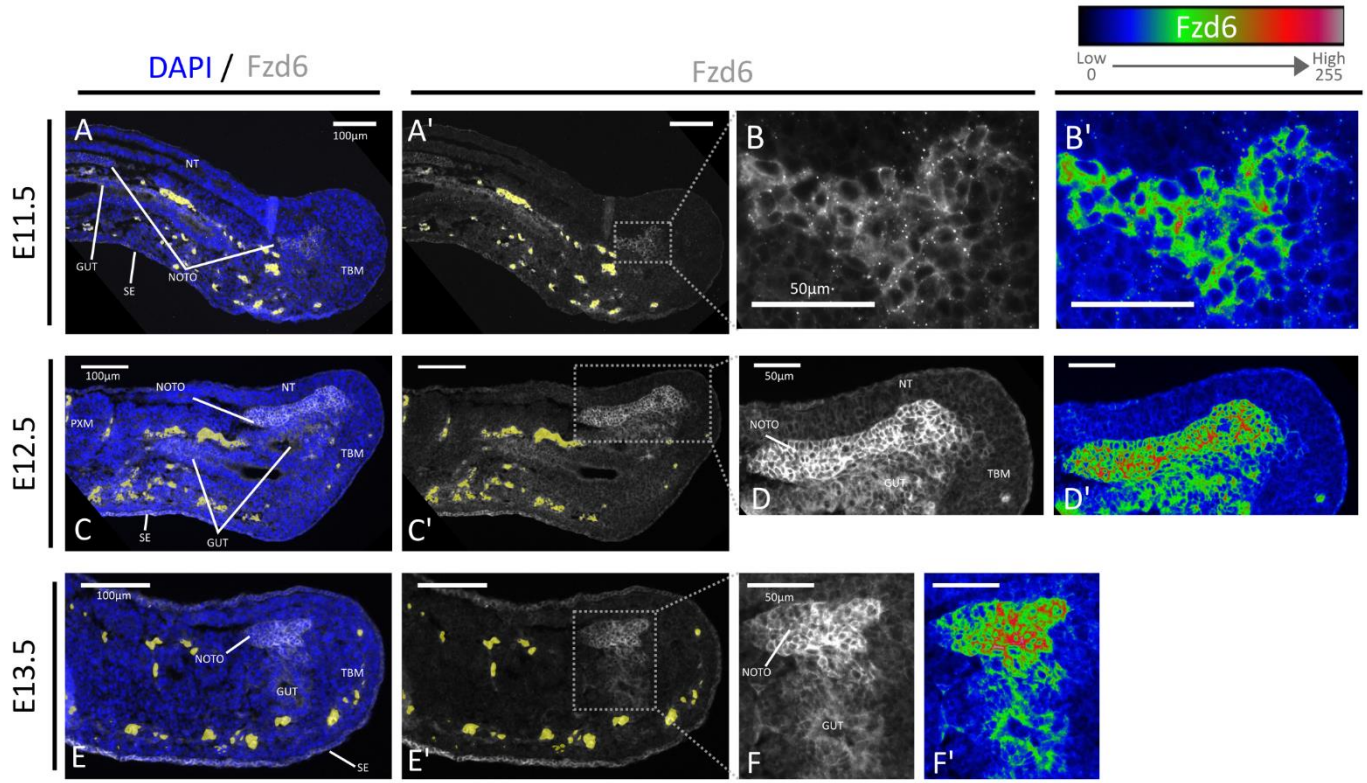

Figure 3.10 – Fzd6 protein profile from E11.5 to E13.5 tailbud. Immunohistochemistry of Fzd6 protein on sagittal and transverse mouse tail bud sections from **(A-B)** E11.5, **(C-D)** E12.5 and **(E-F)** E13.5 embryos. Fzd6 protein is expressed throughout the notochord, including chordoneural hinge (CNH), underlying endoderm and surface ectoderm from E11.5 to E13.5. Notochord (NOTO), surface ectoderm (SE), tail bud mesoderm (TBM), neuroectoderm (NE), paraxial mesoderm (PXM). Fzd6 – Grayscale or Rainbow LUT (detailed above images). DAPI-Blue. Auto-fluorescent red blood cells are labelled yellow with overlay.

3.3.3 NMPs express Vangl2 protein during axial elongation (early headfold - E13.5)

Previously Vangl2 had only been briefly described in the literature, in which mRNA was reported to be expressed in neuroectodermal tissues from E7- E10 (Kibar et al., 2001; Pryor et al., 2014; Torban et al., 2008). Its expression was also described in non-neural tissues in caudal regions however the exact localisation of this was not shown in any detail. To examine these unknowns immunohistochemistry for Vangl2 was performed with Vangl2-ABN373 antibody (Merck Millipore) on sections throughout axial elongation. As Vangl2 protein had previously been reported to be asymmetrically distributed in tissues with active Wnt/PCP signalling (Gao et al., 2011), careful attention was given to the localisation of Vangl2 protein.

In late headfold embryos Vangl2 protein, which was found to be localised to the cell membrane, was expressed broadly throughout the embryo (Fig. 3.11A-B). Generally, the level of Vangl2 expression was lowest in anterior tissue. At the distal regions Vangl2 protein was highest in cells of the notochord, ventral node and crown of the node (Fig. 3.11C). Cells surrounding these areas, including cells of NSB, and dorsal node, also expressed Vangl2, but at lower levels. Asymmetric localisation of Vangl2 was hard to determine in these sections due to the 3D nature of the tissue that was sectioned.

At early somitogenesis stage the difference in expression levels between anterior and posterior tissue was more established (Fig. 3.11D). Cells of the headfold had relatively lower levels of Vangl2 than in cells at the posterior of the embryo (Fig. 3.11E-F). Both newly formed presomitic mesoderm and CLE, where NMPs reside, expressed Vangl2 to the highest levels, however it was difficult to assess if its localisation was asymmetric within cells (Fig. 3.11E).

This trend continued to later stages of somitogenesis (3-4 somites), when high levels of Vangl2 protein were found at the posterior of the embryo, as well as in the

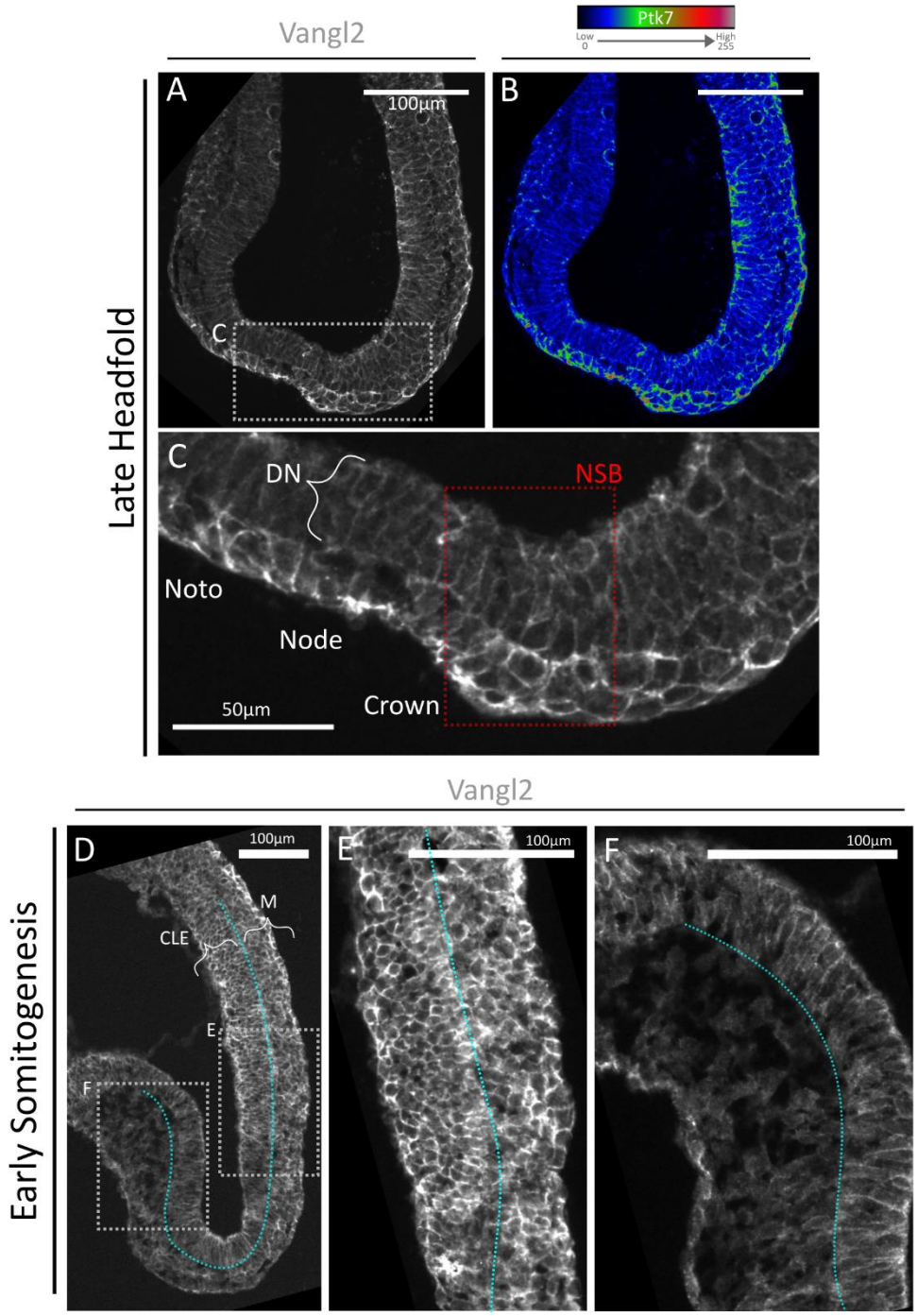

Figure 3.11 – Vangl2 protein profile in late head fold and early somitogenesis embryos.
Immunohistochemistry of Vangl2 protein on **(A-C)** late headfold, and early somitogenesis **(D-F)** mouse sagittal sections. In late headfold embryos, Vangl2 is expressed in the posterior of the embryo (A-B) including cells of the epiblast, and in cells of the notochord (noto), node, crown and node-streak border (NSB), red boxed region (C). Dorsal node (DN) has lower Vangl2 expression. In early somitogenesis embryo sagittal sections (D) Vangl2 is expressed highly in posterior tissues (E), including NMPs in the caudal lateral epiblast (CLE) and presomitic mesoderm (M). Vangl2 is lower in anterior headfolds (F). Vangl2 – Grayscale or Rainbow LUT (detailed above images). In all images, anterior to left, posterior to right.

developing somites (Fig. 3.12A-C). At this stage, Vangl2 protein was present in the cells of the presomitic mesoderm, and in NMPs residing in the CLE. In some cells of the CLE Vangl2 protein appeared to be predominantly localised to lateral membranes rather than apical (cavity-facing) or basal (basement membrane-facing) cell membranes, suggesting that Vangl2 may be asymmetrically localised in these cells (Fig. 3.12D-G). Some cells in the presomitic mesoderm also appeared to have enhanced Vangl2 protein on some membranes relative to others however a pattern in the specific membrane localisation was not clear (Fig. 3.12D-G).

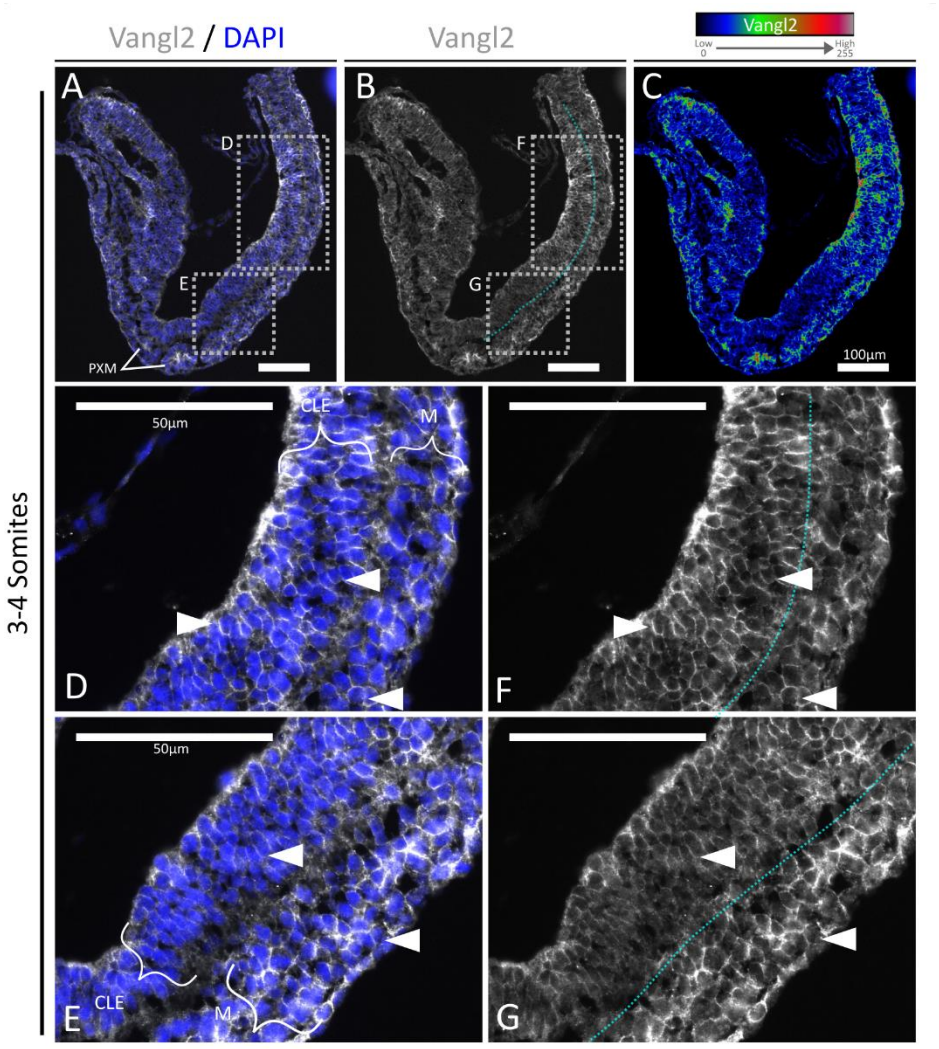

Figure 3.12 – Vangl2 protein profile in 3-4 somite embryos.
Immunohistochemistry of Vangl2 protein on a sagittal 3-4 somite embryo section. Vangl2 is expressed in several tissues including paraxial mesoderm (PXM) (A-C). Magnified posterior regions (D-G), show asymmetric Vangl2 protein localisation (arrowheads) in many NMPs of the caudal lateral epiblast (CLE) and some cells of the presomitic mesoderm (M). Vangl2 – Grayscale or Rainbow LUT (detailed above images). In all images, anterior to left, posterior to right.

At E9.5 Vangl2 protein had a wide distribution across the tail bud. (Fig. 3.13A-B). Inspection of the CNH, verified by T(Bra) expression, showed that Vangl2 was highest in the notochord, but was also present in surrounding tissue including the CNH, where NMPs reside, as well as cells in the gut and neuroectoderm (Fig. 3.13C-D). In more anterior tissue, the neural tube was positive for Vangl2, whilst flanking somites (paraxial mesoderm) were negative (Fig. 3.13E).

At later stages, E10.5-E12.5 (Fig. 3.13G-O), Vangl2 expression remained broad in the tail bud, however cells of the notochord had higher levels of Vangl2 protein, just as in E9.5 (Fig. 3.13I,L,O). As described previously for E9.5, tissue surrounding the notochord remained positive for Vangl2, but at a lower level. In anterior tailbud Vangl2 expression in the neural tube remained high whilst flanking somites had relatively lower levels of Vangl2 (Fig. 3.13M). At all stages from E9.5- E12.5 it was hard to determine if Vangl2 protein distribution within cells was asymmetrically distributed across the tissue, even though some cells clearly had biased localisation of Vangl2 protein across their membrane.

In summary, broad expression of membrane bound Vangl2 was found throughout axial elongation from late headfold to E13.5. Initially Vangl2 was highest in the node region of late headfold embryos, however following the onset of somitogenesis Vangl2 was highly expressed in the CLE where NMPs reside. Interesting cells of the CLE appeared to exhibit asymmetric distribution of Vangl2 akin to previous descriptions of areas containing active Wnt/PCP signalling (Gao et al., 2011). Later in development from E9.5-E12.5 Vangl2 was broadly expressed in the tail bud including the CNH but highest in the notochord, however in these regions asymmetric distribution of Vangl2 was difficult to examine. Additionally in more anterior tail bud tissue, somites expressed Vangl2 to a much lower level than neural tissue in line with previous reports of Vangl2 protein and Vangl2 mRNA in the neural tube (Kibar et al., 2001; Pryor et al., 2014; Torban et al., 2007, 2008).

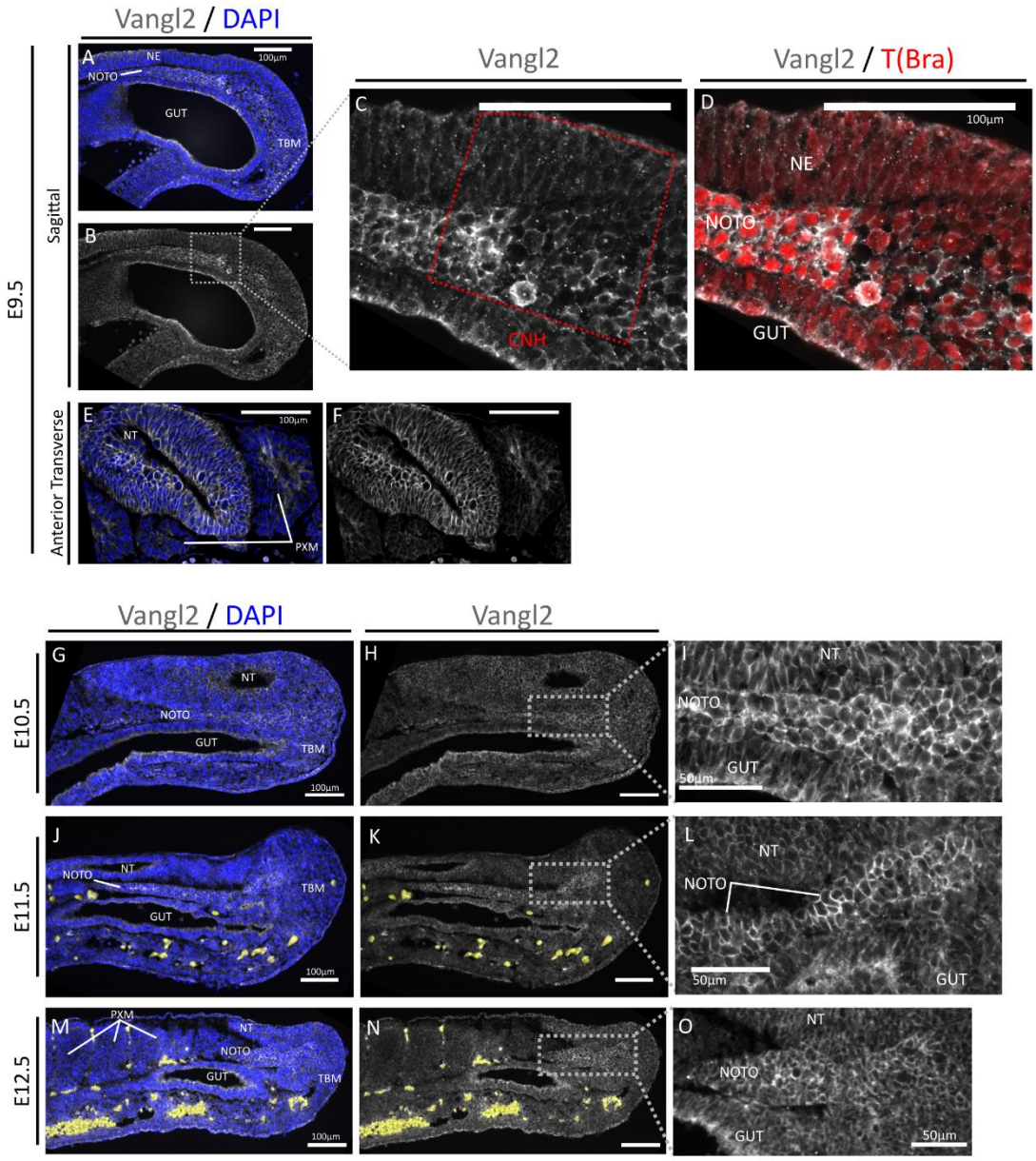

Figure 3.13 – Vangl2 protein profile from E9.5 to E12.5 tail bud.
Immunohistochemistry of Vangl2 protein on **(A-D)** E9.5 sagittal tail bud and **(E-F)** anterior transverse, **(G-I)** E10.5, **(J-L)** E11.5, **(M-O)** E12.5 mouse sections. Vangl2 is broadly expressed in the tail bud from E9.5-E12.5, including cells of the CNH (red dashed box), cells of the tail bud mesoderm (TBM), neuroectoderm (NE), neural tube (NT) and gut, but is highest in the notochord (NOTO). Vangl2 is lowest in paraxial mesoderm (PXM) in anterior sections (E-F). Vangl2 – Grayscale, T(Bra) - Red. In all sagittal images, anterior to left, posterior to right. Auto-fluorescent red blood cells are labelled yellow with overlay.

3.3.4 Sub-optimal Wnt/PCP antibodies

The results described above came from using four out of a total of 32 antibodies that were tested, the other 28 antibodies were sub-optimal and not adequate for use. Before coming to this conclusion attempts were made to improve the immunohistochemistry results using these antibodies.

Antibodies were initially trialled via immunohistochemistry using embryonic tissue fixed in 4% Paraformaldehyde (PFA). After limited success, antigen retrieval, by heating slides (Shi et al., 2011) was trialled on sub-optimal antibodies. Fig. 3.14A-B documents immunohistochemistry using Vangl1 – 176575 (Abcam) on E10.5 tissue fixed with PFA with and without antigen retrieval. Although there was increased signal detection following antigen retrieval this was non-specific and did not reflect Vangl1 expression previously described as specific to the notochord/neural tube (Torban et al., 2008). This trend was typical for all antibodies trialled with antigen retrieval.

In a further attempt to optimise immunohistochemistry, alternative fixation methods: Trichloroacetic acid (TCA) (Hayashi et al., 1999), PFA-Triton (PFA-T) and methanol, were trialled for some antibodies. Overall PFA-T and methanol did not alter specificity of antibody staining when compared with PFA in tissue of interest. However, some differences were seen with TCA fixation. Control samples, including oviduct responded well to TCA fixation, in overall intensity of staining and heterogenetic expression across the tissue in compliance with that previously reported (Fig. 3.14D, Vangl1-176575, for an example). However, despite apparent improvement in control tissues, embryonic tissues showed homogenous and seemingly unspecific staining across whole embryo sections in all cases (Fig. 3.14C).

In summary, steps were taken to optimise these antibodies for Wnt/PCP detection, however despite improvements in staining for control tissues antibody performance remained inadequate for use on embryonic tissue.

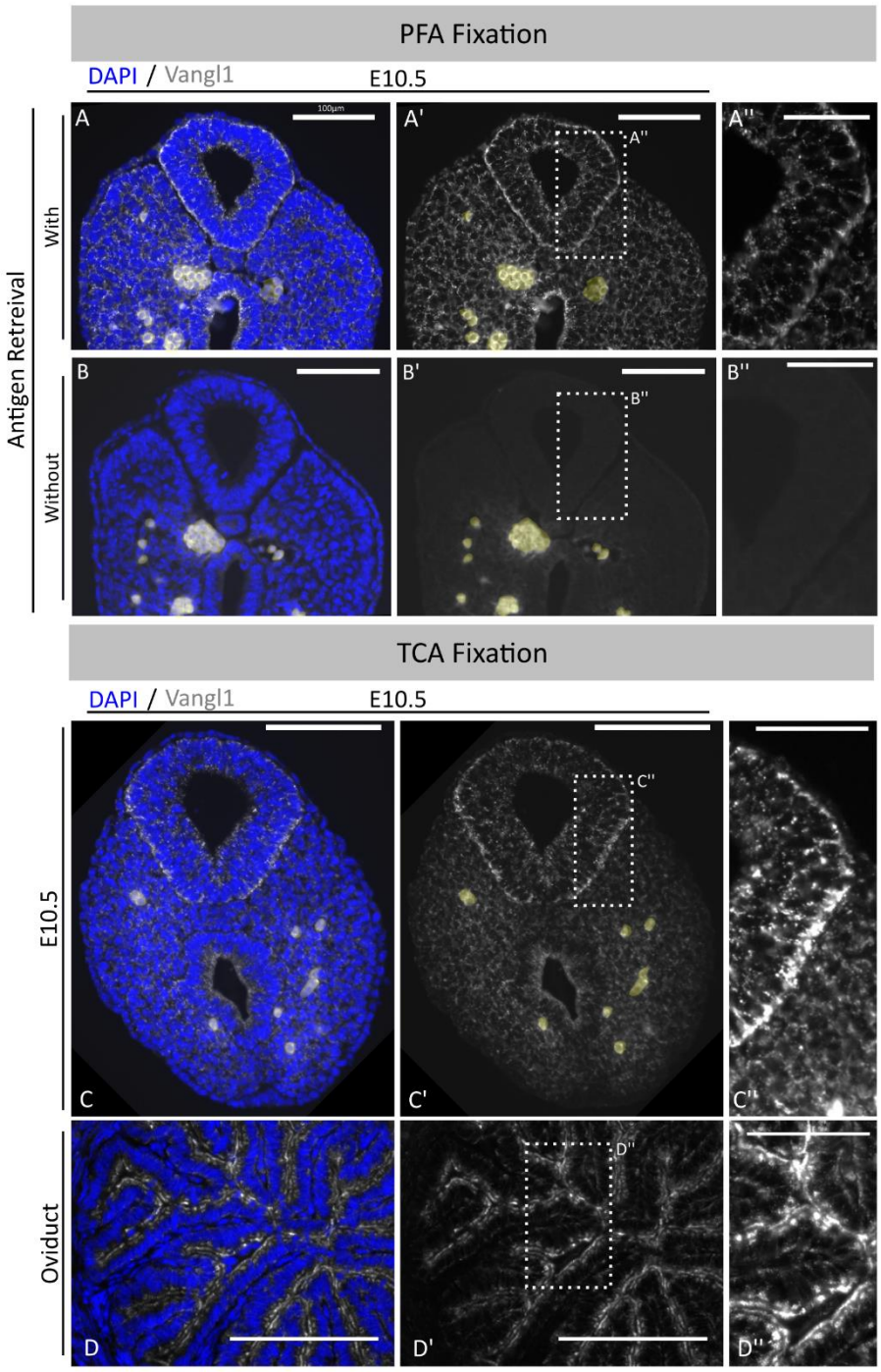

Figure 3.14 Trialled optimisation of immunohistochemistry using antigen retrieval and fixation types.

Immunohistochemistry of Vangl1 protein using Abcam 176575 antibody, on Mouse E10.5 PFA fixed sections **(A)** with and **(B)** without antigen retrieval, and on **(C)** TCA fixed E10.5 and **(D)** positive control oviduct tissue without antigen retrieval. Antibody was diluted 1:100. (A-D) show DAPI (blue) and Vangl2 (greyscale), A'-D' Vangl1 alone, and A''-D'' magnification of A'-D'. Auto-fluorescent red blood cells are labelled yellow with overlay. Antigen retrieval and TCA fixation did not result in the improvement of Vangl1 detection.

3.3.5 Summary of Wnt/PCP component localisation in NMP regions

The data described so far in this chapter (3.2/3.3), unpublished data from the Wilson Lab (Wnt5a/Ptk7 in situs), and the published in situ hybridisation data reviewed in Chapter 1.4.5 (Table. 1.1), were combined and documented in Table. 3.2. Together these data confirm that core Wnt/PCP components *Pk1*, *Celsr1-3* and *Vangl2* and Wnt/PCP co-receptor *Ptk7* are all found in the CLE, the location of NMPs prior to tail bud formation. Additionally, *Wnt5a*, *Fzd6*, *Vangl2* and *Ptk7* were found in the CNH, where NMPs reside in the tail bud during axial elongation. Altogether these data suggest that Wnt/PCP components have the right spatio-temporal profile to potentially regulate NMP behaviour during axial elongation.

Summary of In Situ Data from Publications

	E7.5- E8.5			E8.5	E9.5	E10.5	E11.5	E12.5	E13.5	References
	PS	NSB/node	CLE	TB	TB	TB	TB	TB	TB	
Celsr1	xx	xx	x	x	xx	xx	n/d	n/d	n/d	(Shima *et al.*, 2002; Crompton, Du Roure and Rodriguez, 2007)
Celsr2	x	xx	xx	x	x	x	n/d	n/d	n/d	(Shima *et al.*, 2002; Crompton, Du Roure and Rodriguez, 2007)
Celsr3	x	x	xx	x	n/d	n/d	n/d	n/d	n/d	(Shima *et al.*, 2002; Crompton, Du Roure and Rodriguez, 2007)
Dvl1	x	x	n/s	x	x	x	n/d	n/d	n/d	(Bois *et al.*, 1996)
Dvl2	n/d	n/d	n/d	n/d	n/d	x	n/d	n/d	n/d	(Tissir and Goffinet, 2006)
Dvl3	n/d	n/d	n/d	n/d	n/d	x	n/d	n/d	n/d	(Tissir and Goffinet, 2006)
Fzd1	n/d	n/d	n/d	x	x	x	n/d	n/d	n/d	(Borello *et al.*, 1999)
Fzd2	n/d	n/d	n/d	n/d	n/d	n/d	n/d	n/d	n/d	(Borello *et al.*, 1999)
Fzd3	n/d	n/d	n/d	x	x	xx	n/d	n/d	n/d	(Borello *et al.*, 1999)
Fzd6	n/d	n/d	n/d	x	x	x	n/d	n/d	n/d	(Borello *et al.*, 1999)
Fzd7	n/d	n/d	n/d	-	-	-	n/d	n/d	n/d	(Borello *et al.*, 1999)
Pk1	xx	xx	xx	xx	xx	n/d	n/d	n/d	n/d	(Bekman and Henrique, 2002; Crompton, Du Roure and Rodriguez, 2007)
Pk2	-	x	-	n/d	n/d	n/d	n/d	n/d	n/d	(Crompton, Du Roure and Rodriguez, 2007)
Ptk7	n/d	n/d	n/d	xx	xx	n/d	n/d	n/d	n/d	(Paudyal *et al.*, 2010)
Ror1	-	-	-	-	n/d	n/d	n/d	n/d	n/d	(Matsuda *et al.*, 2001)
Ror2	xx	xx	n/s	xx	xx	xx	xx	n/d	n/d	(Matsuda *et al.*, 2001; Verhey van Wijk *et al.*, 2009)
Vangl1	n/d	n/d	n/d	x	x	x	x	x	x	(Torban *et al.*, 2008; Pryor *et al.*, 2014)
Vangl2	x	x	n/s	x	x	x	n/d	n/d	n/d	(Kibar *et al.*, 2001; Murdoch et al., 2001; Pryor *et al.*, 2014)
Wnt11	x	xx	n/s	xx	x	x	n/d	n/d	n/d	(Kispert *et al.*, 1996)
Wnt5a	xx	x	n/s	xx	xx	n/d	n/d	n/d	n/d	(Takada *et al.*, 1994; Yamaguchi *et al.*, 1999)

Summary of Unpublished Expression Data

		E7.5-E8.5			E9.5		E10.5		E11.5		E12.5		E13.5		Source
		Noto/Node	NSB	CLE	Noto	CNH	Noto	CNH	Noto	CNH	Noto	CNH	Noto	CNH	
Protein (IHC)	Ptk7	x	x	x	x	x	x	x	x	x	x	x	x	x	Fig. 3.4-8
	Ptk7 (uncleaved)				-	x	-	x			-	x			Fig 3.2-3
	Fzd6	xx	x	-	xx	x			xx	x	xx	x	xx	x	Fig. 3.9-10
	Vangl2	xx	x	xx	xx	x	xx	x	xx	x	xx	x			Fig. 3.11-13
mRNA (ISH)	Pk1	x	x	x	x	x	x	x							Fig 3.1
	Ptk7	x	x	x	x	x	x	x							Wilson Lab
	Wnt5a	x	x	x	x	x	x	x							Wilson Lab

Table 3.2 Summary of published in situ reports for genes associated with Wnt/PCP signalling, and summary of findings in this thesis, including unpublished data from the Wilson lab.
Light green **(x)** - reports of genes expressed in primitive streak, node, caudal lateral epiblast or tailbud during axial elongation, Dark green **(xx)** - reports of distinct high expression in these regions, Grey (n/d)- no data or (n/s) no sections of this region reported, Red **(-)** no expression of gene in region. References for published reports or associated figures included on right hand column. Primitive streak (PS), node-streak border (NSB), caudal lateral epiblast (CLE), tail bud (TB), notochord (noto), in situ hybridisation (ISH), immunohistochemistry (ISH).

3.4 Visualising polarity during development by examining organelle location

Planar cell polarity is not only characterised by the presence and asymmetry of key Wnt/PCP protein components but also by the positioning of cellular structures, the most described being the cells of the inner ear whose hair bundles coordinate to orientate in a unified direction when Wnt/PCP is active (Curtin et al., 2003; Montcouquiol et al., 2003; Wang et al., 2006). In lieu of hair bundles during early embryonic development an alternative indicator of polarity was sought. Organelles within cells, including cytoskeleton components (Centrosomes) and endomembranes (Golgi), provided good alternatives, as their relative localisation indicates the polarity of the cell (Bornens, 2008; Burute et al., 2017). Of particular interest was the use of Golgi apparatus to track polarity, which had been previously described in the literature to examine polarity changes during EMT in chick (Boehm et al., 2010; Nakaya and Sheng, 2009).

Therefore, to gather information about polarity in early Mouse development, specifically in regions where NMPs reside, immunohistochemistry was performed using antibodies for nuclear envelope (LaminB1), to track individual cells and Golgi apparatus (GM130) to examine individual cell polarity.

3.4.1 –Optimisation of Nuclear Envelope and Golgi Immunohistochemistry

LaminB1 antibody from Abcam was used to track nuclear envelope in three dimensions in wholemount embryos. LaminB1 protein contributes to the nuclear envelope (Camps et al., 2015) and therefore the use of this antibody permitted the visualisation of the outer surface of the nucleus. This was advantageous versus DAPI, which is not specific to the nuclear envelope, but instead labels the whole nucleus, including structures within. LaminB1 immunohistochemistry was performed on an E6.5 prestreak embryo (Fig. 3.15A). Panning through the embryo showed that nuclei of neighbouring cells were closely associated in all three dimensions, within individual z-planes, and between z-planes (Fig. 3.15Aa-h). Despite this close association being neighbouring cells LaminB1 allowed for easy distinction between individual cells, which would not be possible with DAPI staining. Immunohistochemistry of nuclear

envelope were then performed on later embryonic stages E8.5-E10.5 (Fig. 3.15B-D). Unfortunately, LaminB1 failed to show distinct nuclear envelope staining in thicker specimens, with nuclear envelope intensity decreasing with increasing thickness. This was particularly disappointing for the E9.5 tail bud for which individual cells of the notochord and CNH could were not detectable (Fig. 3.15D).

To improve antibody penetration, increasing primary and secondary antibody temperature was trialled (Fig. 3.16). Unfortunately increasing incubation temperature for primary and/or secondary antibody made no difference to the detection of nuclear envelope in thicker tissue. In all conditions, consistent disparities between LaminB1 detection on the surface and in the core of specimens was present (Fig. 3.16A-D).

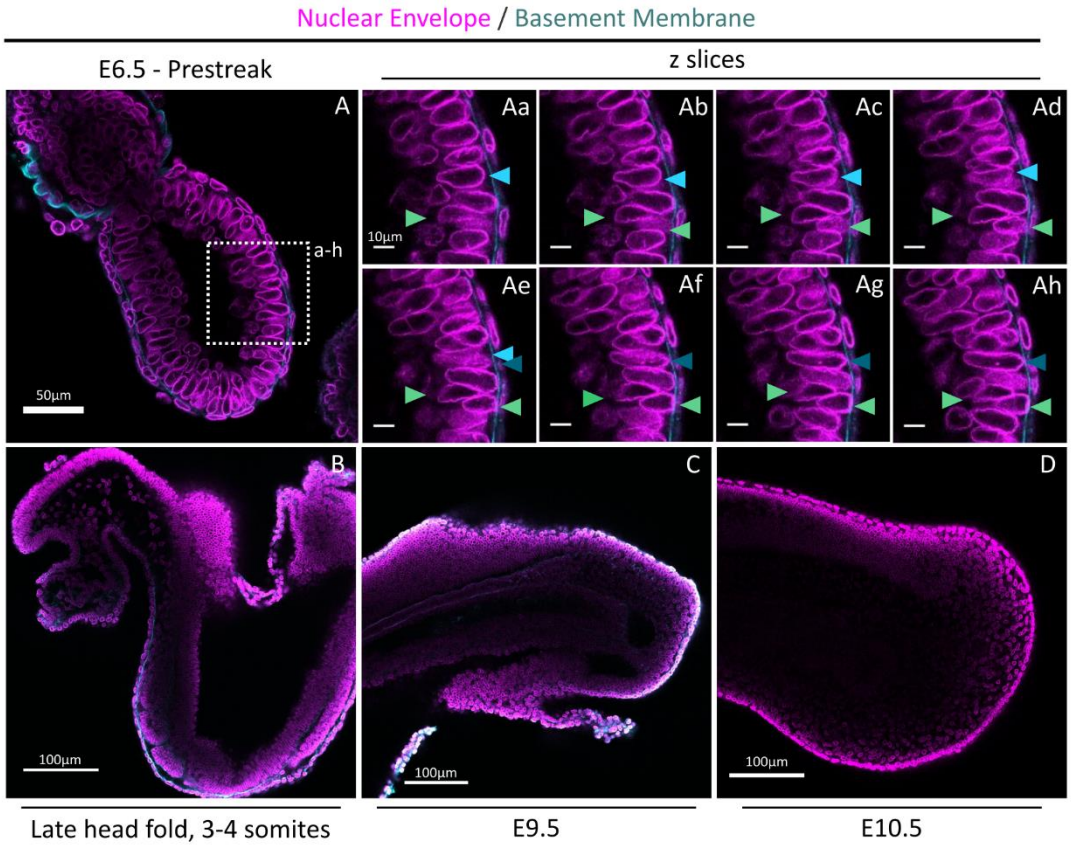

Figure 3.15 LaminB1 (Nuclear Envelope) immunohistochemistry from E6.5 to E10.5.
Wholemount confocal images of LaminB1 immunohistochemistry of **(A)** E6.5 prestreak embryo, with magnified region (Aa-Ah) showing cells are closely associated within (green arrows) and between (blue arrows) z-slices. In **(B)** Late headfold (3-4 somites) (anterior on left, posterior on right), **(C)** E9.5 tail bud and (D) E10.5 tailbud, LaminB1 intensity is lost in thicker tissues. Nuclear envelope - magenta, Basement Membrane - cyan. Embryos positioned anterior to right, posterior to left.

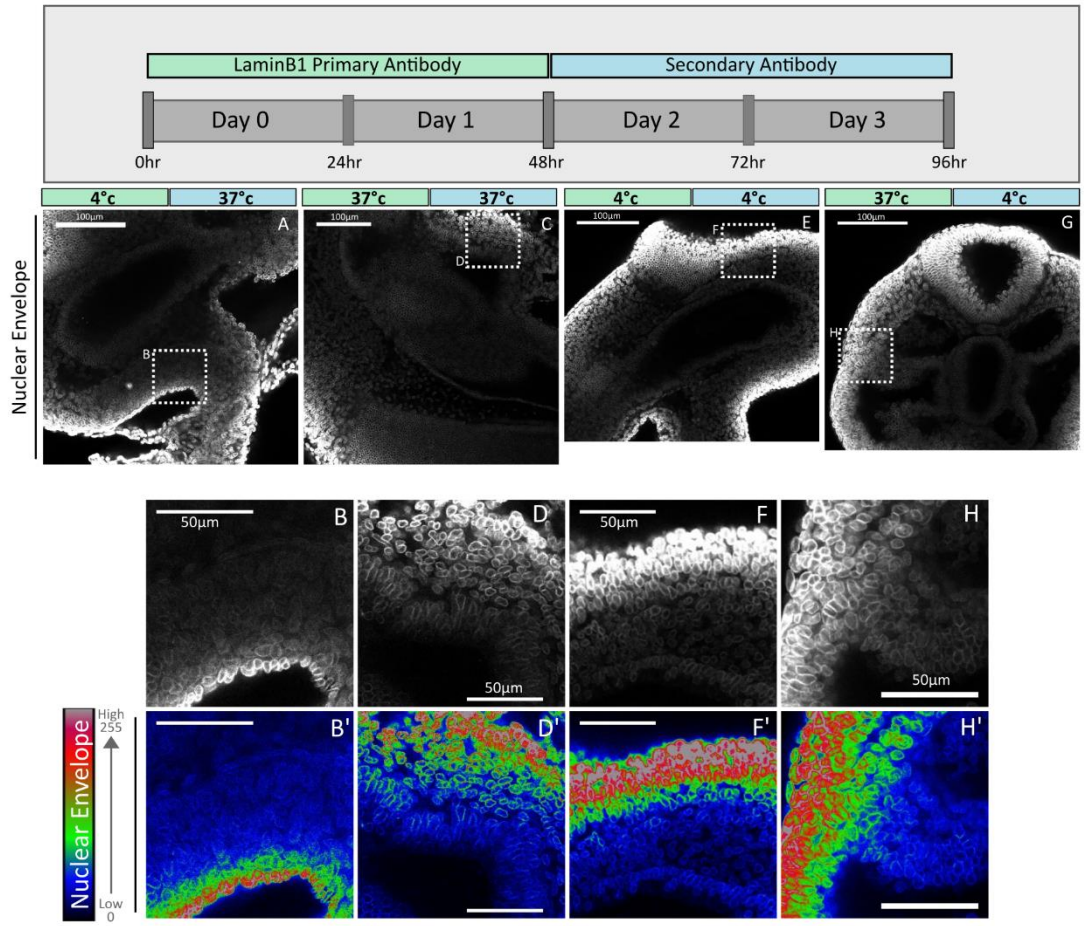

Figure 3.16 LaminB1 (Nuclear Envelope) Trialled Optimisation.
Above is overview of trialled optimisation of LaminB1 immunohistochemistry to improve signal penetrance. Despite increasing temperature of primary and/secondary antibody incubation, a significant disparancy of signal intensity was observed between cells on the surface and those in deeper tissues. (A,C, E,G). 1-4 shows LaminB1 staining (greyscale) for each condition, and magnified area for each B,D,F,H respectively, LaminB1 – grayscale or rainbow LUT.

Optimisation of organelle specific antibodies was then undertaken. An Abcam antibody specific for cis-Golgi matrix protein (GM130), a key protein found in Golgi membrane (Nakamura et al., 1995) was trialled on E7.5 embryos using a number of different fixatives. Immunohistochemistry with methanol was unsuccessful, however fixation with PFA and PFA-Triton enabled visualisation of Golgi (Fig. 3.17A-B). Golgi detection was cleaner, (less background) and clearer (defined punctate staining) with PFA-Triton fixation versus PFA alone. As distinct Golgi visualisation was essential for visual analysis of cell polarity, PFA-Triton fixation was preferentially used as the fixation method in subsequent experiments.

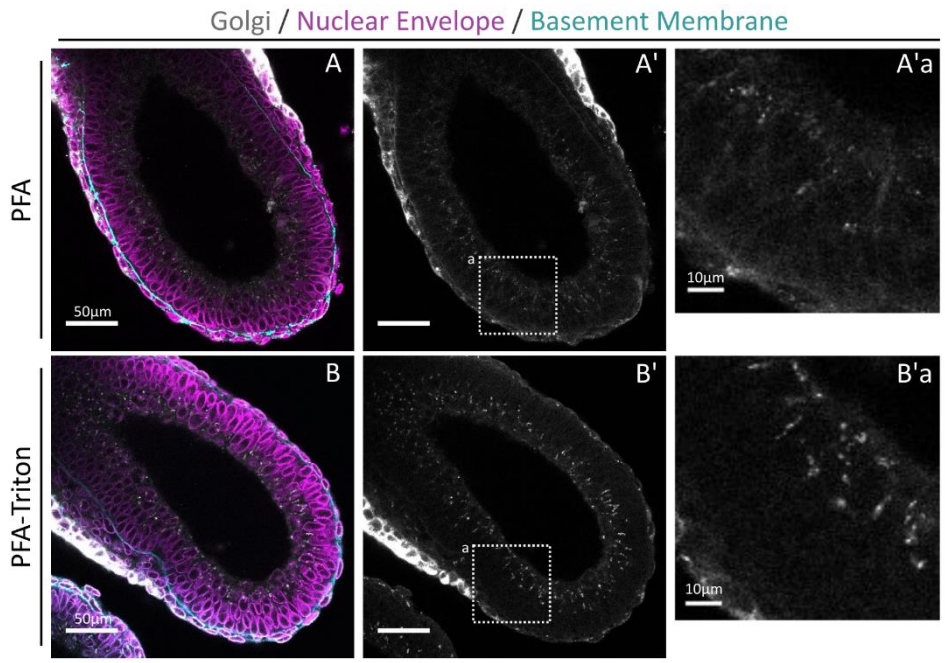

Figure 3.17 GM130 (Golgi) immunohistochemistry optimisation.
GM130 (Golgi) immunohistochemistry on prestreak embryos resulted in cleaner and clearer visualisation of Golgi using **(B)** PFA-Triton fixed embryos versus **(A)** PFA fixation alone. Dashed bounded box depicts magnified images on the right. GM130 (Golgi) – grayscale, basement membrane – cyan, nuclear envelope - magenta.

3.4.2 –Polarity visualisation from prestreak to E11.5

Previously examination of cell polarity dynamics during early Mouse development had only been briefly described in the literature. This was limited to early gastrulation, when polarity of cells was monitored undergoing epithelial to mesenchymal transitions (EMT) in the primitive streak, through analysis of nucleus-centrosome axes (the axis drawn from the nucleus to the centrosome) (Burute et al., 2017). In the epiblast Centrosomes were initially localised close to the cavity, resulting in coordination of nucleus-centrosome axes throughout the epiblast towards the cavity. This coordination was then lost at the onset of EMT when Centrosomes repositioned in individual cells to point towards the streak, resulting in the nucleus-centrosome axes thus becoming inverted as cells travelled through the streak. To understand the dynamics of cell polarity and cell movement in NMP stages in a similar way, nuclear envelope (LaminB1) and optimised Golgi (GM130) co-staining and 3D confocal imaging was performed on embryos from E6 (prestreak) to E11.5.

In pre-streak embryos, epiblast Golgi faced inwards towards the proamniotic cavity as previously described in the literature for Centrosomes (Burute et al., 2017) (Fig. 3.18A). Visually assigned nucleus-Golgi axes (by proximity) indicated that individual cells were polarised towards the cavity and together cells were coordinated in this polarity throughout the epiblast (Fig. 3.18Aa-i).

In streak stage embryos, the streak was located by the absence of basement membrane in transverse views (Fig. 3.19A). Cells of the epiblast not in the primitive streak had Golgi localised close to the proamniotic cavity, suggesting they were polarised towards the cavity akin to cells of pre-streak embryos (Fig. 3.19B). However, cells located in the streak did not show similar alignment of polarity to the proamniotic cavity. Instead their polarity appeared random and uncoordinated (Fig. 3.19B). This was also clear in transverse views were the positioning of Golgi in streak areas was further from the cavity than in the epiblast (Fig. 3.19C-D). These findings were in agreement with previously documented observations during Mouse gastrulation using Centrosomes, and with Golgi staining described for the chick during epithelial to mesenchymal transitions (EMT) (Burute et al., 2017; Nakaya and Sheng, 2009). As these findings were in keeping with previous reports of polarity and cell movement at this stage, later embryos, which had not previously been documented in the literature, were subsequently analysed.

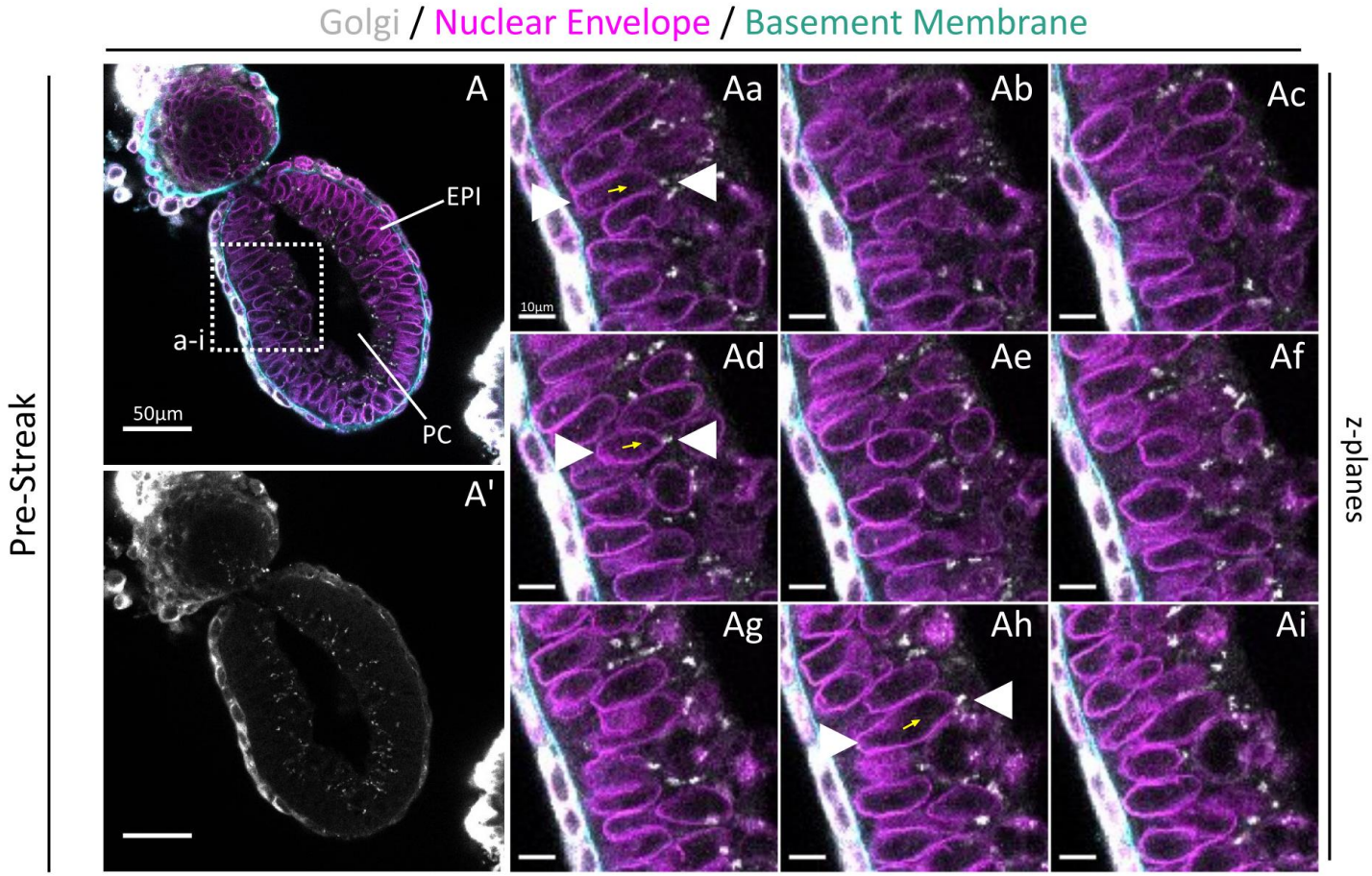

Figure 3.18 - Polarity in pre-streak embryos.
Confocal images from wholemount immuno-histochemistry using Gm130 (Golgi) – grayscale, LaminB1 (nuclear envelope) – magenta and collagen IV (basement membrane) – cyan, on **(A)** pre-streak embryos. Cells of the epiblast (EPI) are aligned to the proamniotic cavity (PC), yellow arrowheads show assigned nucleus-Golgi vector of individual cells bounded by white arrowheads (Aa-Ai)

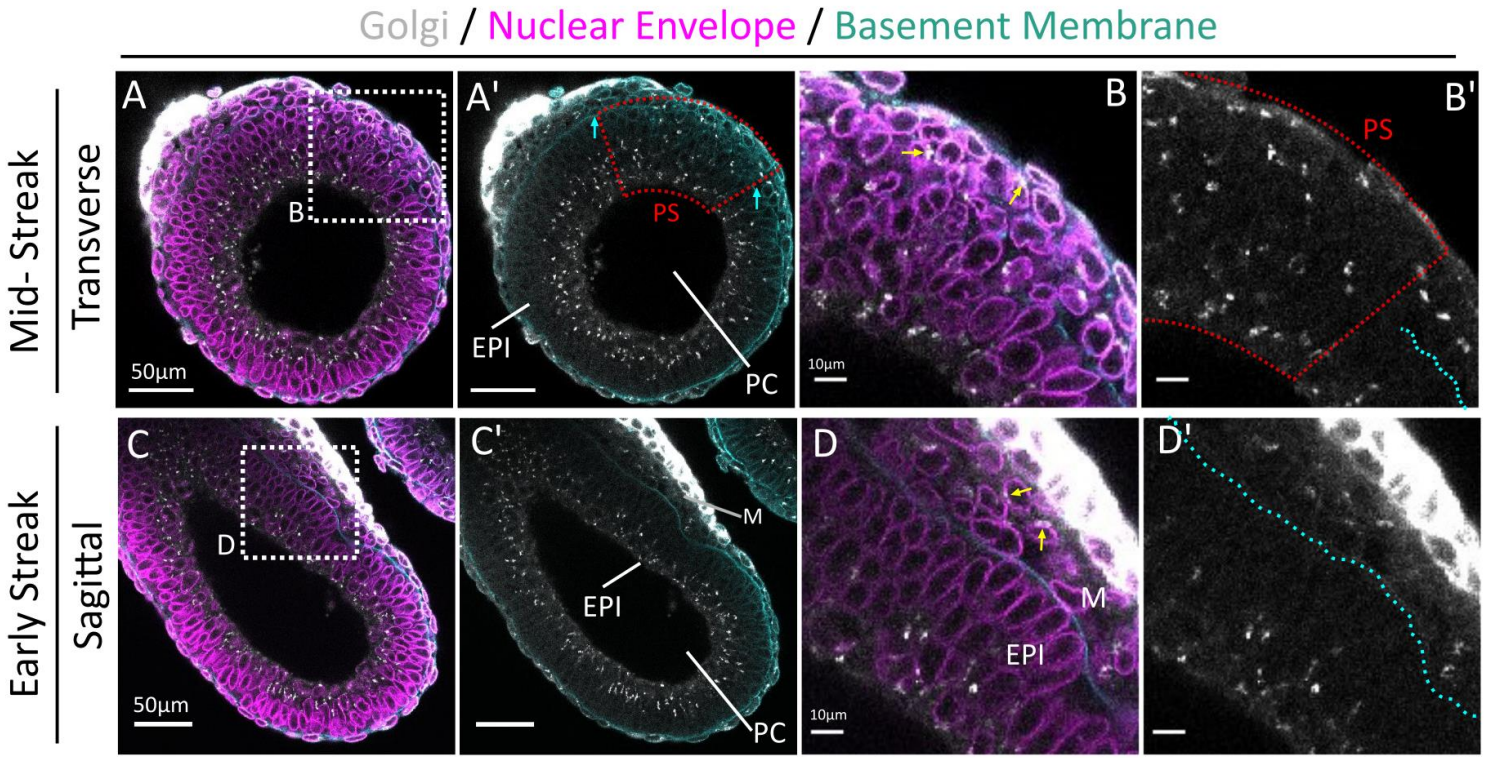

Figure 3.19 - Polarity in mid-streak embryos.
Confocal images from wholemount immunohistochemistry using Gm130(Golgi) – grayscale, LaminB1 (nuclear envelope) – magenta and collagen IV (basement membrane) – cyan, on **(A)** Mid-streak (transverse z-slice) **(B)** early streak (sagittal z-slice). Cells of the epiblast (EPI) are aligned to the proamniotic cavity (PC). In streak embryos, primitive streak (PS) is marked by loss of basement membrane (cyan). Cells within the PS and in the presomitic mesoderm (M) are not coordinated in their polarity (yellow arrows).

A sagittal view of an early somitogenesis embryo, permitted assessment of polarity in multiple tissue types (Fig. 3.20A). Unfortunately, nuclear envelope staining was not adequate to determine the polarity of individual cells, however an impression of polarity was possible by considering the position of Golgi within tissues. In the somites, all Golgi faced the centre of the somite, suggesting that all cells were aligned in their polarity (Fig. 3.20B). Alignment of Golgi was also found in the CLE at the posterior of the embryo where NMPs reside, but not in adjacent presomitic mesoderm where Golgi localisation appeared random (Fig. 3.20C). Examining transverse z-planes of the posterior showed this area in more detail (Fig. 3.21A-E). NMPs within the CLE had Golgi localised to the cavity, whilst cells in the presomitic mesoderm and streak had random Golgi positioning. In addition, cells within the node and crown of the node showed uniform polarity with the Golgi apparatus facing the ventral side of the embryo (Fig. 3.21A). NMPS residing in the CLE remained apical-basally polarised throughout the posterior z-planes, and appeared to exhibit uniform polarity from medial to lateral regions.

At E9.5, the nuclear envelope staining was again incomplete for cells deepest within the tissue, meaning individual cells and their individual polarity could not be determined, however despite this observations of polarity could still be made. Golgi of neuroectodermal cells were polarised toward the ventricular side (Fig. 3.22A-B). Cells in the underlying notochord did not display the same coordination, and Golgi position in this tissue appeared random (Fig. 3.22B). This was akin to the tail bud mesoderm which also exhibited random Golgi localisation (Fig. 3.22C). Transverse views through the posterior of the E9.5 tail supported observations of random Golgi localisation in tail bud mesoderm and coordination of neuroectoderm Golgi to the dorsal edge (Fig. 3.22D). However, this coordination was not consistent throughout the whole neuroectoderm and appeared to be lost at the caudal neuropore, the region which subsequently closes to form the caudal neural tube containing the CNH (Nikolopoulou et al., 2017). At the caudal neuropore localisation of Golgi at the dorsal neuroectoderm edge was observed in lateral regions, however at the midline coordinated Golgi localisation appeared to be lost and instead was random resembling that of cells at the primitive streak (Fig. 3.22D).

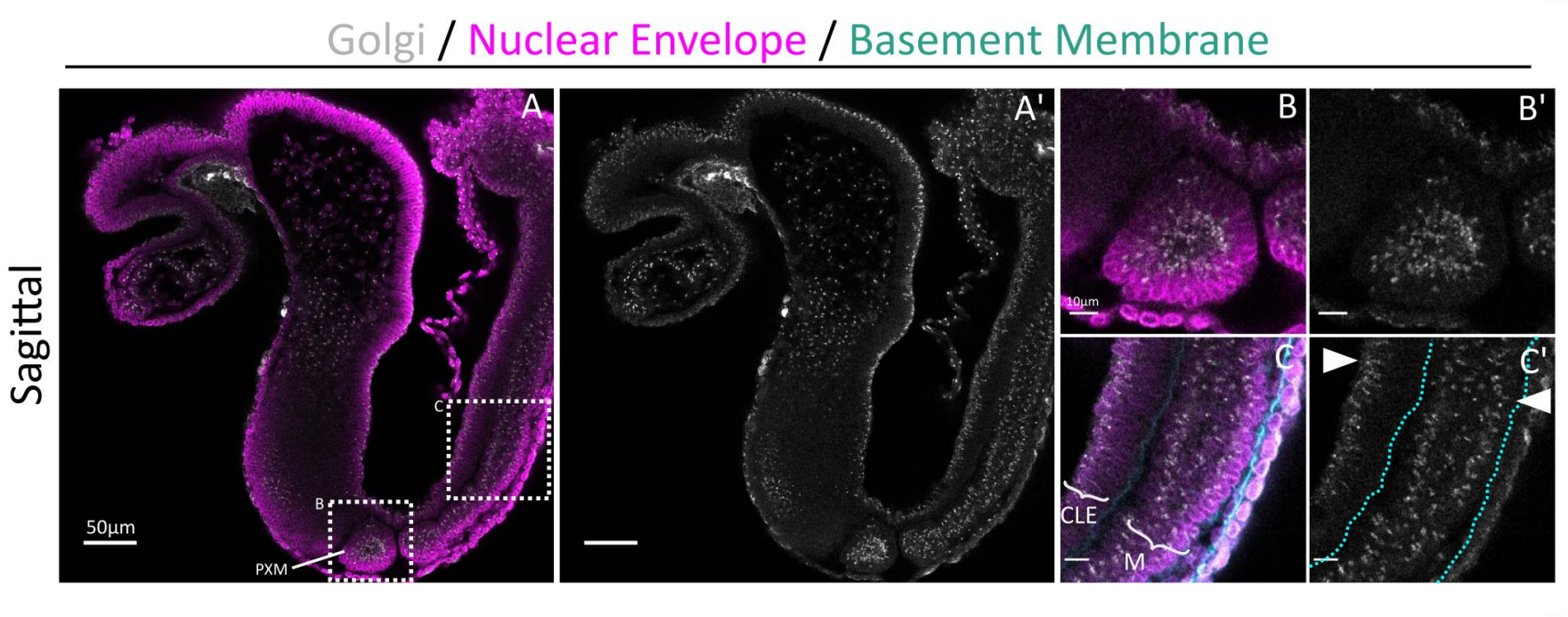

Figure 3.20 - Polarity during early somitogenesis.

Confocal images from wholemount immunohistochemistry using Gm130(Golgi) – grayscale, LaminB1 (nuclear envelope) – magenta and collagen IV (basement membrane) – cyan, on embryo during early somitogenesis. Nuclear envelope staining was not optimal enough to allow the polarity of individual cells to be monitored. **(A)** Sagittal z-slice, showed coordinated Golgi in the **(B)** paraxial mesoderm (PXM) and **(C)** posterior embryo regions including NMPs in the caudal lateral epiblast (CLE) and the presomitic mesoderm (M).

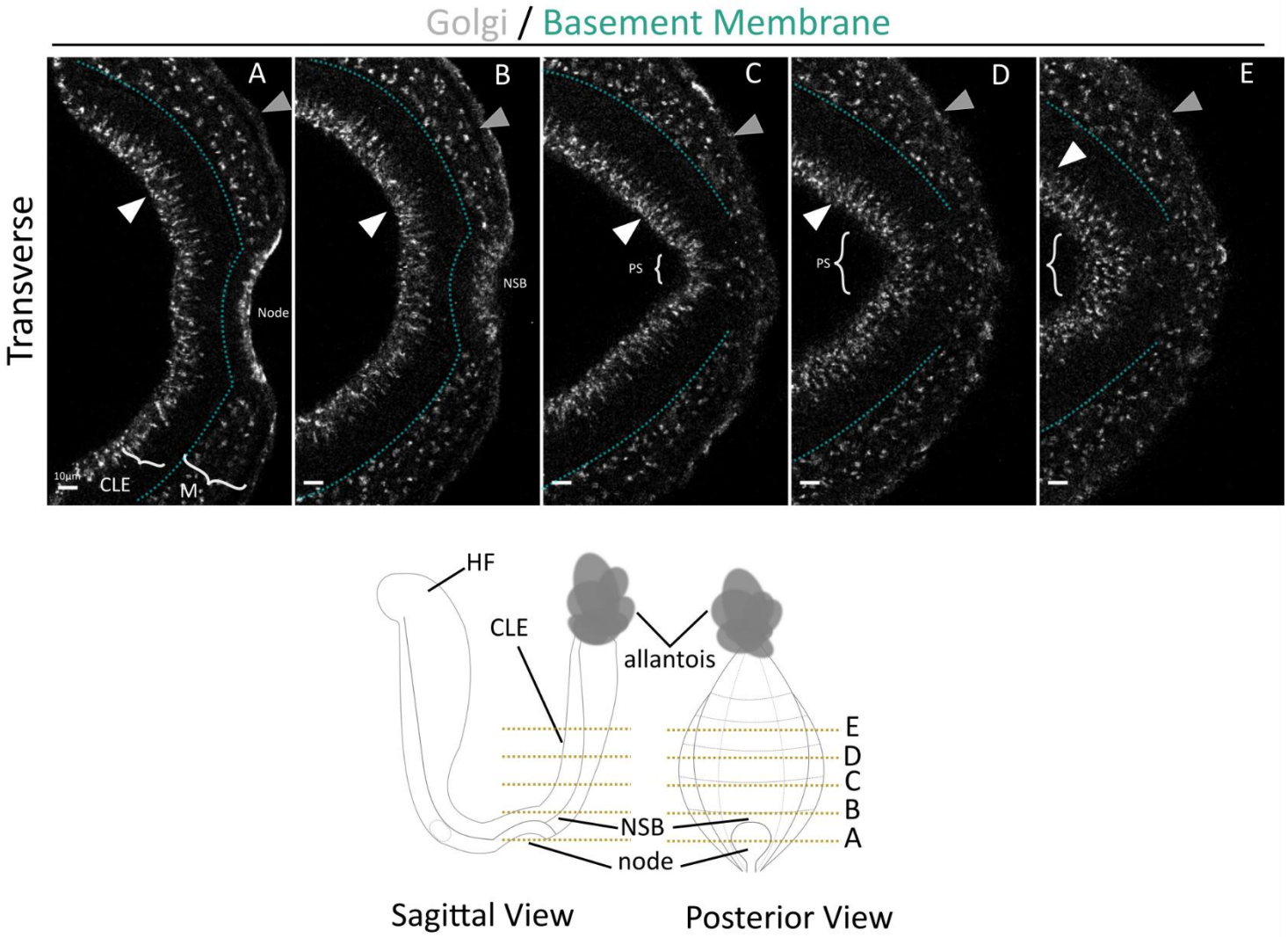

Figure 3.21 - Polarity in the posterior embryo during early somitogenesis.
Confocal images from wholemount immuno-histochemistry using Gm130(Golgi) – grayscale, and collagen IV (basement membrane) – cyan- added dashed line, on embryos during early somitogenesis.
Schematic below indicates approximate distal to proximal location of z-slices (A-E). NMPs in the CLE (white arrows), and cells of the node and the node streak border (NSB) are polarised. Cells of the primitive streak (PS) and presomitic mesoderm (M) (grey arrows) are not.

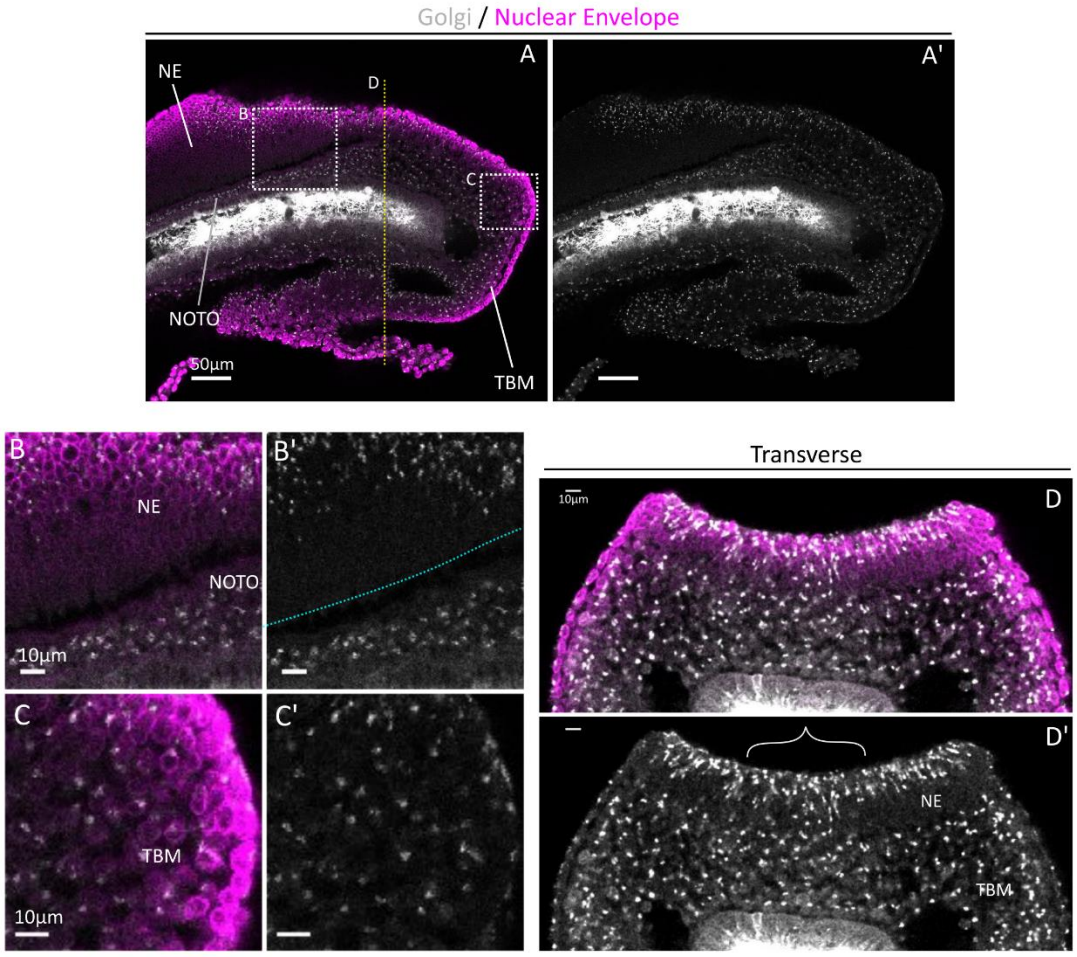

Figure 3.22 - Polarity in E9.5 tail bud.
Confocal images from wholemount immunohistochemistry using Gm130(Golgi) – grayscale, LaminB1 (nuclear envelope) – magenta and collagen IV (basement membrane) – cyan, on E9.5 tail bud. **(A)** Sagittal z-slice, showing coordinated Golgi in the polarised **(B)** neuroectoderm (NE), and uncoordinated Golgi in the notochord (NOTO) and **(C)** tail bud mesoderm (TBM). (D) Transverse z-slice (yellow dashed line on A shows approximate anterior-posterior z-slice position), through CNH region shows cells at the midline (brackets) are not polarised and resemble those found in the streak.

At E10.5 and E11.5 similar observations were made. Golgi in the tail bud mesoderm again had random localisation, whereas Golgi in the neural tube were coordinated (Fig. 3.23 and Fig. 3.24). However, Golgi at the most posterior tip of the neural tube, the CNH, appeared slightly less coordinated than Golgi in the dorsal or more anterior neural tube, at both E10.5 and E11.5 (Fig. 3.23D,F, Fig. 3.24B,E). Transverse views highlighted these differences, with anterior neural tube tissue appearing to have Golgi closely localised to the neural tube cavity, whilst in more posterior neural tube, Golgi within the CNH appeared to be localised randomly akin to those in the primitive streak (Fig. 3.23D,F, Fig. 3.24B,E). This was clearer in E10.5 embryos but also appeared to be present in E11.5.

In summary, the analysis of polarity and cell movement using Golgi positioning in early embryos reflected that previously reported in the literature and thus encouraged analysis of later embryonic stages which had not yet been investigated. In embryos undergoing early somitogenesis cells of the node, node-streak border and NMPs residing in the CLE have uniform polarity towards the amniotic cavity. Conversely this polarity was lost as cells underwent EMT and travelled through the streak, forming unpolarised presomitic mesoderm, akin to observations of previous embryo stages. Across later stages of axial elongation (E9.5 to E11.5) Golgi in mesoderm derivatives; notochord and tail bud mesoderm, were not coordinated in their localisation or alignment. In neuroectoderm, cells were polarised to the dorsal edge, except for regions of the CNH, where NMPs reside. Cells of the CNH appeared to be less coordinated in their polarity with random Golgi localisation reflecting that of the primitive streak. This suggests that NMPs in the CNH may be losing polarity and undergoing cell movements similar to that of the primitive streak.

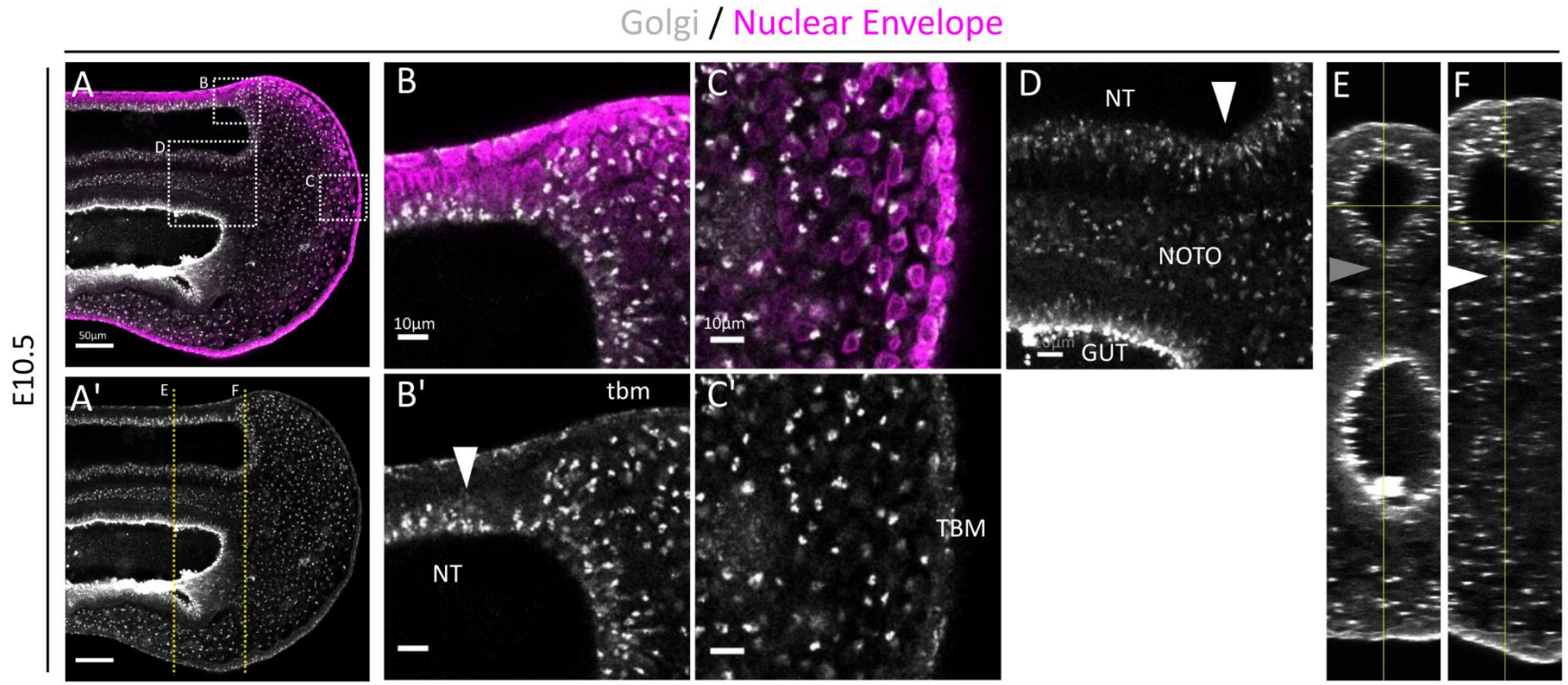

Figure 3.23 - Polarity in E10.5 tail bud.
Confocal images from wholemount immunohistochemistry using Gm130(Golgi) – grayscale, LaminB1 (nuclear envelope) – magenta and collagen IV (basement membrane) – cyan, on **(A)** E10.5 tail bud. At E10.5 cells in the **(B)** neural tube (NT), **(C)** tail bud mesoderm (TBM) and **(D)** notochord (NOTO). Transverse z-slices through **(E)** anterior and **(F)** posterior tail bud (approximate positions of these are shown by yellow dashed lines in **(A)**, show cells in the CNH (white arrows) of posterior slices are less polarised than those in anterior regions (grey arrow).

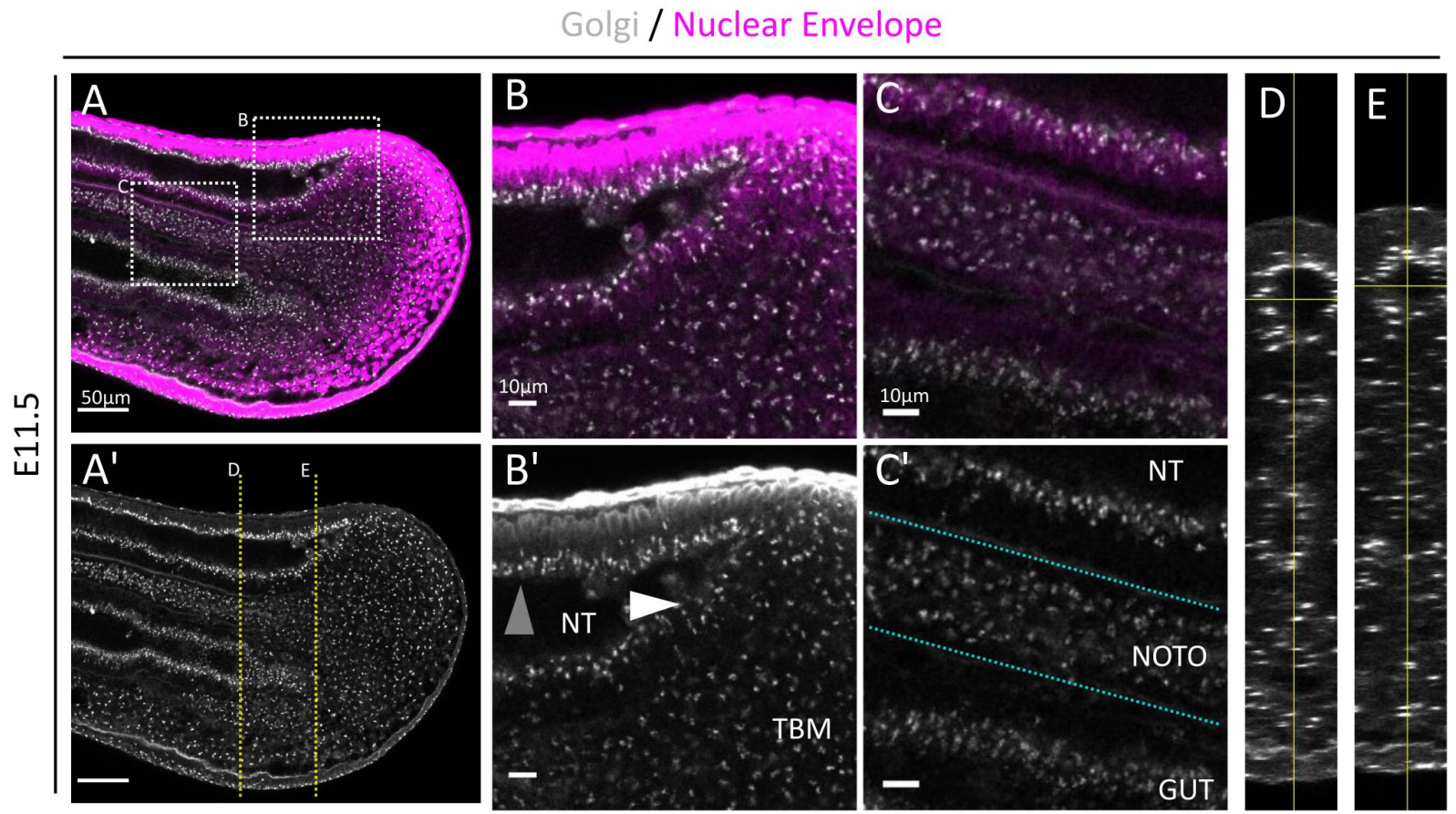

Figure 3.24 - Polarity in E11.5 tail bud.

Confocal images from wholemount immunohistochemistry using Gm130 (Golgi) – grayscale, LaminB1 (nuclear envelope) – magenta and collagen IV (basement membrane) – cyan, on **(A)** E11.5 tail bud. At E10.5 cells in the **(B)** neural tube (NT), **(C)** notochord (NOTO) and Gut are shown. Transverse z-slices through **(D)** anterior and **(E)** posterior tail bud (approximate positions of these are shown by yellow dashed lines in **(A)**. Cells in the CNH (white arrows, **(B')** of posterior regions are less polarised than those in anterior regions (grey arrow). This is also visible in the sagittal anterior and posterior planes of view **(D-E)**.

3.5 Discussion

3.5.1 The profile of Wnt/PCP components implicates Wnt/PCP signalling in regulating NMP behaviour

From the comprehensive review of published expression data for Wnt/PCP components in (1.4.5) it appeared that Wnt/PCP components may be expressed at the right time and in the right place for Wnt/PCP signalling to potentially regulate the behaviour of NMPs. However, this published data was far from complete, specifically for the CLE and CNH, and thus it remained unclear if Wnt/PCP components were indeed expressed there. The objective of the work described in this chapter was to address some of these limitations, with much of the research focused on examining the protein localisation of key Wnt/PCP components in NMP regions.

Pk1, Ptk7 and Vangl2 were all found to be expressed in the CLE, where NMPs reside at the onset of somitogenesis (Fig. 3.1; Fig. 3.2-8; Fig. 3.11-3). The presence of these Wnt/PCP components in the CLE supports the contention that Wnt/PCP signalling could regulate NMP behaviour. Generally, it is assumed that all members of the core Wnt/PCP pathway are needed for this pathway to be active. Despite attempts to investigate the presence of other members including, Celsr, Dvl, Ror and Fzd this was not possible with the available (sub-optimal) antibodies. However, support for the presence of these additional components comes from other published reports. All members of the Celsr family have been reported to be expressed in the CLE (Crompton et al., 2007) and *in situ* hybridisation reports for *Dvl1* and *Ror2* described expression in the adjacent primitive streak but did not report sections to confirm expression in CLE regions (Bois et al., 1996; Matsuda et al., 2001). The only family members that have been shown to be unequivocally absent in CLE regions include Fzd6, which was limited to expression in node, node-streak border, and notochord (Fig. 3.9-10), *Pk2*, and Wnt co-receptor *Ror1* (Crompton et al., 2007; Matsuda et al., 2001). However, these represent single members of larger families which have functional redundancy between members, and as discussed, these other family members including *Pk1* and *Ror2* have been shown to be expressed either in or adjacent to the CLE. Therefore, evidence provided in this thesis, reinforces the belief that most Wnt/PCP components are present in NMPs residing in the CLE supporting their potential role in regulating NMP behaviour.

Previously expression of Wnt/PCP components had been reported in the tail bud but never confirmed in the CNH region, where NMPs reside. This present work confirms that *Pk1*, Vangl2 and Ptk7 are broadly expressed in the tail bud during axial elongation. *Pk1* expression was confirmed in the CNH (Fig. 3.1) from E9.5 to E10.5 in line with previous reports (Bekman and Henrique, 2002; Crompton et al., 2007), and Vangl2 and Ptk7 protein were confirmed to be in the CNH from E9.5 to E12.5/13.5 (Fig. 3.13, Fig.3.2-3, 3.7-8). Despite not being able to verify the presence of other components in the CNH, the continuity between the streak and the CNH that has been reported before (Cambray and Wilson, 2002) suggests that the expression of Wnt/PCP components in the streak may be conserved in the CNH. Of course, this is not yet proven, and further examination of this region is needed to confirm this hypothesis. As with the CLE, few Wnt/PCP components have been reported to be absent in the tail bud, these include, *Ror1* and *Fzd7*. As for other components, many have been reported to be expressed in the tail bud but not confirmed specifically in the CNH. Therefore, despite less reports of Wnt/PCP components in the literature, the work outlined in this chapter has supported the concept that Wnt/PCP signalling may regulate NMPs in the CNH throughout axial elongation.

Another interesting finding is that examined Wnt/PCP components do not appear to weaken in their expression towards the end of axial elongation at E13.5. Moreover it has previously been reported that the expression of components involved in regulation of NMPs, including Fgf8 and Wnt3a decline as tail elongation arrests, with levels significantly decreased by E12.5 (Cambray and Wilson, 2007). Vangl2 (Fig. 3.13), Ptk7 (Fig. 3.8) in CNH and Fzd6 in the notochord (Fig. 3.10) appear to maintain the same expression levels throughout axial elongation including between E12.5-E13.5 stages. This suggests that if Wnt/PCP is involved in regulating NMP behaviour it is not directly regulating the cessation of axial elongation.

3.5.2 Asymmetric distribution of Vangl2 in CLE suggests activity of Wnt/PCP signalling

Asymmetry of Wnt/PCP components is important for the establishment and propagation of Wnt/PCP signalling across polarised tissues, and therefore considered a read out of Wnt/PCP activity. Vangl2 and Fzd6 protein has been previously reported

in the literature in other systems, including the cells of the inner ear and limb bud development, in which their asymmetric distribution is associated with active Wnt/PCP signalling (Gao et al., 2011; Montcouquiol, 2006). I hoped to examine the presence of asymmetry to confirm the activity of Wnt/PCP signalling in NMP regions during axial elongation. In my investigations Vangl2 was found to be localised to the membrane in NMP-containing regions, the CLE and the CNH throughout axial elongation (Fig. 3.11-13). Despite this membrane localisation of Vangl2 identification of asymmetry was difficult in these tissues. Over all stages examined, Vangl2 was only identified as asymmetric across multiple cells during early somitogenesis (Fig. 3.11). Vangl2 protein in NMPs of the CLE appeared to be predominantly localised to lateral membranes and absent from apical (cavity facing) or basal (basement membrane facing) membranes, and thus polarised along the anterior-posterior axis. Although this asymmetry isn't as clear as that previously described for the inner ear, it is akin to that described for epidermis development in which the cells are asymmetrically polarised along the anterior posterior axis (Devenport and Fuchs, 2008; Montcouquiol, 2006). These observations support the hypothesis that Wnt/PCP is active in NMPs residing in the CLE. However, it is not clear if Wnt/PCP is active across all regions of the CLE, thus further investigation into Vangl2 distribution in this tissue is necessary. The CLE is a curved epithelium, making observations of polarity across the tissue difficult. Confocal microscopy may provide the best alternative to analyse the distribution of Vangl2 as it can provide three-dimensional information about Vangl2 localisation. In summary, the observations provided in this chapter confirm that Wnt/PCP is active in some NMPs of the CLE, and promotes investigations into its functional role regulating NMP behaviour at this developmental stage.

Despite identification of membrane localised Vangl2 in NMP regions in all stages examined, coordinated asymmetry of this protein across multiple cells was never clearly identified in the CNH, and this complicates interpretation of whether Wnt/PCP is truly active in NMPs of the tail bud (Fig. 3.12). The reasons for these observations could be threefold; Vangl2 asymmetry could be present but the orientation of the tissue may preclude its visualisation, or Wnt/PCP signalling could be active but its activity does not require asymmetric distribution of components, or these areas may not have Wnt/PCP activity. To understand which possibility is the most likely it is necessary to

take in to consideration findings published for other systems in which Wnt/PCP is active, this is described below.

Reports in dynamic and complex tissues during chordate development, present difficulties in examining asymmetric distribution compared with simple *Drosophila* or vertebrate inner ear models. In Mouse epidermis Vangl2, Celsr and Fzd6 asymmetric localisation has been verified by exploring different planes of view (Devenport and Fuchs, 2008). Sagittal views obscured the asymmetric localisation of components, however, the use of planar views dramatically improved visualisation of asymmetry across many cells. Due to the complex nature of the CNH in the work presented here sagittal sections were utilised. However, this may have prevented easy observation of asymmetric distribution. Unlike the epidermis however, the CNH is not composed of a simple epithelium, but is more complex and three-dimensional. It is therefore difficult to know what plane would be best to examine asymmetric localisation of components. For this reason, future investigations should focus on imaging these cells with confocal imaging which would allow multiplane/multiangle investigations into the distribution of Vangl2 in the CNH.

The second possibility for why coordinated asymmetry is not present, is that asymmetry may not be essential for Wnt/PCP activity. Wnt/PCP signalling has been shown to be essential for the elongation of the limb bud, and CE in the node and notochord in Mouse, however the asymmetric localisation of Wnt/PCP components in these regions have remained elusive. In the limb bud, Vangl2 protein localisation is biased in some cells but the orientation of this bias is not coordinated across the whole tissue (Gao et al., 2011). Additionally, Vangl1 has been reported in the notochord during early Mouse development, but this does not appear to be asymmetric in the majority of cells (Andre et al., 2015). Together this work suggests that asymmetry of Wnt/PCP components including Vangl2 may not need to be coordinated across every cell for Wnt/PCP to be active. However, this idea opposes findings in *Drosophila* in which asymmetry of components is essential for generating and propagating Wnt/PCP across tissues (reviewed in Yang and Mlodzik, 2015). This paradox between *Drosophila* and vertebrate systems may be resolved by considering the complexity and three-dimensional nature of vertebrate systems in which Wnt/PCP may operate via

different mechanisms. However, this proposal remains untested. Overall the pattern of Vangl2 localisation observed in the CNH is akin to other tissues, namely node, notochord and limb bud, in which Wnt/PCP was found to be active, but asymmetric distribution was not visualised in every cell. Thus, the apparent lack of coordination in Vangl2 asymmetry across the CNH, does not necessarily determine that Wnt/PCP is not active in these regions.

Other evidence supports the idea that Wnt/PCP is active in these regions. In Wnt/PCP mutants Vangl1 and Vangl2 asymmetrical localisation is reported to be lost in cells of the inner ear, limb bud and notochord (Andre et al., 2015; Gao et al., 2011; Qian et al., 2007). In these mutants Vangl2 localisation is found to be more unbiased and diffuse across the membranes of individual cells, with an overall loss of signal intensity at boundaries. The Vangl2 localisation observed in the CNH regions does not reflect the Vangl2 distribution in Wnt/PCP mutants. In CNH regions Vangl2 is observed to be intensely localised on some but not all membranes equally, and thus it does not appear to be diffuse or uniformly distributed throughout the membranes of individual cells. Thus, although no coordination in asymmetric distribution of Vangl2 is obvious in these cells, the strong membrane localisation of Vangl2 which is not uniformly distributed, provides support for the idea that Wnt/PCP is active in these regions.

Taken together the distribution of Vangl2 observed in the CNH, along with published observations in other systems supports the idea that Wnt/PCP is likely to be active in the CNH. As mentioned further investigations need to be carried out to understand more about the true nature of Vangl2 localisation in these areas and to examine other read outs of tissue polarity within these areas.

In summary, evidence provided in this thesis lends further support to the belief that Wnt/PCP signalling is active in at least some NMPs of the CLE, encouraging further investigation into its role in regulating NMP behaviour. In addition, conservation of Wnt/PCP activity in the CNH is not as clear from the data collected so its role in this region remains contentious.

3.5.3 Wnt/PCP activity in NMP regions may be regulated by Wnt co-receptor Ptk7

Ptk7 is considered a Wnt signalling co-receptor, and has been identified as an important regulator of the Wnt/PCP pathway in many developmental processes including CE and gastrulation. However, many aspects of Ptk7 signalling function are still unknown and in different contexts it has been shown to interact with components of both Wnt/β-catenin signalling and Wnt/PCP signalling. This interaction with both pathways makes it particularly interesting in terms of NMP behaviour, as NMPs require a tight regulation of Wnt/β-catenin signalling for maintenance and differentiation. Ptk7 had previously been reported to be upregulated in caudal regions of the embryo (Paudyal et al., 2010), and in this chapter a key objective was to verify its expression in NMP regions during axial elongation.

For the identification of Ptk7 protein two antibodies were used, both detected Ptk7 levels to be highest in the tailbud in keeping with previous reports (Paudyal et al., 2010). Additionally in these observations Ptk7 protein was always membrane bound, a localisation known to be associated with Wnt/PCP activity (Berger et al., 2017a). However, notable differences in Ptk7 protein profile across the tailbud were found between the two Ptk7 antibodies. The first antibody (Abcam) recognises a 15 amino acid peptide sequence in the N-terminus found in the extracellular domain of Ptk7 protein, whilst the second antibody (Proteintech) recognises a peptide sequences towards the C-terminus in the cytoplasmic domain. Between these two antibody recognition sites lies a region which can be cleaved by MMP14, resulting in the production of a N-terminal soluble fragment and membrane bound C-terminal (Golubkov et al., 2010). Thus when the first antibody (Abcam) recognises membrane bound protein, this is uncleaved Ptk7. Conversely the second antibody (Proteintech) can detect both cleaved and uncleaved protein. This permitted the identification of regions in which Ptk7 cleavage was or was not present. The second antibody detected all forms of Ptk7, throughout the posterior region of pre-somitic embryos (from E7.5) and the tail bud to the end of axial elongation (E13.5), including NMPs residing in the CLE and CNH. However, the first antibody (Abcam) showed absence of uncleaved protein in the notochord, gut, surface ectoderm and closed neural tube from E9.5-

E12.5. This indicates that MMP-14 is likely to be expressed in these specific areas during axial elongation.

This difference is interesting in terms of how Wnt/PCP might be regulated in these areas. The functional relevance of this cleavage of Ptk7 by MMP14 isn't fully understood, however novel *Ptk7 chuzhoi* mutants which have an additional extracellular cleavage site exhibit neural tube defects synonymous with disruptions in CE and Wnt/PCP signalling (Golubkov and Strongin, 2012). It remains to be determined whether disruption in these mutants is caused by the additional shortening of the extracellular soluble fragment of Ptk7 protein, portions of which have known interactions with Wnt/PCP components (reviewed in Berger, Wodarz and Borchers, 2017), or due to quenching of MMP14 proteolysis which may prevent the normal physiological levels of cleaved Ptk7 protein. Either way, work reported here shows that cleaved Ptk7 is found specifically in the notochord, gut, closed neural tube and surface ectoderm. Interestingly Wnt/PCP regulation of CE has been reported extensively in the notochord, so the fact that cleaved Ptk7 is specifically found here suggests it may be involved the regulation of this process.

Thus, this research has identified the presence of Ptk7 protein in NMP regions throughout axial elongation. Questions remain on the functional role of Ptk7 in these areas, and if cleavage of Ptk7 determines the function of Ptk7. Altogether this evidence promotes further investigation into the role of Ptk7 in NMP dynamics.

3.5.4 Wnt/PCP may regulate other tissues during axial elongation

This chapter identified the presence of *Pk1*, Vangl2, Ptk7 in NMP regions during axial elongation. However strikingly these components were not limited to only NMP regions, and were sometimes even expressed higher in other non-NMP regions. This was particularly the case for Vangl2, whose expression was present in the node and notochord of late headfold embryos (Fig. 3.11), and later was highly expressed in the notochord from E9.5-E12.5 (Fig. 3.13). Additionally, Fzd6 protein was found to be exclusively expressed in the notochord, node and node-streak border in late headfold embryos (Fig. 3.9), and later restricted to notochord, including the anterior most CNH, underlying endoderm and surface ectoderm from E9.5- E13.5 (Fig. 3.9-10).

A role for Wnt/PCP signalling in the notochord is already well established in the literature, in which it regulates cell movements during CE (reviewed in Gray, Roszko and Solnica-Krezel, 2011). Vangl1 protein in the notochord has already been reported (Andre et al., 2015), however the novel identification of Vangl2 and Fzd6 in notochord in the present work, provide further evidence for Wnt/PCP signalling in this tissue. The presence of Wnt/PCP components and signalling in the notochord may initially seem unrelated to NMP behaviour, however the notochord is an important source of signals during development (reviewed in Corallo, Trapani and Bonaldo, 2015). Signals originating from the notochord have been implicated in controlling patterning and proliferation of many tissues across the axis, and furthermore there is also evidence that the posterior most notochord (CNH) may also regulate NMPs. Experiments in chick in which Hensens Node, the chick equivalent of the NSB, was removed, resulted in loss of caudal mesoderm and neural structures despite there still being NMPs in the adjacent CLE (Charrier et al., 1999). Thus, the notochord may acts as a vital niche to maintain NMPs, and disruption to this structure could have drastic effects on NMP behaviour. In this thesis, the identification of Fzd6 and Vangl2 in the notochord, including anterior most node-streak border suggests that Wnt/PCP is active in regions adjacent to NMPs and thus may regulate NMP behaviour. This has important consequences on the interpretation of axial defects exhibited by Wnt/PCP knock out mice. Loss of caudal structures in these mutants may primarily be because of disruption in notochord, rather disruption of Wnt/PCP directly in NMPs. Thus, to tease apart direct and indirect effects of Wnt/PCP signalling on NMP behaviour Wnt/PCP needs to be disrupted in a spatial and temporal specific manner.

3.5.5 Conservation of similar cell polarity dynamics and cell movements between CLE and CNH.

The examination of Wnt/PCP signalling using the localisation of Wnt/PCP components as described above can allow the examination of Wnt/PCP signalling within tissues. However, examining localisation of organelles within the cell can also be used to understand its polarity. Previously polarity changes and movements of cells in the streak had been investigated during gastrulation by examining the localisation of Centrosomes within cells (Burute et al., 2017). The work described in this chapter aimed to understand more about cell movements and polarity in NMP regions by

applying a similar strategy. By co-staining for nuclear envelope and Golgi the polarity of individual cells and the coordination of this polarity across tissues was examined. In this work observations in early gastrulation embryos were akin to those previously described for this stage in the literature (Burute et al., 2017). Cells of the epiblast were initially coordinated in their apical basal polarisation towards the proaminiotic cavity, which was subsequently lost in cells which underwent EMT and moved through the streak to form pre-somitic mesoderm (Fig. 3.19). A model for this process is summarised in (Fig. 3.25).

It was unknown if this process continued in NMP regions, and if the NMPs were polarised or not in the CLE or CNH. The work here provides evidence to suggest that NMPs reside in areas in which similar changes in polarity and dynamic cell movements are taking place. Similar profiles of Golgi localisation were described during early somitogenesis, and in the tail bud. NMPs in the NSB and CLE were coordinated in their polarity toward the pro-amniotic cavity, whilst cells of the streak and presomitic mesoderm did not have coordination of polarity between neighbours (Fig. 3.21). These differences were conserved later in development, when cells within the most posterior neuroepithelium, adjacent to the notochord (CNH), also show uncoordinated Golgi localisation, strikingly different to all other regions of the neural tube (Fig. 3.22D, Fig. 3.23D,F, Fig. 3.24B,E). Thus, the process by which NMPs differentiate, to stay as polarised neural cells or become mesoderm (unpolarised), is likely to be conserved during axial elongation. This finding also implicates regulation of polarity as an important step in this fate choice. However, many questions remain, as it is not clear how polarity may be regulated in these regions. Additionally, the data described here can only determine the presence of apical-basal polarity, with more complex analysis needed to examine planar polarity in these areas. The CLE, which is a flat epithelium is the least morphologically complex region containing NMPs, and thus provides a location in which tissue polarity might be easiest to identify. Moreover, as described above, NMPs in the CLE express both Ptk7 and Vangl2, suggesting Wnt/PCP is active in this area. Initial steps have been taken to quantitatively analyse planar polarity in the CLE using nuclei and Centrosome positioning (Appendix S-Fig.3.1 & 3.2). This is an exciting but complex area of new research, and it is hoped

that it will provide more information about how NMPs are polarised, and the consequence of this polarisation on their behaviour.

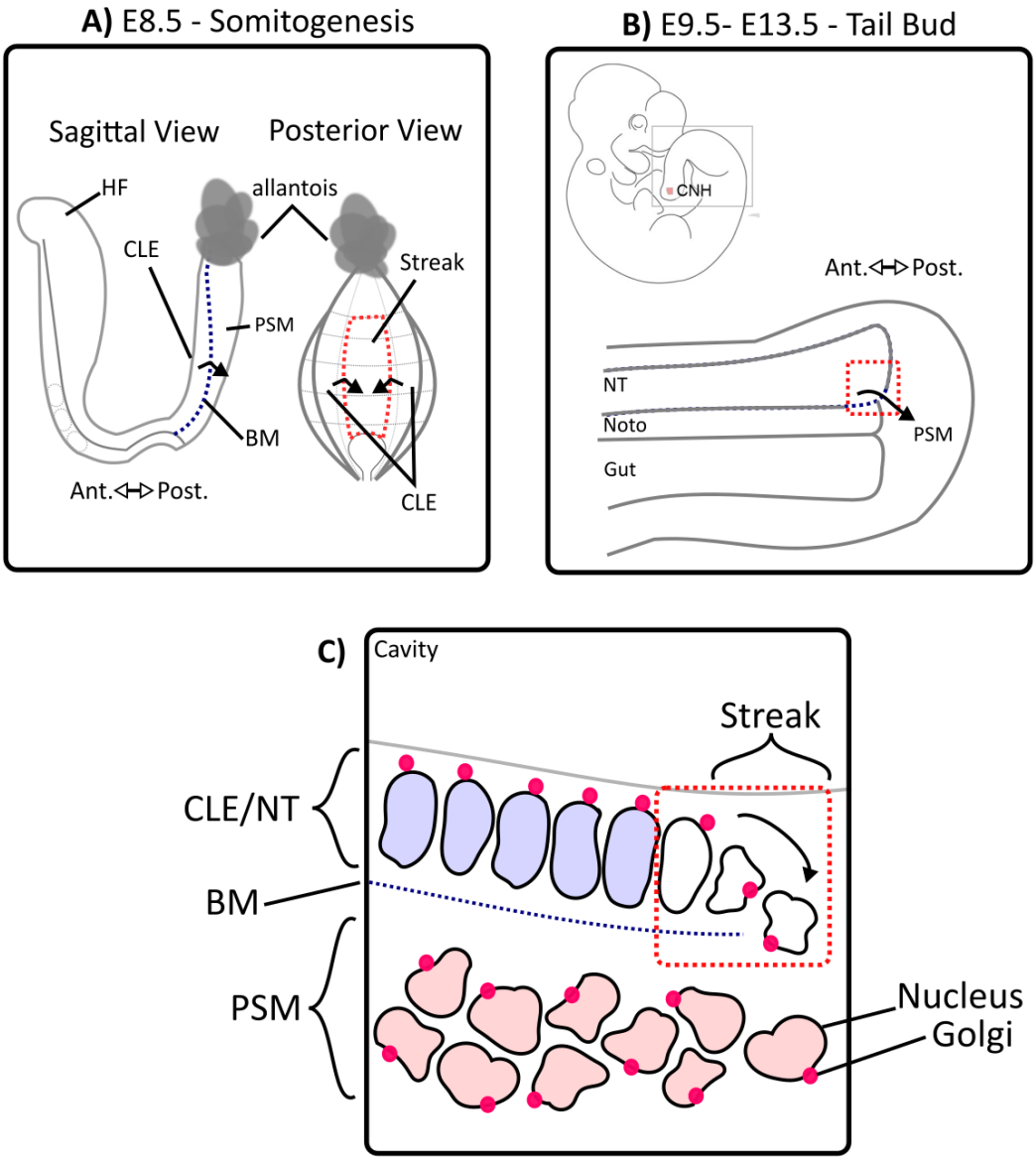

Figure 3.25 - Cell movements in NMP regions during axial elongation.
NMPs in the **(A)** caudal lateral epiblast (CLE) at E8.5 and **(B)** the chordoneural hinge (CNH) from E9.5 to E13.5 appear to undergo similar polarity dynamics and cell movements during axial elongation **(C)**. NMPs (blue) are initially polarised with Golgi (pink) polarised towards the cavity (proamniotic, for CLE and neural tube cavity, for CNH). Subsequently individual NMPs lose coordination of polarity (become unpolarised) (white) and move away from the epithelium to form unpolarised presomitic mesoderm (PSM)(red). This pattern is similar to that described previously for cells moving through the primitive streak (PS) (Burute et al., 2017). BM - Basement membrane, NT - Neural Tube, Noto - Notochord, Ant - Anterior, Post - Posterior.

Chapter 4: Deriving NMPs from EpiLCs *in vitro*

4.1 Introduction & Aims

As mentioned in the introduction (1.3.5), NMPs have been generated *in vitro* from Mouse ESC and EpiSCs through activation of Fgf and Wnt/β-catenin signalling (Gouti et al., 2014; Tsakiridis et al., 2014; Turner et al., 2014). However, both these sources do not represent homogeneous starting populations and within these cultures there can be significant transcriptome variations and both are prone to spontaneous differentiation (reviewed in Morgani, Nichols and Hadjantonakis, 2017). Currently many questions remain unanswered in terms of the robustness or reliability of differentiation from these cells states. As previously mentioned cells cultured in 2i/LIF offer a more homogeneous starting point, with reduced expression of lineage specific markers and significantly less spontaneous differentiation (Silva and Smith, 2008; Silva et al., 2008). Recently an intermediate state between ESCs and EpiSC has been generated from 2i/LIF cultures, from which more robust differentiation could be possible (Hayashi and Saitou, 2013; Hayashi et al., 2011, 2012). These are termed EpiLCs, and following 48 hours of differentiation from 2i/LIF transcriptionally reflect E5.75 embryos. Despite their identification as an advantageous starting population exploration of their functional abilities have been limited to derivation of primordial germ cells. In this chapter I aim to investigate:

- If cells co-expressing T(Bra) and Sox2 (a hallmark of NMPs) can be generated from EpiLCs

And thus:

- What combination of variables are optimal for maximising T(Bra) and Sox2 co-expressing cells
- Determine if these derived putative NMPs from EpiLCs, transcriptionally and functionally equate to *in vitro* EpiSC derived NMPs and *in vivo* NMP respectively

4.2 EpiLC are more homogeneous in morphology than EpiSCs

In my hands culturing EpiSCs was not reproducible due to variable spontaneous differentiation, which in some cases even resulted in terminal differentiation of the whole culture. EpiSCs derived from the same wildtype cell line but of different passage numbers show this spontaneous differentiation, with EpiSC colonies surrounded by more differentiated cells (Fig. 4.1A-B). As mentioned above EpiLC may provide a more homogeneous starting point compared with EpiSCs. Ultimately if the starting point of differentiation is homogeneous then the products of differentiation may have a better chance of a predictable, homogeneous phenotype. Before considering EpiLCs as an alternative source of *in vitro* NMPs, I was interested if EpiLCs display a less heterogeneous phenotype than EpiSCs. Indeed, EpiLCs consistently formed tightly-packed colonies akin to those of EpiSCs but without the presence of differentiated cells (Fig. 4.1C), suggesting they may offer a suitable alternative source of *in vitro* NMPs.

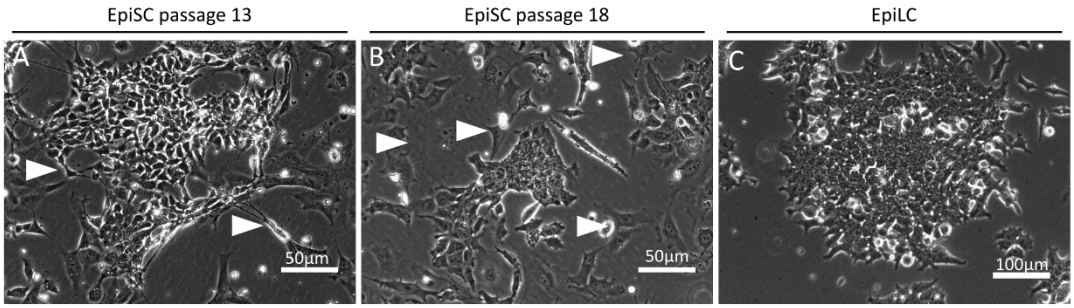

Figure 4.1 – Morphology of EpiSC and EpiLC colonies.
Brightfield images of wildtype (E14Ju09) EpiSCs cultured in N2B27/Activin/FGF, passage 13 **(A)**, passage 18 **(B)** and EpiLCs **(C)** derived from wildtype 2i/LIF cultured cells through culture on fibronectin with N2B27/Activin/FGF/KSR media for 48 hours. Both EpiSCs cultures have more spontaneous differentiation, indicated by larger, less rounded, flatter cells (arrows) than EpiLC cultures however the colony morphology (of both is strikingly similar.

4.3 Putative NMPs, T(Bra) and Sox2 co-expressing cells can be generated from EpiLCs

Due to similarities between EpiSC and EpiLC culture, initial trials to derive NMPs from EpiLCs were conducted using a similar protocol to derive NMPs from EpiSC as described in (Gouti et al., 2014) (Fig. 4.2). Briefly, 2i/LIF cultured cells were placed

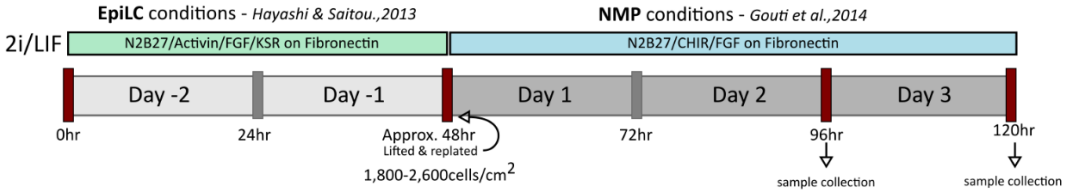

Figure 4.2 – Generating putative NMPs from EpiLCs.
Experimental set up used to derive T(Bra) and Sox2 positive cells from EpiLCs. EpiLC cells were initially derived by seeding 2i/LIF wildtype cultured cells in EpiLC conditions, N2B27/Activin/FGF/KSR media, according to (Hayashi and Saitou, 2013), for approximately 48 hours, before lifting and replating in NMP conditions according to (Gouti et al., 2014) in N2B27/CHIR/FGF for either 2 or 3 days.

in EpiLC conditions for approximately 48 hours as described in (Hayashi and Saitou, 2013). These were then dissociated with Accutase and re-plated in N2B27/CHIR/FGF media on fibronectin in the same manner EpiSC are used to derive NMPs (Gouti et al.,2014). As cell death has been widely reported at Day 3 of EpiLC culture (Hayashi et al., 2011), EpiLCs cells were plated at a number of densities, from 1800cells/cm^2 which is commonly used for derivation of NMPs from EpiSC, to a higher density of 2600 cells/cm^2. NMPs are generally found from Day 2 from EpiSC derivation, and because EpiLCs represent an earlier embryonic state, I expected to see emergence of NMPs on Day 2 or Day 3. To evaluate the presence of NMPs in the culture conditions, T(Bra) and Sox2 co-expression, a hallmark of NMPs, was detected using immunohistochemistry.

At all densities, and at both days, colonies with cells expressing both T(Bra) and Sox2 (T+/S+) were identified (Fig. 4.3). In these cultures, not all observed cells were T+/S+. Some T(Bra) single positive (T+/S-), Sox2 single positive (T-/S+) and double negative for T(Bra) and Sox2 (T-/S-) cells were also found at all plating densities. Overall there was considerable death at all densities, visible by the number of dead cells floating in the culture, ultimately resulting in very few attached colonies remaining in each well (Fig. 4.4). As cell death had been reported previously for EpiLCs and because it is considered as a normal observation in other differentiation systems, I continued to optimise this protocol (Hayashi et al., 2011; Ying and Smith, 2003).

To optimise the plating density a high-throughput system was utilised. Cells were seeded in 96 well plates and collected at Day 2 (Fig. 4.5). Following fixation cells were

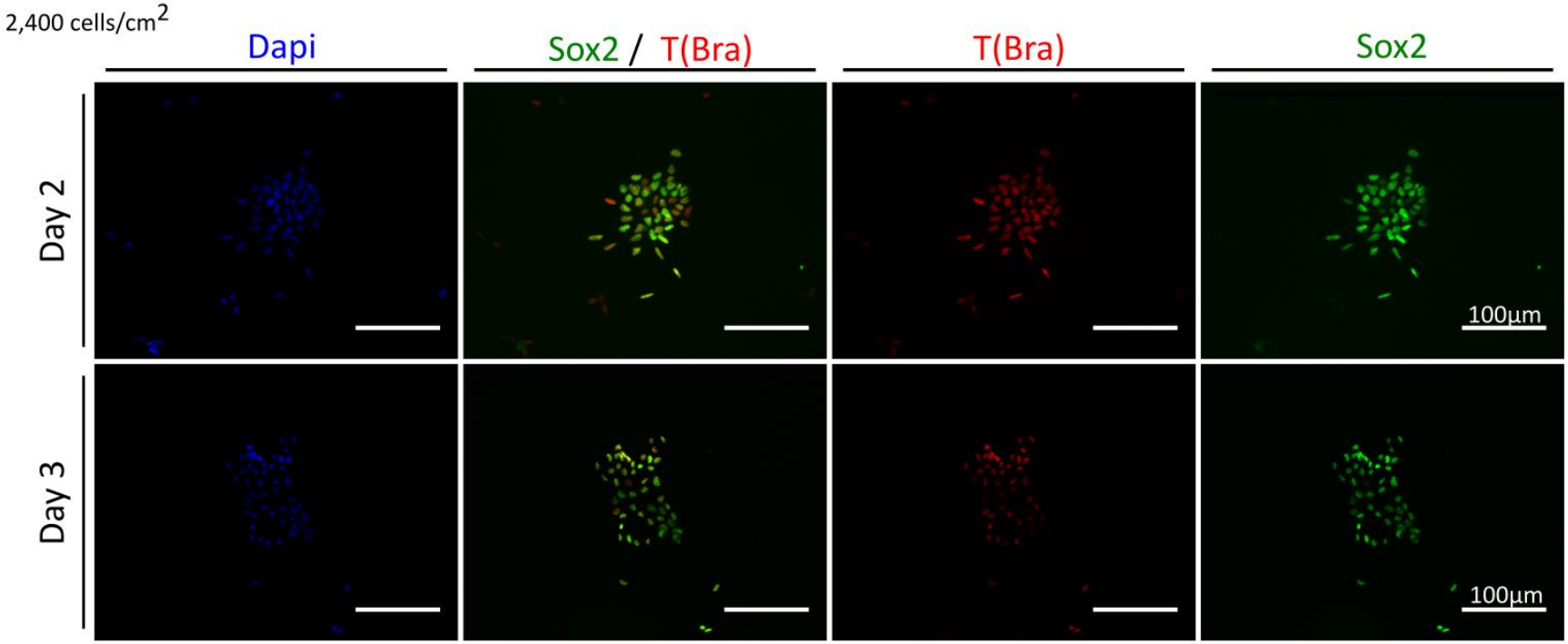

Figure 4.3 – T(Bra) and Sox2 co-expressing cells can be derived from EpiLCs.
T(Bra)-red and Sox2- green immunohistochemistry on cells fixed on either Day 2 or Day 3, show that these cells co-express both markers.

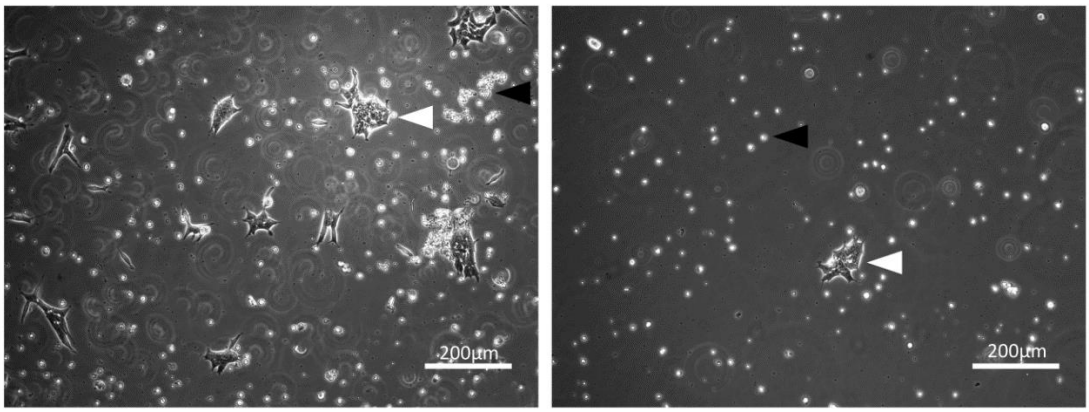

Figure 4.4 – EpiLC cultures contain a high proportion of dead cells.
Day 2 Brightfield images show many dead cells floating in the culture (black arrows) surrounding alive cells attached to the plate (white arrows)

labelled using DAPI, and imaged with an Operetta High-Content Imaging System, which allows the imaging of whole wells/plates. At the plating density reported to produce a high proportion of NMPs (Gouti et al., 2014), very few colonies were present (Fig. 4.5a). Instead a plating density of 260,000 cells/cm^2 generated an equivalent cell density after EpiSC differentiation (Fig. 4.5i).

In summary, T(Bra) and Sox2 co-expressing cells, putative NMPs, can be generated from EpiLC through dual activation of Fgf and Wnt/β-catenin signalling for approximately 48-72 hours, similarly to that previously described from Mouse ESCs and EpiSCs. However due to wide-spread cell death EpiLCs need to be plated at a significantly higher density than EpiSCs.

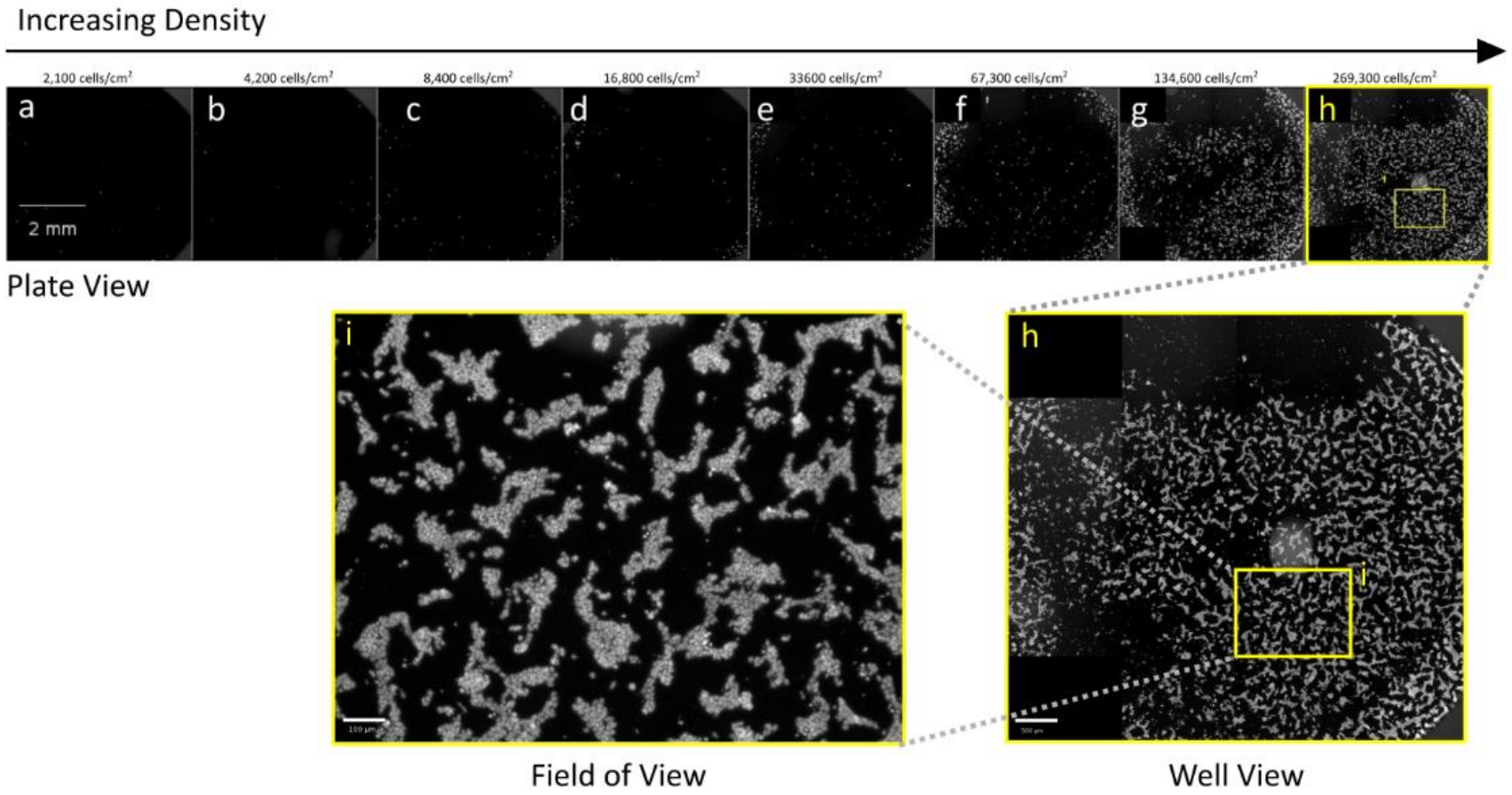

Figure 4.5 – Optimisation of EpiLC plating density.

Plating density of EpiLC was optimised using high-through put system which allowed the imaging of whole 96 well plate wells. DAPI staining is shown for EpiLC cells plated in 96 well plate in NMP promoting conditions for 2 days. Density of cells doubles between each well from left to right (a-h). Well **(h)**, was the optimum density for generating EpiLC-NMP colonies. **(i)** shows single field of view.

4.4 Optimisation of variables to enhance putative NMP proportions

4.4.1 Experimental Set-up

Following optimisation of density, I set up a multivariate experiment to achieve the highest proportion of T+/S+ putative NMPs, from EpiLCs. Overall experimental set-up is documented in (Fig. 4.6).

The variables were:

(1) Timepoint of NMP differentiation. T+/S+ cells were previously observed on both Day 2 and Day 3 in preliminary experiments (Fig. 4.3), so both were examined.

(2) EpiLC differentiation duration. Timepoint of EpiLC/NMP differentiation media change. Cell survival appeared to be variable in experimental repeats where the exact time of replating on Day 2 varied. This may reflect their dynamic gene expression between 24-72 hours of EpiLC culture (Hayashi et al., 2011). Therefore, a systematic series of five timepoints between 42-54 hours in EpiLC conditions was tested to determine whether this affected the efficiency of T+/S+ cell production, these were: 42 hours, 45 hours, 48 hours, 51 hours, and 54 hours into EpiLC differentiation.

(3) Replating of EpiLCs. To test whether the extensive cell death in EpiLC- NMP culture (Fig. 4.4) was a result of passaging cells at the transition from EpiLC to NMPs differentiation, cells were either passaged ('Replated') or not ('Not Replated'). To compensate for the probable increase in cell density from leaving cells attached to the dish during the media change, cells were plated at a series of lower densities for 'Not Replated' condition.

(4) Plating density. It had previously been observed in EpiSC cultures that high cell densities have effects on the level of T(Bra), Tsakiridis/Karagianni (unpublished observations). Therefore a series of densities were assayed at each stage where cells were plated: for culture in 'Not Replated' series, densities between 625-6,250 *cells/cm*^{2} were examined, while in the 'Replated'

series, 2i/LIF cultured cells were plated at 16,000 cells/cm^2 and EpiLCs re-plated at 6,250-132,000 cells/cm^2 .

Image analysis was performed on cells immunostained with T(Bra) and Sox2 antibodies.

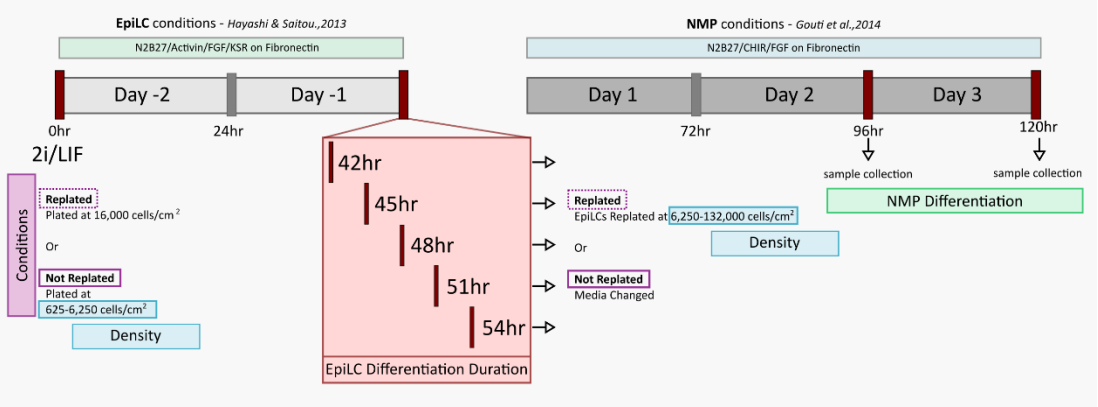

Figure 4.6 – Optimisation of variables to enhance putative NMP proportions.
Experimental set up to optimise variables to enhance putative NMP proportions in EpiLC-NMP cultures. Variables were: **(1)** NMP differentiation, **(2)** EpiLC differentiation duration **(3)** Replating of EpiLCs ('replated' or 'not replated') and **(4)** plating density.

4.4.2 Putative NMPs were more abundant at Day 2

In cultures where NMPs are generated from EpiSC, T+/S+ cells appear following 48 hours of treatment in NMP conditions, and remain in the culture until at least 72 hours. To examine the temporal dynamics of putative NMPs in my EpiLC derived cultures, the presence of T+/S+ cells was compared between Day 2 and Day 3 samples for all conditions.

In 'Not Replated' conditions T+/S+ cells were found consistently at all EpiLC differentiation durations on Day 2 (Fig. 4.7A). In comparison 'Not Replated' conditions at Day 3 did not show the same pattern of T(Bra) and Sox2 co-expression (Fig. 4.7B). Although some T+/S+ cells were present in the culture at Day3, T(Bra) and Sox2 expression appeared mutually exclusive in most cells. This was hard to confirm for all cells, specifically those in more domed colonies, where cells and their expression signal overlapped. These domes tended to have the highest expression of

Sox2 at their core, typically surrounded by T(Bra) positive cells. Flat and sparse cells surrounding large colonies were typically T-/S- in Day 3 cultures.

Similar trends were found in 'Replated' conditions, with Day 2 cultures typically having more T+/S+ cells (Fig. 4.8A), while on Day 3 T(Bra) and Sox2 again appeared to be mutually exclusive in most cells (Fig. 4.8B).

In summary, putative NMPs (T+/S+), were plentiful in Day 2 cultures, however by Day 3, most of these cells had already become T(Bra) and Sox2 single positive. This suggests that differentiation of these putative NMPs present at Day 2 occurs quickly, with cell differentiating to specific lineages between 48-72 hours of culture.

4.4.3 Unbiased analysis to determine the best combination of variables

4.4.3.1 Analysis methodology

Although it was clear that T+/S+ cells were more abundant at Day 2, it was not clear what combination of plating condition, timing of NMP condition transfer or density was optimal to obtain the highest proportion of T+/S+. Thus, further analysis was carried out on the Day2 immunohistochemistry data for 'Not Replated' and 'Replated' conditions. Columbus Software was utilised to determine levels of T(Bra) and Sox2 for individual cells over all conditions, data which were subsequently used to determine the proportion of T+/S+ cells within each condition.

To determine levels of T(Bra) and Sox2 for individual cells segmentation of individual cells was conducted with Columbus software using optimised settings for each plating condition (Fig. 4.9). Despite undergoing optimisation, segmentation performed by the software was not perfect and some errors of over segmentation and under segmentation were detected through manual inspection of segmented field.

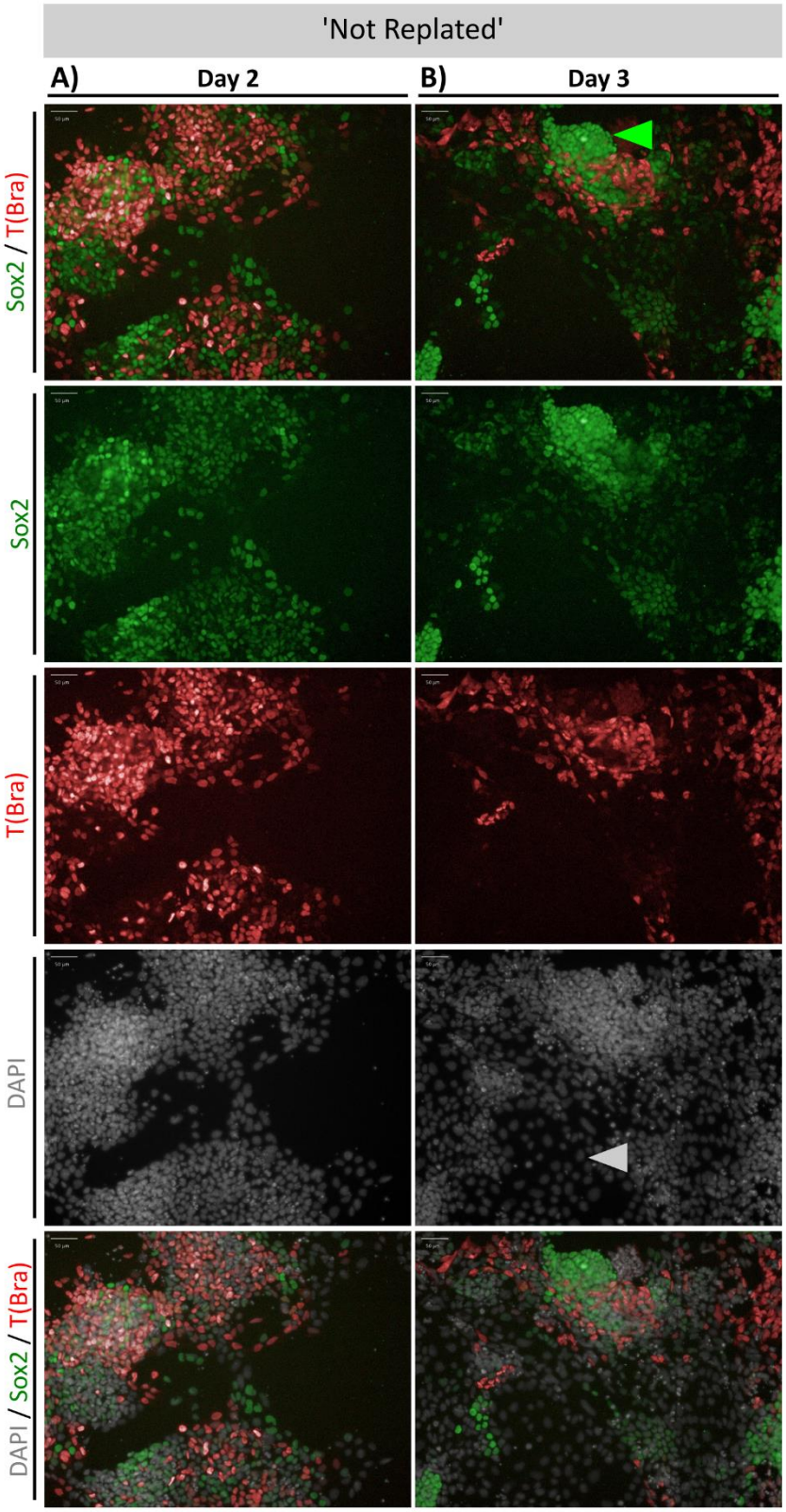

Figure 4.7 – 'Not Replated' cultures at Day 2 and Day 3.

Cells co-expressing T(Bra)- red, and Sox2-green were more abundant in 'Not Replated' conditions on Day 2 than Day 3. In Day 3 'Not Replated' cultures T(Bra) and Sox2 was mutually exclusive for many cells, and cultures were characterised by domed colonies of Sox2 positive cells (green arrow) surrounded by T(Bra) positive cells. Flatter negative cells were also abundant at Day 3 (grey arrow).

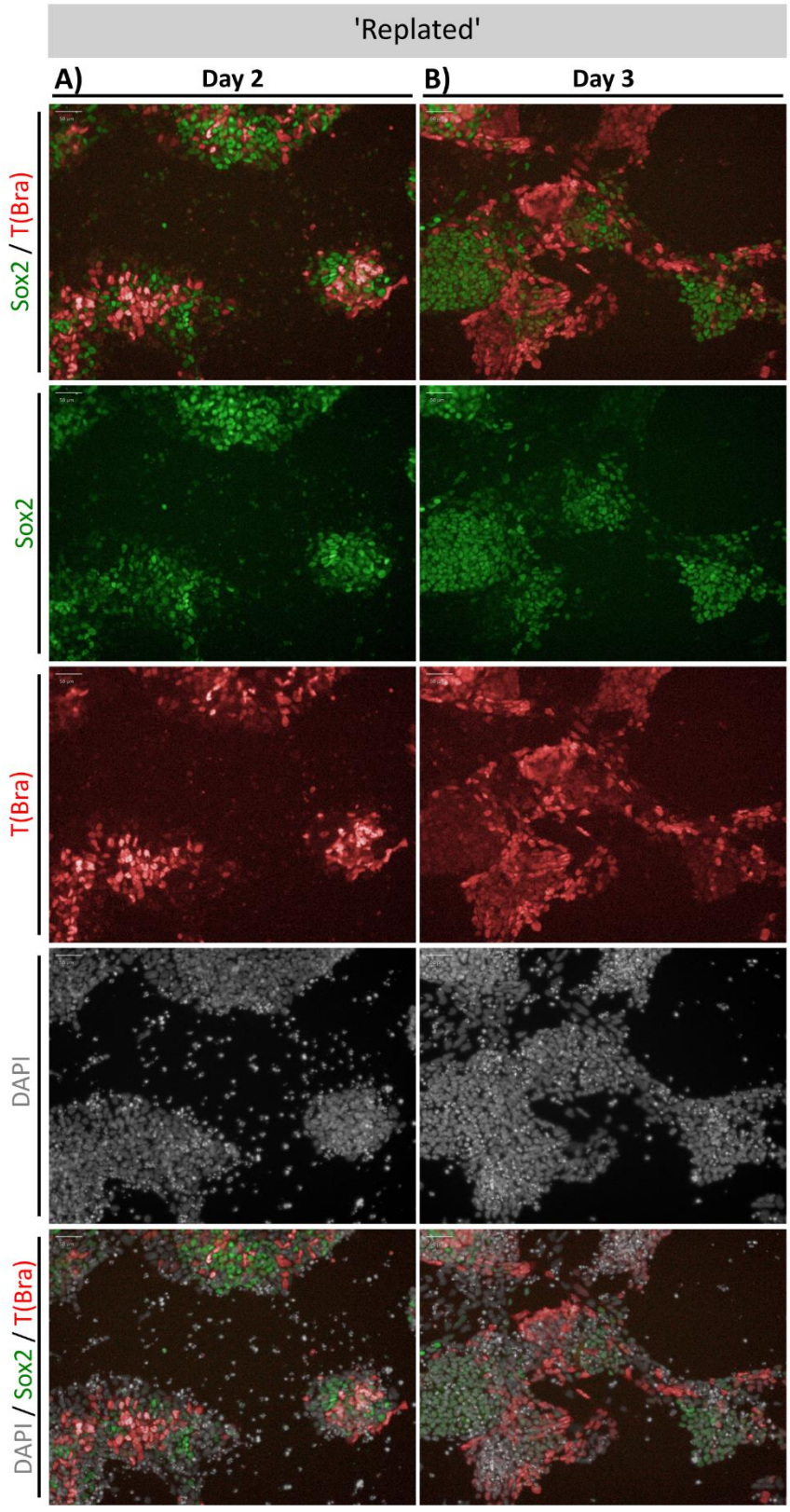

Figure 4.8 – 'Replated' cultures at Day 2 and Day 3.

Cells co-expressing T(Bra)- red, and Sox2-green were more abundant in 'Replated' conditions on Day 2 than Day 3. In Day 3 'Not Replated' cultures T(Bra) and Sox2 was mutually exclusive for many cells, and cultures were characterised by domed colonies of Sox2 positive cells surrounded by T(Bra) positive cells.

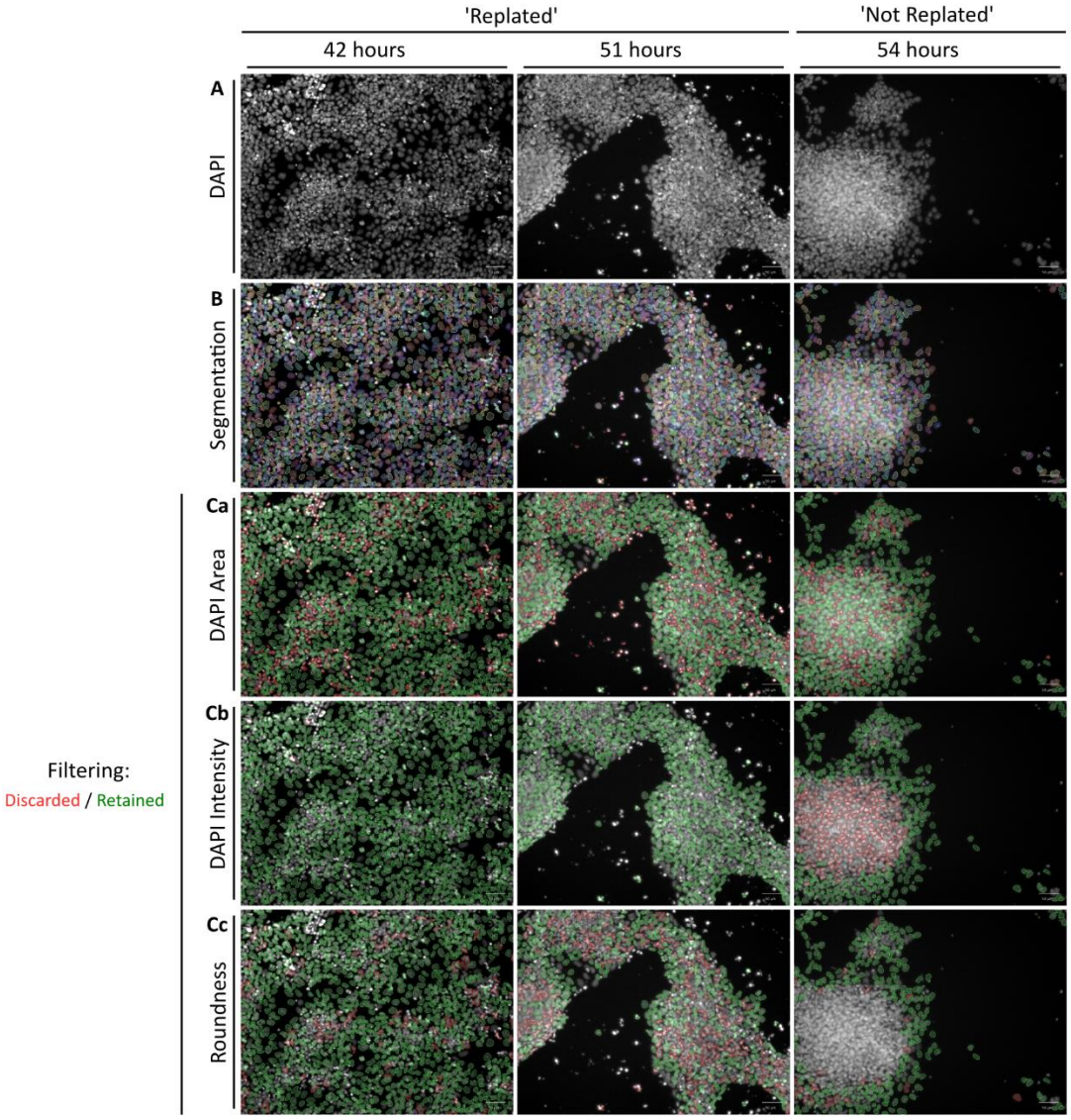

Figure 4.9 – Optimisation and limitations of segmentation by Columbus Software
Images show outcome of segmentation performed by Columbus Software (Perkin Elmer) using optimised settings on immunohistochemistry images for 'Replated' conditions at 42 hours, and 41 hours and 54 hours for 'Not Replated'. **(A)** DAPI only, **(B)** Optimised segmentation **(C)** Filters used to remove mis-segmented cells from the analysis by **(Ca)** DAPI Area **(Cb)** DAPI Intensity and **(Cc)** Cell roundness. (discarded cells – red , kept cells – green).

Incorrectly segmented cells were removed by applying filters based on cell morphology or DAPI intensity, which were optimised for each condition (Fig. 4.9C). These filters removed incorrectly segmented cells based on cell size (DAPI area), DAPI intensity, and roundness of the cells (Fig. 4.9Ca-c). Typically, flatter cultures (e.g. those for shorter EpiLC differentiation in 'Replated' conditions) segmented well. Conversely domed colonies, in which cells were overlapping, did not segment well, with the software unable to distinguish between individual cells. To minimise incorrect segmentation, areas with overlapping cells were removed from the analysis by filtering out cells with high DAPI intensity, and unusual cell shape (usually the result of under-segmentation). For 'Not Replated' conditions this resulted in the exclusion of many cells from the analysis, but those that were included were mostly correctly segmented and thus still valuable for the analysis (Fig. 4.9).

Following segmentation, the levels of T(Bra) and Sox2 were reported for each individual cell via Columbus software. Note data from well 'Not Replated' at 48 hour EpiLC differentiation at highest density was excluded from further analysis due to abnormally high DAPI values which filtered out too many cells. To calculate the proportion of cells that were double positive for T(Bra) and Sox2, minimum threshold levels for both channels were defined by judgement of negative expression levels. For each well, cells were then assigned to four quadrants based on these parameters: double negative (T-/S-), T(Bra) single positive (T+/S-). Sox2 single positive (T-/S+) and double positive (T+/S+). To compare between wells, proportion of cells in these quadrants was calculated for all wells, and are documented (Fig. 4.10), including total cell numbers for each (Fig. 4.10B). Additionally, to observe trends within variables, the average proportion of cells for each quadrant for 'Not Replated' and 'Replated' by density and by EpiLC differentiation duration were calculated (Fig. 4.10).

4.4.3.2 Putative NMP proportions are higher in the absence of replating step

Comparing the proportion of T+/S+ cells between 'Not Replated' and 'Replated' showed that 'Not Replated' wells typically had a higher proportion of putative NMPs across all EpiLC differentiation lengths and densities (Fig. 4.10A). Examining average T+/S+ proportions across all EpiLC differentiation lengths showed that 'Not Replated'

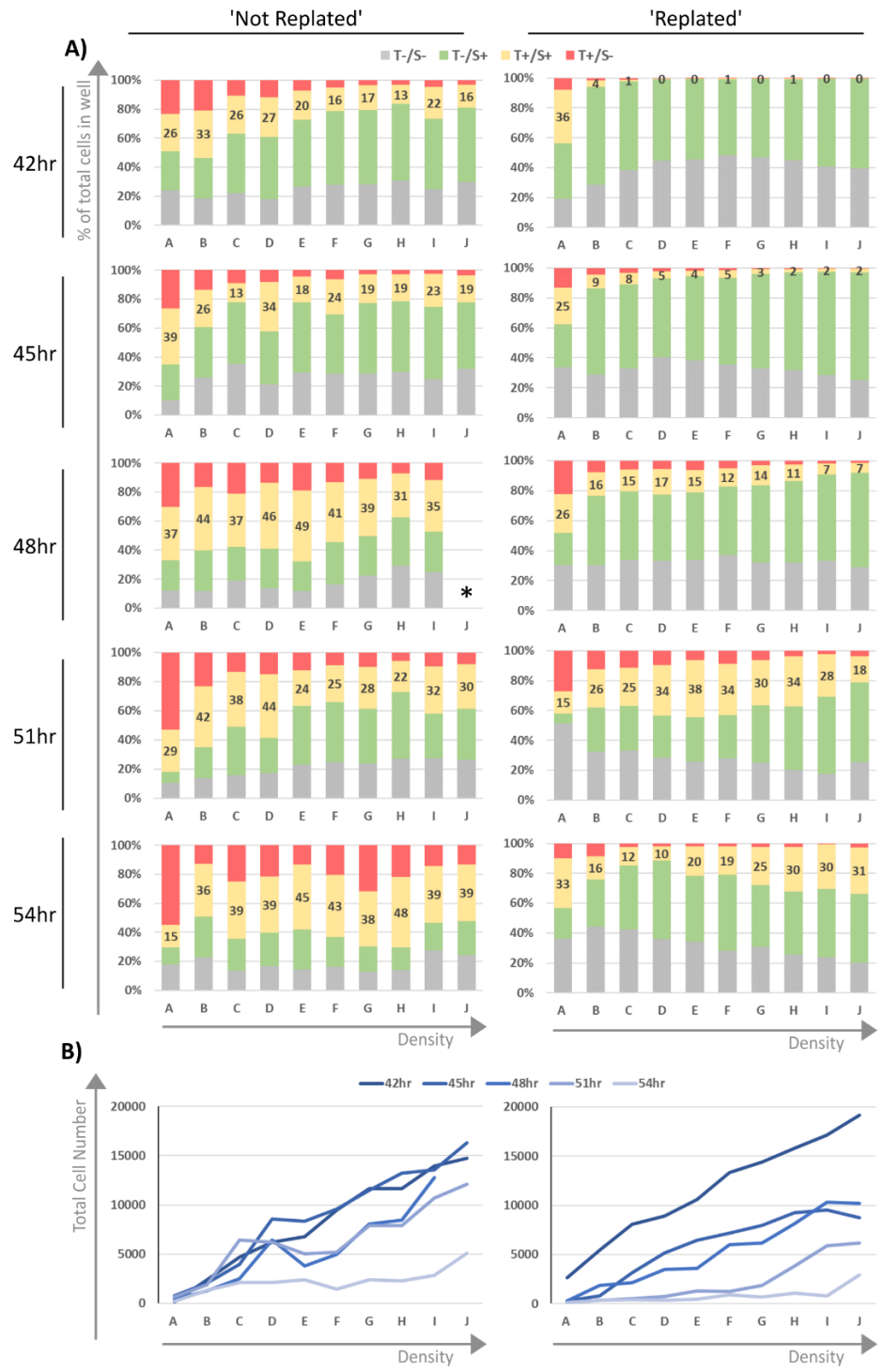

Figure 4.10 – Proportion of T(Bra) and Sox2 double positive cells and total number of cells per variable.

(A) Cells from each condition were split quadrants in terms of their T(Bra) and Sox2 intensity. These were: T(Bra) single positive (T+/S-)- red, Sox2 single positive (T-/S+)-green, double positive (T+/S+)-yellow - percentage of total well shown, and double negative (T-/S-)- grey. Thresholds for Sox2 and T(Bra) were set based on visual analysis of positivity. **(B)** Total cells counted in each well for each condition. A-J, low density to high density. * this sample was excluded due to the loss of too many cells during segmentation filtering. N=1 for each condition.

typically had twice as many putative NMPs across densities compared with wells from ‘Replated’ conditions (Fig. 4.10A). Thus, not replating cells from EpiLC during NMP derivation was key to achieving high levels of putative NMPs. Notability ‘not replating’ was not associated with reduced cell death in the culture, with an overall similar extent of death between ‘Not Replated’ and ‘Replated’ samples.

In ‘Replated’ wells the proportion of T(Bra) positive cells (T+/S+ and T+/S-) was lower than that for ‘Not Replated’ wells (Fig 4.10A,4.11A). This showed that T(Bra) expression was generally lower in ‘Replated’ versus ‘Not Replated’ conditions and could potentially be the limiting factor in overall NMP number. For both conditions, the highest proportion of T+/S+ cells were typically found at the lowest plating densities, when the proportion of T+/S- was also highest. Conversely the proportion of T-/S+ cells was highest at higher densities. Thus, T(Bra) and Sox2 positivity appeared to be inversely correlated.

Figure 4.11 – Averaged proportions of EpiLC-NMPs per density and per EpiLC differentiation. Averages by density and by EpiLC differentiation length outlined in Fig. 4.10. Percentages of T+/S+ (EpiLC-NMPs) are included on bar chart.

In summary, dissociating and replating EpiLCs before transferring to NMP conditions has a negative effect on the proportion of putative NMPs and T(Bra) positive cells. Additionally, putative NMP proportions are highest at lower densities however this effect is less influential than the 'Replating' variable.

4.4.3.3 Increasing duration of EpiLC differentiation enhances putative NMPs proportions

EpiLCs exhibit a dynamic transcriptome between 24-72 hours of EpiLC culture (Hayashi et al., 2011). Thus, I was interested whether EpiLC differentiation length affected the efficiency of putative NMP production. Comparing T+/S+ proportions over EpiLC differentiation lengths for both conditions, the proportion of putative NMPs were typically lower for shorter EpiLC differentiation lengths, 42-45 hours (Fig. 4.10A). This was particularly striking in 'Replated' conditions for 42 hours differentiation timepoint, in which many wells exhibited 0% putative NMPs proportions. Conversely 'Replated' conditions at 54 hours of EpiLC differentiation at the same densities exhibited proportions of putative NMPs between 10-31% (Fig. 4.10A). Highest putative NMP proportions were found for longer EpiLC differentiation lengths (48-54hr) for 'Not Replated' conditions. Averaging proportions of quadrants for all well densities, showed that on average 40%, 32% and 38% of cells after 48hr, 51hr and 54 hr EpiLC differentiation respectively, of total cell numbers are putative NMPs (Fig. 4.11B). Thus, in summary increasing duration of EpiLC differentiation before transferring cells to NMP conditions results in an enrichment of putative NMPs proportions.

However, cells with longer EpiLC differentiation duration were prone to detaching from the plate, and this was reflected in overall lower numbers of cell analysed for these conditions (Fig. 4.10B). In both 'Not Replated' and 'Replated' conditions, for 42-51hours of EpiLC differentiation conditions, the number of cells included in the analysis increased with increasing plating density. However, for those that underwent 54 hours of EpiLC differentiation total cell numbers remained low even with increasing cell seeding densities. Detaching of cells was confirmed by inspection of stitched field of view images (Fig. 4.12). 'Not Replated' condition wells in which media was changed following 54 hours of EpiLCs differentiation had large areas in which cells are absent (Fig. 4.12B). This was a drastic reduction in well coverage

compared to those cultured in EpiLC conditions for only 41 hours, which had cells distributed equally over the entire well (Fig.4.12A). To investigate this further 'Replated' conditions were compared in a similar manner. Wells for which EpiLCs differentiation was longer had significant loss in well coverage relative to those with less EpiLC differentiation (Fig. 4.12C-D). Cell colonies between these wells also differed in terms of their morphology, with colonies being more domed with longer EpiLC differentiation (Fig. 4.12E-F). Together this suggests that duration of EpiLC differentiation determines how well cells attach to the well substrate and each other.

Considering all variables, conditions in which cells were not dissociated and replated, and which had a longer EpiLC differentiation, resulted in the highest proportions of putative NMPs. However, considering the significant detachment of cells after 54 hours of EpiLC differentiation, 51 hours of EpiLC differentiation provide an alternative condition for appropriate for use in future experiments.

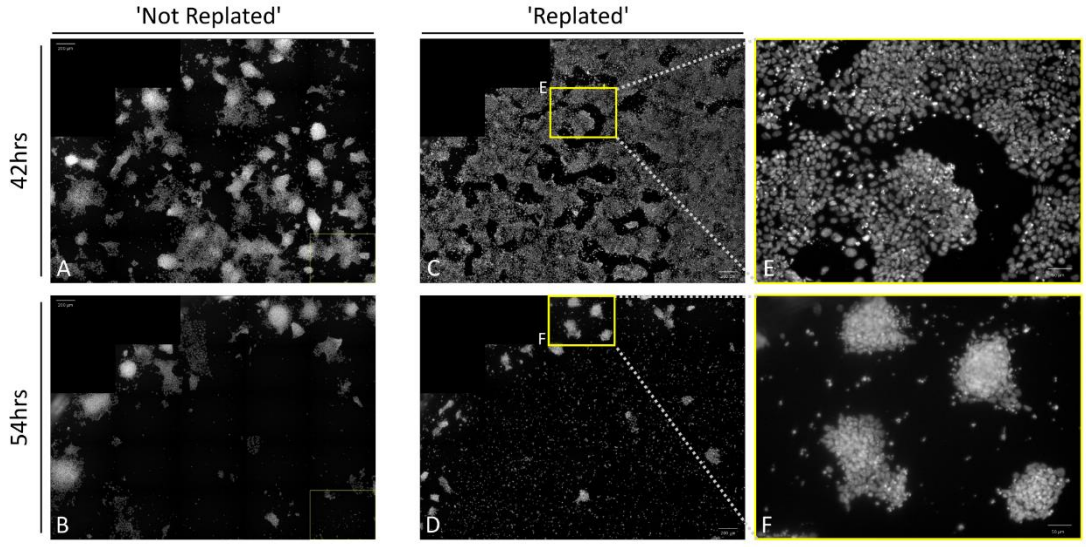

Figure 4.12– Colony morphology is dependent on length of EpiLC differentiation.
In both 'Not Replated' and 'Replated' Conditions, cells with longer EpiLC differentiation were prone to detaching from the plate. 'Not Replated' **(A)** at 42 hours, and **(B)** at 54 hours. 'Replated' **(C)** at 42 hours, and **(D)** at 54 hours. Closer inspection of 'Replated' conditions (plated at the same density) showed that cell colonies with longer EpiLC differentiation were also more domed, shorter **(E)** versus **(F)** longer EpiLC differentiation.

4.5 qRT-PCR comparison between NMPs derived from EpiSCs and EpiLCs

4.5.1 Experimental overview

Following the optimisation of variables to maximise putative NMP numbers from EpiLCs (4.4), I was interested whether putative NMPs generated from EpiLCs were transcriptionally equivalent to EpiSC derived NMPs. The differences in gene mRNA expression profiles were compared using qRT-PCR analysis. To maximise putative NMP numbers from EpiLCs and limit cell detachment, samples were collected from conditions with 51 hours of EpiLC differentiation, without replating ('Not Replated' condition) at Day 2 (Fig. 4.13). Additionally, to examine the further differentiation of these cells, samples were additionally collected at Day 3. Control samples included in the analysis were, 2i/LIF culture starting population, EpiLC at 51 hours, NMPs derived from EpiSCs (48 hours) and their EpiSC starting population (all N=3 biological replicates, except EpiSC N=4, and Oct4 N=2).

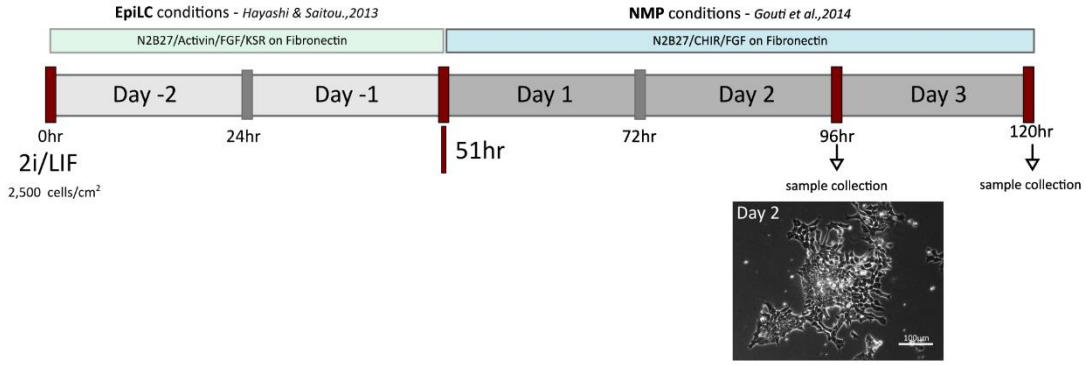

Figure 4.13 – qRT-PCR to compare NMPs derived from EpiSC and EpiLC.
Overview of EpiLC-NMP derivation to collect samples for qRT-PCR. Brightfield image shows typical colony of Day 2 sample.

4.5.2 EpiLC derived NMPs Day 2 are most similar to EpiSC derived NMPs

qRT-PCR results for all samples are documented in (Fig. 4.14) and (Fig. 4.15), all expression levels were calculated relative to 2i/LIF and error bars represent calculated standard error of the mean (SEM). qRT-PCR was performed for the analysis of pluripotency, NMP associated and lineage specification markers.

Pluripotency marker *Oct4* was expressed at negligible levels in EpiLC derived NMPs for Day 2 and Day 3, comparable to those for EpiSC NMPs samples and much lower than levels for 2i/LIF and EpiLCs which are associated with more pluripotent states (Fig. 4.14A). The expression of *Sox2*, a pluripotency marker in early development and later a marker of neural lineage, was twice as high in NMPs derived from EpiLCs than those from EpiSCs. As *Oct4* was low in these samples, the increase in *Sox2* indicated higher level of neural identity in NMPs derived from EpiLCs versus those from EpiSCs, which was further increased in Day 3 samples. Together these markers indicate that putative NMPs from EpiLCs lose pluripotency to a similar extent to EpiSC derived NMPs, but may have more neural characteristics.

Next primitive streak markers characteristic of embryo and *in vitro* derived NMPs were investigated , these were, *Fgf8* (Crossley and Martin, 1995), *Cdx2* (Beck et al., 1995; Deschamps and van Nes, 2005), *Evx1* (Bastian and Gruss, 1990; Cambray and Wilson, 2007), *Nkx1.2* (Schubert et al., 1995), *Ptk7* (Lu et al., 2004), *Wnt3a* (Takada *et al.*, 1994) and *T(Bra)* (additionally a mesoderm marker)(Wilkinson et al., 1990) (Fig. 4.14B). NMPs derived from EpiSC and EpiLCs showed comparable levels of *Fgf8*, *Cdx2*, *Evx1*, *Nkx2.1* and *Ptk7*, suggesting a similarity between these two populations. However, *Wnt3a* and *T(Bra)* were significantly lower in NMPs derived from EpiLCs versus those from EpiSCs (verified using two-tailed unpaired *t* test).

Thus, despite similarities in gene expression characteristic of NMPs, NMPs derived from EpiLCs and EpiSC are not identical. Expression of *T(Bra)* and *Wnt3a* are generally associated with Wnt/β-catenin signalling, and therefore suggested that this pathway may be less active in NMPs derived from EpiLCs. Comparing Day 2 and Day 3 EpiLC derived NMPs, Day 3 samples tended to exhibit lower levels of NMP markers, in keeping with the idea that they might be losing NMP identity and differentiating.

In development, the anterior-posterior identity of axial tissues is regulated by the sequential activation of the *Hox* genes along the axis (Deschamps and van Nes, 2005). A selection of Hox genes were examined to compare the axial identity of these two NMPs populations. *HoxA4* is associated with anterior cervical domains (Horan et al., 1994), *HoxA6* with thoracic domains (Kostic and Capecchi, 1994), and *HoxD13* with

caudal domains (Deschamps and van Nes, 2005). *HoxA4* and Hoxa6 had previously been reported to be higher in EpiSC derived NMPs compared to EpiSC (Gouti et al., 2014). This trend was also present for EpiLC derived NMPs, which had higher levels of *HoxA4* and *HoxA6* compared with EpiSCs (Fig. 4.14C). *HoxA4* and *HoxA6* tended to be higher in putative NMPs derived from EpiLC than those from EpiSC, suggesting there may be subtle differences between the two populations. Previously low expression of *HoxD13* had been reported in EpiSC derived NMP culture (Gouti et al., 2014). In line with this, all samples tested for *HoxD13*, including EpiLC derived NMPs exhibited low expression levels. In summary, NMPs derived from EpiLCs displayed upregulation of specific *Hox* genes characteristic of EpiSC derived NMPs.

To further dissect similarities between NMPs derived from EpiSC and EpiLCs, lineage specific markers were investigated (Fig. 4.15). Markers of emergent paraxial mesoderm *Tbx6* (Chapman et al., 1996) and skeletal and cardiac mesoderm *Mesp1* (Saga et al., 1996), were lower in EpiLC derived NMPs, suggesting this culture contained less mesoderm fated cells (Fig. 4.15A). Conversely EpiLC NMPs had higher levels of both neural lineage markers *Pax6* (Bernier et al., 2001) and Sox1 (Pevny et al., 1998) compared with EpiSC derived NMPs (Fig. 4.15B). Moreover, *Sox1* levels were significantly higher in EpiLC-NMPs day 3 samples than day 2 samples suggesting increasing neural differentiation in these samples. Finally endoderm markers *FoxA2* (also present in node/notochord) (Sasaki and Hogan, 1993), and *Sox17*(Kanai-Azuma et al., 2002) showed distinct differences between the two NMP populations (Fig. 4.15C). FoxA2 was significantly lower in NMPs derived from EpiLCs, while *Sox17* was higher compared to EpiSC derived NMPs.

Overall the profile of many developmental markers in EpiLC derived NMPs corresponded to those of EpiSC NMPs, suggesting many parallels between these two populations. This was especially true for many genes characteristically upregulated in *in vivo* and *in vitro* NMPs including specific Hox genes. However, NMPs derived from EpiLCs did show some distinct differences, with significantly lower levels of *Wnt3a* and *T(Bra)* and mesoderm lineage markers, indicating a deficiency in Wnt/β-catenin signalling. Concurrently EpiLC NMP also exhibited higher transcript levels of neural lineage markers. Thus, despite many similarities between the two populations some

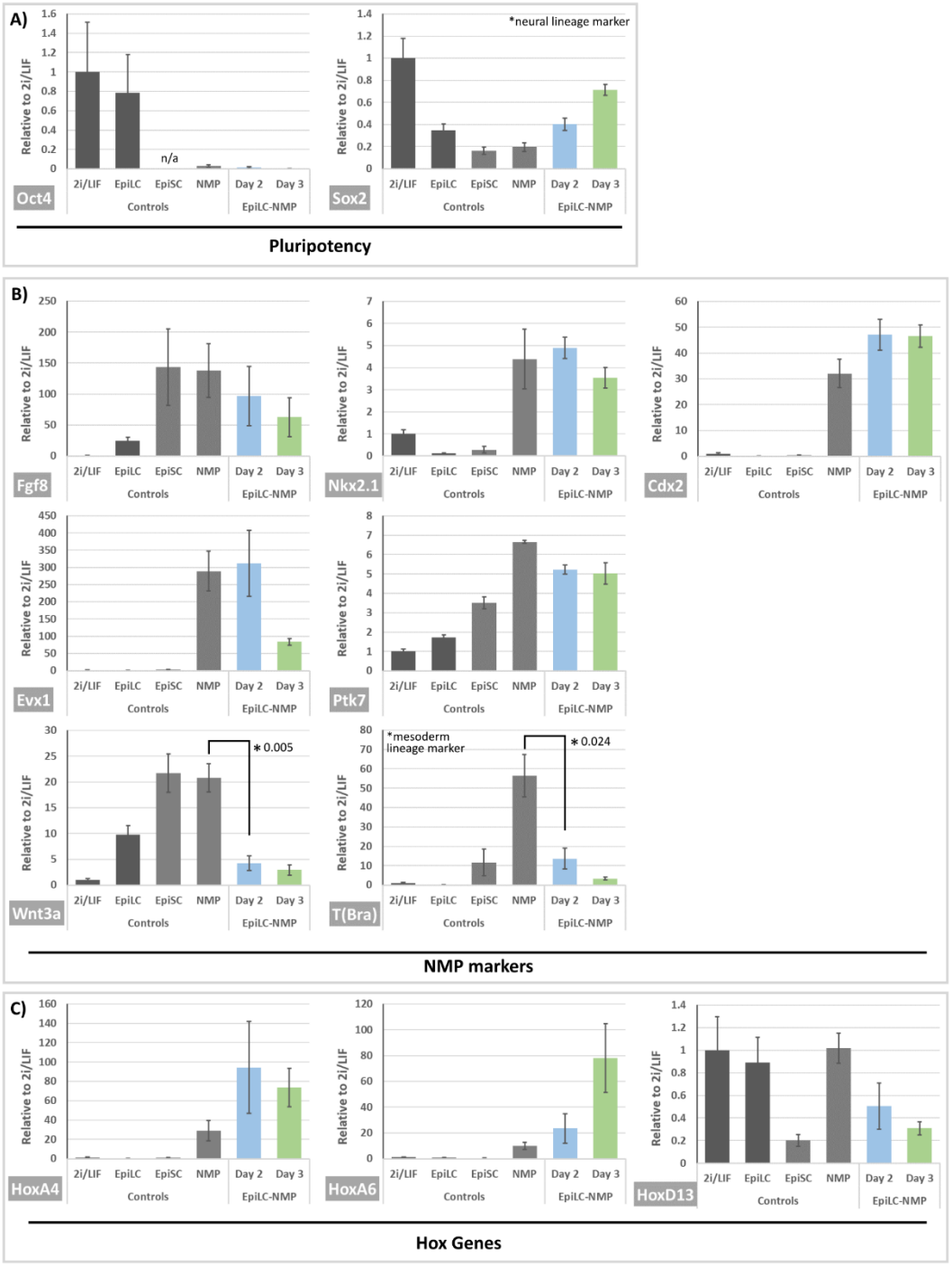

Figure 4.14 –qRT-PCR analysis to compare NMP derived from EpiSC and EpiLC - Pluripotency, NMP and Hox genes.

qRT-PCR analysis of genes **(A)** associated with pluripotency, **(B)** upregulated *in vivo* NMPS and additionally **(C)** Hox genes. Levels of gene expression are all relative to 2i/LIF sample. Errorbars represent standard error of the mean, N=3 for all genes except O*ct4* (N=2) and EpiSC (N=4). Statistical significance was assessed by performing a t test (two-tailed), p-values are shown. * indicates if a gene is associated with additional tissue types. EpiLC sample was collected following 51 hours of EpiLC differentiation, and NMP sample is from 48 hours of NMP differentiation from EpiSCs.

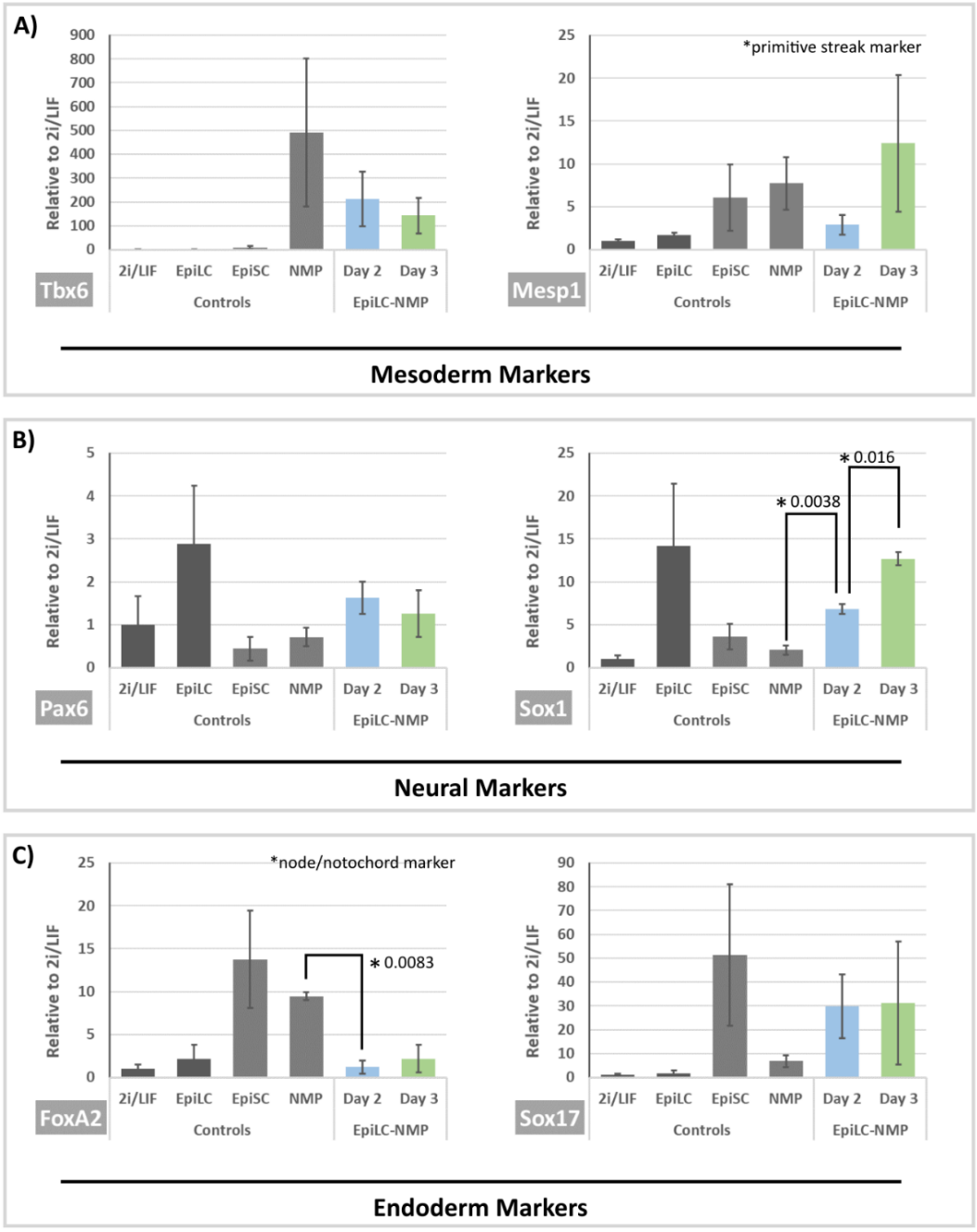

Figure 4.15 –qRT-PCR analysis to compare NMP derived from EpiSC and EpiLC - Mesoderm, Neural and Endoderm associated genes.

qRT-PCR analysis of genes **(A)** associated with mesodermal **(B)** neural and **(C)** endoderm tissues. Details are the same as those described for Fig. 4.14.

differences did exist.

4.6 NMPs derived from EpiLCs and EpiSCs express similar levels of Wnt/PCP components

Although expression of Wnt/PCP components during *in vivo* development had been described in the literature, albeit sparsely, no investigation of Wnt/PCP component expression in *in vitro* cultures has ever been reported. For this reason, and to compare the differences between EpiLC and EpiSC derived NMPs, immunohistochemistry for Fzd6, Ptk7 and Vangl2, was carried out on cells cultured in different conditions (Fig. 4.16-8).

Fzd6 protein was only present at low levels in 2i/LIF and EpiLC cultures, where protein was found to be diffuse and not membrane specific (Fig. 4.16A-F). Fzd6 protein levels were increased in EpiLC derived NMPs, and more specific to the cell surface (Fig. 4.16G-I), but lower compared to EpiSC and EpiSC derived NMPs in which the protein was more abundant (Fig. 4.16J-O). Fzd6 which is specific to notochord during in vivo development (3.3.2) appeared ubiquitously expressed in EpiSCs and EpiSC derived NMPs, as well as EpiSC, suggesting Wnt/PCP signalling may be present in these cultures.

Ptk7 protein was detected using Proteintech antibody which recognises both cleaved and uncleaved forms of Ptk7 protein. Membrane bound Ptk7 protein was observed ubiquitously in all culture conditions tested (Fig. 4.17). However distinct Ptk7 levels were observed, with Ptk7 protein more abundant and more intense at the cell membrane in NMPs derived from either EpiSC and EpiLC, and EpiSC (Fig. 4.17I-R) compared to 2i/LIF and EpiLC cultures (Fig. 4.17A-F).

Vangl2 protein was detected in low levels in 2i/LIF and EpiLC cultures, for which protein distribution appeared diffuse and not membrane specific (Fig. 4.18A-F). Vangl2 protein was much higher in EpiSCs, and NMPs derived from both EpiSC and EpiLCs. In these cultures Vangl2 localisation was not diffuse but instead localised to the cell membrane, and for all NMP samples appeared to be intensely localised in some cells more than others.

Overall, immunofluorescence intensity tended to increase with the differentiation state of the cell cultures, with NMPs having the highest levels of Wnt/PCP components examined. This aligns with previous descriptions of these components after gastrulation (3.3.1-3.3.3), suggesting Wnt/PCP may be active from this point in *in vivo* and *in vitro* systems. Comparing the levels between NMPs derived from EpiSCs and EpiLCs, Ptk7 and Vangl2 tended to be similar, however Fzd6 appeared to be slightly lower in NMPs derived from EpiLCs.

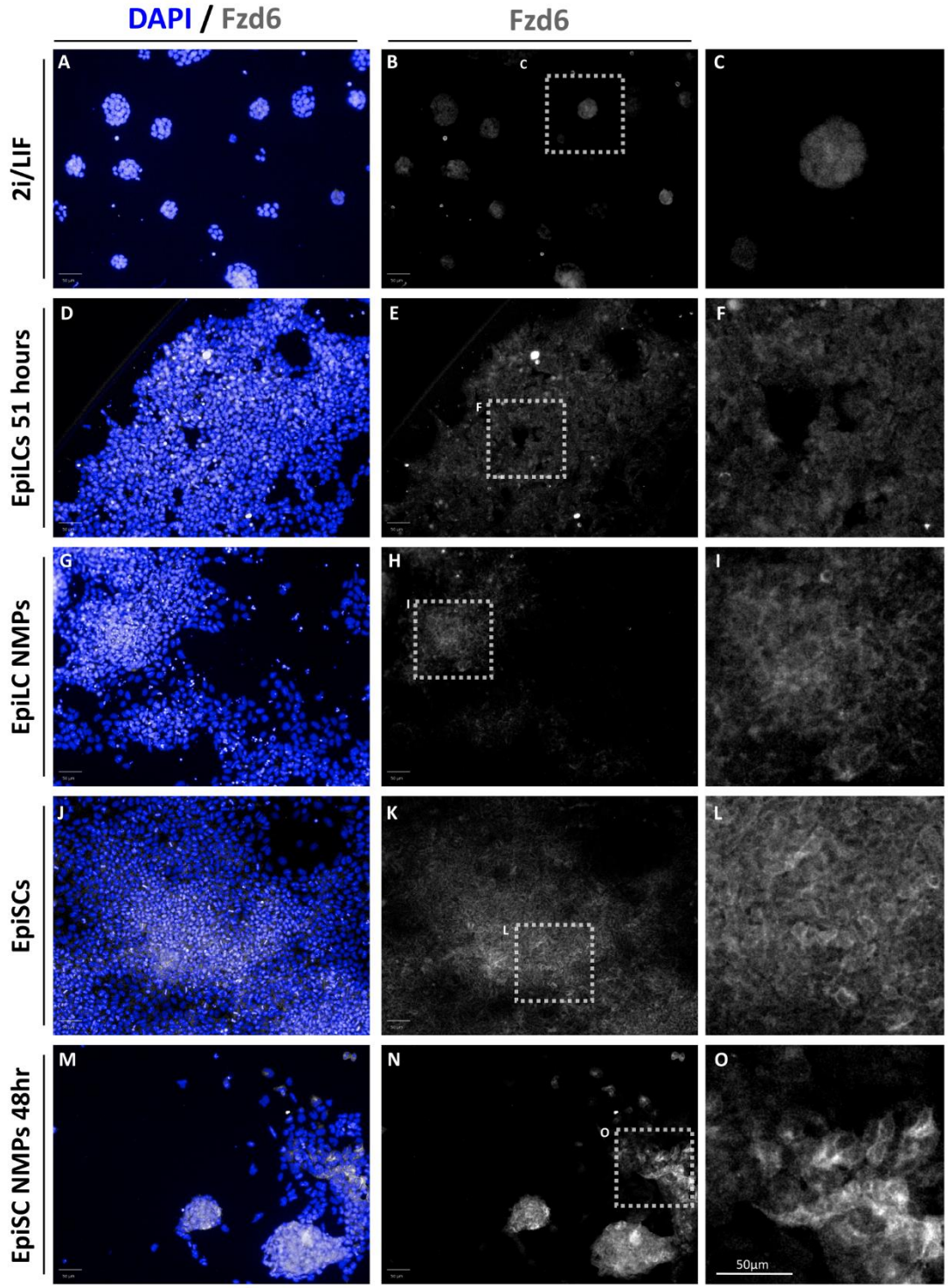

Figure 4.16 - Fzd6 expression in *in vitro* cultures.
Figure shows immunohistochemistry of Fzd6- greyscale, in *in vitro* cultures of **(A-C)** 2i/LIF, **(D-F)** EpiLCs (51 hours), **(G-I)** EpiLC derived NMPs, **(J-L)** EpiSCs, and **(M-O)** EpiSC derived NMPs Day 2 of differentiation. DAPI - blue

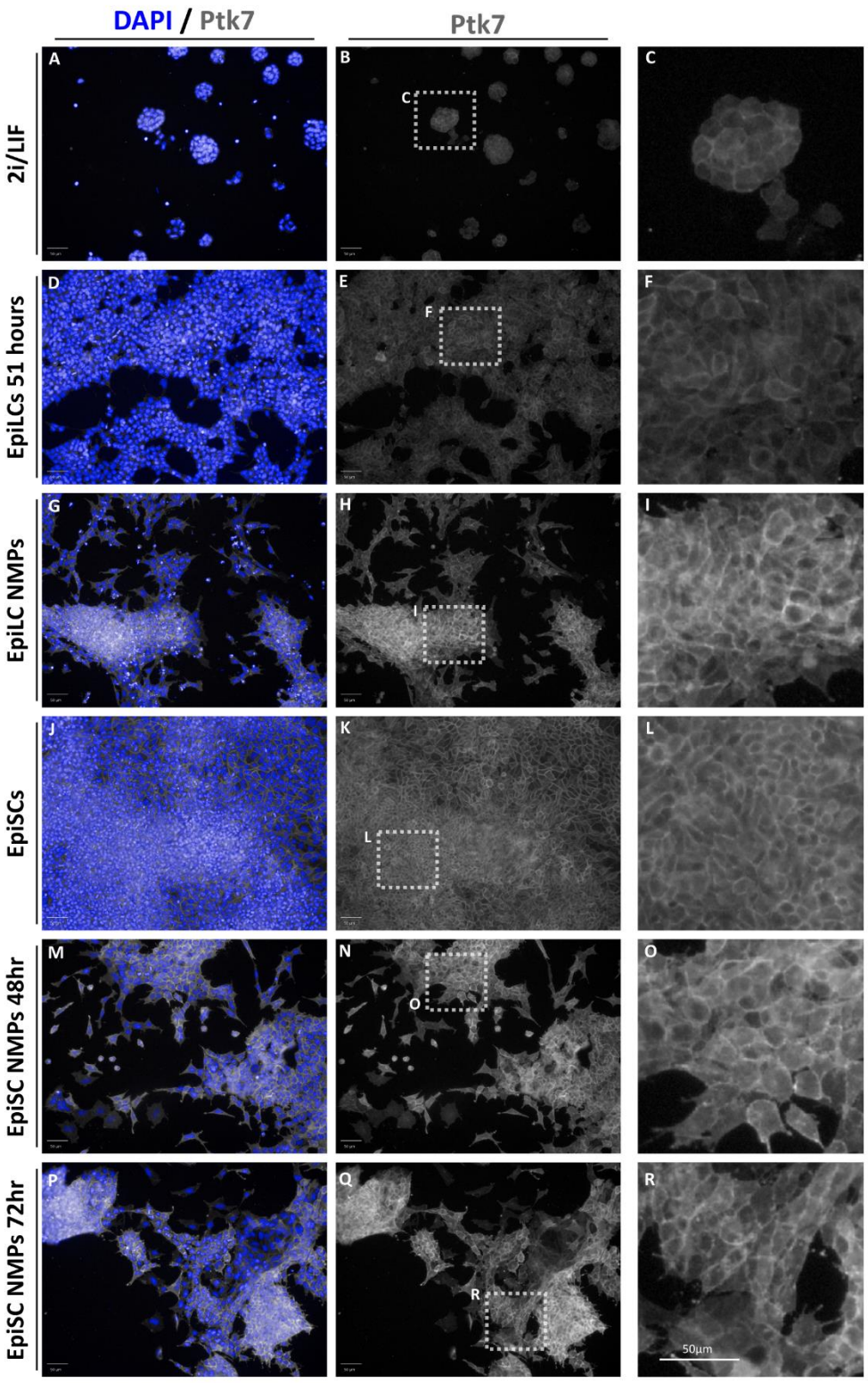

Figure 4.17 - Ptk7 expression in *in vitro* cultures.
Figure shows immunohistochemistry of Ptk7- greyscale, in *in vitro* cultures of **(A-C)** 2i/LIF, **(D-F)** EpiLCs (51 hours), **(G-I)** EpiLC derived NMPs, **(J-L)** EpiSCs, and **(M-O)** EpiSC derived NMPs Day 2 **(P-R)** and Day 3 of differentiation. DAPI - blue

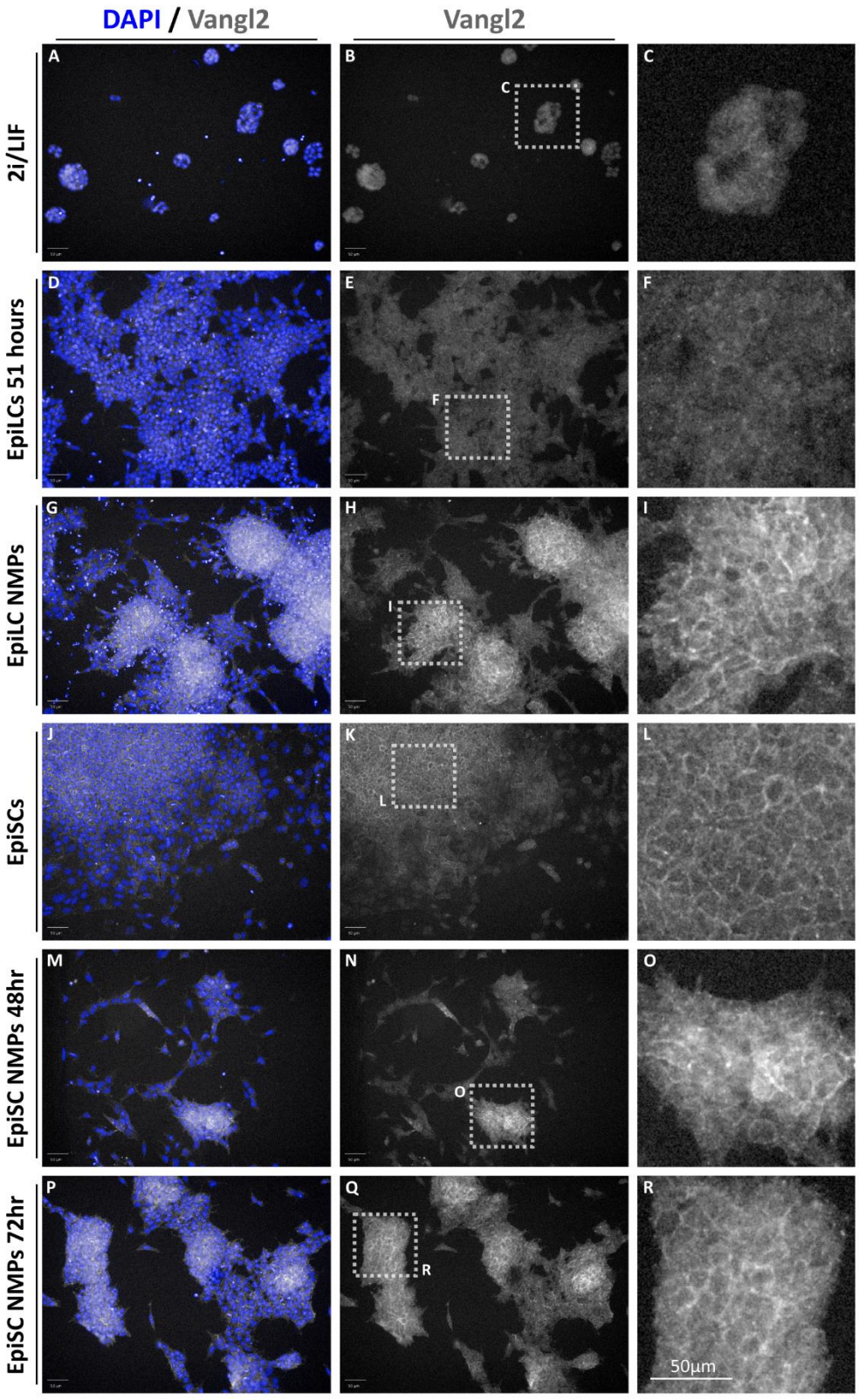

Figure 4.18 - Vangl2 expression in *in vitro* cultures.
Figure shows immunohistochemistry of Vangl2- greyscale, in *in vitro* cultures of **(A-C)** 2i/LIF, **(D-F)** EpiLCs (51 hours), **(G-I)** EpiLC derived NMPs, **(J-L)** EpiSCs, and **(M-O)** EpiSC derived NMPs Day 2 **(P-R)** and Day 3 of differentiation. DAPI - blue

4.7 Grafting of prospective EpiLC derived NMPs

Grafting conducted by Prof Val Wilson, Ex Vivo Embryo Culture and Imaging aided by Dr Filip Wymeersch.

Following the identification of similarities between NMPs derived from EpiSC and EpiLCs, I was interested to test if these cells also exhibited parallels in their *in vivo* developmental potential. NMPs derived from EpiSC had previously been shown to extensively contribute to both neural and mesodermal tissues when grafted to the Node-streak Border (NSB), the site of NMPs at the onset of somitogenesis (Fig. 4.20B) (Gouti et al., 2014).

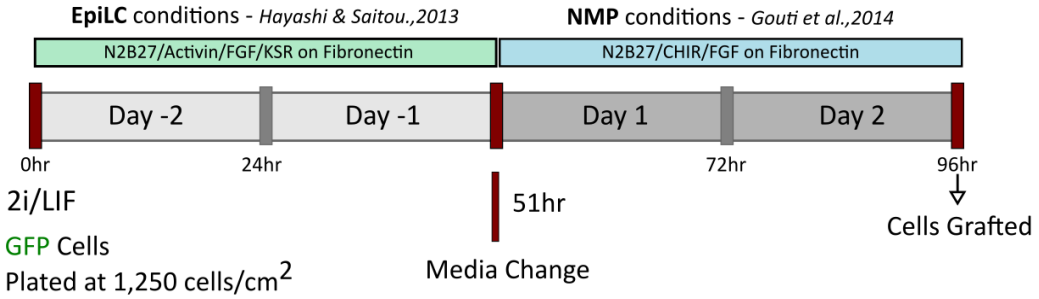

Figure 4.19 – Experimental overview of grafting GFP positive EpiLC-NMPs to NSB of wildtype embryos - Cell Differentiation.
Cell lines ubiquitously expressing GFP were seeded from 2i/LIF to EpiLC cuture conditions for 51 hours, and subsequently in NMP conditions for 2 days

Thus, to assess the functional capabilities of prospective NMPs derived from EpiLCs, these were grafted in the same manner. NMPs from EpiLCs were generated from two ubiquitously expressing GFP 2i/LIF cultured cells, C2 (Guo et al., 2009) and A-EGFP (Gilchrist et al., 2003) under optimised conditions (Fig. 4.19). Small groups of GFP transgenic cells were grafted in the NSB of wildtype embryos at 2-3 somite stage. They were initially imaged, to assess the success of the grafting, before being placed in to *ex vivo* rolling culture for 48 hours (Fig. 4.20). Embryos were then collected, dissected and imaged a final time.

.

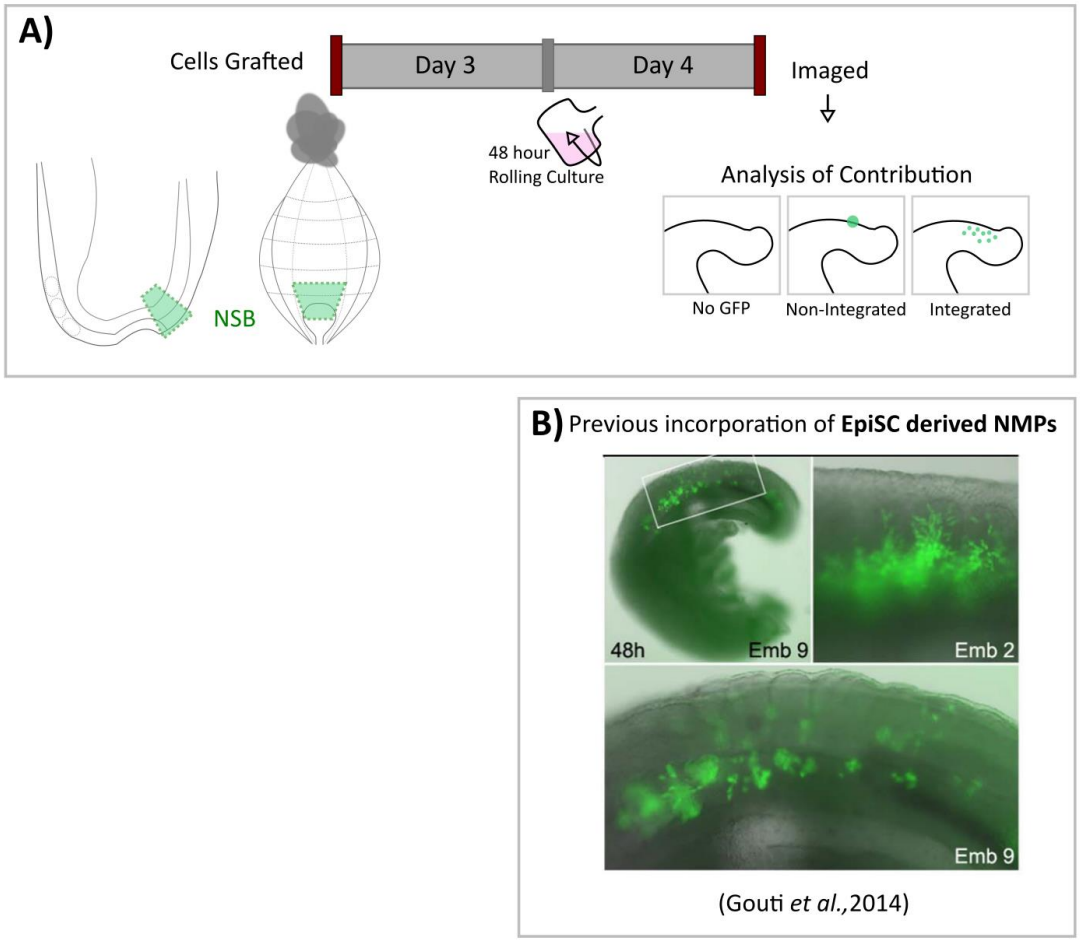

Figure 4.20 – Experimental overview of grafting GFP positive EpiLC-NMPs to NSB of wildtype embryos - Cell Grafting.

Cells lines ubiquitously expressing GFP were seeded from 2i/LIF to EpiLC cuture conditions for 51 hours, and subsequently in NMP conditions for 2 days, **(A)** were then grafted in to the NSB (NMP region) of wildtype embryos. Following imaging they were further grown in rolling culture for 48 hours before imaging again to determine contribution to the embryo. Contribution of GFP positive cells to wholemount embryos was classified as either, no GFP, non-integrated or integrated. To be classified as integrated, GFP positive cells had to be widely dispersed among wildtype (GFP negative) cells and not as a clump. As a control EpiLCs cultured for approximately 48 hours were also grafted in the same way. **(B)** EpiSC-NMPs previously contributed extensively to the caudal axis when grafted to the NSB in the same manner (Gouti et al., 2014).

Contribution of GFP positive cells was scored using images of wholemount embryos and assigned to three categories: no GFP, non-integrated or integrated (Fig. 4.20A). To be classified as integrated, GFP positive cells had to be widely dispersed among wildtype (GFP negative) cells, whereas non-integrated cells formed self-adherent clumps. 2i/LIF cultured cells cultured for 48 hours in EpiLC conditions are transcriptionally akin to pre-gastrulation embryos (Hayashi et al., 2011), and therefore these were additionally grafted as a negative control group as they were expected to not integrate. Contribution analysis is summarised in Table 4.1 below.

Table 4.1 – Contribution of GFP cells lines and cell types following grafting

C2 Cell Line

Cell Type	Contribution		
	No GFP	Non-Integrated	Integrated
EpiLC NMPs	5/6	1/6	0/6
EpiLC (control)	0/2	2/2	0/2

A-EGFP Cell Line

Cell Type	Contribution		
	No GFP	Non-Integrated	Integrated
EpiLC NMPs	0/6	2/6	4/6
EpiLC (control)	0/3	3/3	0/3

Grafting of the C2-GFP cell line resulted in no successful integration of either EpiLC or EpiLC-NMPs, this data is documented in (S-Fig. 4.1). In contrast, grafting using the A-EGFP cell line resulted in successful integration of GFP positive cells in 4/6 grafts using EpiC-NMPs (Fig. 4.21A-H) compared with the EpiLC control group for which integrated cells were not observed (0/3) (Fig. 4.22A-E). The successful integration of EpiLC-NMPs into these embryos showed contribution to tissues of the tail bud (Fig. 4.21B,D), and trunk (Fig. 4.21F,H) with verification of specific tissue contribution dependent on future examination of sections. The remaining two out of the six EpiLC-NMP grafted embryos contained only non-integrated GFP clumps (Fig. 4.21I-L). However these clumps were also observed in embryos with successful EpiLC-NMP integration (2/4) (Fig. 4.21B,H), suggesting EpiLC-NMPs had low contribution efficiency. Collectively this data suggests that EpiLC-NMPs can contribute to caudal tissues when grafted to in vivo NMP regions, with verification of specific tissue contribution dependent on future examination of sections. However, compared with the extensive incorporation of EpiSC-NMPs described previously

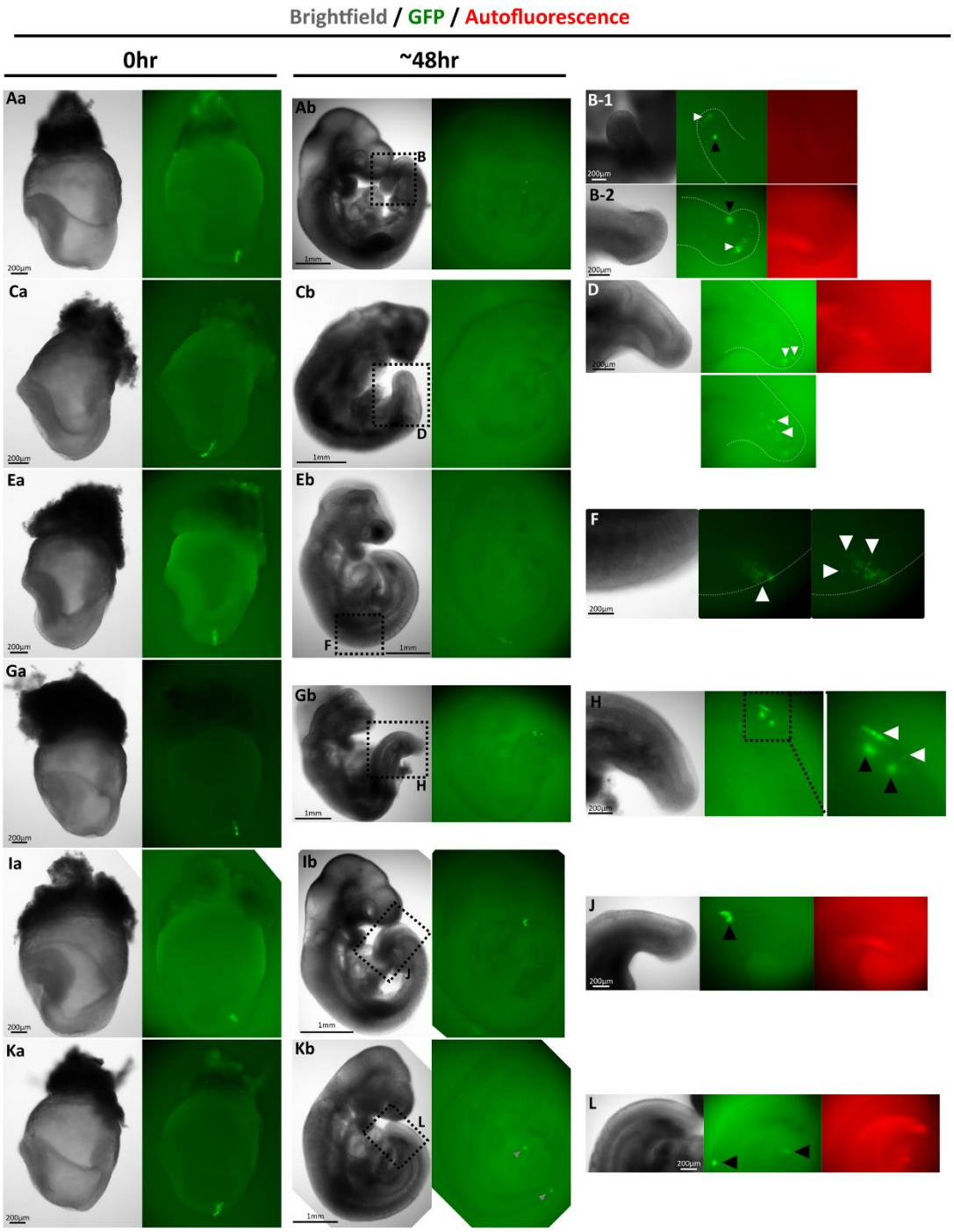

Figure 4.21 – EpiLC-NMPs can contribute to axial tissue when grafted to NMP regions.
Figure shows initial grafts (first column **Aa-Ka**) of EpiLC derived NMPs in to the NSB of E8.5 embryos at 0hr for 6 embryos in total, as well as images of **(Ab-Kb)** wholemount and **(B,D,F,H,J,L)** magnification of GFP+ contribution after approximately 48 hours of rolling culture. Embryos A-G show incorporated GFP+ cells contributing to axial tissues, and embryos I-K have non-integrated GFP clumps. GFP – green and auto fluorescence captured with the RFP channel – red. Integrated cells (white arrows), non-integrated clumps (black arrows). Overall the level of integration was lower than that previously described for EpiSC-NMPs. (Fig. 4.20B).

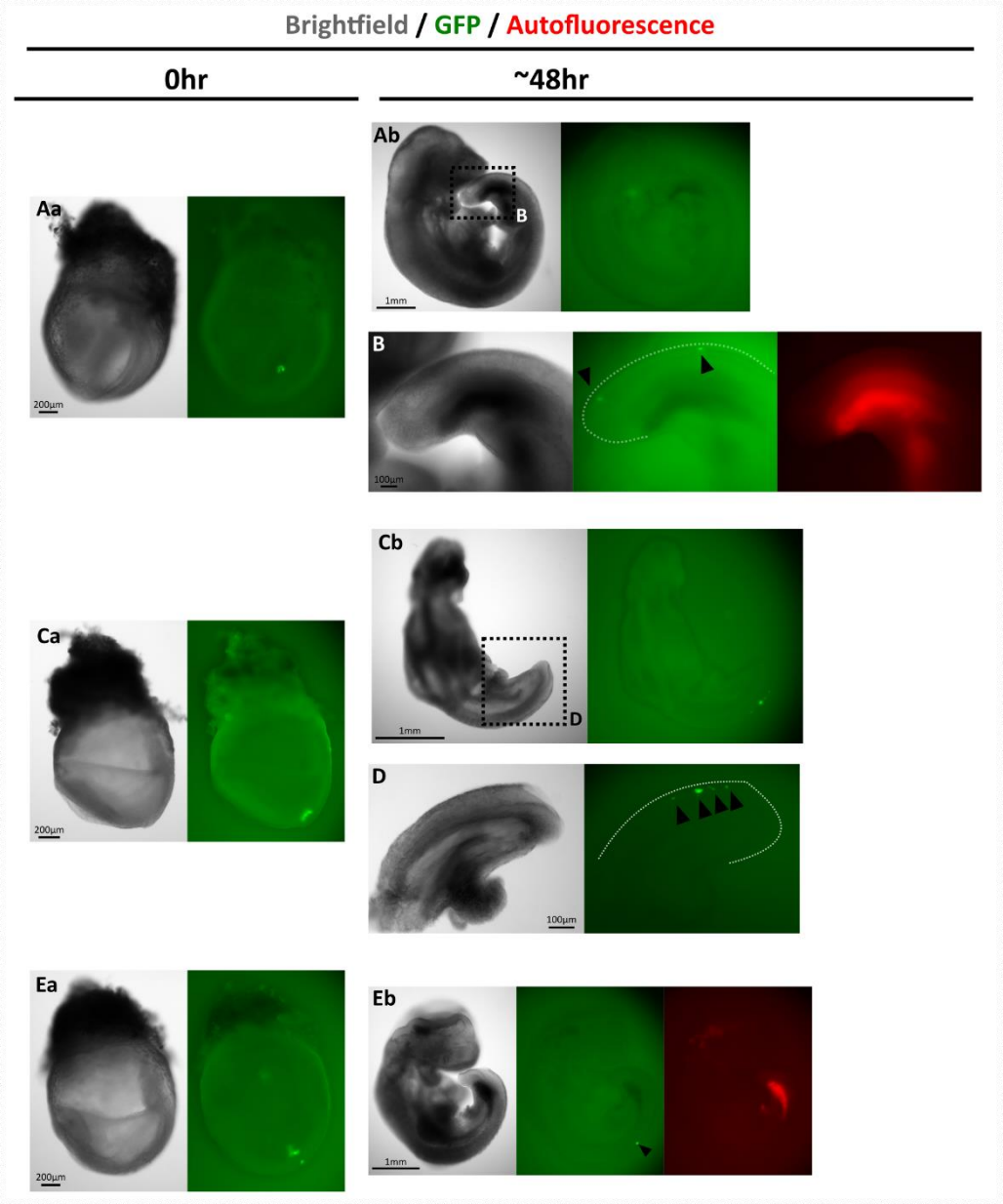

Figure 4.22 - EpiLCs cannot integrate when grafted to the NMP regions.
Figure shows **(Aa-Ea)** initial grafts of EpiLC (differentiated for approx. 48-52 hours) in to the NSB of E8.5 embryos at 0hr for 3 embryos in total, as well as images of (Ab-Eb) wholemount and (B,D) magnification of GFP+ areas after approximately 48 hours of rolling culture. All embryos show no integration of grafts. Non-integrated clumps (black arrows). GFP – green and autofluorescence captured with the RFP channel – red.

(Gouti et al., 2014), ultimately EpiLC-NMPs appear to have inferior NMP functionally in this context.

4.8 Discussion

4.8.1 NMPs can be derived from EpiLCs

EpiLCs represent a so-called 'formative' state, and are a homogeneous population of cell generated from 2i/LIF cultures. Following 48 hours of EpiLC differentiation cells are transcriptionally akin to E5.75 embryos (Hayashi et al., 2011). In the work described in this chapter the objective was to assess if NMPs could be derived from EpiLCs, a seemingly advantageous starting population versus more heterogenous EpiSCs. The work has demonstrated the robust derivation of T(Bra) and Sox2 double positive cells, characteristic of NMPs, from EpiLC culture, through activation of Fgf and Wnt/β-catenin signalling (Fig. 4.2-4.3), the traditional method of deriving NMPs from EpiSCs and ESCs (LIF/FCS) cultures (Gouti et al., 2014).

The effect of multiple variables on putative NMP proportions in these cultures was additionally explored using a high-throughput system and permitted the identification of optimal conditions for EpiLC-NMP derivation (Fig. 4.10-11). Finally, these optimised EpiLC-NMP cultures were compared with EpiSC-NMP cultures with regard to their transcriptional profile (Fig. 4.14-15), Wnt/PCP component expression (Fig. 4.16-18) and *in vivo* function (Fig. 4.21) to determine any inherent differences. Despite some apparent differences, overall many parallels existed between EpiLC-NMP and EpiSC-NMP cultures, providing evidence that EpiLC-NMP are similar to *in vivo* NMPs. In summation, this work deriving NMPs from homogeneous EpiLCs sources provides evidence of a novel *in vitro* differentiation protocol capable of producing cultures that mimic *in vivo* NMPs.

4.8.2 Comparison of derivation of NMPs from EpiLCs and EpiSCs

Following 48 hours of EpiLC differentiation, EpiLCs transcriptionally represent E5.75 embryos (Hayashi et al., 2011). On the other hand, EpiSCs which are derived from E5.5- E7.5 embryos, represent a later differentiation state termed 'primed', reflected by their expression of lineage markers (Brons et al., 2007; Kojima et al., 2014b; Tesar et al., 2007). As EpiLCs and EpiSCs represent different embryonic states, it was of particular interest to study what the consequences would be for moving to EpiLCs to EpiLC to NMP deriving conditions.

Overall it was apparent that derivation of NMPs from EpiLCs results in a phase of extensive cell death (Fig. 4.4). This phase does not occur when deriving NMPs from EpiSCs and, ultimately meant that plating density was 100x higher for EpiLCs compared with that for EpiSC to have the same plate coverage (Fig. 4.5). Even the adjustment of 'not replating' cells did not prevent this extensive cell death. However the process of EpiSC derivation from pluripotent ESCs is also characterised by extensive cell death that persists over many cell passages until EpiSCs are fully derived (Turco et al., 2012). Given these points it appears that cell death is a 'normal' and essential process in differentiation from more pluripotent states.

In NMP derivation from EpiLCs this process occurs quickly compared with the prolonged process of EpiSC derivation, and does not appear to impede progress to NMP differentiation. In fact death has also been described in other differentiation processes including neural differentiation (Ying and Smith, 2003). It is considered that cells unable to convert to new conditions and differentiate accordingly, are eliminated by apoptosis (reviewed in Morgani, Nichols and Hadjantonakis, 2017). In conclusion, the extensive death exhibited by EpiLCs towards NMP cultures mimics that of EpiSC derivation, and thus appears to be a normal process of cell differentiation. Derivation of NMPs from EpiLCs has the advantage in that it is quicker than deriving EpiSCs, which is prolonged and can be a heterogenous process (Bernemann et al., 2011). Nonetheless, whether the difference in the timing of the described extensive death between EpiLCs and EpiSCs has advantages in terms of the final NMPs derived, remains to be determined.

Another striking difference between NMP derivation from EpiLC and EpiSC was the temporal dynamics of T(Bra) and Sox2 co-expression. This co-expression, characteristic of NMPs was used to determine the presence of NMPs in the culture. T(Bra) and Sox2 co-expression appears following 48 hours of culture of EpiSC in NMP conditions, and persists for a further 48 hours approximately before expression becomes mutually exclusive (Gouti et al., 2014). In this chapter, it was shown that T(Bra) and Sox2 double positive cells, are present following 48 hours of culture of EpiLC in NMPs conditions (Fig. 4.3). This double positivity does not appear to persist, with T(Bra) and Sox2 becoming mutually exclusive in just 24 hours, suggesting they

had differentiated (Fig. 4.7B). Yet upon examination of the transcriptional data EpiLC-NMPs at this time do not appear to have lost their NMP identity, with markers of NMPs continuing to be expressed at a similar level to samples taken 24 hours previously (Fig. 4.14B,C). Moreover, they did not appear to be more differentiated when lineage specific markers were examined (Fig. 4.15).

In conclusion, the temporal dynamics of NMPs in EpiLC-NMP cultures needs further refinement to understand differences between EpiLC-NMPs and EpiSC-NMPs. Further investigations could utilise confocal microscopy to substantiate the proportions of T(Bra) and Sox2 double positive cells at 72 hours (Day 3) of EpiLC-NMP differentiation. This should also be complemented with a time course of transcriptional profiling to further describe the behaviour of cells in this dynamic differentiation process.

Of all the variables investigated, two appeared to be most important in determining the proportion of EpiLC-NMPs present in the culture. The first was the process of replating the EpiLCs before placing them in to NMP culture conditions. Reliably EpiLC-NMPs were more abundant in cultures in which cells were not detached and replated, but instead where only the media was changed (Fig. 4.11). Thus, the process of disrupting cell-cell contacts was obstructive to overall NMP numbers. Cell-cell contacts are also important for EpiSCs, which require passaging in small clumps of cells to survive (Chenoweth et al., 2010; Tesar et al., 2007). Moreover, the colonies of EpiSC and EpiLC cultures at 48 hours appeared strikingly similar, with cells closely associated (Fig. 4.1). This supports the idea that cell-cell contacts are important for regulating T(Bra) and Sox2 levels during differentiation toward NMPS, perhaps even implicating Wnt/PCP signalling for which cell-cell contacts are thought to be crucial. Considering this, Wnt/PCP components Fzd6 (Fig. 4.16,O), Ptk7 (Fig. 4.17I,O,R) and Vangl2 (Fig. 4.18I,O,R), were all identified in NMPs derived from EpiSC and EpiLC. In fact, Ptk7 and Vangl2 were even expressed in EpiSC cultures albeit to a lower level (Fig. 4.17-18L). Together this evidence supports the idea that cell-cell contacts are important for derivation of NMPs from EpiLCs and EpiSC, and additionally that this derivation may be mediated by the same Wnt/PCP signalling.

The second variable which enhanced EpiLC-NMP proportions was the length of EpiLC differentiation. Cultures which had longer EpiLC differentiation tended to have higher EpiLC-NMP proportions (Fig. 4.11). This finding is somewhat counter intuitive as these cells had waited the longest to receive 'posteriorising' signals from CHIR and Fgf treatment, and therefore potentially risk becoming more anteriorised. Nevertheless, EpiLC differentiation is a dynamic process, with many genes upregulated as EpiLCs differentiate, including *Wnt3a* and *Fgf5*, which may enhance NMP derivation (Hayashi et al., 2011). Another thing to consider is that the colonies in cultures with longer EpiLC differentiation are more domed, with cells appearing to be more closely associated (Fig. 4.12). As discussed above cell-cell contacts appear to be important for enhancement of EpiLC-NMPs, so this could also play an important role. In conclusion, longer EpiLC differentiation was associated with increased EpiLC-NMP number, however the exact mechanisms by which this is achieved remains to be fully understood.

4.8.3 EpiLC-NMPs and EpiSC-NMPs are similar but distinct

Comparison between NMPs derived from EpiLCs and EpiSCs was possible through examination of their transcriptional profile and *in vivo* potential. Some of the identified differences and similarities between the two populations are now discussed.

Transcriptionally EpiLC-NMPs and EpiSC-NMPs were analogous in concurrent downregulation of pluripotency markers and upregulation of gene associated with *in vivo* NMPs from their starting population, EpiLCs and EpiSCs respectively (Fig. 4.14). Moreover EpiSC-NMPs and EpiLC-NMPs were more like one another than any other control cell type included in the analysis. With that said, specific differences did emerge from the transcriptional analysis. With significantly lower *Wnt3a* and *T(Bra)* mRNA in EpiLC-NMPs it was evident that Wnt/β-catenin signalling was diminished in these samples compared with EpiSC-NMPs (Fig. 4.14B). This was also evident in the general (not significant) decrease in mesoderm specific markers (Fig. 4.15A) and marked (significant for Sox1) increase in neural markers of EpiLC-NMPs (Fig. 4.15B) compared with EpiSC-NMPs.

In conclusion despite the co-expression of T(Bra) and Sox2 protein, as well as the specific expression of NMP expression markers, EpiLC-NMPs appear to have concurrently a lower mesodermal and higher neural identity compared to EpiSC-NMPs. This is likely to have consequences on their differentiation potential, indeed preliminary evidence from these current investigations suggest that there may be a neural bias of these cells, with significantly increased levels of Sox1 in Day 3 EpiLC-NMP differentiation samples which was not matched by increases in examined mesoderm markers (Fig. 4.15). With that said, the inclusion of larger spectrum of mesoderm and neural markers would be essential in future investigations to confirm any potential differentiation bias.

Following the confirmation of similarities between EpiSC-NMPs and EpiLC-NMPs with transcriptional analysis, EpiLC-NMPs were tested functionally with *in vivo* grafting to NMP sites. EpiLC-NMPs were grafted to the NSB, in which NMPs reside and their tissue contribution was analysed the following day. EpiSC-NMPs grafted to this region had previously incorporated extensively to the caudal axis of embryos in 15/15 embryos (Gouti et al., 2014).

Despite contributing to some caudal tissues, EpiLC-NMPs showed less efficiency in their contribution with only 5/6 embryos exhibiting integration of grafted cells (Fig. 4.21). EpiLC-NMPs did not appear to have a bias to either mesodermal or neural tissues, however future examination of sections is essential to confirm this. Thus, despite similarities in gene expression and T(Bra) and Sox2 co-expression EpiLC-NMPs are not functionally equivalent.

This poorer contribution could have occurred for several reasons. Sub-optimal integration is characteristic of developmental asynchrony where two tissues do not match developmentally and the ability of the donor cells to colonise the host embryo is restricted. Thus, suggesting that grafted EpiLC-NMPs might not represent the exact temporal profile of NMPs needed for integration to host embryos. In this study *HoxA4*, *HoxA6* and *HoxD13* were also examined to determine any potential asymmetry. *Hox* genes are expressed in a spatio-temporal manner during embryo development (Deschamps and van Nes, 2005). No significant differences were identified between the EpiSC-NMPs and EpiLC-NMPs samples (Fig. 4.14C). Despite this preliminary

evidence against developmental asynchrony the examination of more *Hox* genes is necessary to allow for a more robust conclusion.

Another explanation for the sub-optimal contribution of EpiLC-NMPs could be because of a reduction in the overall number of grafted cells with NMP potential. As the same technique was used for grafting of EpiLC-NMPs in this thesis and for EpiSC-NMPs previous reported (Gouti et al., 2014), the reduction in NMP number would be most likely to be due to a dilution of NMP number in a mixed population of EpiLC-NMP cultures. Indeed, considering the T(Bra) and Sox2 analysis only 48% of the cells were reported as T(Bra) and Sox2 double positive even in the most optimal conditions (Fig. 4.10A). This is a dramatic reduction from the 90% reported for NMP derivation from EpiSCs (Gouti et al., 2014). However, for this analysis many cells had to be excluded due to the highly-domed nature of EpiLC-NMP colonies (Fig. 4.9). Thus, the estimation in EpiLC-NMP number reported in these experiments is likely to represent an underestimation of the absolute number of NMPs in EpiLC-NMP cultures. Further investigations are essential to get a better estimate of true proportions of NMPs in EpiLC-NMPs cultures. This might be done using confocal imaging which would allow the co-expression of T(Bra) and Sox2 to be determined in these domed colonies. Moreover, grafting experiments provide only an indication of the NMP potential of these cells, but cannot confirm if these cells are truly bipotent, and can contribute to both neural and mesodermal lineages. To do this retrospective clonal analysis of single-cell seeding of EpiLC-NMPs would need to be carried out, similar to those described for EpiSC-NMPs (Tsakiridis and Wilson, 2015). These experiments, in which clones generated by single cells are analysed in terms of their expression of lineage specific markers, would also indicate any inherent bias of these EpiLC-NMPs.

To sum up, the transcriptional analysis and functional testing of EpiLC-NMPs revealed many similarities between EpiSC-NMPs and EpiLC-NMPs, suggesting these cells are much alike. Transcriptional differences appear modest, however functionally EpiLC-NMPs are less efficiently with *in vivo* grafting. Further experiments are essential to understand the true reason for this, and to determine if EpiLC-NMPs truly represent bipotential progenitors. With that said, evidence presented in this thesis endorses the

use of EpiLCs as a novel starting population for the generation of cells which have many properties of *in vivo* NMPs and *in vitro* EpiSC-NMPs.

4.8.4 Derivation of EpiLC-NMPs requires further optimisation

Even the most optimised conditions for derived EpiLC-NMPs resulted in approximately 50% of the culture co-expressing T(Bra) and Sox2 (Fig. 4.10) versus the 90% of NMPs described from EpiSC (Gouti et al., 2014). Although this could be an under estimation of NMP number due to the exclusion of many domed colonies which could not be segmented accurately, and thus not included in the analysis. However low numbers of T(Bra) and Sox2 co-expressing cells could be due to suboptimal levels of Fgf or CHIR (Wnt/β-ctaenin signalling) which are essential for NMP derivation. Moreover, in the high-throughput screen for optimal conditions, the neural marker Sox2 tended to dominate the cultures. With only a few exceptions, Sox2 expression was consistently higher versus T(Bra) for all conditions tested (Fig. 4.10B). Furthermore, the lower levels of *Wnt3a* and *T(Bra)* (Fig. 4.14B), genes associated Wnt/β-catenin signalling, and the higher levels of neural markers compared with EpiSC-NMPs (Fig. 4.15B), support the idea that EpiLC-NMPs cultures exhibit neural bias. Furthermore, maintaining the correct balance between T(Bra) and Sox2 is thought to be crucial for deriving NMPs (Koch et al., 2017). Moreover, reported optimisation of EpiSC-NMPs, proved that suboptimal levels of Fgf or CHIR was enough to drastically reduce NMP numbers, and enhance the emergence of Sox single positive cells at the detriment of T(Bra) positive cells (Gouti et al., 2014). Indeed Fgf has been shown to inhibit neural differentiation (Greber et al., 2010), and T(Bra) being a direct target of Wnt/β-catenin signalling (Wilkinson et al., 1990).

Taken together, evidence points to a suboptimal level of Fgf and CHIR in EpiLC-NMP cultures. In future experiments Fgf and CHIR should be titrated to determine optimal levels. As T(Bra) expression appears to be the limiting factor simple titration experiments could be carried out using a T(Bra)- GFP reporter cell line (Tsakiridis and Wilson, 2015). This simple method would also circumvent the limitations that come with segmenting domed colonies.

As discussed above, this present work indicates some routes to optimisation but shows future research is needed, building on these new insights. Ideally this would allow for the eventual development of a robust protocol to produce cultures containing a high proportion of pure EpiLC-NMPs. Only at this point would it be prudent to compare the robust-ness and quality of NMPs derived from EpiSCs and EpiLCs, to determine if one source is superior over the other. With that said, the EpiLC-NMP protocol as it stands already offers an alternative starting population for NMP differentiation protocols which avoids the need of EpiSCs derivation which can be unpredictable and variable (Bernemann et al., 2011).

Chapter 5: Manipulating Wnt/PCP signalling in NMPs

5.1 Introduction & Aims

As previously described in the introduction (1.4.5) there is a growing body of evidence to suggest that Wnt/PCP may play a role in regulating NMP behaviour. This evidence includes reports of Wnt/PCP component expression in caudal regions during axial elongation. Additionally, there is a loss of caudal tissue in Wnt/PCP mutants, associated with dysregulation of NMP maintenance and/or differentiation (Table. 1.1). Moreover, this is supported by the identification of core Wnt/PCP components *Pk1* (3.2) and Vangl2 (3.3.3), and Wnt/PCP co-receptor Ptk7 (3.3.1) expression in *in vivo* NMPs during axial elongation in this thesis. Still, these components were not solely limited to expression in NMPs but were also identified in adjacent regions, including the notochord. Further of Wnt/PCPs role, its receptor, Fzd6 (3.3.2) is uniquely expressed in notochord, including that adjacent to NMPs in the CNH. Consequently, the localisation of Wnt/PCP components in adjacent regions complicates the interpretation of axial defects in Wnt/PCP mutants. Essentially, loss of caudal structures could either be a direct consequence of NMP specific disruption of Wnt/PCP or an indirect consequence of extensive Wnt/PCP disruption in the posterior of the embryo. Hence to fully dissect the role of Wnt/PCP signalling in regulating NMP maintenance and differentiation directly, conditional targeting of Wnt/PCP disruption is essential. Conditional disruptions of Wnt/PCP have been demonstrated in the literature, through the introduction of exogenous Wnt/PCP components (Albors et al., 2015; Guirao et al., 2010; Sienknecht et al., 2011). Consequently, the delicate balance of antagonistic interactions between components are disturbed, leaving Wnt/PCP signalling in these cells defunct.

Other questions remain regarding the regulation of Wnt/β-catenin signalling during axial elongation. Activation of this pathway is implicated in the maintenance of NMPs as well as their differentiation to mesoderm. Nevertheless, it is not known how this dual role of Wnt/β-catenin signalling is achieved. The recent identification of seemingly inhibitory influences of Wnt/PCP pathway components on Wnt/β-catenin signalling, advocates a potential role of Wnt/PCP in regulating NMP behaviour. Of

interest is Wnt co-receptor Ptk7, which can promote Wnt/PCP while attenuating Wnt/β-catenin signalling in Zebrafish development (Hayes et al., 2014). Notwithstanding, these remain uncharted areas of investigation in terms of NMPs during Mouse axial elongation.

Based on the above, the aim of the research described in this chapter was to advance knowledge of the role of Wnt/PCP signalling in NMP behaviour with a goal of answering key questions that remain unsolved including:

(1) Is Wnt/PCP activity in NMPs involved in the regulation of NMP maintenance and/or differentiation?

(2) Does Ptk7 have an active role in Wnt/PCP activity in NMPs?

To address these, experimental goals included:

- Adaption and utilisation of tools to conditionally disrupt Wnt/PCP signalling in *in vitro* and *in vivo* NMP systems
- Systematic study of the effects of disrupting Wnt/PCP signalling on NMP maintenance and differentiation in these systems

5.2 Wnt/PCP perturbation *in vivo*

5.2.1 Generation of Wnt/PCP overexpression constructs

As outlined in the above the introduction of exogenous wildtype Wnt/PCP components is enough to disrupt Wnt/PCP. Electroporation offers a simple method through which exogenous DNA can be precisely introduced into a small number of cells. Electroporation of CLE and NSB had recently been optimised, and therefore provided a method by which exogenous Wnt/PCP components could be introduced specifically in NMPs (Huang et al., 2015). More importantly in this thesis the identification of Ptk7 (Fig. 3.5-3.6) and asymmetric Vangl2 (Fig. 3.12) implicated the activity of Wnt/PCP in this region. In total five fluorescently labelled gene overexpression plasmids were generated for use in *in vivo* electroporation experiments (Fig. 5.1). These included CAG-*Vangl2*-T2A-RFP (**CAG-Vangl2**), CAG-*Pk1*-T2A-RFP (**CAG-Pk1**), and CAG-*Ptk7*-T2A-RFP (**CAG-Ptk7**) generated based on wildtype sequences.

Despite reports of Wnt/PCP disruption with overexpression of Pk1 and Vangl2 (Albors et al., 2015), comparable disruptions had not been fully described for Ptk7 overexpression. Instead dominant negative constructs had been reported to disrupt Ptk7 function. A soluble Ptk7 (sPtk7), consisting of only small portion of extracellular Ptk7 domain including the cleavage site of MMP14 results in neural tube defects characteristic of *Ptk7 chuzhoi* mutants (in which an extra MMP14 cleavage site is present) (Paudyal et al., 2010; Shin et al., 2008). Thus, endogenous Ptk7 activity may be disrupted by competing for its cleavage by MMP14. This was potentially interesting in terms of NMP regulation as distinct regions of Ptk7 protein proteolysis were identified during axial elongation (3.3.1). Hence, two putative dominant negative Ptk7 constructs were generated, CAG-*Ptk7*ΔICD-T2A-RFP (**CAG-Ptk7ΔICD**) and CAG-s*Ptk7*-T2A-RFP (**CAG-sPtk7)**. CAG-sPtk7, had the same sequence as the soluble Ptk7 described in (Shin et al., 2008), consisting of only a small portion of the extracellular domain (6^{th} and 7^{th} Ig domains) of wildtype Ptk7. Putative dominant negative CAG-Ptk7ΔICD included all extracellular Ig domains, the transmembrane domain of wildtype Ptk7, but no intracellular domain (ΔICD). This construct was generated to potentially compete with endogenous Ptk7 for binding of extracellular

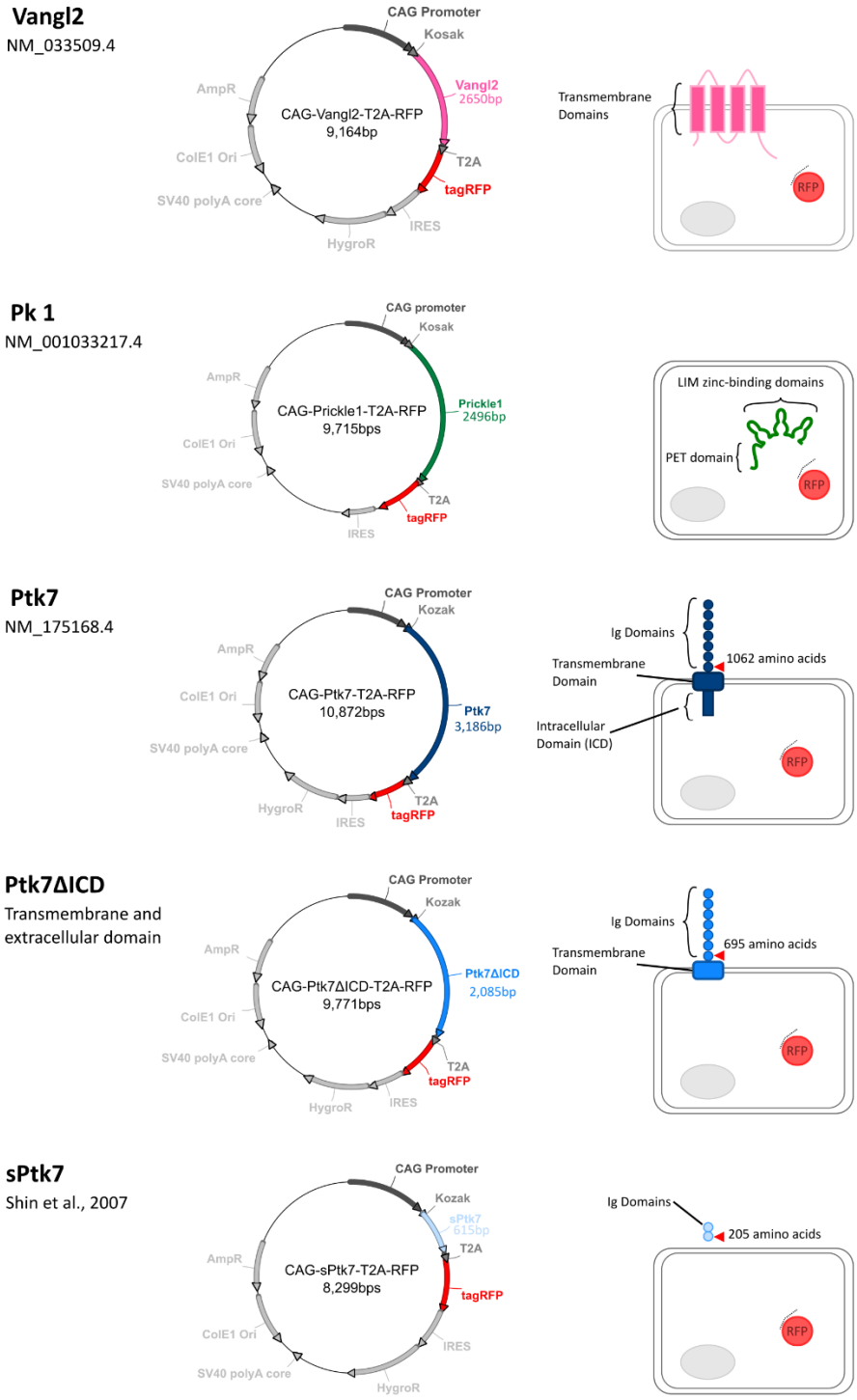

Figure 5.1 – Generated Wnt/PCP overexpression RFP labelled plasmids.
Figure shows plasmid maps for generated overexpression plasmids. Each plasmid is labelled with the Wnt/PCP gene of interest, the NCBI sequence from which it was cloned, as well as the structure or reference paper they were generated based on. All plasmids drive gene of interest with CAG promotor and kozak sequences, with gene of interest linked to tag red fluorescent protein (RFP) with T2A sequence encoding a 2A cleavage peptide. Also included is expected post-translation structure and location of protein. For Ptk7 constructs MMP-14 cleavage site is indicated by red arrow. ICD – intracellular domain, Ig – immunoglobulin.

interaction partners reported to include Wnt3a, Wnt5a and Ror2 (reviewed in Berger, Wodarz and Borchers, 2017).

All plasmids were designed to have the gene of interest, driven upstream by a CAG promotor, known to promote high level of gene expression (Niwa et al., 1991; Okabe et al., 1997) followed by a Kosak sequence to aid initiation of translation (De Angioletti et al., 2004). The stop codon of each gene was replaced by a T2A sequence followed by tag Red Fluorescent Protein (tagRFP). Inclusion of the T2A sequence, meant the protein of interest would be fused to the RFP via a self-cleavage 2A peptide (Kim et al., 2011; Ryan et al., 1991). These 'self-cleaving' peptides are though to function by disrupting the ribosome during translation which leads to the separation of two adjacent peptides (Kim et al., 2011). This system allows for accurate reporting of protein expression without compromising the activity or stability of the protein. This was important for the proteins of interest, specifically Vangl2 and Ptk7 which have been shown to interact with components via regions near to their Carboxyl-terminus (Belotti et al., 2012; Montcouquiol, 2006; Puppo et al., 2011; Shnitsar and Borchers, 2008; Torban et al., 2004; Wehner et al., 2011; Yao et al., 2004).

5.2.2 Electroporation of Wnt/PCP constructs in NMPs

Electroporation and embryo culture was performed by MSc Student Catarina Matins Costa and Dr Filip Wymeersch.

To determine if perturbation of Wnt/PCP signalling by overexpression of either Vangl2, Ptk7 or Pk1 would affect cell fate decisions of NMPs, overexpression constructs were electroporated into Mouse embryos in NMP containing regions (CLE and NSB) (Fig. 5.2A). An RFP overexpression plasmid was used as a control. Following 2 hours of *ex vivo* rolling culture, embryos were examined for RFP expression. Those correctly targeted, reported frfby RFP expression, were further cultured for 22 hours after which they were dissected, imaged, fixed, embedded and cryosectioned (Fig. 5.2B). In transverse embryo sections RFP intensity was low, but bright enough to see without use of RFP antibody staining. RFP was localised to the cytoplasm, and was also frequently found as aggregations, small red fluorescent dots (Fig. 5.3D). Before undergoing analysis to identify a possible bias in the fate of

electroporated NMPs, the overexpression of Wnt/PCP components in electroporated cells was confirmed.

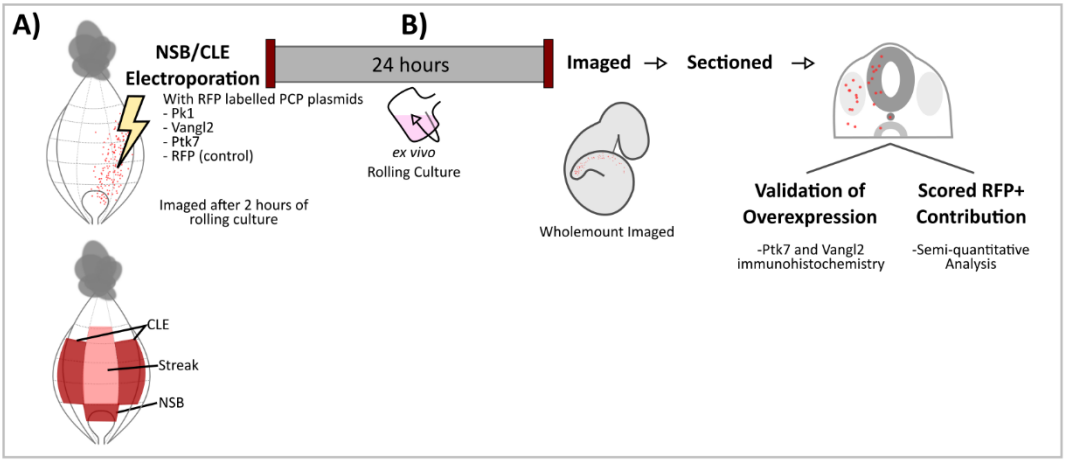

Figure 5.2 – Experimental set up for electroporation of E8.5 embryos with Wnt/PCP overexpression plasmids.
Figure shows experimental set up for analysis of electroporation of Wnt/PCP plasmids. **(A)** E8.5 embryos were electroporated with fluorescently labelled Wnt/PCP overexpressing plasmids, targeting specifically NMP regions, the caudal lateral epiblast (CLE) and the node-streak border (NSB). **(B)** Following 2 hours of *ex vivo* culture, wholemount embryos were imaged and selected for further *ex vivo* culture based on the presence cells expressing RFP. Following a total of 24 *ex vivo* rolling culture, the embryos were imaged, fixed, embedded and sectfioned in preparation for further analysis.

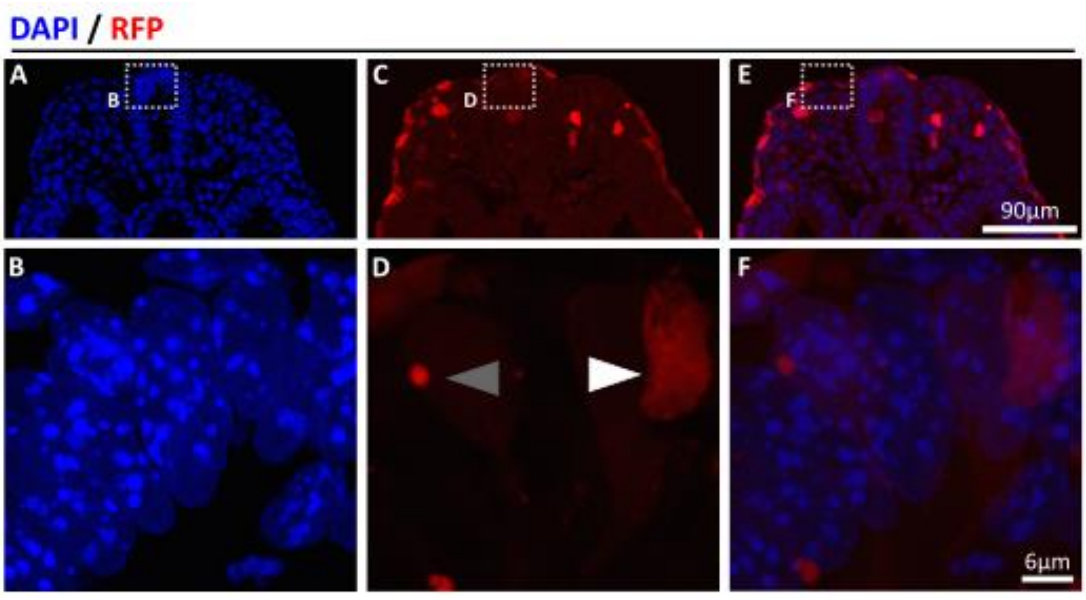

Figure 5.3 – Red Fluorescent Protein was aggregated or localised to the cytoplasm.
Transverse sections of electroporated embryos show the localisation of RFP. RFP was found as aggregates (grey arrow) and in the cytoplasm (white arrow). DAPI - blue, RFP - red.

5.2.2.1 Validation of electroporated Wnt/PCP constructs

Immunohistochemistry and imaging was performed by MSc Student Catarina Martins Costa

To verify that RFP expression was associated with an increase of Wnt/PCP protein, immunohistochemistry of Vangl2 and Ptk7 on electroporated embryo sections were performed using antibodies specific to each respective protein (Fig. 5.4). Vangl2 and Ptk7 proteins were only found at the cell membrane as expected, and never in aggregates (Fig. 5.4D,L). RFP positive cells had higher levels of each respective protein versus RFP negative cells, which expressed only endogenous Ptk7 and Vangl2. The different localisation of RFP (cytoplasm) and Wnt/PCP proteins (cell membrane) within the cell also indicated correct cleavage of T2A peptide. In conclusion, cells electroporated specifically overexpressed Wnt/PCP components. Consequently, the value of further analysis of electroporated cells to examine their potential fate bias was confirmed.

5.2.2.2 Ptk7 or Vangl2 overexpression impedes NMP neural differentiation and NMP persistence in the CNH

DAPI staining, section scoring and targeted electroporation diagrams were carried out by MSc Student Catarina Costa

With the purpose of identifying a bias in the fate of electroporated NMPs, semi-quantitative analysis was performed to examine the contribution of electroporated cells to specific tissue lineages along the axis. At least 5 embryos with similar targeted electroporated areas (specifically in the midline and CLE), for each treatment group were selected for analysis. Every other slide (containing between 5-6 sections) was scored for the presence of RFP+ cells anteriorly to posteriorly (Fig. 5.5A), starting from where the first RFP+ cell was found (Fig. 5.5B). Each section was scored based on the percentage contribution of RFP+ cells per tissue type (versus all cells in that tissue type). These tissues were either PXM (somites, presomitic mesoderm and tail bud mesoderm) or neural tube (NT), or additionally in more posterior tissue the CNH (Fig. 5.5C), representative images documented in (Fig. 5.6). The density of RFP+ contribution in each was graded: negative (0% RFP+), Low (1-20%), Medium (20-60%) or high (>60%) (Fig. 5.5D). Representative images illustrating the

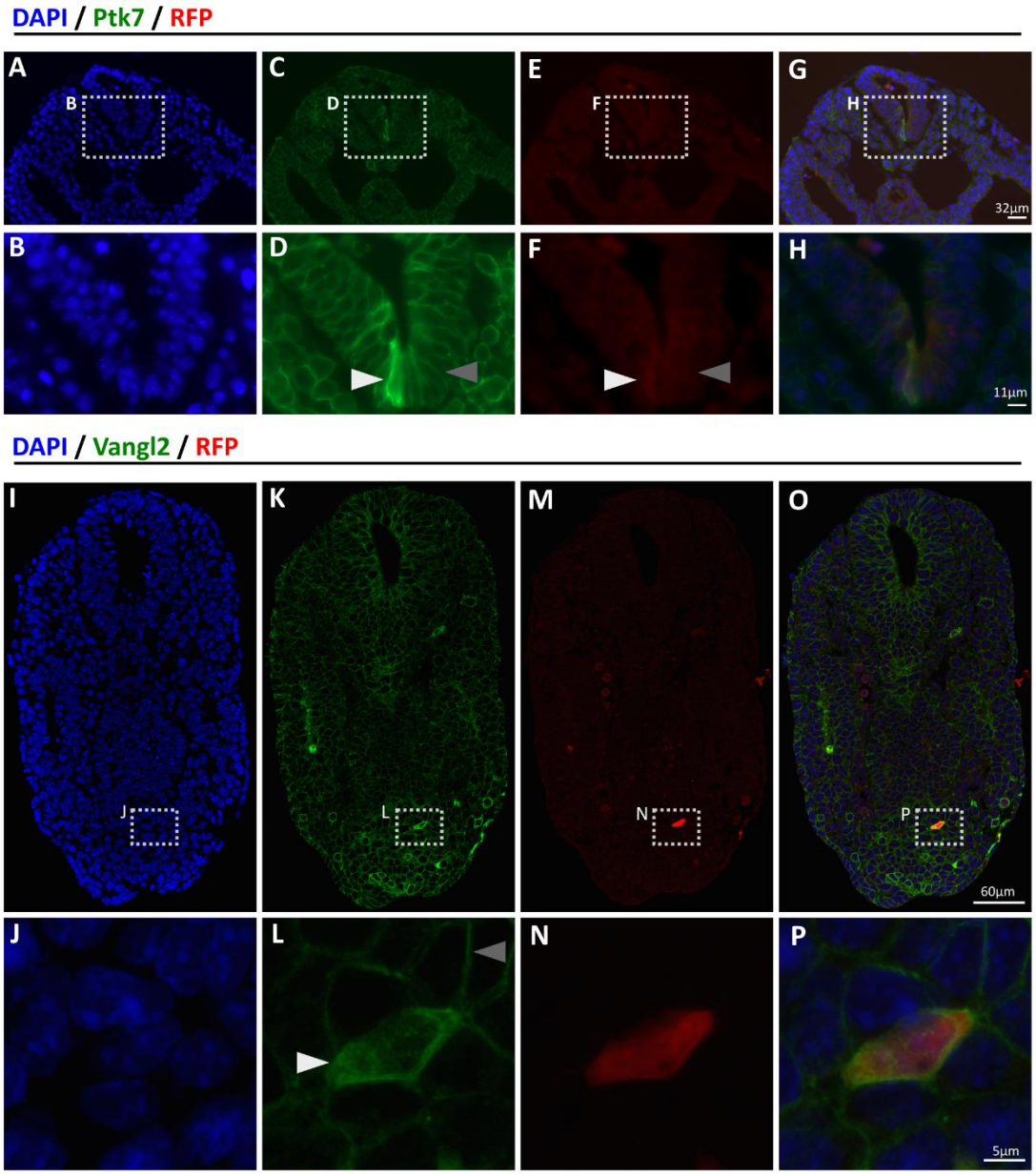

Figure 5.4 – Ptk7 and Vangl2 are overexpressed in targeted electroporated cells.
(A-H) Ptk7 immunohistochemistry on transverse sections of CAG-Ptk7-T2A-RFP electroporated embryos shows targeted (RFP positive – white arrow) cells have increased levels of Ptk7 (green) compared with un-electroporated (RFP negative – grey arrow) neighbours. **(I-P)** Vangl2 immunohistochemistry on transverse sections of CAG-Vangl2-T2A-RFP electroporated embryos shows targeted (RFP positive – white arrow) cells have increased levels of Vangl2 - green compared with un electroporated (RFP negative – grey arrow) neighbours.

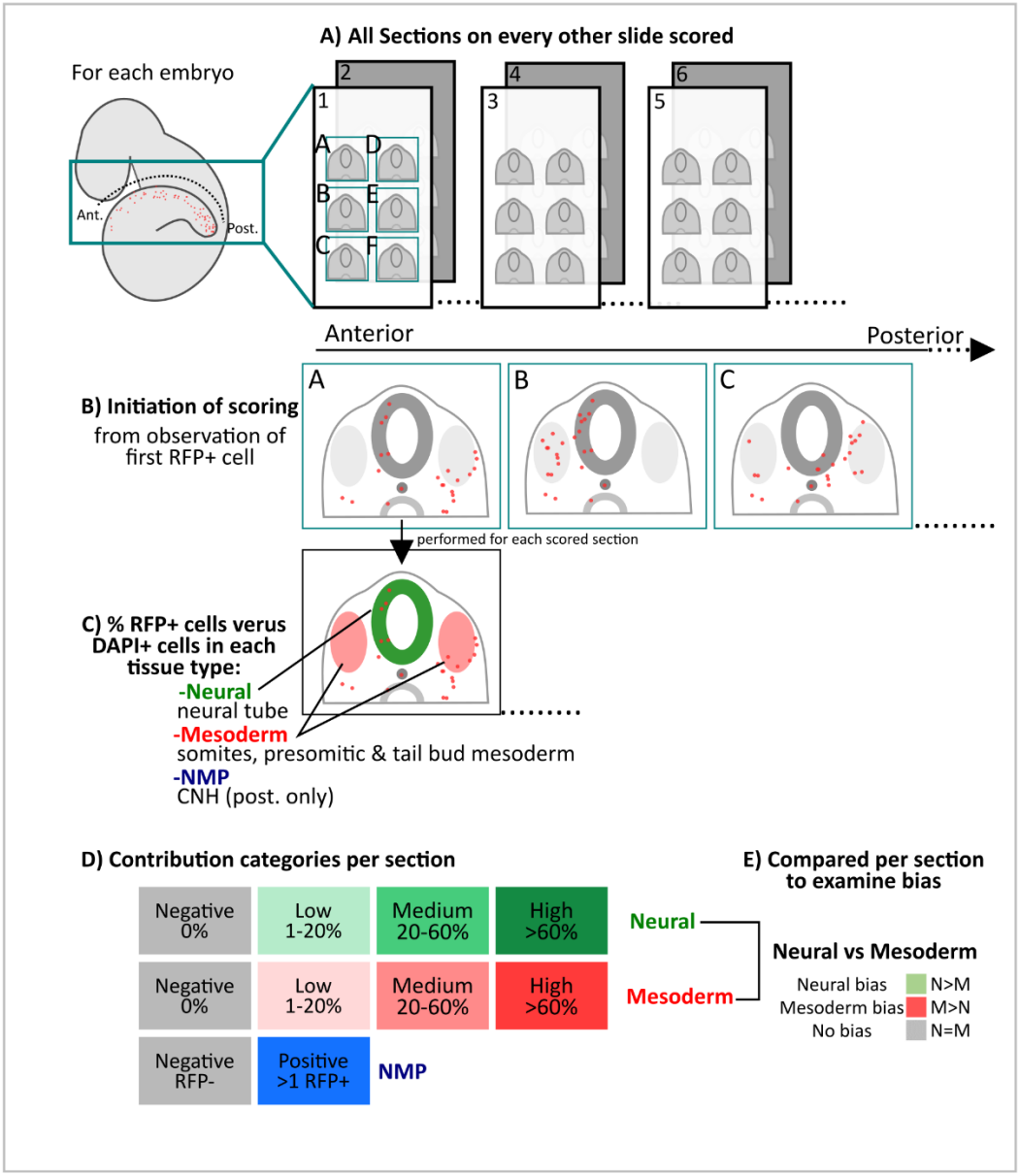

Figure 5.5 –Overview of semi-quantitative analysis of RFP+ contribution.
To identify any potential bias in the fate of electroporated NMPs, semi-quantitative analysis undertaken. **(A)** For each embryo, every other slide containing between 5-6 sections was **(B)** scored for the presence of RFP+ cells sequentially from anterior to posterior sections, beginning from where the first RFP+ cell was found. **(C)** Each individual section was scored based on the percentage contribution of RFP+ cells per tissue type (versus all cells-DAPI in that tissue type), tissue types were neural, mesoderm and neuromesodermal progenitors (NMPs) (in posterior CNH sections only). **(D)** The density of RFP+ cells within each tissue was graded into categories. **(E)** To investigate a potential lineage-bias the relative levels of RFP+ density was calculated by comparing the category of contribution between neural and mesoderm.

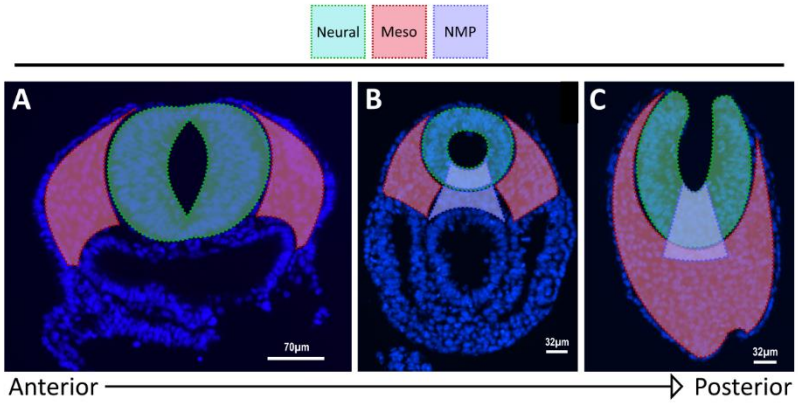

Figure 5.6 – Representative anterior to posterior images of tissue types scored.
Representative images to show regions scored across the axis from **(A)** anterior through **(B)** to the most posterior tissue **(C)**. Neural (green) included neural tube, Mesoderm (meso) (red) included paraxial mesoderm (anterior) and tail bud mesoderm (posterior), and finally the NMPs region (purple) was the CNH which was limited to posterior sections.

categorisation of RFP+ levels for mesoderm, including sections were RFP was aggregated are documented in (Fig. 5.7).

To evaluate the capacity of electroporated NMPs to differentiate to either lineage or remain in the NMP region, the contribution to the neural, mesoderm and CNH was calculated for each embryo. This is represented as percentage of each category across all sections (Fig.5.5D / Fig. 5.8a-11a). To further investigate a potential lineage bias, the relative levels of neural versus mesoderm RFP+ contribution per scored section was calculated by comparing contribution categories (Fig. 5.5 E). Each section was categorised to have either, neural bias -neural contribution was greater than mesoderm (N>M), mesoderm bias - mesoderm contribution was greater than neural (M>N), or no bias - in which categories were equal for both lineages (N=M). These are represented as percentage of each category across all scored sections (Fig. 5.8b-5.11b). Results of this analysis for each embryo is documented for RFP control (Fig. 5.8), Ptk7 (Fig. 5.9), Pk1 (Fig. 5.10) and Vangl2 (Fig. 5.11). Supplementing examination of individual embryos, results were pooled per experimental group and averaged in terms of RFP+ density for each tissue type and tissue bias (Fig. 5.12).

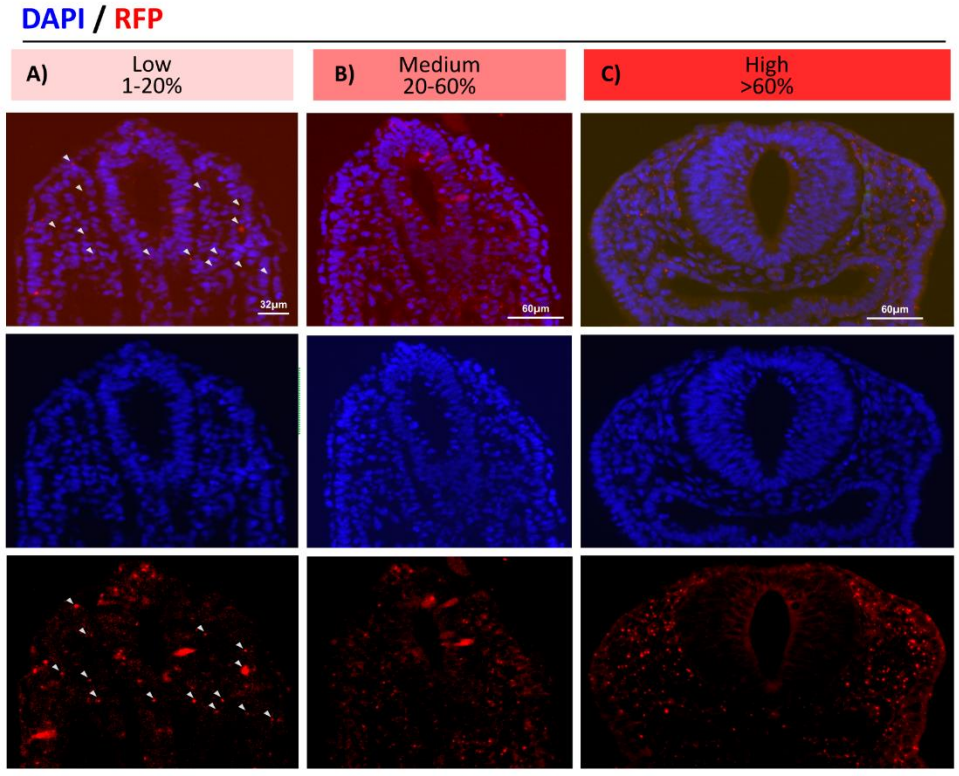

Figure 5.7 – Representative sections of RFP+ mesoderm contribution.
Representative images show categorised contribution, here for mesoderm. **(A)** section with low (1-20%) contribution, in which only a low number of aggregates (white arrows) were present, **(B)** medium (20-60%) and **(C)** High (>60%) contribution of RFP+ cells to mesoderm tissues.

Individual embryos for control group displayed unique variance in lineage contribution which appeared to be related to targeted electroporated area (Fig. 5.8). Embryos 1,5,6 exhibited enhanced contribution to mesoderm lineages. With a higher proportion of all sections containing at least 20% RFP+ positivity in mesoderm tissue, versus contribution to neural (Fig. 5.8c), and additionally more mesoderm versus neural contribution within sections (Fig. 5.8d). Consequently these findings were not unexpected as these embryos were electroporated in regions associated with bias to mesoderm lineages (streak and posterior tissue) (Cambray and Wilson, 2007; Wymeersch et al., 2016). Conversely embryos with more lateral electroporation, Embryos 2 and 4, displayed preference to neural contribution, both between and within sections. Moreover embryo 3 in which electroporation included streak and CLE, had no significant preference to either lineage. Despite variation in lineage bias between individual embryos, the overall lineage contribution was balanced when these were averaged for the whole group (Fig. 5.10). In total 87% and 89% of all sections

contained RFP+ contribution in neural or mesoderm respectively (Fig. 5.10A,B). Furthermore 37% and 35% of all sections contained at least medium (20%+) levels of RFP+ density in neural or mesoderm respectively. In addition, within individual sections there were comparable levels of bias towards mesoderm or neural tissues, suggesting an overall balance in NMP differentiation toward either lineage. 30% and 35% of sections displayed preference to neural or mesoderm contribution, and 35% with equal mesoderm and neural contribution (Fig. 5.10C). Notably in the control group, RFP+ NMPs were always found in the CNH of all analysed embryos, with contribution to 97% of all CNH sections (Fig. 5.10D). In summary, despite variability between individual embryos, overall NMPs gave rise to both neural and mesodermal lineages in a balanced way, and additionally persisted in the CNH. This confirmed that electroporated NMPs cells are viable and behave as expected in this assay, and permitted further analysis of embryos electroporated with Wnt/PCP constructs.

Pk1 electroporated embryos displayed similar trends in lineage and CNH contributions. Overall the percentage of negative sections was slightly higher in Pk1 group but comparable to control group. In total 22% and 24% of Pk1 sections were negative for RFP+ cells in neural and mesoderm tissue respectively, versus 13% and 11% (control group) (Fig. 5.12A,B). Consistent with the control group, the relative levels of mesoderm or neural contribution across sections, and neural verses mesoderm within sections was variable between individual embryos (Fig. 5.10a-b). Considering this variation, no clear association between lineage bias and electroporated region in these individual embryos could be identified. Overall the lineage bias per section in the Pk1 group reflected the balance described previously for the control. The proportion of individual sections with mesoderm or neural bias was comparable at 35% and 29%, even if slightly higher for mesoderm, with the remaining 35% displaying equal balance of neural and mesoderm contribution (Fig. 5.12C). Pk1 electroporated embryos additionally showed similar contribution to CNH sections versus controls. 100% of CNH sections contained RFP+ cells compared with 97% for control group (Fig. 5.12D).

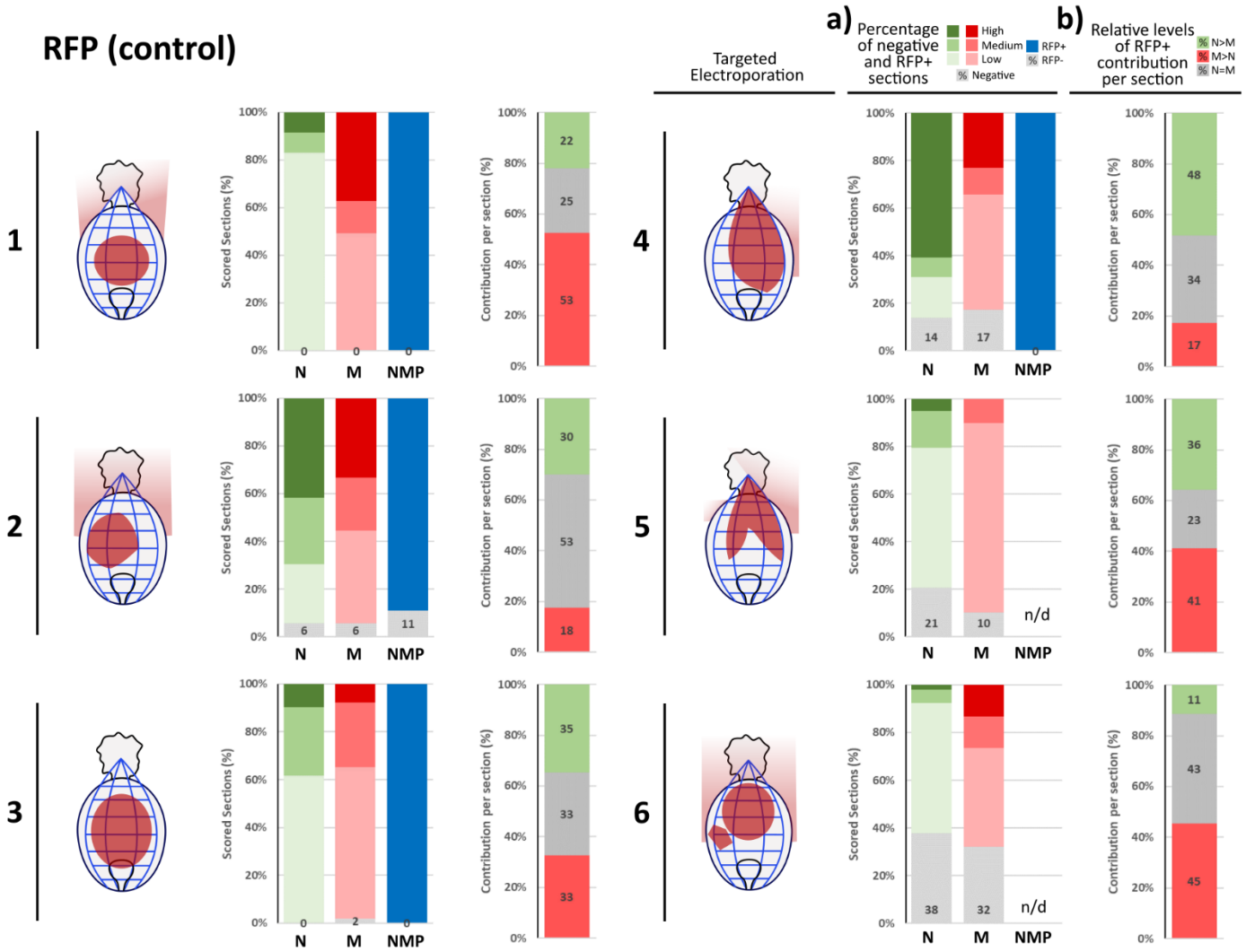

Figure 5.8 - Single embryo results for electroporation with CAG-RFP.

Results of semi-quantitative analysis for individual embryos for CAG-RFP electroporated embryos. For each embryo, a schematic representation is included to indicate the approximate targeted area (red) based on images taken 2 hours following electroporation including off-targeted areas represented by red surround **(a)** The percentage of all scored sections in each RFP density category, for neural (green), mesoderm (red) and NMP (blue) tissues. Percentage of sections with no contribution is shown as a number on the bar chart **(b)** Relative levels of neural versus mesoderm RFP+ contribution per individual section, grey indicating proportion of those with equal contribution to both tissues. The percentage in each category is shown by the number. (N- neural, M-mesoderm, NMP-neuromesodermal progenitor.

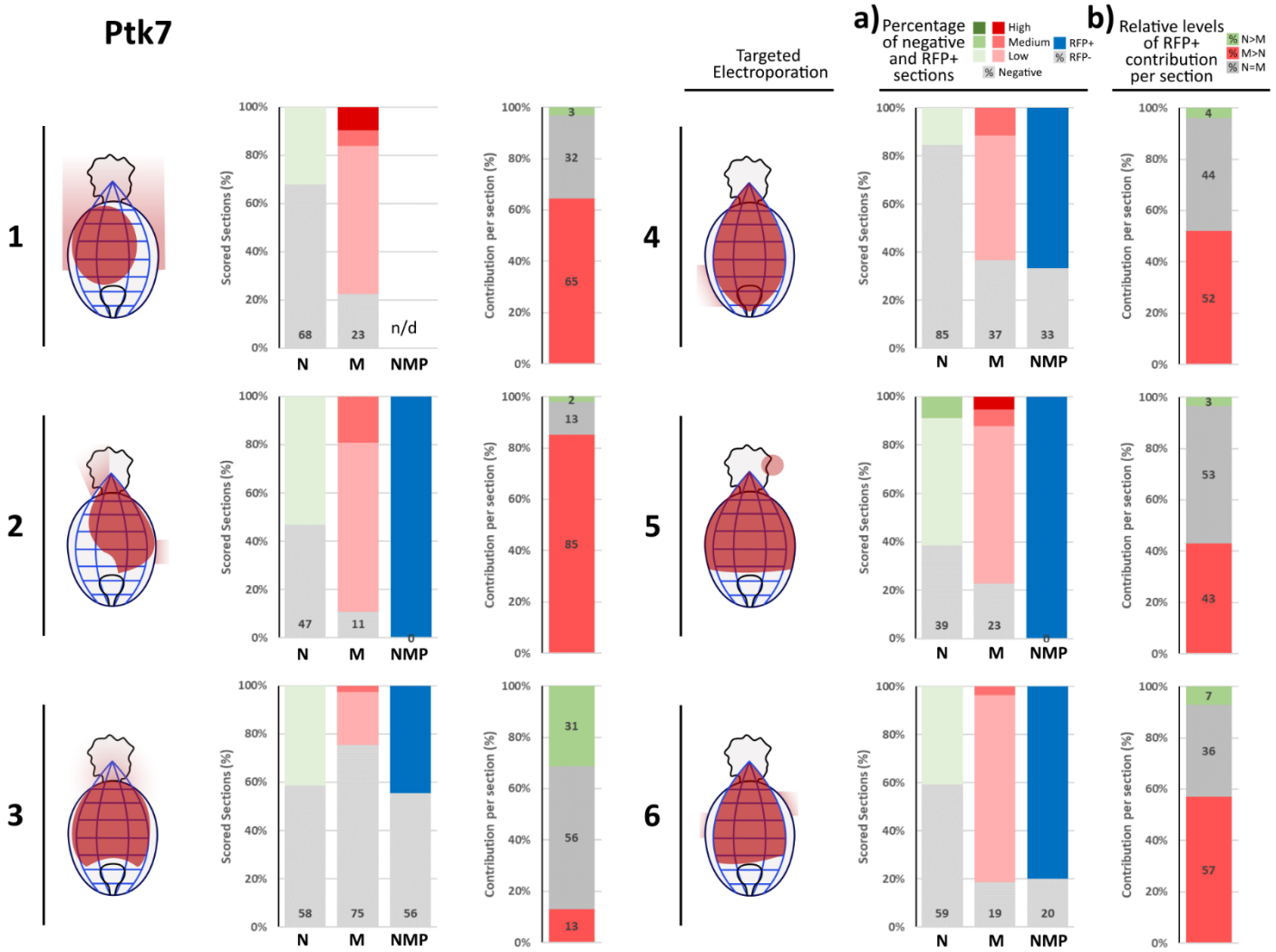

Figure 5.9 - Single embryo results for electroporation with CAG-Ptk7.
Results of semi-quantitative analysis for individual embryos for CAG-Ptk7 electroporated embryos. For each embryo, a schematic representation is included to indicate the approximate targeted area (red) based on images taken 2 hours following electroporation including off-targeted areas represented by red surround **(a)** The percentage of all scored sections in each RFP density category, for neural (green), mesoderm (red) and NMP (blue) tissues. Percentage of sections with no contribution is shown as a number on the bar chart **(b)** Relative levels of neural versus mesoderm RFP+ contribution per individual section, grey indicating proportion of those with equal contribution to both tissues. The percentage in each category is shown by the number. (N- neural, M- mesoderm, NMP- neuromesodermal progenitor.

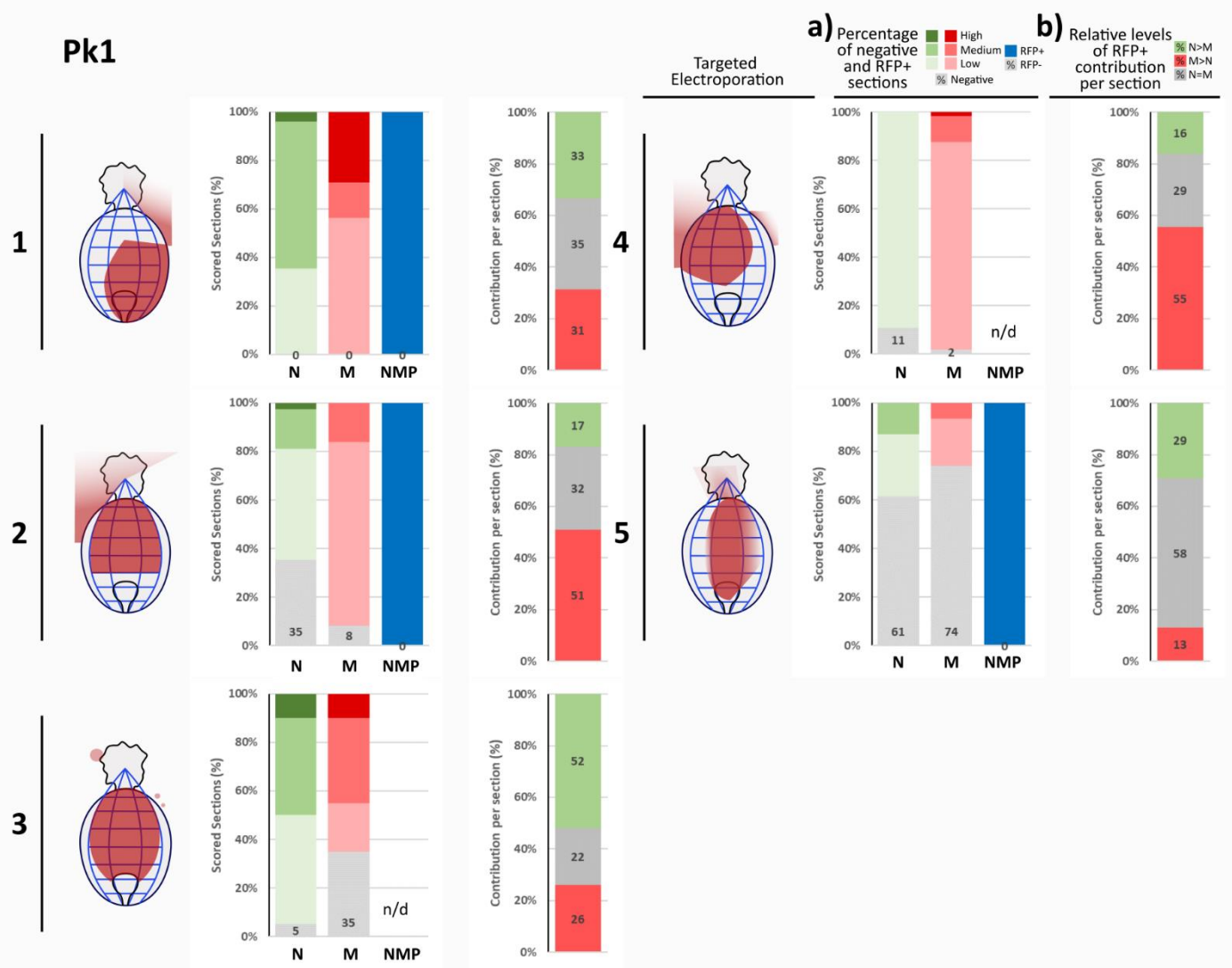

Figure 5.10 - Single embryo results for electroporation with CAG-Pk1. Results of semi-quantitative analysis for individual embryos for CAG-Pk1 electroporated embryos. For each embryo, a schematic representation is included to indicate the approximate targeted area (red) based on images taken 2 hours following electroporation including off-targeted areas represented by red surround **(a)** The percentage of all scored sections in each RFP density category, for neural (green), mesoderm (red) and NMP (blue) tissues. Percentage of sections with no contribution is shown as a number on the bar chart **(b)** Relative levels of neural versus mesoderm RFP+ contribution per individual section, grey indicating proportion of those with equal contribution to both tissues. The percentage in each category is shown by the number. (N- neural, M-mesoderm, NMP-neuromesodermal progenitor.

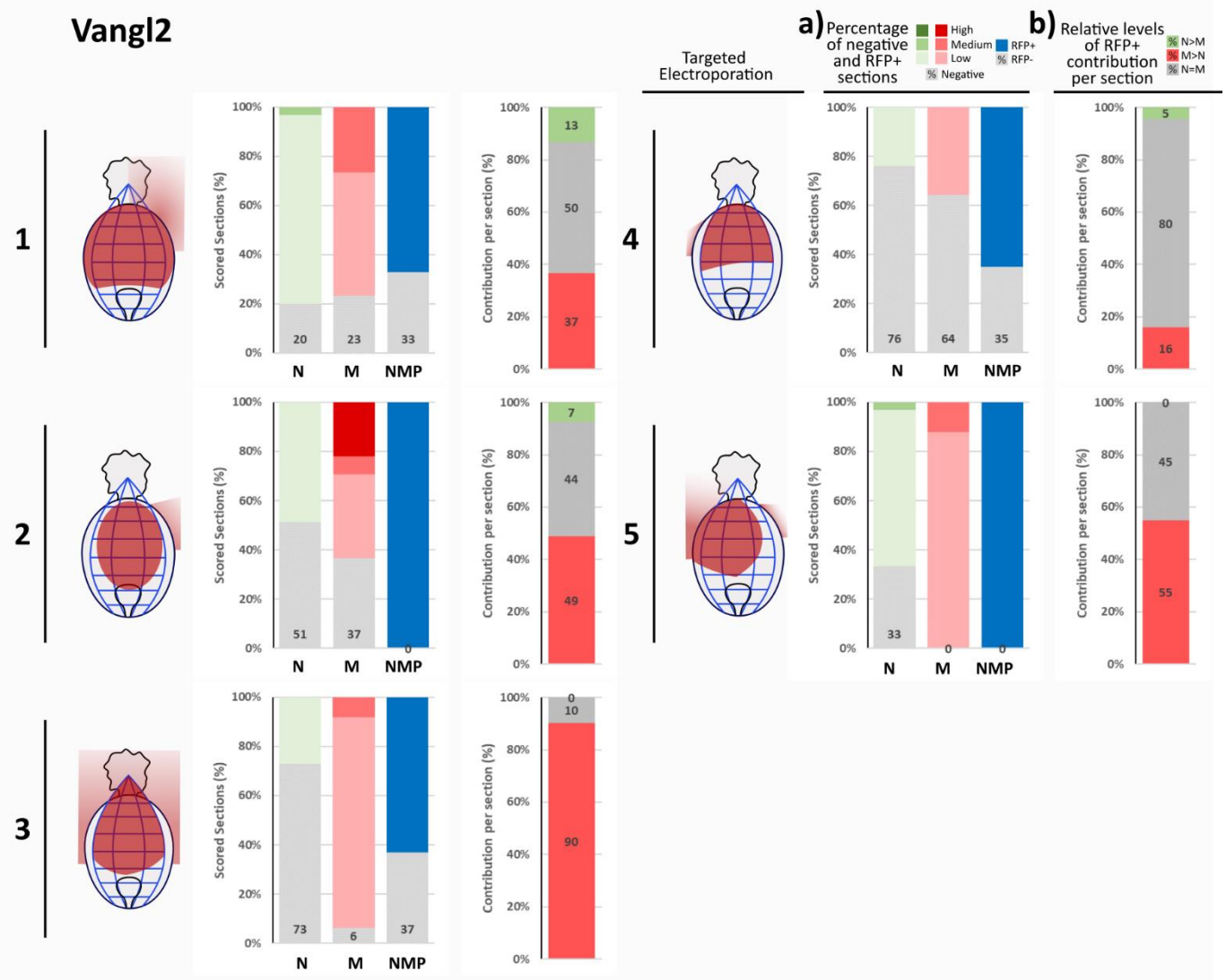

Figure 5.11 - Single embryo results for electroporation with CAG-Vangl2.

Results of semi-quantitative analysis for individual embryos for CAG-Vangl2 electroporated embryos. For each embryo, a schematic representation is included to indicate the approximate targeted area (red) based on images taken 2 hours following electroporation including off-targeted areas represented by red surround **(a)** The percentage of all scored sections in each RFP density category, for neural (green), mesoderm (red) and NMP (blue) tissues. Percentage of sections with no contribution is shown as a number on the bar chart **(b)** Relative levels of neural versus mesoderm RFP+ contribution per individual section, grey indicating proportion of those with equal contribution to both tissues. The percentage in each category is shown by the number. (N- neural, M-mesoderm, NMP-neuromesodermal progenitor.

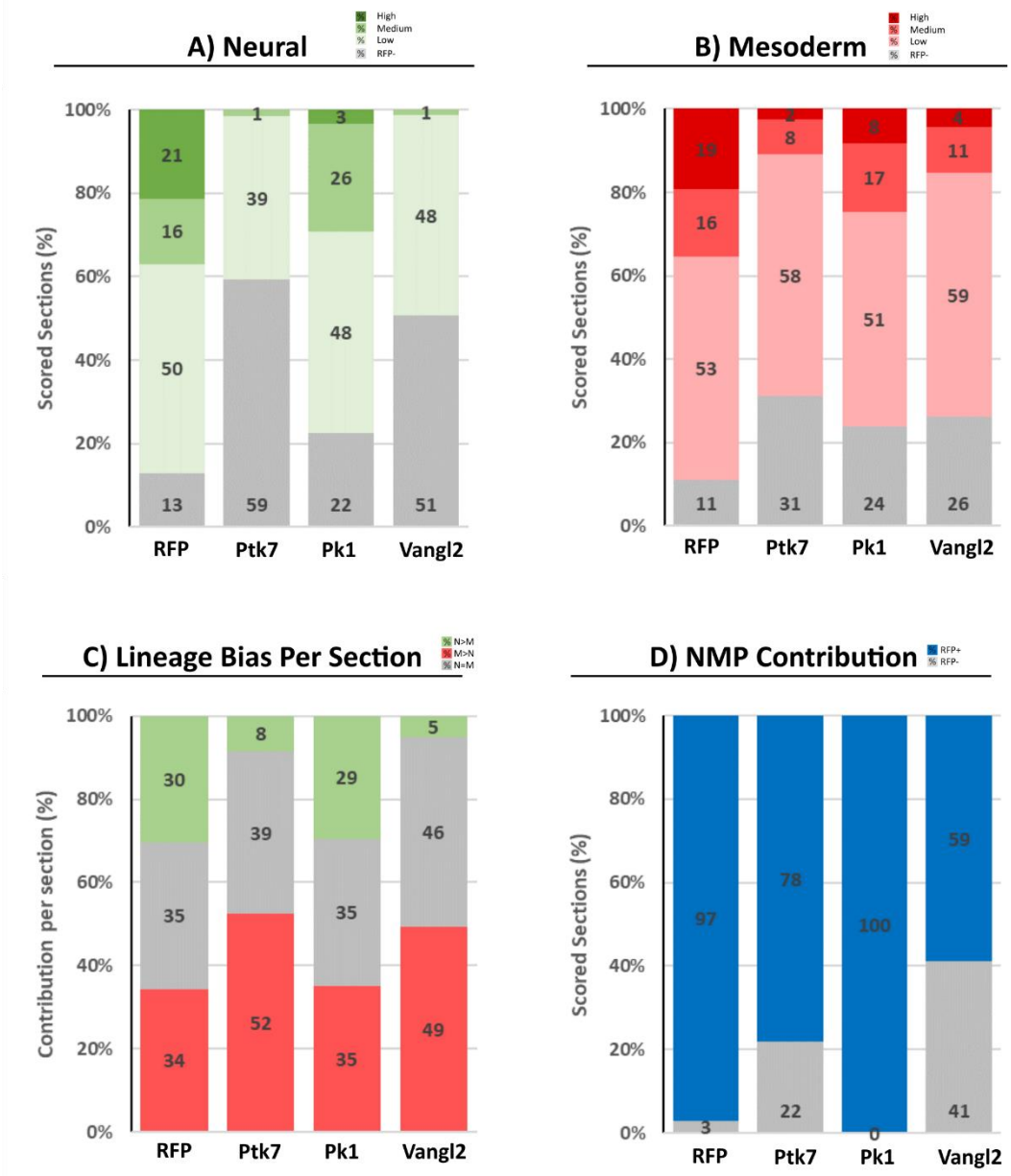

Figure 5.12 - Comparison of average RFP+ contributions between groups.
Averaged percentages of scored sections for each group according to RFP+ density in **(A)** Neural, **(B)** Mesoderm or **(D)** NMP. **(C)** Neural versus mesoderm contribution per section averaged for each group. Percentages shown for each category. Colour code as stated in Fig. 5.8-11.

In summary electroporation of Pk1 did not affect the bias of tissue specific or CNH contribution of NMPs, akin to that described previously for control group.

Distinctly diverging results were found for Ptk7 and Vangl2 electroporation compared with both control and Pk1 electroporation groups. Overall the proportions of sections with neural contribution in Vangl2 and Ptk7 were markedly reduced compared with control. 59% and 51% of sections examined over all Ptk7 and Vangl2 embryos

respectively, had no RFP+ cell contribution (Fig. 5.12A). Furthermore, in Ptk7 and Vangl2 groups no sections contained High (>60%) neural contribution, compared to 21% for control group. Mesoderm contribution was less affected in Ptk7 and Vangl2 groups but did exhibit an increase in number of sections with no RFP+ contribution compared with control, (31% Ptk7, 26% Vangl2 and 11% control) (Fig. 5.12B). Most revealing however was a shift in the balance between neural and mesodermal lineages within sections (Fig. 5.12C). Proportion of individual sections with higher contribution to mesoderm versus neural tissue sections was 52% for Ptk7 and 49% in Vangl2 groups, much higher than 35% reported for control (Fig. 12C). Conversely only 8% of Ptk7 and 5% of Vangl2 group sections had bias toward neural contribution within cells, drastically lower than the 30% previously described for the control group. Thus, cells electroporated with either Vangl2 or Ptk7 appeared to have reduced differentiation to neural lineages.

This bias was also clearly identifiable through examination of individual embryos. In Ptk7 electroporated group only one individual embryo (embryo 3), out of six, had more sections with RFP+ contribution in neural tissue than that for mesoderm tissue (Fig. 5.9a), and had a larger proportion of individual sections with neural > mesoderm bias compared with mesoderm > neural bias (Fig. 5.9b). In comparison, only a single embryo (embryo 1), out of five, in the Vangl2 electroporated group displayed a marginally higher proportion of neural RFP+ sections (80%) than mesoderm RFP+ sections (77%) (Fig. 5.11a). Yet all embryos in the Vangl2 electroporated group displayed a preference for neural lineage when proportions of mesoderm and neural contribution was compared within sections (Fig. 5.11b).

Regarding NMP maintenance, both Ptk7 and Vangl2 electroporation groups exhibited reduced contribution to the NMP regions compared with control group. RFP+ cells were localised in the CNH region in 78% and 59% of scored CNH sections for Ptk7 and Vangl2 respectively, significantly lower than 97% previously described for RFP control group (Fig. 5.12D). Taken together this evidence suggests that targeted overexpression of Vangl2 and Ptk7 in NMPs prevents their normal differentiation to neural but not mesodermal lineages, and additionally prevents NMPs from persisting within the CNH

To summarise this experiment, exogenous DNA was incorporated into NMPs during early somitogenesis through a targeted electroporation technique. Contribution of cells, targeted with electroporation of control constructs, showed that the behaviours of targeted NMPs was normal, and they subsequently gave rise to cells of neural and mesoderm lineage in equal measure, as well as persisting in the CNH through self-renewal (Fig. 5.13A). Similar contribution to tissues of both lineages and CNH was evident when NMPs were instead electroporated with Pk1 constructs. In contrast, discernible differences in NMP behaviour were apparent when Vangl2 or Ptk7 constructs were electroporated (Fig. 5.13B). Overall the proportion of electroporated NMP descendants forming neural tissues was substantially reduced, as to where the number of descendants contributing in the progenitor zone (CNH) (Fig. 5.13B). Additionally, electroporated cells appeared to preferentially contribute to cells of mesodermal lineages versus neural lineages. Thus, overexpression of Wnt/PCP components Ptk7 and Vangl2 is adequate to alter the behaviour of NMPs, both in terms of their maintenance and differentiation choices.

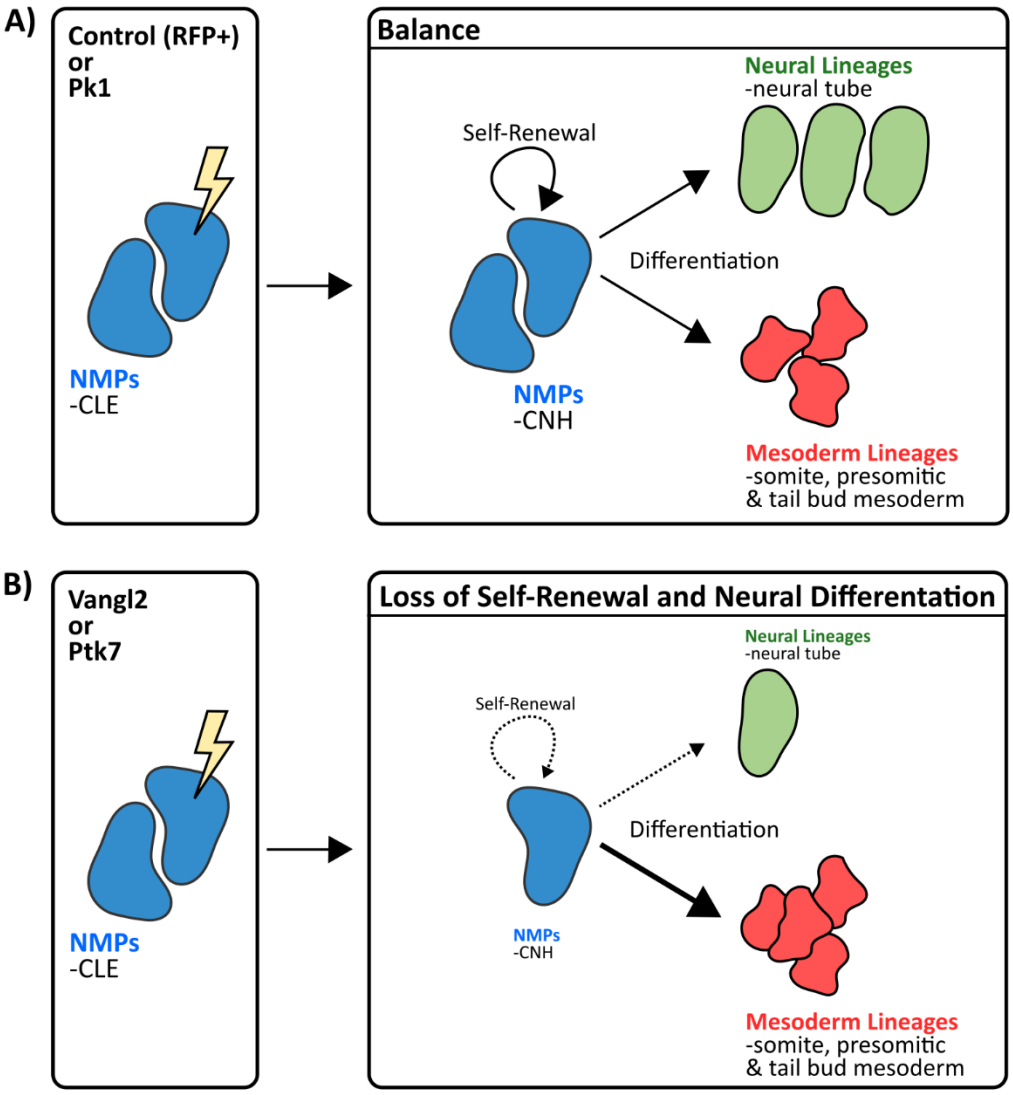

Figure 5.13 - Overexpression of Ptk7 and Vangl2 disrupts NMP behaviour.
(A) Electroporation of neuromesodermal progenitors (NMPs) in the caudal lateral epiblast (CLE) with Pk1 or RFP (control) overexpression constructs results in these NMPs contributing to all tissues as normal, with descendants persisting in the chorodoneural hinge (CNH) through self-renewal, and differentiating to contribute to both mesodermal and neural lineages equally. **(B)** Electroporation of NMPs in the CLE with Vangl2 or Ptk7 overexpression constructs results in these NMPS contributing to less cells of neural lineages and NMPs of the CNH. Thus, NMPs lose their ability to persist in the CNH, and additionally exhibit a bias towards mesodermal lineages at the expense of neural lineages.

5.3 Wnt/PCP perturbations *in vitro*

The *in vivo* overexpression assays described above permitted the collection of strong evidence supporting the role of Vangl2 and Ptk7 in regulating NMP behaviour. Motivated by these findings, mechanisms underlying the cell fate bias induced by Wnt/PCP component overexpression were investigated. These *in vivo* experiments constitute a sensitive and reliable technique for testing the function of specific genes during development, however it is time consuming, difficult to scale up and the timing of perturbation is limited by accessibility. Furthermore, the ability to derive NMPs in *in vitro* assays provides an alternative more accessible system in which investigations can be undertaken. Crucially in Chapter 4 the presence of Fzd6 (Fig. 4.16), Ptk7 (Fig. 4.17) and Vangl2 (Fig. 4.18) proteins in *in vitro* derived NMPs were identified. The identification of Wnt/PCP components in these culture systems implicates the activity of Wnt/PCP signalling further supporting the alternative use of *in vitro* assays to study the role of Wnt/PCP in NMPs.

5.3.1 Generation of inducible Wnt/PCP mutant cell lines as a novel tool to modulate Wnt/PCP signalling during NMP differentiation

Introduction of exogenous DNA in *in vitro* culture systems is possible using electroporation in a similar manner to that described above for *in vivo* systems. Nonetheless a more robust system which would allow the overexpression of Wnt/PCP components in a more controllable way was advocated. Specifically, one able to overexpress components homogenously across a whole culture dish at any desired timepoint. For this reason an inducible cell line system recently published by (Iacovino et al., 2011) was utilised. This system permits the generation of gene of interest inducible cells lines, which over express inserted gene of interest with the simple addition of dox to the media. This is achieved through the insertion of incoming DNA (gene of interest - GOI) using an ICE (inducible cassette exchange) target locus which is located downstream of a doxycycline (tetracycline) responsive promoter (TRE) (Iacovino et al., 2011).

Cell lines were generated by subcloning (GOI-T2A-RFP), from the plasmids described in (Fig. 5.1) and nucleofecting each of them into the specialised receiver cell line. The

inclusion of T2A-RFP ensured that Wnt/PCP induction could be monitored simply. In total five Wnt/PCP overexpression-RFP cell lines were generated in 2i/LIF conditions, these were cPtk7, cPtk7ΔICM, csPtk7, cPk1 and cVangl2. A RFP only inducible cell line was additional generated for use as a control (cRFP) (generated by Matt Malaguti, Lowell Lab).

5.3.2 Validation of inducible Wnt/PCP cell lines

Pk1 clone picking and induction efficiency analysis in collaboration with MSc Student Catarina Martins Costa

5.3.2.1 Efficiency of Dox-induction is substantial for all generated cell lines

All clones for each cell line showed high induction efficiency, as determined by flow cytometry (S-Fig.5.1) or fluorescent microscopy, (S-Fig.5.2). For Ptk7 and Ptk7ΔICM picked clones, induction was verified visually by inducing gene expression through addition of dox and checking RFP levels in alive cells after 24 hours. 100% of clones for both Ptk7 (8/8) and Ptk7ΔICM (7/7) cells lines showed good induction of RFP after 24 hours following the addition of dox. RFP appeared to homogenous for all cell clones, except for Ptk7 clone 6, in which was more heterogenous. RFP positive cells were never found in controls which were not treated with dox. To understand more about the dynamics and variation of induction between generated cell lines and clonal lines, more detailed analysis was done using flow cytometry. A threshold of RFP positivity was applied to each sample using wildtype 2i/LIF cells as a control for RFP positivity. Overall the RFP levels of all control (-dox) samples were comparable to that for wildtype 2i/LOF cells, with negligible averages of RFP positive cells. For all clonal lines and for all genes, there was a significant shift in RFP increasing expression between +dox and -dox treatment group. This shift affected the whole population for most clonal lines, except for sPtk7 clones 1,2,3, which appeared to have a minor separate negative population of cells. Average RFP positivity was high for all cell lines, 99.9% (sPtk7), 86.1% (Pk1), 89% (Vangl2) and 99.5% RFP. Cell lines with the highest inducibility had the lowest variability between clones, and vice versa. No differences in morphology or survival between -dox and +dox treated cells for all gene inducible cell lines.

The clones chosen for use in experiments in this thesis were, Ptk7 - Clone 3, Ptk7ΔICM - Clone 5, sPtk7 - Clone 2, RFP - clone 1, Pk1 - clone 5, Vangl2 - clone 3.

The efficiency of induction of each clone was verified using fluorescent microscopy for cPtk7 and cPtk7ΔICM cell lines cultured in 2i/LIF conditions (Fig. 5.14A). 24 hours after the addition of dox in 2i/LIF culture conditions, RFP appeared to be homogenously distributed in all cells of the culture for both cell lines (Fig. 5.14Aa,c). RFP positive cells were never found in controls in which addition of dox was absent (Fig. 5.14Ab,d).

To understand more about the dynamics and variation of induction between generated cell lines more refined and detailed analysis was executed for the remaining cell lines using flow cytometry in 2i/LIF culture conditions. A threshold of RFP positivity was calculated using wildtype 2i/LIF cultured cells (negative for RFP). All cell lines exhibited negligible induction of RFP in the absence of dox in 2i/LIF culture (Fig. 5.14B) (csPtk7 0%, cPk1 0%, cVangl2 0.2% and cRFP 0.5%). In contrast 24 hours following dox induction all cell lines exhibited extensive levels of RFP positivity in 2i/LIF culture. The highest was for cRFP, in which 99% of cells were RFP positive, with csPtk7, cPk1 and cVangl2 having 98%, 90.1% and 85.5% RFP positivity respectively (Fig. 5.14Ba-d).

Taken together the visual and flow cytometry analysis of generated cell lines, showed robust and high inducibility of inserted gene of interest, as visualised by RFP expression levels. Importantly this induction was specific to the addition of dox to the culture. In addition, no differences in morphology or survival were visible between -dox and +dox treated cells for all inducible cell lines.

5.3.2.2 RFP faithfully reports Wnt/PCP component overexpression

To verify that induced RFP positivity observed by fluorescence microscopy and flow cytometry was associated with an increase of Wnt/PCP protein, immunohistochemistry of Ptk7 and Vangl2 were conducted on fixed wells of cVangl2 and cPtk7 respectively. cPtk7 cultures incubated without dox had low levels of endogenous Ptk7 protein (Fig. 5.15Af). Conversely the levels of Ptk7 protein following 24 hours of dox were notably higher (Fig. 5.15Ac). Additionally, highest

levels of Ptk7 protein were associated with higher RFP expression levels. Similar increases in Vangl2 protein were obtained in cVangl2 cultures treated with dox for 24 hours, for which RFP induction was confirmed by flow cytometry (data not shown). Without dox treatment, the levels of Vangl2 protein were significantly lower, akin to expected endogenous levels (Fig. 5.15Be).

In conclusion, the addition of dox to Wnt/PCP cell lines results in increased levels of Wnt/PCP components, which can be monitored by the presence of RFP. Consequently, this permitted the use of these cell lines to investigate the role of Wnt/PCP in NMP *in vitro* cultures.

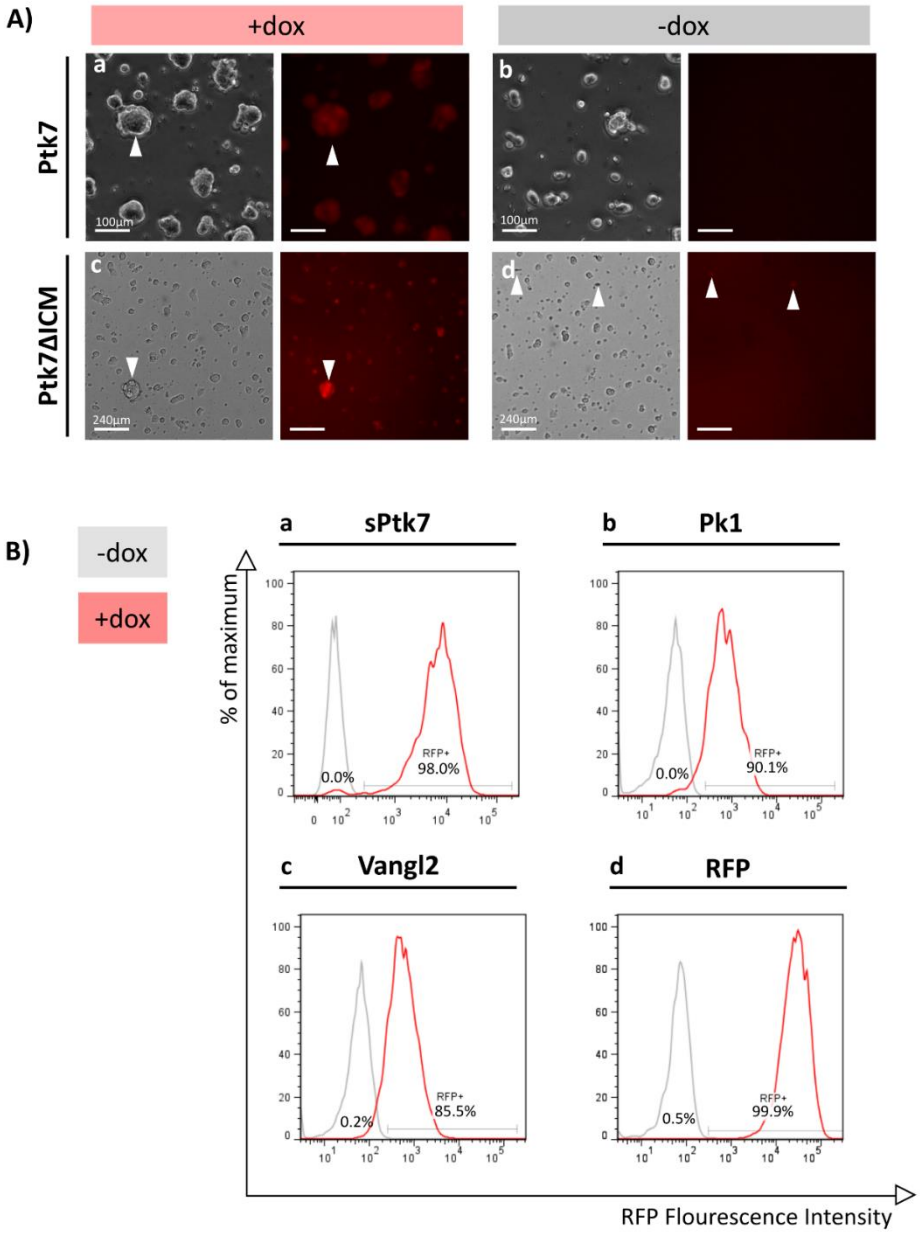

Figure 5.14 - Wnt/PCP inducible overexpression cell lines show high levels of inducibility.
(A) Brightfield and RFP live images taken of generated Ptk7 and PtkΔICM inducible cell lines, in the presence (+dox)**(a,c)** and absence (-dox)**(b,d)** of dox in 2i/LIF culture conditions. All cells show homogenous for RFP induction (white arrows) in +dox conditions. RFP was never found in cells not treated with dox (white arrows show RFP autofluorescence in detached cell).**(B)** Flow cytometry analysis of **(a)** sPtk7, **(b)** Pk1, **(c)** Vangl2, and **(d)** RFP inducible cell lines, in 2i/LIF culture conditions with dox (+dox – red) and without dox (-dox – grey). All show high levels of levels of RFP positivity. Threshold of RFP positivity based wildtype (non-fluorescent) 2i/LIF.

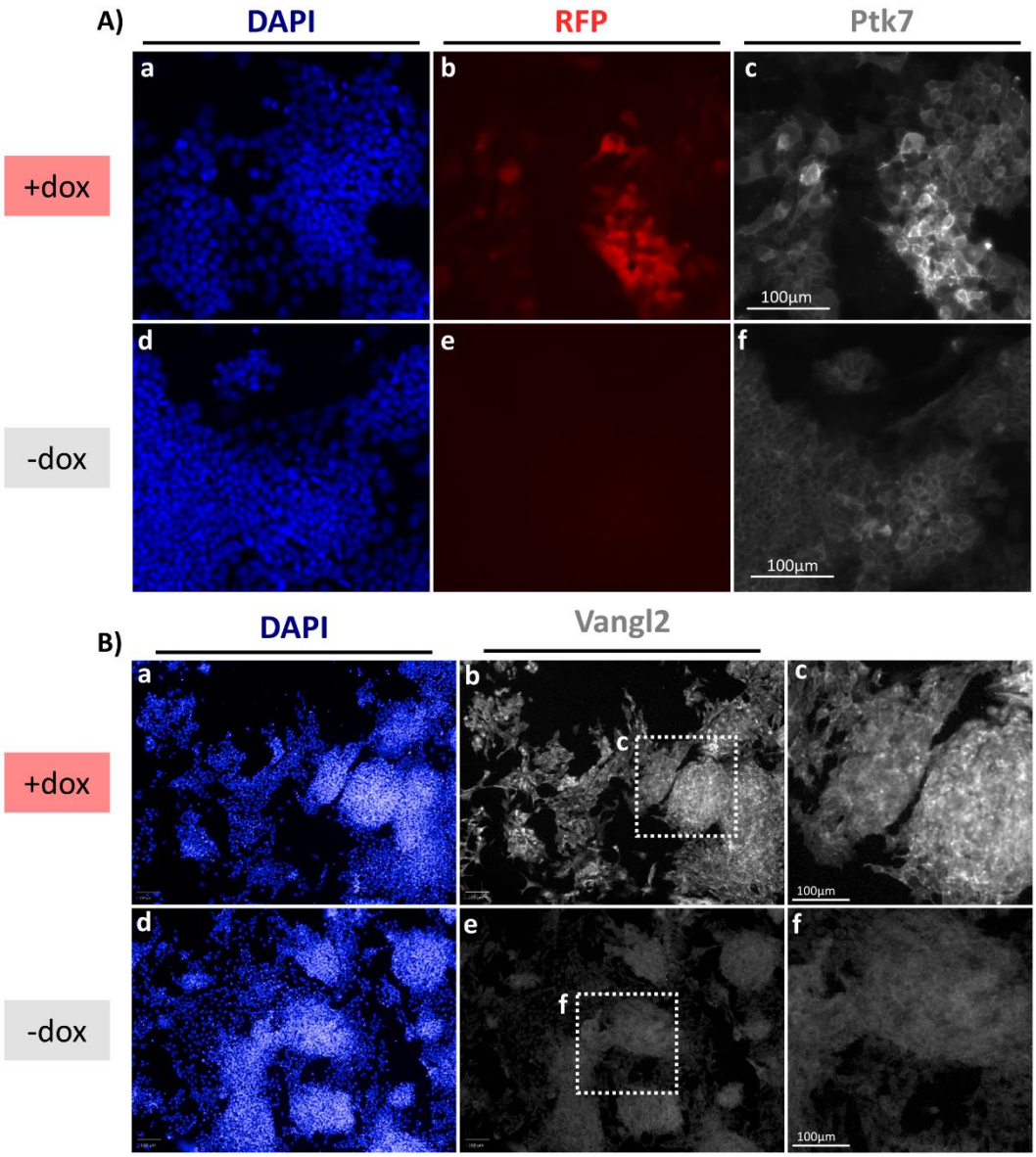

Figure 5.15 - Inducible cell lines overexpress Wnt/PCP components.
(A) Immunohistochemistry of Ptk7 overexpressing cell lines, show that Ptk7 is expressed at a higher in cultures were dox (+dox) has been added (c), compared to endogenous level of Ptk7 seen in the absence of dox (-dox control) (f). Increase in Ptk7 protein also corresponded increased levels of RFP (b). **(B)** Immunohistochemistry of Vangl2 protein on Vangl2 inducible cells lines, with (b-c) and without dox (e-f) show that Vangl2 protein is found at a higher level when induced, compared to endogenous Vangl2 protein (-dox control).

5.3.3 Overexpressing Wnt/PCP components in EpiLC derived NMPs

In Chapter 4 a novel *in vitro* differentiation protocol was presented which mimicked the developmental stages of NMPs during axial elongation. It was decided to take advantage of the scalability of this *in vitro* assay to test if the described effects of overexpressing Wnt/PCP components *in vivo* (5.2) can be mirrored in this *in vitro* assay.

Media used to derive NMPs *in vitro* traditionally contains (CHIR), a potent activator of Wnt/β-catenin signalling (Henrique et al., 2015). CHIR inhibits cytoplasmic glycogen synthase kinase 3 (GSK3) which has known interactions with Dvl family proteins. As Dvl family proteins are also shared by the Wnt/PCP pathway it is not clear if CHIR additionally disrupts Wnt/PCP signalling through its inhibition of GSK3 protein. Consequently, to investigate the true effect of overexpressing Wnt/PCP in NMPs derived from EpiLCs CHIR was not included in the culture. Alternatively, recombinant Wnt3a protein was used to activate Wnt/β-catenin signalling in these cultures. This alternative Wnt agonist had been utilised previously to derive NMPs from EpiSCs and had generated T(Bra) and Sox2 co-expressing cells to the same extent as CHIR (Gouti et al., 2014).

In Chapter 2 the expression of Wnt/PCP components Fzd6 (Fig. 4.16), Ptk7 (Fig. 4.17) and Vangl2 (Fig. 4.18) in *in vitro* culture conditions was reported. Thus, suggesting that Wnt/PCP may be active in EpiLC-NMPs and may have a role in regulating NMP differentiation. Additionally, the level of these proteins tended to increase with differentiation state, low in EpiLC and higher in EpiLC-NMPs, thus suggesting that Wnt/PCP component expression is upregulated on the way to NMP state. Therefore Wnt/PCP signalling may additionally be important for the derivation of NMPs *in vitro*. To test the effect of Wnt/PCP overexpression in the process of NMP derivation and differentiation from NMPs, dox was added to cultures in a time dependent manner. These preliminary investigations are described below.

5.3.3.1 Overexpression of Wnt/PCP components *in vitro* does not substantially alter T(Bra) and Sox2 during NMP derivation

To test the effect of Wnt/PCP overexpression during the derivation of NMPs, EpiLC-NMPs were derived from 2i/LIF cultures for each Wnt/PCP cell line using the optimised protocol from Chapter 4 (Fig. 5.16). Dox was added to induce Wnt/PCP component overexpression at the transition between EpiLC and EpiSC culture conditions (+dox). Subsequently cells were collected 48 hours later for analysis. Negative controls samples were also included for each cell line, in which dox was not added (-dox). Two replicates were set up for each cell line.

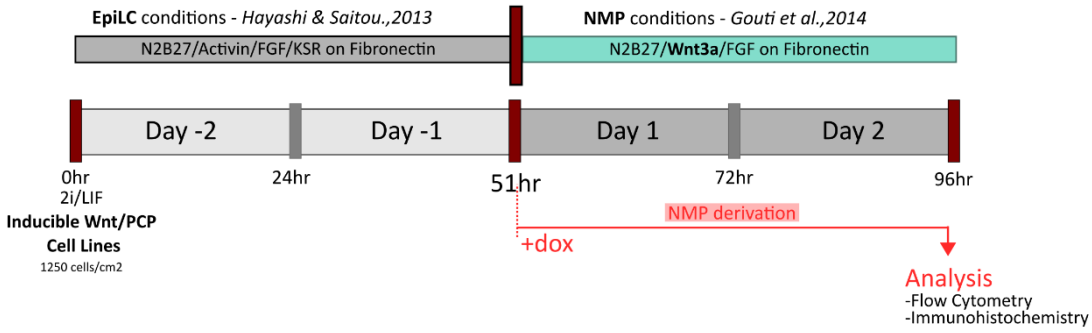

Figure 5.16 - Overexpressing Wnt/PCP components during NMP derivation.
Experimental design for overexpressing Wnt/PCP components during NMP derivation from EpiLCs. Dox was added to the media following 51 hours of EpiLC differentiation, and samples were collected 48 hours later for analysis with flow cytometry and immunohistochemistry.

As induction efficiency had only been previously examined in 2i/LIF culture conditions, the induction efficiency EpiLC-NMPs was examined to ensure it remained high despite the more differentiated culture state. RFP levels were inspected using flow cytometry (Fig. 5.17). RFP positivity for each sample was determined using a threshold of RFP positivity determined by an untargeted parental cell line sample (negative for RFP). Overall induction levels for all cell lines were high with at least 90% of cells being RFP positive (Fig. 5.17A-F) (cPtk7- 90.3%, cPtk7ΔICM - 99.9%, csPtk7 - 100%, cPk1 - 96.6%, cVangl2 - 95.5%, cRFP - 99.5%, respectively). However, cell lines that had the highest induction efficiency also displayed small levels of induction without doxycycline (-dox). This was highest for

csPtk7 and cRFP (control), which respectively displayed 9.1% and 7.8% of RFP positive cells without the addition of dox (Fig. 5.17C,F). Despite this small level of induction in controls without dox, the induction was significantly higher in the +dox samples, and thus comparisons between the two samples would still be valuable.

In summary, overexpression cell lines had high levels of induction following the addition of dox in cell differentiating toward NMP state. Despite some induction without dox addition, the differences between +dox and -dox (control) groups was substantial enough for all cell lines to warrant analysis of differences between treatment groups.

In the *in vivo* NMP assays described previously (5.2), the overexpression of Vangl2 and Ptk7 in NMPs disrupted differentiation to neural lineages as well as inhibiting their persistence in the CNH (NMP progenitor zone). To assess the effect of Wnt/PCP component overexpression on NMP derivation *in vitro*, the levels of T(Bra) and Sox2 were analysed and compared for +dox and -dox (control) samples for all cell lines using immunohistochemistry. Any differences in neural marker Sox2 would indicate changes in the neural potential of these cells, and additionally analysis of T(Bra) would allow the examination of NMP number. As this *in vitro* assay resulted in the overexpression of Wnt/PCP components in at least 90% of cells (as verified by flow cytometry), I expected any changes to be extensive throughout the culture.

Unfortunately, despite extreme care and sensitive processing, many cells were lost during the immunohistochemistry process. However, given that most cells would be overexpressing the Wnt/PCP components (90%, based on flow analysis), it was expected that a reduction in cells would not obstruct the identification of real differences between treatment groups. Acquired images underwent segmentation as described previously in Chapter 4, and values for T(Bra) and Sox2 expression intensity were generated.

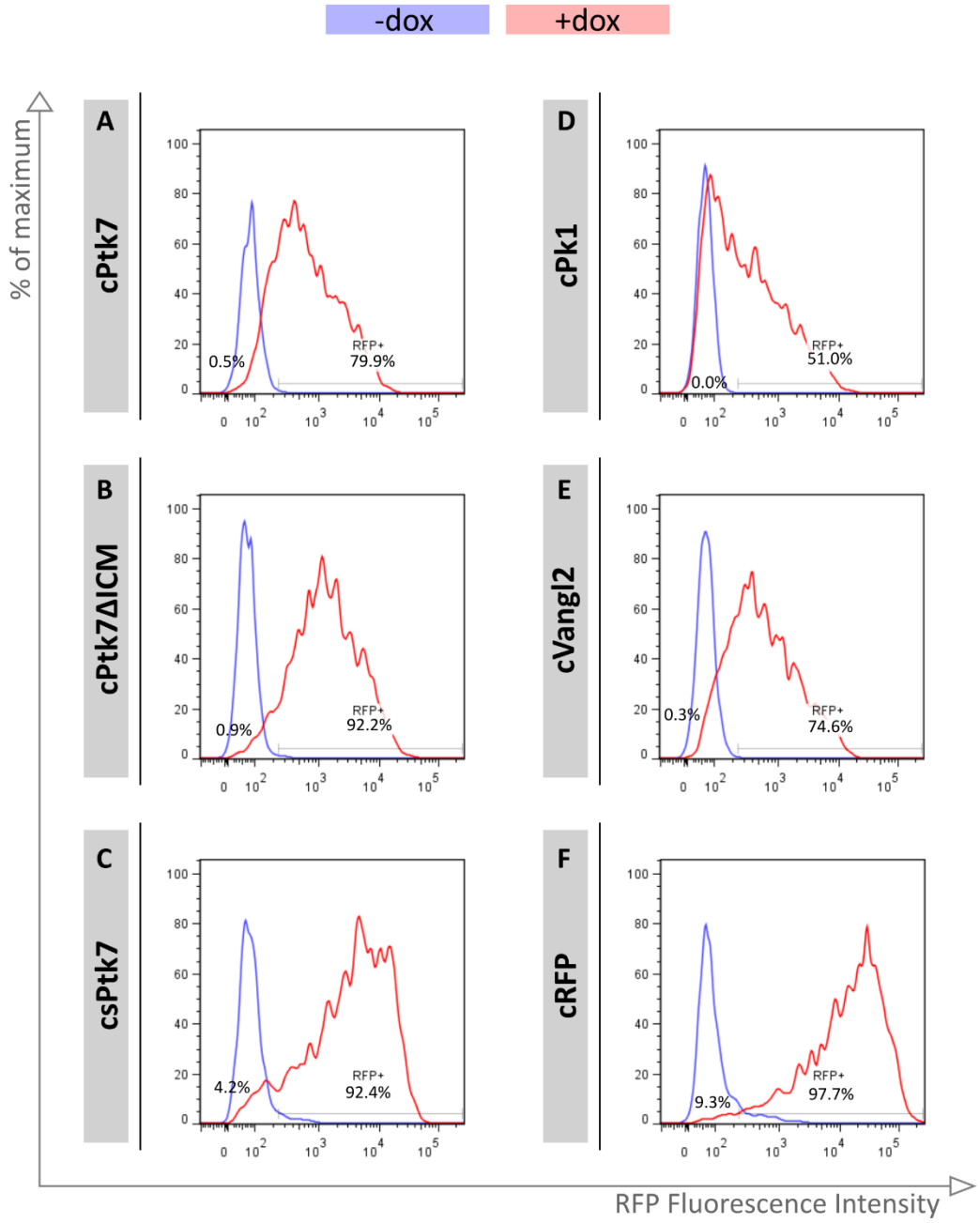

Figure 5.17 - Flow cytometry analysis to verify induction during NMP derivation.
Inducible cells lines **(A)** cPtk7, **(B)** cPtk7ΔICM, **(C)** csPtk7, **(D)** cPk1, **(E)** cVangl2 and **(F)** cRFP all showed high levels of inducibility when dox was added in EpiLC conditions. Additionally, controls in which dox was not added showed low levels of RFP intensity but this is overall significantly lower than that for dox (+dox) samples. Flow cytometry analysis was performed as described in Fig. 5.14.

To understand the inherent variability of this assay, RFP control cell lines were examined first. For the RFP control the mean T(Bra) intensity observed was steady between replicates of each treatment type (Fig. 5.18A), however between treatment types there was a considerable variation (means were 190 for both -dox replicates, and 224 and 223 for +dox replicates). This was also apparent when Sox2 intensity was examined between replicates and treatment groups (Fig. 5.18B). In -dox replicates mean Sox2 intensity was 137(R1) and 149(R2), however for +dox replicates these were considerably lower at 114(R1) and 105(R2). Thus, despite the only difference being overexpression of RFP, the intensity profiles of T(Bra) and Sox2 between +dox and -dox treatment groups was substantial. When the mean of both replicates was compared between treatment groups the standard deviation was 24 for both T(Bra) and Sox2 intensity. This indicated that there was considerable noise in this assay. Meaning, any differences identified between treatment groups of the other cell types, would have to be larger than this baseline variation to be considered significant.

Differences in Sox2 and T(Bra) intensity between treatment groups was then carried out on all other Wnt/PCP overexpression cell lines. For T(Bra) the standard deviation between means from -dox and +dox treatment groups was consistently the exact same or lower than that detected for RFP (control), csPtk7-24, cPtk7ΔICM- 15, csPtk7- 12, cPk1 - 13, cVangl2 - 18 versus RFP control -24) (Fig. 5.18C,E & Fig. 5.19A,C,E). This indicated that overexpressing Wnt/PCP components had no detectable affect within this assay. Moreover, Sox2 intensity differences between treatment groups was conservative. For four out of five Wnt/PCP cell lines, the standard deviation between means of treatment group replicates was lower than that described for cRFP control (cPtk7 - 11, csPtk7- 9, cPk1 - 7, versus control - 24) (Fig. 5.18D, Fig. 5.19B,C), particularly for Vangl2 whose standard deviation was only 1 (Fig. 5.19F). However, cPtk7ΔICM cell line in which Ptk7 transmembrane and extracellular is overexpressed, had a standard deviation of 31 (Fig. 5.18D). For this group the average Sox2 intensity without dox treatment was 162, and with dox treatment decreased to 118, suggesting that the overexpression of this Ptk7 fragment may inhibit the acquisition of neural identity in these cells (Fig. 5.18F).

In summary, upon examination of Sox2 and T(Bra) intensity between +dox and -dox, no substantial differences in phenotype were observed for any cell lines. The only notable difference was a reduction of Sox2 following induction of Ptk7ΔICM construct, but more replicates would need to be carried out to confirm the robustness of this finding. Due to the lack of significant differences in T(Bra) and Sox2 intensity, the number of T(Bra) and Sox2 co-expressing cells were not investigated.

5.3.3.2 Overexpression of Wnt/PCP components *in vitro* does not substantially alter NMP differentiation

Another outstanding question was whether over expressing Wnt/PCP components would have a greater effect on NMP differentiation, akin to what was observed in *in vivo* electroporation experiments. EpiLC-NMPs were derived from all Wnt/PCP inducible cells lines. Dox was added to NMPs, and then analysis was carried out 24 hours later following their subsequent differentiation as described in Chapter 4 (Fig 5.20).

To ensure induction of Wnt/PCP components, samples underwent flow cytometry analysis as described previously in 5.3.3.1. Clear reductions in inducibility efficiency were apparent compared with that previously described above for EpiLC induction (Fig. 5.15). Most notably cPk1 induction was reduced from 96.6% of cells with RFP positivity (in EpiLC) to 51% (in NMPs) (Fig. 5.21D). All other cell lines exhibited at least 74% induction, specific values were, cPtk7- 79.9%, cPtk7ΔICM - 92.2%, csPtk7 - 92.4%, cVangl2 - 74.6% and cRFP (control) - 97.7% (Fig. 5.21A-C,E-F). As with induction in EpiLCs, RFP positivity was also found in -dox controls. RFP expression was negligible in cPtk7, cPtk7ΔICM, cPk1 and cVangl2 cultures, in which less than 1% of cells expressed RFP (Fig. 5.21A-B,D-E). Conversely csPtk7 and cRFP cell cultures had 4.2% and 9.3% of cell expressing RFP respectively (Fig. 5.21C,F).

In summary, there was a reduction in inducibility of cells lines in NMP conditions compared to that previously described at EpiLCs state. Regardless all cell lines nevertheless exhibited high levels of induction following the addition of dox. Moreover, despite low induction without dox addition, the differences between +dox and -dox (control) groups was substantial enough for all cell lines to warrant analysis of differences between treatment groups.

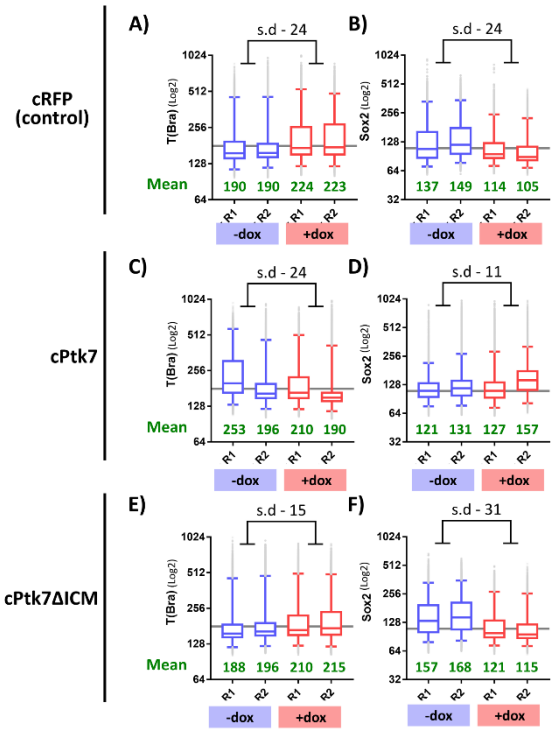

Figure 5.18 - T(Bra) and Sox2 intensity following induction during NMP derivation - RFP (control), Ptk7 and Ptk7ΔICM cell lines.

Box and whisker plots showing the distribution of T(Bra) and Sox2 intensity per well in conditions with (+dox) and without (-dox) dox addition during NMP derivation from EpiLCs. Two replicates are shown for each inducible cell line (R1/R2). Box and whisker plots show minimum, maximum, median, the upper and the lower quartiles, and below the mean intensity value (green). Standard deviations were calculated by comparing the average mean (of both replicates) between conditions (+dox/-dox).

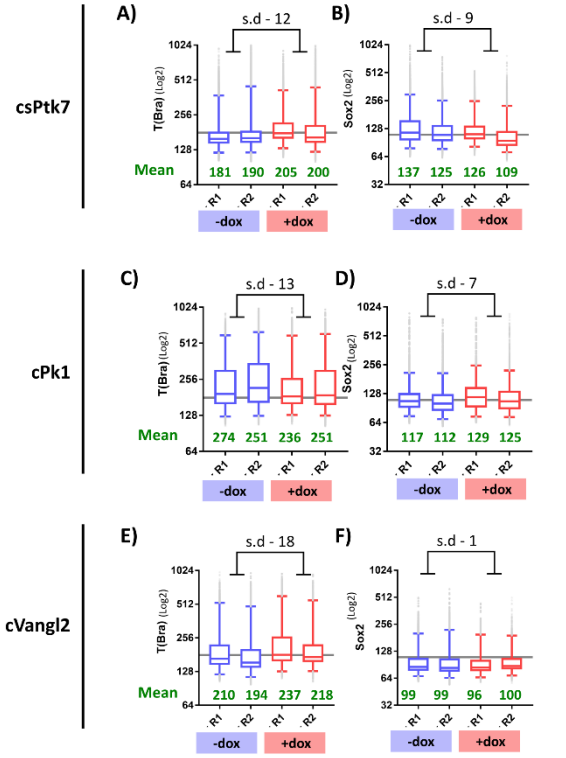

Figure 5.19 - T(Bra) and Sox2 intensity following induction during NMP derivation - sPtk7, Pk1 and Vangl2 cell lines.

Box and whisker plots showing the distribution of T(Bra) and Sox2 intensity per well in conditions with (+dox) and without (-dox) dox addition during NMP derivation from EpiLCs. Two replicates are shown for each inducible cell line (R1/R2). Box and whisker plots show minimum, maximum, median, the upper and the lower quartiles, and below the mean intensity value (green). Standard deviations were calculated by comparing the average mean (of both replicates) between conditions (+dox/-dox).

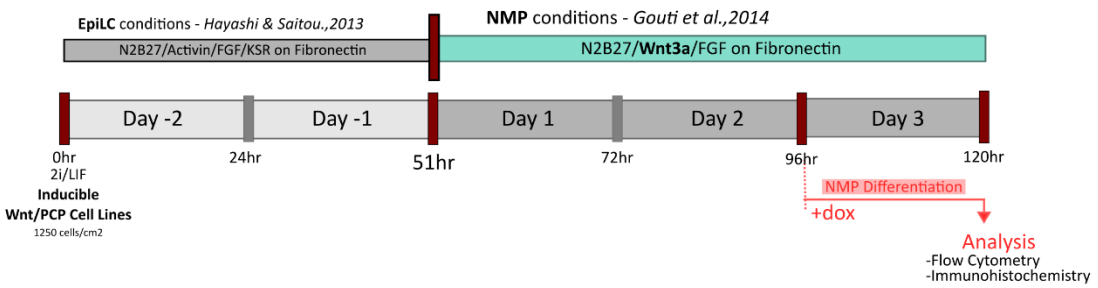

Figure 5.20 - Overexpressing Wnt/PCP components during NMP differentiation.
Experimental design for overexpressing Wnt/PCP components during NMP differentiation from EpiLCs. Dox was added to the media following 2 days of NMP differentiation, and samples were collected 24 hours later for analysis with flow cytometry and immunohistochemistry.

In the *in vivo* NMP assays described previously (5.2), the overexpression of Vangl2 and Ptk7 in NMPs prevented differentiation to neural lineages as well as inhibiting their persistence in the CNH (NMP progenitor zone). To assess the effect of Wnt/PCP component overexpression on NMP differentiation *in vitro*, the levels of T(Bra) and Sox2 were analysed using whole well microscopy and compared for +dox and -dox (control) samples for all cell lines using immunohistochemistry. As cultures are dense following 3 days of NMP differentiation it is impossible to segment images, however given that at least 50% of cells (as verified by flow cytometry) overexpressed the Wnt/PCP components, any changes were expected to be apparent through visual comparison. Any differences in expression of neural marker Sox2 between -dox and +dox treatment would indicate a change in the neural potential of these cells.

Whole well images made of stitched fields of view for each cell line and condition are documented in (Fig. 5.22-24). High RFP expression in +dox but not -dox conditions for each cell lines confirmed the high level of Wnt/PCP expression induction previously reported with flow cytometry. Examining cRFP control (Fig. 5.22A), Sox2 expression was dominant in both +dox and -dox conditions, and T(Bra) was also present but to a lower extent. There were no clear phenotypic differences between +dox and -dox control. In cPtk7 cell samples Sox2 dominance was not as apparent as that for cRFP control, though Sox2 expression between +dox and -dox wells were comparable (Fig. 5.22B). Moreover, so was the overall expression of T(Bra) in the

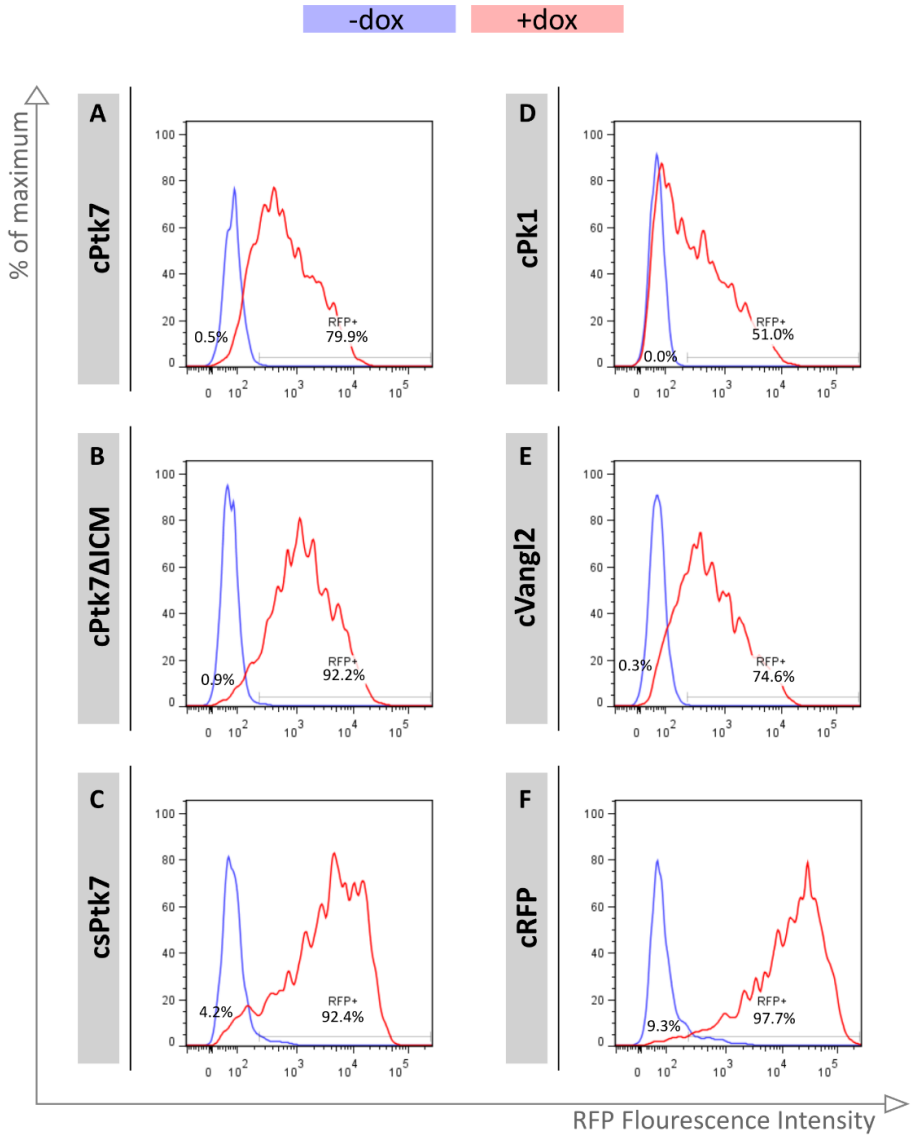

Figure 5.21 - Flow cytometry analysis to verify induction during NMP differentiation.
Inducible cells lines **(A)** cPtk7, **(B)** cPtk7ΔICM, **(C)** csPtk7, **(D)** cPk1, **(E)** cVangl2 and **(F)** cRFP all showed high levels of inducibility when dox was added following 2 days of NMP differentiation. Additionally, controls in which dox was not added show some low levels of RFP intensity but this is overall significantly lower than that for dox (+dox) samples. Flow cytometry analysis was performed as described in Fig. 5.14.

dish, implying that Ptk7 overexpression had no notable effect on EpiLC-NMP differentiation in this assay. For cPtk7ΔICM and csPtk7 cell lines, Sox2 was dominant in the culture versus T(Bra) levels following 24 hours of NMP differentiation, illustrating an obvious preference for neural differentiation for these cell lines (Fig. 5.23A-B). Sox2 protein levels were comparable in +dox and -dox conditions for these cell lines, suggesting that overexpression of Ptk7ΔICM and sPtk7 construct had minimal global effects on the culture. This also appeared to be true for Pk1 and Vangl2

overexpression, although comparisons were more difficult due to significant cell detachment during immunohistochemistry processing (Fig. 5.24A-B). With that said, there appeared to be no discernible differences between +dox and -dox treatment groups for both these cell lines.

In summary, no detectable differences were found between with and without Wnt/PCP component overexpression, suggesting they may have negligible impacts on Sox2 or T(Bra) intensity during the 24hours examined.

Taken together, the overexpression of Wnt/PCP during NMP derivation and NMP differentiation *in vitro*, did not appear to have an obvious effect on either T(Bra) or Sox2 expression. Consequently, Wnt/PCP may not be important for NMP derivation or differentiation. Conversely the lack of phenotype could also reflect the suitability of the assay. In the NMP derivation experiment there was considerable variation in the control cell line, and thus inherent variability in the assay may be masking the effect of overexpressing Wnt/PCP components. Furthermore, it was impossible to examine subtle effects in the whole well fluorescent microscopy images of the NMP differentiation experiment. To conclude, despite the lack of phenotype when Wnt/PCP components are overexpressed during NMP derivation and differentiation, additional more refined experiments are essential to assert these initial findings.

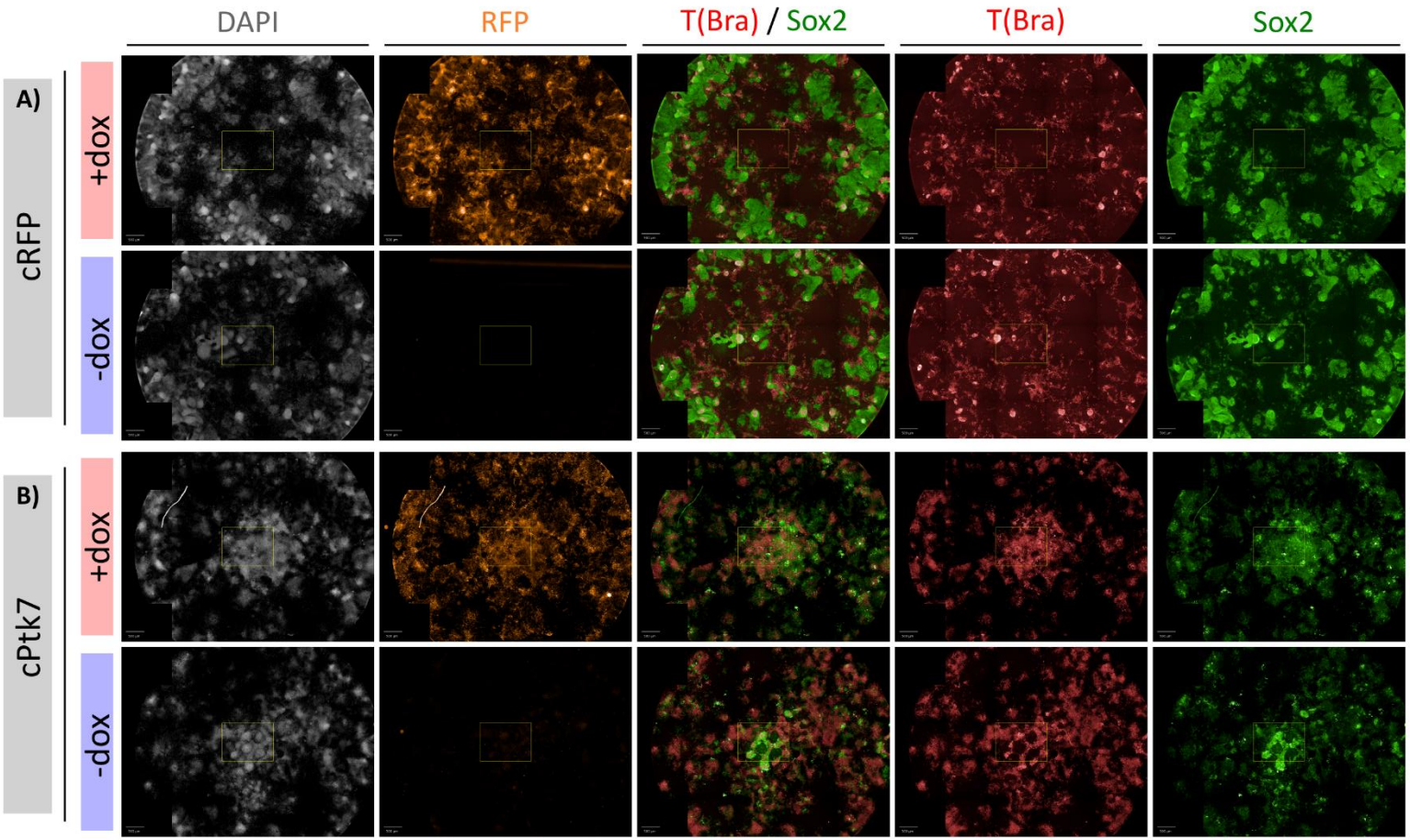

Figure 5.22 - T(Bra) and Sox2 intensity following induction during NMP differentiation - RFP(control) and Ptk7.
Immunohistochemistry of T(Bra) and Sox2 for (A) cRFP (control) and (B) cPtk7 cell lines, in conditions were dox was present (+dox) or absent (-dox) during EpiLC-NMP differentiation.

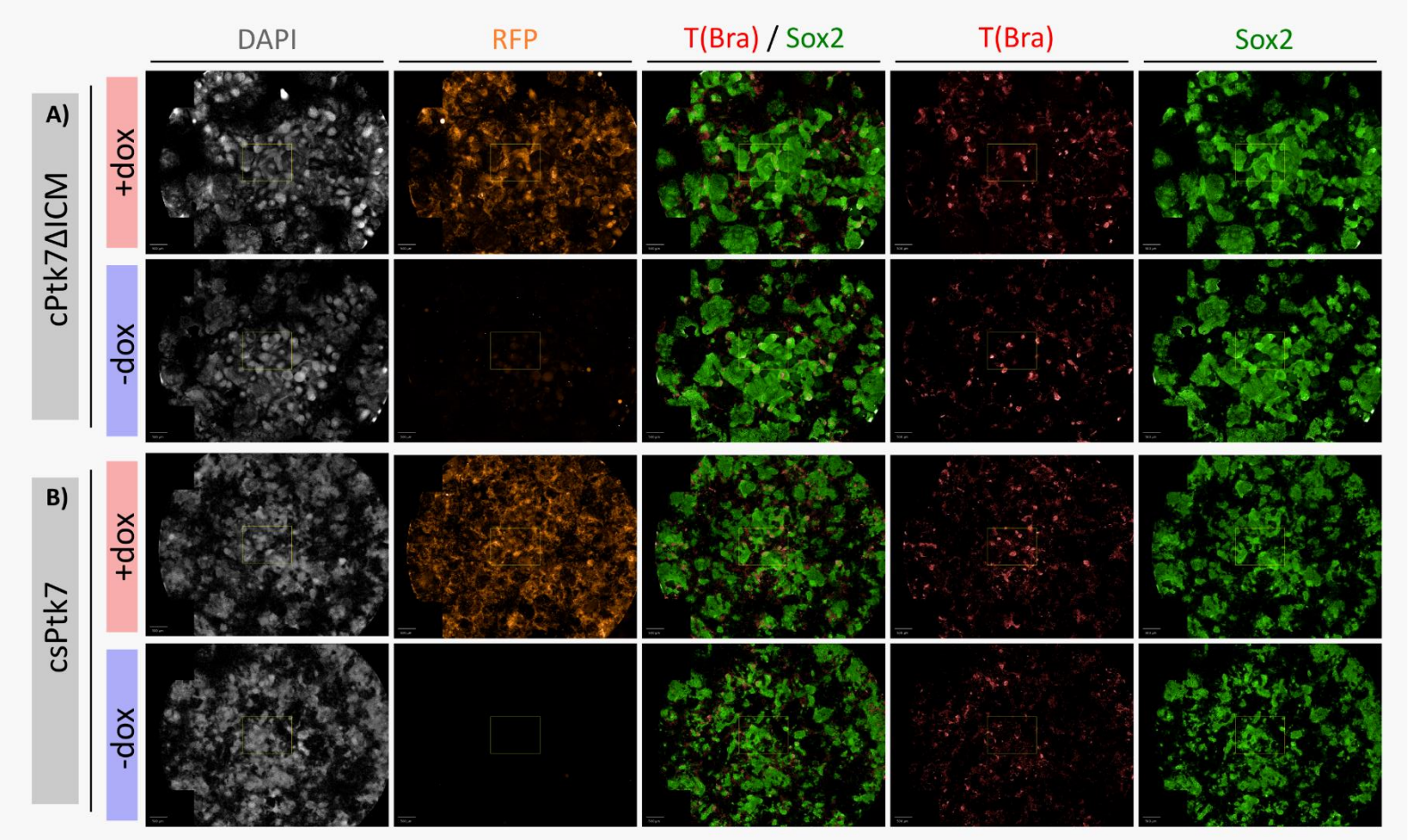

Figure 5.23 - T(Bra) and Sox2 intensity following induction during NMP differentiation - Ptk7ΔICM and sPtk7.
Immunohistochemistry of T(Bra) and Sox2 for **(A)** cPtk7ΔICM and **(B)** csPtk7 cell lines, in conditions were dox was present (+dox) or absent (-dox) during EpiLC-NMP differentiation.

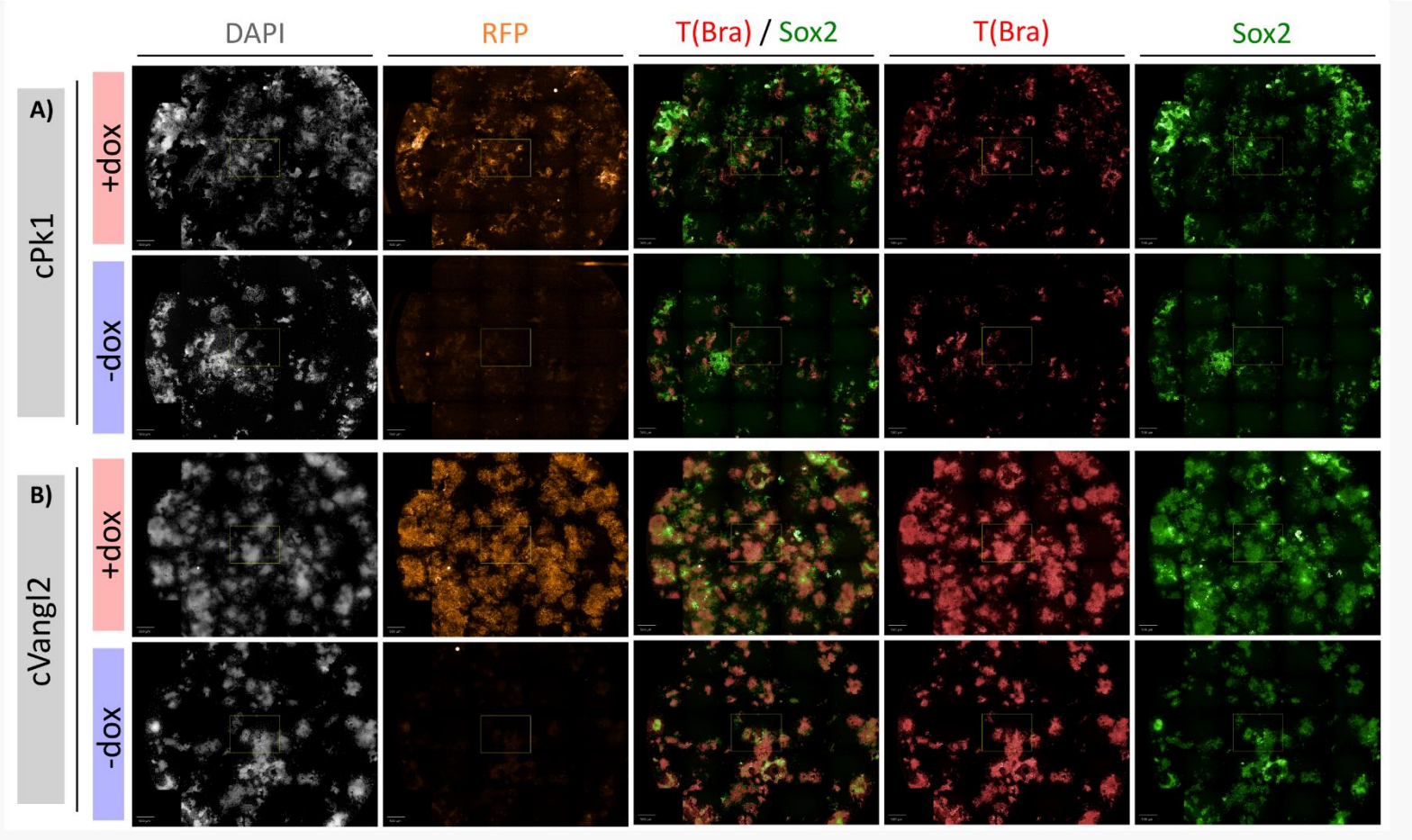

Figure 5.24 - T(Bra) and Sox2 intensity following induction during NMP differentiation - Pk1 and Vangl2.
Immunohistochemistry of T(Bra) and Sox2 for **(A)** Pk1 and **(B)** Vangl2 cell lines, in conditions were dox was present (+dox) or absent (-dox) during EpiLC-NMP differentiation.

5.3 Discussion

As previously discussed in the introduction (1.4) there is a growing body of evidence to suggest Wnt/PCP plays a role in regulating NMP behaviour. Research presented in Chapter 3 (3.2 and 3.3) and Chapter 4 (4.6) confirmed that Wnt/PCP components Fzd6, Ptk7 and Vangl2 are expressed in or adjacent to *in vivo* NMP regions, and in *in vitro* NMPs respectively. Furthermore Wnt/PCP mutants are characterised by axial truncations, in which caudal structures are lost during axial development. This phenotype is generally associated with improper regulation of NMP self-renewal or their tissue specific differentiation. However due to the global effect of these knock outs remained unclear whether phenotypes were a direct effect on disrupting Wnt/PCP in NMPs specifically or due to widespread changes in the posterior of the embryo.

For this reason, the aim of the work reported in this chapter was to advance knowledge of the role of Wnt/PCP signalling specifically in terms of regulating NMP behaviour. To achieve this, experimental goals included the generation of *in vivo* and *in vitro* tools to manipulate Wnt/PCP in *in vitro* and *in vivo* systems. Overexpression Wnt/PCP plasmids were developed for use in electroporation experiments which specifically allow the integration of Wnt/PCP components in *in vivo* NMPs at the start of somitogenesis, and the subsequent disruption of Wnt/PCP signalling. This permitted the dissection of global roles for Wnt/PCP in the general tailbud (Wnt/PCP knockouts), and the specific roles of Wnt/PCP in NMPs at this distinct timepoint in development (this thesis). In complement to *in vivo* systems, a previously described method of conditionally overexpressing genes (Iacovino et al., 2011, 2014), was adapted to allow for the conditional overexpression of Wnt/PCP components *in vitro*. Using these two systems the roles of Wnt/PCP signalling in NMPs were investigated by examining the tissue type contribution of NMPs with disrupted Wnt/PCP signalling. These findings are discussed further below.

5.3.1 Overexpression of Vangl2 but not Pk1 impedes NMP neural differentiation and NMP persistence in the CNH *in vivo*

Initial investigations of the role of Wnt/PCP began in *in vivo* systems focused on the CLE, the location of NMPs during early somitogenesis. Earlier in this thesis (Chapter 2) core Wnt/PCP component Vang2 (Fig. 3.12) and Pk1 (Fig. 3.1), as well as Wnt/PCP

co-receptor Ptk7 (Fig. 3.6) were found to be expressed in this region, suggesting these may be directly involved in regulating NMPs. Moreover, Vangl2 was identified as asymmetrically expressed in this area, further supporting the idea that Wnt/PCP signalling was active in NMPs that reside there.

This location is targetable by electroporation (Huang et al., 2015), a system that had been utilised to disrupt Wnt/PCP in previous vertebrate systems (Albors et al., 2015; Guirao et al., 2010). Overexpression of Wnt/PCP components is considered enough to overwhelm the delicately balanced system of antagonistic interactions between components that are essential for the initiation and propagation of Wnt/PCP signalling through tissues. Therefore, in order to further understand the relationship between Wnt/PCP signalling and NMP behaviour overexpression plasmids for Vangl2, Pk1 and Ptk7, were therefore generated. This permitted a 'triple attack' on the Wnt/PCP machinery, at the level of membrane, cytoplasm, and co-receptor respectively (Fig. 5.1), all components I had identified to be present in this region.

The plasmids were electroporated in to the CLE of embryos, and following 24 hours of ex vivo culture underwent analysis. This experiment aimed to address three questions. These were, does Wnt/PCP disruption (1) prevent normal NMP differentiation to mesoderm or neural lineages? (2) alter the balance of NMP differentiation between mesoderm and neural lineages? (3) change the persistence of NMPs in the progenitor region (CNH)? The inclusion of a cleavable T2A flanked by a RFP protein permitted the descendants of electroporated NMPs to be tracked, permitting the identification of any bias in NMP behaviour when Wnt/PCP was disrupted.

Analysis of control group, electroporated with RFP control plasmid confirmed that electroporated NMPs were viable and behaved normally, contributing to both neural and mesodermal tissues equally and persisting in the NMP region (CNH) (Fig. 5.8) (Cambray and Wilson, 2007; Huang et al., 2015; Wymeersch et al., 2016). Compared to controls, Pk1 did not significantly affect the persistence of NMPs in the CNH, suggesting NMP self-renewal was not affected by Pk1 overexpression (Fig. 5.12D). Moreover, NMPs electroporated with Pk1 showed little reduction in contribution to mesoderm or neural tissues, between which there was no obvious bias (Fig. 5.12A-C).

Conversely a strikingly different phenotype was obtained with the electroporation of Vangl2 (Fig. 5.11). Vangl2 overexpression resulted in an overall reduction in contribution along the axis (Fig. 5.12A-B) and to NMPs of the CNH (Fig. 5.12D). This strongly suggests that Vangl2 overexpression inhibits the ability of NMPs to remain in the progenitor region, and thus contribute to less axial tissue. Additionally, a bias between mesodermal and neural contribution was also identified by comparing the contribution of descendants within individual sections (Fig. 5.12C). A dramatic loss of neural contribution bias compared with control groups was observed, which implicates a role for Wnt/PCP signalling in NMP neural differentiation.

This distinction in phenotype between Vangl2 and Pk1 overexpression was not expected based on their previously reported roles in Wnt/PCP signalling. As mentioned in the Introduction (1.4.3.1), when Wnt/PCP is active, membrane localised Vangl2 and cytoplasmic Pk1, are co-localised and form a complex with Celsr proteins on one side of the cell (reviewed in Yang and Mlodzik, 2015). Pk proteins are recruited to the membrane by Vangl proteins where they function to inhibit Fzd-Dvl complexes forming nearby (Bastock, 2003; Das et al., 2004; Jenny et al., 2003; Tree et al., 2002). Thus, Vangl2 and Pk1 are thought to be essential for the initiation of core Wnt/PCP protein asymmetry, and subsequent Wnt/PCP signalling. Furthermore the overexpression of Pk1 or Vang2 during spinal cord regeneration of Axolotl results in similar phenotypes (Albors et al., 2015). Despite these reports, the evidence supplied by this current work suggests distinct roles for Vangl2 and Pk1 in the maintenance and differentiation of NMPs. This idea is supported by other evidence where they are known to have discrete interactions with other Wnt/PCP components. As mentioned earlier, Pk1 is known to interact with cytoplasmic components, including Dvl, whose downstream targets converge on cytoskeletal regulation. On the other hand Wnt5a has been shown to mediate the formation of complexes between Vangl2 and Wnt co-receptor Ror2, resulting in the phosphorylation of Vangl2 protein (Gao et al., 2011). In addition Vangl2 may also interact with Fzd, when they are co-localised at the edges of neighbouring cells through Celsr bridging (Chen et al., 2008; Lawrence et al., 2008; Struhl et al., 2012; Strutt and Strutt, 2008; Wu and Mlodzik, 2008).

In conclusion, despite the close association between Vangl2 and Pk1 in Wnt/PCP initiation and propagation, the distinct interactions with other component may explain the different phenotypes observed. The unique reported interaction of Vangl2 with Ror2 which is mediated by Wnt5a highlights a particularly interesting avenue for further investigation, especially given that expression of these components has been reported in NMP regions during axial elongation (Fig. 3.15) (Matsuda et al., 2001; Takada et al., 1994b; Verhey van Wijk et al., 2009; Yamaguchi et al., 1999b). Nevertheless, many questions remain in terms of how changes in NMP behaviour are mediated by Wnt/PCP.

Wnt/PCP has also been implicated in determining the orientation of cell divisions (reviewed in Gray, Roszko and Solnica-Krezel, 2011), and therefore may be a mechanism by which Wnt/PCP regulates NMP maintenance of NMPs in the progenitor zone. Of course, tracking cell division in NMPs *in vivo* can be extremely difficult due to their location within the tail bud. With that said, *in vitro* models could offer a more accessible system in which this could be examined.

It is possible that the difference in phenotypes between Pk1 and Vangl2 overexpression is not mediated by dysregulation of downstream cytoskeletal targets (downstream of Pk1) but perhaps by interactions between cells mediated by Vangl2. Moreover, given the derivatives of NMPs are either highly polarised (neural cells) or not (cells of mesoderm) (Fig. 3.20-22), the ability of NMPs to differentiate to either lineage may be determined by their ability to activate Wnt/PCP. It is not a stretch to imagine a NMP overexpressing Vangl2, unable to activate Wnt/PCP and coordinate with neighbouring cells, and thus subsequently travelling through the streak to form unpolarised mesoderm.

5.3.2 Ptk7 overexpression impedes NMP neural differentiation and NMP persistence in the CNH *in vivo*

Electroporation of Ptk7 in NMPs *in vivo* resulted in a strikingly similar phenotype to that described for Vangl2. Electroporation of Ptk7 reduced the capacity of NMPs to contribute to neural tissue and persist in NMPs regions (Fig. 5.9, Fig. 5.12). This similarity between Ptk7 and Vangl2 overexpression was somewhat surprising, as Ptk7 and Vangl2 have distinct roles in Wnt/PCP signalling. Unlike Vangl2, Ptk7 is not

considered a core Wnt/PCP component, but rather a Wnt co-receptor. Ptk7 interacts with components of the Wnt/PCP pathway, including Wnt5a (Martinez et al., 2015) and fellow co-receptor Ror2 (Martinez et al., 2015; Podleschny et al., 2015). However Ptk7's additional interactions with Wnt/β-catenin signalling family members, Wnt3a (Peradziryi et al., 2011) and β-catenin (Puppo et al., 2011), make its downstream actions unclear and perhaps context dependent. Furthermore as Ptk7 has not been overexpressed before in NMPs it is difficult to interpret its actions. Moreover, the parallels between Vangl2 overexpression which disrupts Wnt/PCP and Ptk7 overexpression, could be interpreted as an anti-Wnt/PCP influence of Ptk7, with increased Ptk7 mediated actions inhibiting Wnt/PCP signalling.

With that said, the identical phenotypes between Vangl2 and Ptk7 also implicates a common mechanism of action of their overexpression. Vangl2 and Ptk7 are not known to interact directly with knock out of either not affecting the localisation of the other (Paudyal et al., 2010). Conversely they both share Ror2 as a common interaction partner (Gao et al., 2011; Martinez et al., 2015; Podleschny et al., 2015), which is not shared by Pk1. Another connection between Vangl2 and Ptk7 is metalloproteinase MMP14. Vangl2 has been implicated in regulating the availability of MMP14 (Williams et al., 2012). When Vangl2 is knocked down in Zebrafish studies, the availability of MMP14 outside the cell increases, implicating Vangl2 in regulation of MMP14 availability. Moreover Ptk7 is cleaved by MMP14 in its extracellular domain generating a secreted extracellular fragment (Golubkov et al., 2010). Wnt/PCP axial truncation phenotypes are apparent in *Ptk7 chuzhoi* mutants which an extra MMP-14 cleavage site suggesting MMP-14 cleavage may be important aspect of Ptk7 interaction with Wnt/PCP (Paudyal et al., 2010).

In conclusion despite no direct interactions between Ptk7 and Vangl2 reported in the literature, indirect links between these proteins are clear. Moreover, these connections provide some explanation for the parallel NMP behaviour phenotypes that are determined when they are overexpressed, and unlock an exciting new area of investigation going forward. Nonetheless, many questions remain unanswered. For example, it is not clear if asymmetry of components is essential for NMP regulation? Also how does disrupting MMP14 affect NMP behaviours and what are the actions of

cleaved and uncleaved Ptk7? Additional tools are now available precisely for such investigations. As described in 5.2.1, modified Ptk7 constructs, sPtk7 and Ptk7ΔICM (Fig. 5.1), have been generated but not yet utilised in electroporation experiments. These would allow further dissection of the role of Ptk7 in NMP behaviour. Specifically, sPtk7 contains the small extracellular portions of Ptk7 which contains the MMP14 cleavage site. This would enable the verification of MMP14 role in the Ptk7-Vangl2 regulation of NMP behaviour.

5.3.3 Wnt/PCP has distinct roles in regulating NMP behaviour

Previously Wnt/PCP mutants have been found to exhibit severe axial defects with an overall loss of caudal structures. Detailed examination of several of these mutants, demonstrated many mesoderm defects due to disruptions in CE and EMT (Andre et al., 2015; Paudyal et al., 2010; Yen et al., 2009). Moreover, an accumulation of NMPs had been reported in *Wnt5a/Wnt11* double knock outs (Andre et al., 2015). The work undertaken in this chapter does not demonstrate any similar defects or disruptions in the mice with specific overexpression of Ptk7 and Vangl2 in NMPs. In contrast to the accumulation of NMPs in the streak of global knock outs Wnt/PCP mutants, NMPs electroporated with Ptk7 or Vangl2 did not show any complications when travelling through the streak, and incorporated normally with neighbouring cells of the neural tube and mesoderm (Fig. 5.7). In fact, less rather than more electroporated cells were found in NMPs regions (CNH), suggesting cells with disrupted Wnt/PCP actively leave NMPs regions through the primitive streak (Fig. 5.12). Additionally NMPs with Ptk7 and Vangl2 overexpression preferentially contributed to mesoderm tissue, in contrast to loss of mesoderm described for Ptk7 mutants (Yen et al., 2009).

In conclusion, the effect of disrupting Wnt/PCP globally during early development is vastly different to localised disruption of Wnt/PCP in NMPs. This suggests that CE and EMT phenotypes in Wnt/PCP mutants are not a direct consequence of losing Wnt/PCP signalling in NMPs. This dual role of Wnt/PCP in caudal tissues is not particularly surprising, given that Wnt/PCP components were identified in other tissues including notochord, situated adjacent to NMPs residing in the CNH and node-streak border (3.2). This underlines the importance of studying Wnt/PCPs role in NMPs in a conditional system.

5.3.4 Discrete actions of overexpressing Wnt/PCP *in vitro* and *in vivo* systems

Motivated by observations using *in vivo* systems, an alternative high-throughput and accessible system in which the mechanism underlying Wnt/PCP signalling in NMPs could be further investigated was sought. The ability to derive NMPs in *in vitro* assays provided a suitable alternative, and importantly Wnt/PCP components had been identified in these cell cultures previously (4.6).

Thus, overexpression cell lines were generated using an adaptable dox inducible *in vitro* system described previously (Iacovino et al., 2011, 2014). The results indicate that inducibility was high in both 2i/LIF (Fig. 5.14) and EpiLC cultures (Fig.5.17, Fig. 5.21), with at least 50% of total cells overexpressing the Wnt/PCP gene of interest. Subsequently, these cell lines were used to test the effect of Wnt/PCP overexpressing at two distinct timepoints. The first, during derivation of EpiLC-NMPs and the second, during differentiation from EpiLC-NMPs, using the EpiLC-NMP derivation protocol previously described in Chapter 4. T(Bra) and Sox2 levels were used as a read out of any effects on NMP behaviour by Wnt/PCP overexpression.

In the NMP derivation experiment there was no evidence of an effect of induction. However, the considerable variation in the control cell line between induced and non-induced population (Fig. 5.18A-B), and this inherent variability in the assay may mask the effect of overexpressing Wnt/PCP components (Fig. 5.18-19). Furthermore, no differences were identified between induced and non-induced populations during NMP differentiation. However, it was impossible to examine subtle effects in the whole well fluorescent microscopy images of this NMP differentiation experiment (Fig. 5.22-24). To conclude, no obvious phenotype was observed when Wnt/PCP components were overexpressed during *in vitro* NMP derivation or differentiation.

The results reported above create something of a paradox between the observable phenotype of Wnt/PCP overexpression in *in vivo* assays, but not in *in vitro* assays. This could be for several reasons, one of which could be due to limitations of the *in vitro* assays used. Further investigations should focus on refining these assays to confirm the presence of a phenotype. For example, confocal microscopy of these cultures would provide more accurate dynamics of T(Bra) and Sox2 intensities, and may permit

the identification of subtle phenotypes. Conversely, increasing the length of time Wnt/PCP components are induced for, may allow for more observable phenotypes.

Another rationale for the lack of phenotype could be that Wnt/PCP is not being disrupted. This is highly unlikely given that the same gene sequences were used in both *in vitro* and *in vivo* inducible systems (Fig. 2.1). Additionally, the induction of Ptk7 and Vangl2 was shown to be specifically overexpressed in these cell lines upon the addition of dox to a significant level (Fig. 5.15). Unfortunately, disruption of Wnt/PCP signalling is difficult to monitor, as many downstream effectors converge on cytoskeletal changes. However, given that Wnt/PCP and Wnt/β-catenin may be antagonistic, perhaps examining activation of Wnt/β-catenin may allow the confirmation of Wnt/PCP disruption. As described in the introduction (1.4) Wnt/PCP activity can also be monitored by examining the intrinsic asymmetry of individual cells. Thus, disruptions to Wnt/PCP signalling in these cell cultures could potentially be inferred from examining patterns of organelle positioning between cells. Moreover, this would also provide a method to confirm disruptions of Wnt/PCP in *in vitro* cultures when components are overexpressed.

Finally, another possible reason for the lack of phenotype in *in vitro* assays is that these assays may represent a sub-optimal model of *in vivo* NMP development. Despite many similarities transcriptionally and functionally between *in vitro* and *in vivo* derived NMPs (reviewed in Henrique et al., 2015) their environments are distinct. NMPs *in vitro* are confined to flat two-dimensional cultures, whereas *in vivo* NMPs are integrated in a complex three-dimensional architecture. Moreover NMPs *in vivo* are close to other tissues which may act as a niche sustaining their development and behaviour. These supporting cells are simply not present in *in vitro* cultures, the consequences of which are not fully understood. Thus, future development of three-dimensional culture systems may provide a more fitting system in which Wnt/PCP and polarity of NMPs could be investigated.

Chapter 6: Conclusion and Working Model

Although the role of Wnt/PCP in regulation of NMPs in early embryonic development was suspected the mechanisms and the dynamic nature of this regulation were poorly defined. This thesis set out to provide a finer grained view of that relationship in several key areas. This thesis aimed to explore the hypothesis that Wnt/PCP regulated NMP behaviour in two ways. First by examining the localisation of Wnt/PCP components in NMP regions during axial elongation *in vivo* (Chapter 3) and *in vitro* (Chapter 4). Secondly by disrupting Wnt/PCP signalling conditionally in NMPs, and observing any change in NMP behaviour (Chapter 5). Based on these findings a working model has been created to describe the potential mechanisms by which Wnt/PCP controls NMP behaviour (Fig. 6.1).

Based on the literature Wnt/PCP activity is likely to be regulated by both internal and external factors (Fig. 6.1A). Intrinsically, cells need to have Wnt/PCP machinery in order for asymmetry to take place and for cells to become polarised (reviewed in Yang and Mlodzik, 2015). Even when only one component is lost (in knock out mutants), the result is severe disruptions to planar polarity which has dramatic consequences for axial development. External factors suspected of influencing Wnt/PCP in NMP regions have included Wnt5a, a key ligand in Wnt/PCP signalling, and co-receptors such as Ptk7 and Ror2.

This thesis has confirmed and extended some of the existing findings. In this thesis, Ptk7, Vangl2 and *Pk1* were identified in NMPs regions throughout axial elongation (3.2/3.3). Moreover, confirming NMPs have internal and external factors associated with Wnt/PCP activation (Fig. 6.1A). Furthermore, monitoring of polarity and cell movement in NMPs regions, using organelle positioning, illustrated that similar dynamics of polarity are continuing in NMP regions throughout axial elongation (summarised in Fig 3.25). Cells in the NMP regions (CLE and neuroectoderm of the CNH), are initially coordinated in their polarity. This coordination is subsequently lost in some cells, which migrate to become cells of the mesoderm, with those left behind thus forming future neural tissues (Fig. 6.1A).

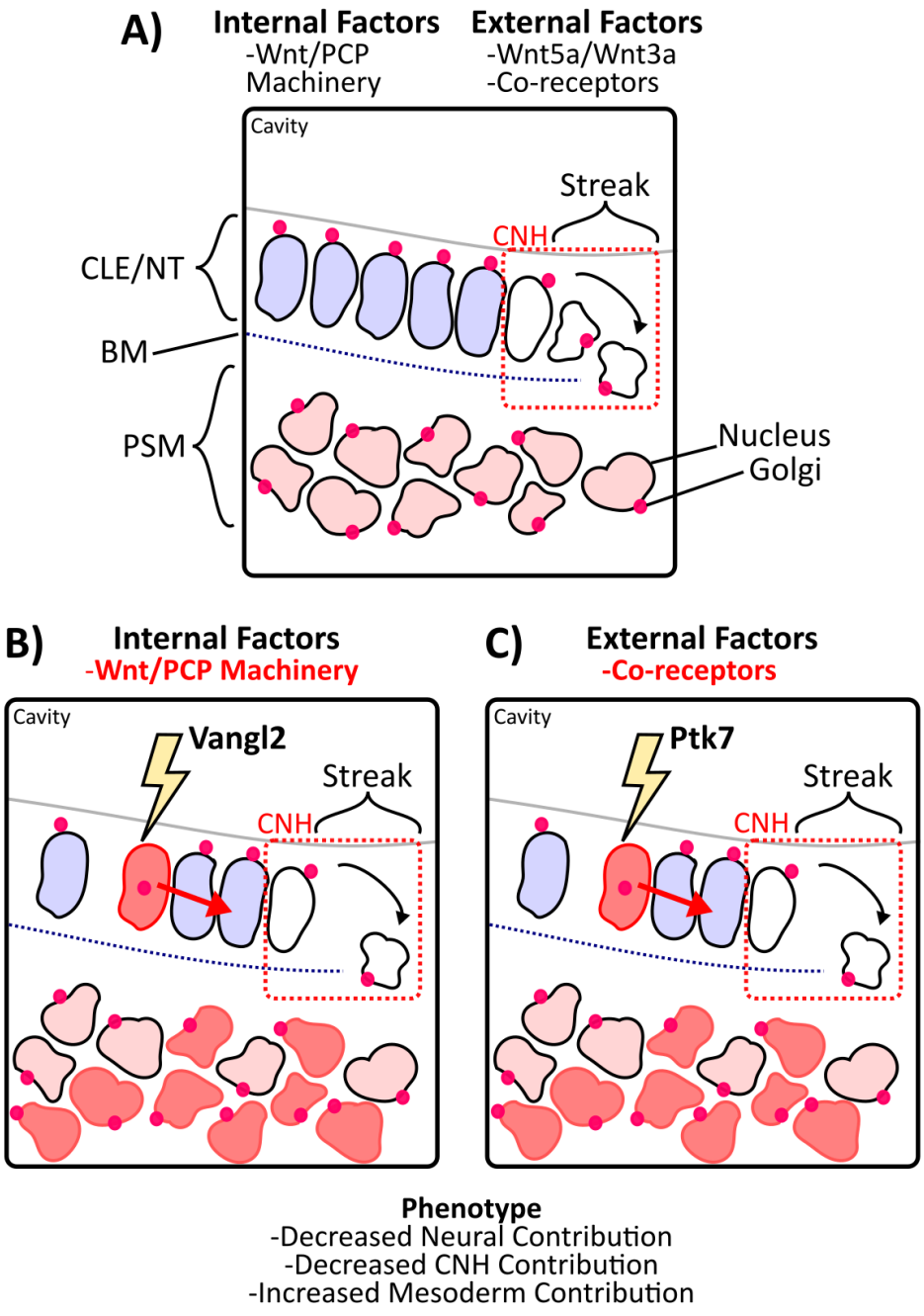

Figure 6.1: Working Model of Wnt/PCP regulation of NMP behaviour.
(A) Wnt/PCP activity is regulated by both internal and external factors. NMPs in early somitogenesis reside in the caudal lateral epiblast (CLE) and then the posterior neural tube (NT), known as the chordoneural hinge (CNH) following tail bud formation (see Fig. 3.25). NMPs in these areas lose polarity as they travel through the streak to form presomitic mesoderm (PSM), with those remaining forming neural tissue. When Wnt/PCP is disrupted at the level of **(B)** Wnt/PCP machinery with overexpression (via electroporation) of Vangl2, or at the level of **(C)** co-receptors with the overexpression (via electroporation) of Ptk7, a similar phenotype is observed. Electroporated cells (red outline) are less likely to remain in the neuroepithelium, or in the CNH region (red dashed box), and instead actively form presomitic mesoderm (PSM), thus shifting the balance of NMP fate choice and maintenance.

Disrupting Wnt/PCP illustrated that Wnt/PCP is indeed key for this NMP behaviour. Disrupting Wnt/PCP by overexpressing components of core machinery, Vangl2 (Fig. 6.1B) or co-receptor, Ptk7 (Fig. 6.1C), specifically in the CLE, resulted in a distinct phenotype. NMPs were unable to contribute to neural lineages as they would normally with these cells preferentially choosing mesodermal fate. Additionally, the ability of NMPs to persist in the CNH was decreased when Wnt/PCP was disrupted. Thus, regulation of NMP behaviour is dependent on Wnt/PCP signalling through Vangl2 and Ptk7 expression. Furthermore, this phenotype was not shared by cytoplasmic component Pk1 overexpression, suggesting that regulation of NMP behaviour is independent of Pk1.

Altogether, this research implicates Wnt/PCP signalling as an important regulator of NMP behaviour, however many questions remain regarding the mechanism behind this regulation. With Wnt/PCP disruptions known to be important for coordinated cell polarity between neighbours, is NMP fate controlled by cell-cell contact alone? Or does Wnt/PCP directly or indirectly control downstream activation of genes important for NMP status, such as T(Bra) and Sox2? Moreover, does Wnt/PCP act antagonistically with Wnt/β-catenin signalling to strike a balance between differentiation and maintenance of NMPs? Indeed, Vangl2 and Ptk7 share interactions with Ror2 an additional Wnt co-receptor, thus is Ror2 the master regulator of NMP behaviour? Additionally, Vangl2 can control the localisation of MMP14, which is important for the cleavage of Ptk7 during CE. Thus, does this represent an additional layer of Wnt/PCP control of NMP behaviour?

In conclusion, this work successfully extends our knowledge on Wnt/PCP mediated control of NMP differentiation and maintenance, and provide a finer grained description of the relationships between them. It accomplished this by the development and deployment of novel research tools and the use of both *in vivo* and *in vitro* techniques. However new insights provided raise a whole new series of questions. Answering these will require further investigation, as well as application and development of new methodologies.

References

Albors, A.R., Tazaki, A., Rost, F., Nowoshilow, S., Chara, O., and Tanaka, E.M. (2015). Planar cell polarity-mediated induction of neural stem cell expansion during axolotl spinal cord regeneration. Elife 1–29.

Andre, P., Song, H., Kim, W., Kispert, A., and Yang, Y. (2015). Wnt5a and Wnt11 regulate mammalian anterior-posterior axis elongation. Development dev.119065-.

De Angioletti, M., Lacerra, G., Sabato, V., and Carestia, C. (2004). β+45 G → C: A novel silent β-thalassaemia mutation, the first in the Kozak sequence. Br. J. Haematol. *124*, 224–231.

Antic, D., Stubbs, J.L., Suyama, K., Kintner, C., Scott, M.P., and Axelrod, J.D. (2010). Planar cell polarity enables posterior localization of nodal cilia and left-right axis determination during mouse and Xenopus embryogenesis. PLoS One *5*.

Arkell, R.M., and Tam, P.P.L. (2012). Initiating head development in mouse embryos: integrating signalling and transcriptional activity. Open Biol. *2*, 120030–120030.

Arnold, S.J., and Robertson, E.J. (2009). Making a commitment: cell lineage allocation and axis patterning in the early mouse embryo. Nat. Rev. Mol. Cell Biol. *10*, 91–103.

Avilion, A.A., Nicolis, S.K., Pevny, L.H., Perez, L., Vivian, N., and Lovell-Badge, R. (2003). Multipotent cell lineages in early mouse development on SOX2 function. Genes Dev. *17*, 126–140.

Axelrod, J.D. (2001). Unipolar membrane association of Dishevelled mediates Frizzled planar cell polarity signaling. Genes Dev. *15*, 1182–1187.

Axelrod, J.D., Miller, J.R., Shulman, J.M., Moon, R.T., and Perrimon, N. (1998). Differential recruitment of dishevelled provides signaling specificity in the planar cell polarity and Wingless signaling pathways. Genes Dev. *12*, 2610–2622.

Bastian, H., and Gruss, P. (1990). A murine even-skipped homologue, Evx 1, is expressed during early embryogenesis and neurogenesis in a biphasic manner. EMBO J. *9*, 1839–1852.

Bastock, R. (2003). Strabismus is asymmetrically localised and binds to Prickle and Dishevelled during Drosophila planar polarity patterning. Development *130*, 3007–3014.

Beck, F., Erler, T., Russell, A., and James, R. (1995). Expression of Cdx-2 in the mouse embryo and placenta: Possible role in patterning of the extra-embryonic membranes. Dev. Dyn. *204*, 219–227.

Becker, K., Jährling, N., Saghafi, S., and Dodt, H.U. (2013). Immunostaining, dehydration, and clearing of mouse embryos for ultramicroscopy. Cold Spring Harb. Protoc. *2013*, 743–744.

Beddington, B.R.S.P. (1983). Histogenetic and neoplastic potential of different regions of the mouse embryonic egg cylinder. J. Embryol. Exp. Morphol. *204*, 189–204.

Beddington, R.S. (1994). Induction of a second neural axis by the mouse node. Development *120*, 613–620.

Beddington, R.S.P., and Robertson, E.J. (1999). Axis development and early asymmetry in mammals. Cell *96*, 195–209.

Beddington, R.S., Rashbass, P., and Wilson, V. (1992). Brachyury--a gene affecting mouse gastrulation and early organogenesis. Development *165*, 157–165.

Bekman, E., and Henrique, D. (2002). Embryonic expression of three mouse genes with homology to the Drosophila melanogaster prickle gene. Gene Expr. Patterns *2*, 73–77.

Bellomo, D., Lander, A., Harragan, L., and Brown, N.A. (1996). Cell proliferation in mammalian gastrulation: The ventral node and notochord are relatively quiescent. Dev. Dyn. *205*, 471–485.

Belotti, E., Puvirajesinghe, T.M., Audebert, S., Baudelet, E., Camoin, L., Pierres, M., Lasvaux, L., Ferracci, G., Montcouquiol, M., and Borg, J.P. (2012). Molecular Characterisation of Endogenous Vangl2/Vangl1 Heteromeric Protein Complexes. PLoS One *7*.

Ben-Haim, N., Lu, C., Guzman-Ayala, M., Pescatore, L., Mesnard, D., Bischofberger, M., Naef, F., Robertson, E.J., and Constam, D.B. (2006). The Nodal Precursor Acting via Activin Receptors Induces Mesoderm by Maintaining a Source of Its Convertases and BMP4. Dev. Cell *11*, 313–323.

Berger, H., Breuer, M., Peradziryi, H., Podleschny, M., Jacob, R., and Borchers, A. (2017a). PTK7 localization and protein stability is affected by canonical Wnt ligands. J. Cell Sci. *130*,

1890–1903.

Berger, H., Wodarz, A., and Borchers, A. (2017b). PTK7 Faces the Wnt in Development and Disease. Front. Cell Dev. Biol. *5*, 1–7.

Bernemann, C., Greber, B., Ko, K., Sterneckert, J., Han, D.W., Araúzo-Bravo, M.J., and Schöler, H.R. (2011). Distinct developmental ground states of epiblast stem cell lines determine different pluripotency features. Stem Cells *29*, 1496–1503.

Bernier, G., Vukovich, W., Neidhardt, L., Herrmann, B.G., and Gruss, P. (2001). Isolation and characterization of a downstream target of Pax6 in the mammalian retinal primordium. Development *128*, 3987–3994.

Bin-Nun, N., Lichtig, H., Malyarova, A., Levy, M., Elias, S., and Frank, D. (2014). PTK7 modulates Wnt signaling activity via LRP6. Development *141*, 410–421.

Blankenship, J.T., Backovic, S.T., Sanny, J.S.S.P., Weitz, O., and Zallen, J.A. (2006). Multicellular Rosette Formation Links Planar Cell Polarity to Tissue Morphogenesis. Dev. Cell *11*, 459–470.

Boehm, B., Westerberg, H., Lesnicar-Pucko, G., Raja, S., Rautschka, M., Cotterell, J., Swoger, J., and Sharpe, J. (2010). The role of spatially controlled cell proliferation in limb bud morphogenesis. PLoS Biol. *8*.

Bois, P., Stead, J.D., Bakshi, S., Williamson, J., Neumann, R., Moghadaszadeh, B., and Jeffreys, A.J. (1996). Isolation and characterization of mouse Dishevelled-3. Dev. Dyn. *207*, 253–262.

Bonnerot, C., Rocancourt, D., Briand, P., Grimber, G., and Nicolas, J.F. (1987). A beta-galactosidase hybrid protein targeted to nuclei as a marker for developmental studies. Proc. Natl. Acad. Sci. U. S. A. *84*, 6795–6799.

Borello, U., Buffa, V., Sonnino, C., Melchionna, R., Vivarelli, E., and Cossu, G. (1999). Differential expression of the Wnt putative receptors Frizzled during mouse somitogenesis. Mech. Dev. *89*, 173–177.

Bornens, M. (2008). Organelle positioning and cell polarity. Nat. Rev. Mol. Cell Biol. *9*, 874–886.

Borovina, A., Superina, S., Voskas, D., and Ciruna, B. (2010). Vangl2 directs the posterior tilting and asymmetric localization of motile primary cilia. Nat. Cell Biol. *12*, 407–412.

Boulet, A.M., and Capecchi, M.R. (2012). Signaling by FGF4 and FGF8 is required for axial elongation of the mouse embryo. Dev. Biol. *371*, 235–245.

Brons, I.G.M., Smithers, L.E., Trotter, M.W.B., Rugg-gunn, P., Sun, B., Chuva, S.M., Lopes, D.S., Howlett, S.K., Clarkson, A., Ahrlund-richter, L., et al. (2007). Derivation of pluripotent epiblast stem cells from mammalian embryos. Nature *448*, 191–196.

Burute, M., Prioux, M., Blin, G., Young, J., Tseng, Q., and Bessy, T. (2017). Polarity Reversal by Centrosome Repositioning Primes Cell Scattering during Epithelial-to-Mesenchymal Transition Article Polarity Reversal by Centrosome Repositioning Primes Cell Scattering during Epithelial-to-Mesenchymal Transition. Dev. Cell *40*, 168–184.

Caddy, J., Wilanowski, T., Darido, C., Dworkin, S., Ting, S.B., Zhao, Q., Rank, G., Auden, A., Srivastava, S., Papenfuss, T.A., et al. (2010). Epidermal Wound Repair is Regulated by the Planar Cell Polarity Signaling Pathway. Dev. Cell *19*, 138–147.

Cambray, N., and Wilson, V. (2002). Axial progenitors with extensive potency are localised to the mouse chordoneural hinge. Development *129*, 4855–4866.

Cambray, N., and Wilson, V. (2007). Two distinct sources for a population of maturing axial progenitors. Development *134*, 2829–2840.

Camps, J., Erdos, M.R., and Ried, T. (2015). The role of lamin B1 for the maintenance of nuclear structure and function. Nucleus *6*, 8–14.

Carvajal-Gonzalez, J.M., Roman, A.-C., and Mlodzik, M. (2016). Positioning of centrioles is a conserved readout of Frizzled planar cell polarity signalling. Nat. Commun. *7*, 11135.

Casey, E.S., O'Reilly, M. a, Conlon, F.L., and Smith, J.C. (1998). The T-box transcription factor Brachyury regulates expression of eFGF through binding to a non-palindromic response element. Development *125*, 3887–3894.

Chapman, D.L., and Papaioannou, V.E. (1998). Three neural tubes in mouse embryos with mutations in the T-box gene Tbx6. Nature *391*, 695–697.

Chapman, D.L., Agulnik, I., Hancock, S., Silver, L.M., and Papaioannou, V.E. (1996). Tbx6,

a mouse T-Box gene implicated in paraxial mesoderm formation at gastrulation. Dev. Biol. *180*, 534–542.

Charrier, J.B., Teillet, M.A., Lapointe, F., and Le Douarin, N.M. (1999). Defining subregions of Hensen's node essential for caudalward movement, midline development and cell survival. Development *126*, 4771–4783.

Chawengsaksophak, K., de Graaff, W., Rossant, J., Deschamps, J., and Beck, F. (2004). Cdx2 is essential for axial elongation in mouse development. Proc. Natl. Acad. Sci. *101*, 7641–7645.

Chen, W.S., Antic, D., Matis, M., Logan, C.Y., Povelones, M., Anderson, G.A., Nusse, R., and Axelrod, J.D. (2008). Asymmetric Homotypic Interactions of the Atypical Cadherin Flamingo Mediate Intercellular Polarity Signaling. Cell *133*, 1093–1105.

Chenoweth, J.G., Mckay, R.D.G., and Tesar, P.J. (2010). Epiblast stem cells contribute new insight into pluripotency and gastrulation. Dev. Growth Differ. *52*, 293–301.

Ciruna, B., and Rossant, J. (2001). Mesoderm Cell Fate Specification and Morphogenetic Movement at the Primitive Streak. Dev. Cell *1*, 37–49.

Concha, M.L., and Adams, R.J. (1998). Oriented cell divisions and cellular morphogenesis in the zebrafish gastrula and neurula : a time-lapse analysis. Development *125*, 983–994.

Conlon, F.L., Lyons, K.M., Takaesu, N., Barth, K.S., Kispert, A., Herrmann, B., and Robertson, E.J. (1994). A primary requirement for nodal in the formation and maintenance of the primitive streak in the mouse. Development *120*, 1919–1928.

Corallo, D., Trapani, V., and Bonaldo, P. (2015). The notochord: Structure and functions. Cell. Mol. Life Sci. *72*, 2989–3008.

Cortijo, C., Gouzi, M., Tissir, F., and Grapin-Botton, A. (2012). Planar Cell Polarity Controls Pancreatic Beta Cell Differentiation and Glucose Homeostasis. Cell Rep. *2*, 1593–1606.

Crompton, L.A., Du Roure, C., and Rodriguez, T.A. (2007). Early embryonic expression patterns of the mouse Flamingo and Prickle orthologues. Dev. Dyn. *236*, 3137–3143.

Crossley, P.H., and Martin, G.R. (1995). The mouse Fgf8 gene encodes a family of

polypeptides and is expressed in regions that direct outgrowth and patterning in the developing embryo. Development *121*, 439–451.

Curtin, J.A., Quint, E., Tsipouri, V., Arkell, R.M., Cattanach, B., Copp, A.J., Henderson, D.J., Spurr, N., Stanier, P., Fisher, E.M., et al. (2003). Mutation of Celsr1 Disrupts Planar Polarity of Inner Ear Hair Cells and Causes Severe Neural Tube Defects in the Mouse. Curr. Biol. *13*, 1129–1133.

Das, G., Jenny, A., Klein, T.J., Eaton, S., and Mlodzik, M. (2004). Diego interacts with Prickle and Strabismus/Van Gogh to localize planar cell polarity complexes. Development *131*, 4467–4476.

Deans, M.R., Antic, D., Suyama, K., Scott, M.P., Axelrod, J.D., and Goodrich, L. V. (2007). Asymmetric Distribution of Prickle-Like 2 Reveals an Early Underlying Polarization of Vestibular Sensory Epithelia in the Inner Ear. J. Neurosci. *27*, 3139–3147.

DeChiara, T.M., Kimble, R.B., Poueymirou, W.T., Rojas, J., Masiakowski, P., Valenzuela, D.M., and Yancopoulos, G.D. (2000). Ror2, encoding a receptor-like tyrosine kinase, is required for cartilage and growth plate development. Nat. Genet. *24*, 271–274.

Delfino-Machin, M., Delfino-Machín, M., Lunn, J.S., Breitkreuz, D.N., Akai, J., Storey, K.G., Delfino-Machin, M., Delfino-Machín, M., Lunn, J.S., Breitkreuz, D.N., et al. (2005). Specification and maintenance of the spinal cord stem zone. Development *132*, 4273–4283.

Deng, C., Shen, M.M., Daugherty, C., Ornitz, D.M., and Leder, P. (1994). Murine FGFR-1 is required for early postimplantation growth and axial organization. Genes Dev. *8*, 3045–3057.

Deschamps, J., and van Nes, J. (2005). Developmental regulation of the Hox genes during axial morphogenesis in the mouse. Development *132*, 2931–2942.

Devenport, D., and Fuchs, E. (2008). Planar Polarization in Embryonic Epidermis Orchestrates Global Asymmetric Morphogenesis of Hair Follicles. Nat. Cell Biol. *10*, 1257–1268.

Dorey, K., and Amaya, E. (2010). FGF signalling: diverse roles during early vertebrate embryogenesis. Development *137*, 3731–3742.

Doudney, K., and Stanier, P. (2005). Epithelial cell polarity genes are required for neural tube closure. Am. J. Med. Genet. Part C Semin. Med. Genet. *135C*, 42–47.

Economides, K.D., Zeltser, L., and Capecchi, M.R. (2003). Hoxb13 mutations cause overgrowth of caudal spinal cordand tail vertebrae. Dev. Biol. *256*, 317–330.

Etheridge, S.L., Ray, S., Li, S., Hamblet, N.S., Lijam, N., Tsang, M., Greer, J., Kardos, N., Wang, J., Sussman, D.J., et al. (2008). Murine dishevelled 3 functions in redundant pathways with dishevelled 1 and 2 in normal cardiac outflow tract, cochlea, and neural tube development. PLoS Genet. *4*.

Evans, M.J., and Kaufman, M.H. (1981). Establishment in culture of pluripotential cells from mouse embryos. Nature *292*, 154–156.

Evans, A.L., Faial, T., Gilchrist, M.J., Down, T., Vallier, L., Pedersen, R.A., Wardle, F.C., and Smith, J.C. (2012). Genomic targets of Brachyury (T) in differentiating mouse embryonic stem cells. PLoS One *7*.

Forlani, S., Lawson, K. a, and Deschamps, J. (2003). Acquisition of Hox codes during gastrulation and axial elongation in the mouse embryo. Development *130*, 3807–3819.

Formstone, C.J., and Little, P.F.R. (2001). The flamingo-related mouse Celsr family (Celsr1-3) genes exhibit distinct patterns of expression during embryonic development. Mech. Dev. *109*, 91–94.

Gao, B., Song, H., Bishop, K., Elliot, G., Garrett, L., English, M.A., Andre, P., Robinson, J., Sood, R., Minami, Y., et al. (2011). Wnt Signaling Gradients Establish Planar Cell Polarity by Inducing Vangl2 Phosphorylation through Ror2. Dev. Cell *20*, 163–176.

Gardner, R.L. (1998). Contributions of blastocyst micromanipulation to the study of mammalian development. BioEssays *20*, 168–180.

Le Garrec, J.-F., Ragni, C. V., Pop, S., Dufour, A., Olivo-Marin, J.-C., Buckingham, M.E., and Meilhac, S.M. (2013). Quantitative analysis of polarity in 3D reveals local cell coordination in the embryonic mouse heart. Development *140*, 395–404.

Gho, M., and Schweisguth, F. (1998). Frizzled signalling controls orientation of asymmetric sense organ precursor cell divisions in Drosophila. Nature *394*, 178–181.

Gibson, D.G. (2011). Enzymatic assembly of overlapping DNA fragments. Methods Enzymol. *498*, 349–361.

Gilchrist, D.S., Ure, J., Hook, L., and Medvinsky, A. (2003). Labeling of hematopoietic stem and progenitor cells in novel activatable EGFP reporter mice. Genesis *36*, 168–176.

Golubkov, V.S., and Strongin, A.Y. (2012). Insights into ectodomain shedding and processing of protein-tyrosine pseudokinase 7 (PTK7). J. Biol. Chem. *287*, 42009–42018.

Golubkov, V.S., Chekanov, A. V., Cieplak, P., Aleshin, A.E., Chernov, A. V., Zhu, W., Radichev, I.A., Zhang, D., Dong, P.D., and Strongin, A.Y. (2010). The Wnt/planar cell polarity protein-tyrosine kinase-7 (PTK7) is a highly efficient proteolytic target of membrane type-1 matrix metalloproteinase: Implications in cancer and embryogenesis. J. Biol. Chem. *285*, 35740–35749.

Golubkov, V.S., Aleshin, A.E., and Strongin, A.Y. (2011). Potential relation of aberrant proteolysis of human protein tyrosine kinase 7 (PTK7) chuzhoi by membrane type 1 matrix metalloproteinase (MT1-MMP) to congenital defects. J. Biol. Chem. *286*, 20970–20976.

Gong, Y., Gong, Y., Mo, C., Mo, C., Fraser, S.E., and Fraser, S.E. (2004). Planar cell polarity signalling controls cell division orientation during zebra sh gastrulation. Nature *430*, 689–693.

Goodrich, L. V. (2008). The Plane Facts of PCP in the CNS. Neuron *60*, 9–16.

Gouti, M., Tsakiridis, A., Wymeersch, F.J., Huang, Y., Kleinjung, J., Wilson, V., and Briscoe, J. (2014). In vitro generation of neuromesodermal progenitors reveals distinct roles for wnt signalling in the specification of spinal cord and paraxial mesoderm identity. PLoS Biol. *12*.

Gray, R.S., Roszko, I., and Solnica-Krezel, L. (2011). Planar Cell Polarity: Coordinating Morphogenetic Cell Behaviors with Embryonic Polarity. Dev. Cell *21*, 120–133.

Greber, B., Wu, G., Bernemann, C., Joo, J.Y., Han, D.W., Ko, K., Tapia, N., Sabour, D., Sterneckert, J., Tesar, P., et al. (2010). Conserved and Divergent Roles of FGF Signaling in Mouse Epiblast Stem Cells and Human Embryonic Stem Cells. Cell Stem Cell *6*, 215–226.

Greco, T.L., Takada, S., Newhouse, M.M., McMahon, J.A., McMahon, A.P., and Camper, S.A. (1996). Analysis of the vestigial tail mutation demonstrates that Wnt-3a gene dosage regulates mouse axial development. Genes Dev. *10*, 313–324.

Gros, J., Hu, J.K.H., Vinegoni, C., Feruglio, P.F., Weissleder, R., and Tabin, C.J. (2010).

WNT5A/JNK and FGF/MAPK pathways regulate the cellular events shaping the vertebrate limb bud. Curr. Biol. *20*, 1993–2002.

Gubb, D., and Garcia-Bellido, A. (1982). A genetic analysis of the determination of cuticular polarity during development in Drosophila melanogaster. J. Embryol. Exp. Morphol. *68*, 37–57.

Guirao, B., Meunier, A., Mortaud, S., Aguilar, A., Corsi, J.-M., Strehl, L., Hirota, Y., Desoeuvre, A., Boutin, C., Han, Y.-G., et al. (2010). Coupling between hydrodynamic forces and planar cell polarity orients mammalian motile cilia. Nat. Cell Biol. *12*, 341–350.

Guo, G., Yang, J., Nichols, J., Hall, J.S., Eyres, I., Mansfield, W., and Smith, A. (2009). Klf4 reverts developmentally programmed restriction of ground state pluripotency. Development *136*, 1063–1069.

Guo, N., Hawkins, C., and Nathans, J. (2004). Frizzled6 controls hair patterning in mice. Proc. Natl. Acad. Sci. *101*, 9277–9281.

Hadjantonakis, A.-K., Formstone, C.J., and Little, P.F.R. (1998). MCelsr1 is an evolutionarily conserved seven-pass transmembrane receptor and is expressed during mouse embryonic development. Mech. Dev. *78*, 91–95.

Hadjantonakis, A.K., Sheward, W.J., Harmar, A.J., de Galan, L., Hoovers, J.M., and Little, P.F. (1997). Celsr1, a neural-specific gene encoding an unusual seven-pass transmembrane receptor, maps to mouse chromosome 15 and human chromosome 22qter. Genomics *45*, 97–104.

Hamblet, N.S. (2002). Dishevelled 2 is essential for cardiac outflow tract development, somite segmentation and neural tube closure. Development *129*, 5827–5838.

Hayashi, K., and Saitou, M. (2013). Generation of eggs from mouse embryonic stem cells and induced pluripotent stem cells. Nat. Protoc. *8*, 1513–1524.

Hayashi, K., Yonemura, S., Matsui, T., and Tsukita, S. (1999). Immunofluorescence detection of ezrin/radixin/moesin (ERM) proteins with their carboxyl-terminal threonine phosphorylated in cultured cells and tissues. J. Cell Sci. *112 (Pt 8)*, 1149–1158.

Hayashi, K., Ohta, H., Kurimoto, K., Aramaki, S., and Saitou, M. (2011). Reconstitution of the mouse germ cell specification pathway in culture by pluripotent stem cells. Cell *146*,

519–532.

Hayashi, K., Ogushi, S., Kurimoto, K., Shimamoto, S., Ohta, H., and Saitou, M. (2012). Offspring from oocytes derived from in vitro primordial germ cell-like cells in mice. Science *338*, 971–975.

Hayes, M., Naito, M., Daulat, A., Angers, S., and Ciruna, B.G. (2013). Ptk7 promotes non-canonical Wnt/PCP-mediated morphogenesis and inhibits Wnt/β-catenin-dependent cell fate decisions during vertebrate development. Development *140*, 1807–1818.

Hayes, M., Gao, X., Yu, L.X., Paria, N., Henkelman, R.M., Wise, C.A., and Ciruna, B. (2014). ptk7 mutant zebrafish models of congenital and idiopathic scoliosis implicate dysregulated Wnt signalling in disease. Nat. Commun. *5*, 4777.

Heisenberg, C.-P., Tada, M., Rauch, G.-J., Saude, L., Concha, M.L., Geisler, R., Stemple, D.L., Smith, J.C., and Wilson, S.W. (2000). Silberblick / Wnt11 mediates convergent extension movements during zebrafish gastrulation. Nature *405*, 76–81.

Henrique, D., Abranches, E., Verrier, L., and Storey, K.G. (2015). Neuromesodermal progenitors and the making of the spinal cord. Development *142*, 2864–2875.

Ho, H.-Y.H., Susman, M.W., Bikoff, J.B., Ryu, Y.K., Jonas, a. M., Hu, L., Kuruvilla, R., and Greenberg, M.E. (2012). Wnt5a-Ror-Dishevelled signaling constitutes a core developmental pathway that controls tissue morphogenesis. Proc. Natl. Acad. Sci. *109*, 1–8.

Hogan, B., Beddington, R., Costantini, F., and Lacy, E. (1994). Manipulating the mouse embryo, 2nd Edition.

Horan, G.S., Wu, K., Wolgemuth, D.J., and Behringer, R.R. (1994). Homeotic transformation of cervical vertebrae in Hoxa-4 mutant mice. Proc. Natl. Acad. Sci. U. S. A. *91*, 12644–12648.

Hua, Z.L., Chang, H., Wang, Y., Smallwood, P.M., and Nathans, J. (2014). Partial interchangeability of Fz3 and Fz6 in tissue polarity signaling for epithelial orientation and axon growth and guidance. Development *141*, 3944–3954.

Huang, Y., Osorno, R., Tsakiridis, A., and Wilson, V. (2012). In Vivo Differentiation Potential of Epiblast Stem Cells Revealed by Chimeric Embryo Formation. Cell Rep. *2*, 1571–1578.

Huang, Y., Wilkie, R., and Wilson, V. (2015). Methods for Precisely Localized Transfer of Cells or DNA into Early Postimplantation Mouse Embryos. J. Vis. Exp. e53295.

Iacovino, M., Bosnakovski, D., Fey, H., Rux, D., Bajwa, G., Mahen, E., Mitanoska, A., Xu, Z., and Kyba, M. (2011). Inducible cassette exchange: A rapid and efficient system enabling conditional gene expression in embryonic stem and primary cells. Stem Cells *29*, 1580–1587.

Iacovino, M., Roth, M.E., and Kyba, M. (2014). Rapid genetic modification of mouse embryonic stem cells by inducible cassette exchange recombination. Methods Mol. Biol. *1101*, 339–351.

Jenny, A., Darken, R.S., Wilson, P.A., and Mlodzik, M. (2003). Prickle and strabismus form a functional complex to generate a correct axis during planar cell polarity signaling. EMBO J. *22*, 4409–4420.

Jurand, A. (1974). Some aspects of the development of the notochord in mouse embryos. J. Embryol. Exp. Morphol. *32*, 1–33.

Jurberg, A.D., Aires, R., Nóvoa, A., Rowland, J.E., and Mallo, M. (2014). Compartment-dependent activities of Wnt3a/β-catenin signaling during vertebrate axial extension. Dev. Biol. *394*, 253–263.

Kanai-Azuma, M., Kanai, Y., Gad, J.M., Tajima, Y., Taya, C., Kurohmaru, M., Sanai, Y., Yonekawa, H., Yazaki, K., Tam, P.P.L., et al. (2002). Depletion of definitive gut endoderm in Sox17-null mutant mice. Development *129*, 2367–2379.

Kibar, Z., Vogan, K.J., Groulx, N., Justice, M.J., Underhill, D.A., and Gros, P. (2001). Ltap, a mammalian homolog of Drosophila Strabismus/Van Gogh, is altered in the mouse neural tube mutant Loop-tail. Nat. Genet. *28*, 251–255.

Kibar, Z., Bosoi, C.M., Kooistra, M., Salem, S., Finnell, R.H., Marco, P. De, Merello, E., Bassuk, A.G., and Capra, V. (2010). Novel Mutations in VANGL1 in Neural Tube Defects. Hum. Mutat. *30*, 1–13.

Kikuchi, A., Yamamoto, H., Sato, A., and Matsumoto, S. (2012). Wnt5a: Its signalling, functions and implication in diseases. Acta Physiol. *204*, 17–33.

Kim, J.H., Lee, S.R., Li, L.H., Park, H.J., Park, J.H., Lee, K.Y., Kim, M.K., Shin, B.A., and

Choi, S.Y. (2011). High cleavage efficiency of a 2A peptide derived from porcine teschovirus-1 in human cell lines, zebrafish and mice. PLoS One *6*, 1–8.

Kinder, S.J., Tsang, T.E., Quinlan, G.A., Hadjantonakis, A.K., Nagy, A., and Tam, P.P. (1999). The orderly allocation of mesodermal cells to the extraembryonic structures and the anteroposterior axis during gastrulation of the mouse embryo. Development *126*, 4691–4701.

Kinder, S.J., Tsang, T.E., Wakamiya, M., Sasaki, H., Behringer, R.R., Nagy, a, and Tam, P.P. (2001). The organizer of the mouse gastrula is composed of a dynamic population of progenitor cells for the axial mesoderm. Development *128*, 3623–3634.

Kispert, A., Vainio, S., Shen, L., Rowitch, D.H., and McMahon, A.P. (1996). Proteoglycans are required for maintenance of Wnt-11 expression in the ureter tips. Development *122*, 3627–3637.

Koch, F., Scholze, M., Wittler, L., Schifferl, D., Sudheer, S., Grote, P., Timmermann, B., Macura, K., and Herrmann, B.G. (2017). Antagonistic Activities of Sox2 and Brachyury Control the Fate Choice of Neuro-Mesodermal Progenitors. Dev. Cell 1–13.

Kojima, Y., Kaufman-Francis, K., Studdert, J.B., Steiner, K.A., Power, M.D., Loebel, D.A.F., Jones, V., Hor, A., De Alencastro, G., Logan, G.J., et al. (2014a). The transcriptional and functional properties of mouse epiblast stem cells resemble the anterior primitive streak. Cell Stem Cell *14*, 107–120.

Kojima, Y., Tam, O.H., and Tam, P.P.L. (2014b). Timing of developmental events in the early mouse embryo. Semin. Cell Dev. Biol. *34*, 65–75.

Komiya, Y., and Habas, R. (2008). Wnt signal transduction pathways. Organogenesis *4*, 68–75.

Kostic, D., and Capecchi, M.R. (1994). Targeted disruptions of the murine Hoxa-4 and Hoxa-6 genes result in homeotic transformation of components of the vertebral column. Mech. Dev. *46*, 231–247.

Kroiher, M., Miller, M.A., and Steele, R.E. (2001). Deceiving appearances: Signaling by “dead” and “fractured” receptor protein-tyrosine kinases. BioEssays *23*, 69–76.

Lawrence, P.A., Struhl, G., and Casal, J. (2007). Planar cell polarity: one or two pathways? Nat. Rev. Genet. *8*, 555–563.

Lawrence, P.A., Struhl, G., and Casal, J. (2008). Planar Cell Polarity: A Bridge Too Far? Curr. Biol. *18*, 959–961.

Lawson, K.A. (1999). Fate mapping the mouse embryo. Int. J. Dev. Biol. *775*, 773–775.

Lawson, K.A., Meneses, J.J., and Pedersen, R.A. (1991). Clonal analysis of epiblast fate during germ layer formation in the mouse embryo. Development *113*, 891–911.

Lee, J., Andreeva, A., Sipe, C.W., Liu, L., Cheng, A., and Lu, X. (2012). PTK7 regulates myosin II activity to orient planar polarity in the mammalian auditory epithelium. Curr. Biol. *22*, 956–966.

Lei, Y.-P., Zhang, T., Li, H., Wu, B.-L., Jin, L., and Wang, H.-Y. (2010). VANGL2 mutations in human cranial neural-tube defects. N. Engl. J. Med. *362*, 2232–2235.

Lijam, N., Paylor, R., McDonald, M.P., Crawley, J.N., Deng, C.X., Herrup, K., Stevens, K.E., Maccaferri, G., McBain, C.J., Sussman, D.J., et al. (1997). Social interaction and sensorimotor gating abnormalities in mice lacking Dvl1. Cell *90*, 895–905.

Liu, C., Lin, C., Gao, C., May-Simera, H., Swaroop, A., and Li, T. (2014). Null and hypomorph Prickle1 alleles in mice phenocopy human Robinow syndrome and disrupt signaling downstream of Wnt5a. Biol. Open *3*, 861–870.

Liu, P., Wakamiya, M., Shea, M.J., Albrecht, U., Behringer, R.R., and Bradley, A. (1999). Requirement for Wnt3 in vertebrate axis formation. Nat. Genet. *22*, 361–365.

Logan, C.Y., and Nusse, R. (2004). the Wnt Signaling Pathway in Development and Disease. Annu. Rev. Cell Dev. Biol. *20*, 781–810.

Lu, C.C., Brennan, J., and Robertson, E.J. (2001). From fertilization to gastrulation: axis formation in the mouse embryo. Curr. Opin. Genet. Dev. *11*, 384–392.

Lu, X., Borchers, A.G.M., Jolicoeur, C., Rayburn, H., Baker, J.C., and Tessier-Lavigne, M. (2004). PTK7 / CCK-4 is a novel regulator of planar cell polarity in vertebrates. Nature *430*, 93–98.

Majumdar, A., Vainio, S., Kispert, A., McMahon, J., and McMahon, A.P. (2003). Wnt11 and Ret/Gdnf pathways cooperate in regulating ureteric branching during metanephric kidney development. Development *130*, 3175–3185.

Mao, Y., Mulvaney, J., Zakaria, S., Yu, T., Morgan, K.M., Allen, S., Basson, M.A., Francis-West, P., and Irvine, K.D. (2011). Characterization of a Dchs1 mutant mouse reveals requirements for Dchs1-Fat4 signaling during mammalian development. Development *138*, 947–957.

Marks, H., Kalkan, T., Menafra, R., Denissov, S., Jones, K., Hofemeister, H., Nichols, J., Kranz, A., Francis Stewart, A., Smith, A., et al. (2012). The transcriptional and epigenomic foundations of ground state pluripotency. Cell *149*, 590–604.

Martin, G.R. (1981). Isolation of a pluripotent cell line from early mouse embryos cultured in medium conditioned by teratocarcinoma stem cells. Proc. Natl. Acad. Sci. U. S. A. *78*, 7634–7638.

Martin, B.L., and Kimelman, D. (2012). Canonical Wnt Signaling Dynamically Controls Multiple Stem Cell Fate Decisions during Vertebrate Body Formation. Dev. Cell *22*, 223–232.

Martin, P., and Cockroft, D.L. (2008). Culture of postimplantation mouse embryos. Methods Mol. Biol. *461*, 7–22.

Martinez, S., Scerbo, P., Giordano, M., Daulat, A.M., Lhoumeau, A.C., Thomé, V., Kodjabachian, L., and Borg, J.P. (2015). The PTK7 and ROR2 protein receptors interact in the vertebrate WNT/Planar cell polarity (PCP) pathway. J. Biol. Chem. *290*, 30562–30572.

Mathis, L., and Nicolas, J.F. (2000). Different clonal dispersion in the rostral and caudal mouse central nervous system. Development *127*, 1277–1290.

Matsuda, T., Nomi, M., Ikeya, M., Kani, S., Oishi, I., Terashima, T., Takada, S., and Minami, Y. (2001). Expression of the receptor tyrosine kinase genes, Ror1 and Ror2, during mouse development. Mech. Dev. *105*, 153–156.

McGrew, M.J., Sherman, A., Lillico, S.G., Ellard, F.M., Radcliffe, P.A., Gilhooley, H.J., Mitrophanous, K.A., Cambray, N., Wilson, V., and Sang, H. (2008). Localised axial progenitor cell populations in the avian tail bud are not committed to a posterior Hox identity. Development *135*, 2289–2299.

Mikels, A.J., and Nusse, R. (2006). Purified Wnt5a protein activates or inhibits β-catenin-TCF signaling depending on receptor context. PLoS Biol. *4*, 570–582.

Mlodzik, M. (2002). Planar cell polarization: Do the same mechanisms regulate Drosophila tissue polarity and vertebrate gastrulation? Trends Genet. *18*, 564–571.

Mlodzik, M. (2016). The Dishevelled Protein Family (Elsevier Inc.).

Montcouquiol, M. (2006). Asymmetric Localization of Vangl2 and Fz3 Indicate Novel Mechanisms for Planar Cell Polarity in Mammals. J. Neurosci. *26*, 5265–5275.

Montcouquiol, M., Rachel, R.A., Lanford, P.J., Copeland, N.G., Jenkins, N.A., and Kelley, M.W. (2003). Identification of Vangl2 and Scrb1 as planar polarity genes in mammals. Nature *423*, 173–177.

Morgani, S., Nichols, J., and Hadjantonakis, A.-K. (2017). The many faces of Pluripotency: in vitro adaptations of a continuum of in vivo states. BMC Dev. Biol. *17*, 7.

Mossie, K., Jallal, B., Alves, F., Sures, I., Plowman, G.D., and Ullrich, A. (1995). Colon carcinoma kinase-4 defines a new subclass of the receptor tyrosine kinase family. Oncogene *11*, 2179–2184.

Murdoch, J.N., Doudney, K., Paternotte, C., Copp, A.J., and Stanier, P. (2001). Severe neural tube defects in the loop-tail mouse result from mutation of Lpp1, a novel gene involved in floor plate specification. Hum. Mol. Genet. *10*, 2593–2601.

Murdoch, J.N., Damrau, C., Paudyal, A., Bogani, D., Wells, S., Greene, N.D.E., Stanier, P., and Copp, A.J. (2014). Interactions between planar cell polarity genes cause diverse neural tube defects. Dis. Model. Mech. *3*, 1153–1163.

Naiche, L. a, Holder, N., and Lewandoski, M. (2011). FGF4 and FGF8 comprise the wavefront activity that controls somitogenesis. Proc. Natl. Acad. Sci. *108*, 4018–4023.

Nakamura, N., Rabouille, C., Watson, R., Nilsson, T., Hui, N., Slusarewicz, P., Kreis, T.E., and Warren, G. (1995). Characterization of a cis-Golgi matrix protein, GM130. J. Cell Biol. *131*, 1715–1726.

Nakaya, Y., and Sheng, G. (2008). Epithelial to mesenchymal transition during gastrulation: An embryological view. Dev. Growth Differ. *50*, 755–766.

Nakaya, Y., and Sheng, G. (2009). An amicable separation: Chick's way of doing EMT. Cell Adhes. Migr. *3*, 160–163.

Nichols, J., and Smith, A. (2009). Naive and Primed Pluripotent States. Cell Stem Cell *4*, 487–492.

Nicolas, J.F., Mathis, L., Bonnerot, C., and Saurin, W. (1996). Evidence in the mouse for self-renewing stem cells in the formation of a segmented longitudinal structure, the myotome. Development *122*, 2933–2946.

Nikolopoulou, E., Galea, G.L., Rolo, A., Greene, N.D.E., and Copp, A.J. (2017). Neural tube closure: cellular, molecular and biomechanical mechanisms. Development *144*, 552–566.

Nishita, M., Itsukushima, S., Nomachi, A., Endo, M., Wang, Z., Inaba, D., Qiao, S., Takada, S., Kikuchi, A., and Minami, Y. (2010). Ror2/Frizzled complex mediates Wnt5a-induced AP-1 activation by regulating Dishevelled polymerization. Mol. Cell. Biol. *30*, 3610–3619.

Niwa, H., Yamamura, K., and Miyazaki, J. (1991). Efficient selection for high-expression transfectants with a novel eukaryotic vector. Gene *108*, 193–199.

Noctor, S.C., Flint, A.C., Weissman, T.A., Dammerman, R.S., and Kriegstein, A.R. (2001). Neurons derived from radial glial cells establish radial units in neocortex. Nature *409*, 714–720.

Nomachi, A., Nishita, M., Inaba, D., Enomoto, M., Hamasaki, M., and Minami, Y. (2008). Receptor tyrosine kinase Ror2 mediates Wnt5a-induced polarized cell migration by activating c-Jun N-terminal kinase via actin-binding protein filamin A. J. Biol. Chem. *283*, 27973–27981.

Nomi, M., Oishi, I., Kani, S., Suzuki, H., Matsuda, T., Yoda, A., Kitamura, M., Itoh, K., Takeuchi, S., Takeda, K., et al. (2001). Loss of mRor1 enhances the heart and skeletal abnormalities in mRor2-deficient mice: redundant and pleiotropic functions of mRor1 and mRor2 receptor tyrosine kinases. Mol. Cell. Biol. *21*, 8329–8335.

Nowotschin, S., Ferrer-Vaquer, A., Concepcion, D., Papaioannou, V.E., and Hadjantonakis, A.K. (2012). Interaction of Wnt3a, Msgn1 and Tbx6 in neural versus paraxial mesoderm lineage commitment and paraxial mesoderm differentiation in the mouse embryo. Dev. Biol. *367*, 1–14.

O'Toole, E., Greenan, G., Lange, K.I., Srayko, M., and Müller-Reichert, T. (2012). The role of γ-tubulin in centrosomal microtubule organization. PLoS One *7*.

Oishi, I., Suzuki, H., Onishi, N., Takada, R., Kani, S., Ohkawara, B., Koshida, I., Suzuki, K., Yamada, G., Schwabe, G.C., et al. (2003). The receptor tyrosine kinase Ror2 is involved in non-canonical Wnt5a/JNK signalling pathway. Genes to Cells *8*, 645–654.

Okabe, M., Ikawa, M., Kominami, K., Nakanishi, T., and Nishimune, Y. (1997). "Green mice" as a source of ubiquitous green cells. FEBS Lett. *407*, 313–319.

Okuda, H., Miyata, S., Mori, Y., and Tohyama, M. (2007). Mouse Prickle1 and Prickle2 are expressed in postmitotic neurons and promote neurite outgrowth. FEBS Lett. *581*, 4754–4760.

Olivera-Martinez, I., Harada, H., Halley, P.A., and Storey, K.G. (2012). Loss of FGF-Dependent Mesoderm Identity and Rise of Endogenous Retinoid Signalling Determine Cessation of Body Axis Elongation. PLoS Biol. *10*.

Osorno, R., Tsakiridis, A., Wong, F., Cambray, N., Economou, C., Wilkie, R., Blin, G., Scotting, P.J., Chambers, I., and Wilson, V. (2012). The developmental dismantling of pluripotency is reversed by ectopic Oct4 expression. Development *139*, 2288–2298.

Paudyal, A., Damrau, C., Patterson, V.L., Ermakov, A., Formstone, C., Lalanne, Z., Wells, S., Lu, X., Norris, D.P., Dean, C.H., et al. (2010). The novel mouse mutant, chuzhoi, has disruption of Ptk7 protein and exhibits defects in neural tube, heart and lung development and abnormal planar cell polarity in the ear. BMC Dev. Biol. *10*, 87.

Peradziryi, H., Kaplan, N. a, Podleschny, M., Liu, X., Wehner, P., Borchers, A., and Tolwinski, N.S. (2011). PTK7/Otk interacts with Wnts and inhibits canonical Wnt signalling. EMBO J. *30*, 3729–3740.

Peradziryi, H., Tolwinski, N.S., and Borchers, A. (2012). The many roles of PTK7: A versatile regulator of cell-cell communication. Arch. Biochem. Biophys. *524*, 71–76.

Pevny, L.H., Sockanathan, S., Placzek, M., and Lovell-Badge, R. (1998). A role for SOX1 in neural determination. Development *125*, 1967–1978.

Podleschny, M., Grund, A., Berger, H., Rollwitz, E., and Borchers, A. (2015). A PTK7/Ror2 Co-Receptor Complex Affects Xenopus Neural Crest Migration. PLoS One *10*, e0145169.

Pop, S., Dufour, A.C., Le Garrec, J.F., Ragni, C. V., Cimper, C., Meilhac, S.M., and Olivo-Marin, J.C. (2013). Extracting 3D cell parameters from dense tissue environments:

Application to the development of the mouse heart. Bioinformatics *29*, 772–779.

Preibisch, S., Saalfeld, S., and Tomancak, P. (2009). Globally optimal stitching of tiled 3D microscopic image acquisitions. Bioinformatics *25*, 1463–1465.

Pryor, S.E., Massa, V., Savery, D., Andre, P., Yang, Y., Greene, N.D.E., and Copp, A.J. (2014). Vangl-dependent planar cell polarity signalling is not required for neural crest migration in mammals. Development *141*, 3153–3158.

Puppo, F., Thomé, V., Lhoumeau, A.-C., Cibois, M., Gangar, A., Lembo, F., Belotti, E., Marchetto, S., Lécine, P., Prébet, T., et al. (2011). Protein tyrosine kinase 7 has a conserved role in Wnt/β-catenin canonical signalling. EMBO Rep. *12*, 43–49.

Qian, D., Jones, C., Rzadzinska, A., Mark, S., Zhang, X., Steel, K.P., Dai, X., and Chen, P. (2007). Wnt5a functions in planar cell polarity regulation in mice. Dev. Biol. *306*, 121–133.

Quesada-Hernández, E., Caneparo, L., Schneider, S., Winkler, S., Liebling, M., Fraser, S.E., and Heisenberg, C.P. (2010). Stereotypical cell division orientation controls neural rod midline formation in zebrafish. Curr. Biol. *20*, 1966–1972.

Rashbass, P., Wilson, V., Rosen, B., and Beddington, R.S.P. (1994). Alterations in gene expression during mesoderm formation and axial patterning in Brachyury (T) embryos. Int. J. Dev. Biol. *38*, 35–44.

Rivera-Perez, J.A., and Magnuson, T. (2005). Primitive streak formation in mice is preceded by localized activation of Brachyury and Wnt3. *288*, 363–371.

Roszko, I., Sawada, A., and Solnica-Krezel, L. (2009). Regulation of convergence and extension movements during vertebrate gastrulation by the Wnt/PCP pathway. Semin. Cell Dev. Biol. *20*, 986–997.

Rousset, R., Mack, J.A., Wharton, K.A., Axelrod, J.D., Cadigan, K.M., Fish, M.P., Nusse, R., and Scott, M.P. (2001). naked cuticle targets dishevelled to antagonize Wnt signal transduction. Genes Dev. 658–671.

Ryan, M.D., King, A.M.Q., and Thomas, G.P. (1991). Cleavage of foot-and-mouth disease virus polyprotein is mediated by residues located within a 19 amino acid sequence. J. Gen. Virol. *72*, 2727–2732.

Saburi, S., Hester, I., Fischer, E., Pontoglio, M., Eremina, V., Gessler, M., Quaggin, S.E., Harrison, R., Mount, R., and McNeill, H. (2008). Loss of Fat4 disrupts PCP signaling and oriented cell division and leads to cystic kidney disease. Nat. Genet. *40*, 1010–1015.

Saburi, S., Hester, I., Goodrich, L., and McNeill, H. (2012). Functional interactions between Fat family cadherins in tissue morphogenesis and planar polarity. Development *139*, 1806–1820.

Saga, Y., Hata, N., Kobayashi, S., Magnuson, T., Seldin, M.F., and Taketo, M.M. (1996). MesP1: a novel basic helix-loop-helix protein expressed in the nascent mesodermal cells during mouse gastrulation. Development *122*, 2769–2778.

Saiz, N., and Plusa, B. (2013). Early cell fate decisions in the mouse embryo. Reproduction *145*, R65-80.

Sambrook, J., and W Russell, D. (2001). Molecular Cloning: A Laboratory Manual. Cold Spring Harb. Lab. Press. Cold Spring Harb. NY 999.

Sarkar, A., and Hochedlinger, K. (2013). The Sox family of transcription factors: Versatile regulators of stem and progenitor cell fate. Cell Stem Cell *12*, 15–30.

Sasaki, H., and Hogan, B.L. (1993). Differential expression of multiple fork head related genes during gastrulation and axial pattern formation in the mouse embryo. Development *118*, 47–59.

Savory, J.G. a, Bouchard, N., Pierre, V., Rijli, F.M., De Repentigny, Y., Kothary, R., and Lohnes, D. (2009). Cdx2 regulation of posterior development through non-Hox targets. Development *136*, 4099–4110.

Schepers, G.E., Teasdale, R.D., and Koopman, P. (2002). Twenty Pairs of Sox. Dev. Cell *3*, 167–170.

Schubert, F.R., Fainsod, A., Gruenbaum, Y., and Gruss, P. (1995). Expression of the novel murine homeobox gene Sax-1 in the developing nervous system. Mech. Dev. *51*, 99–114.

Schwabe, G.C., Trepczik, B., Süring, K., Brieske, N., Tucker, A.S., Sharpe, P.T., Minami, Y., and Mundlos, S. (2004). Ror2 Knockout Mouse as a Model for the Developmental Pathology of Autosomal Recessive Robinow Syndrome. Dev. Dyn. *229*, 400–410.

Seifert, J.R.K., and Mlodzik, M. (2007). Frizzled/PCP signalling: a conserved mechanism regulating cell polarity and directed motility. Nat. Rev. Genet. *8*, 126–138.

Selleck, M.A.J., and Stern, C.D. (1991). Fate mapping and cell lineage analysis of Hensen's node in the chick embryo. Development *112*, 615–626.

Sepich, D.S., Usmani, M., Pawlicki, S., and Solnica-Krezel, L. (2011). Wnt/PCP signaling controls intracellular position of MTOCs during gastrulation convergence and extension movements. Development *138*, 543–552.

She, Z.Y., and Yang, W.X. (2015). SOX family transcription factors involved in diverse cellular events during development. Eur. J. Cell Biol. *94*, 547–563.

Shi, D., Komatsu, K., Hirao, M., Toyooka, Y., Koyama, H., Tissir, F., Goffinet, A.M., Uemura, T., and Fujimori, T. (2014). Celsr1 is required for the generation of polarity at multiple levels of the mouse oviduct. Development *141*, 4558–4568.

Shi, S.-R., Shi, Y., and Taylor, C.R. (2011). Antigen Retrieval Immunohistochemistry. J. Histochem. Cytochem. *59*, 13–32.

Shima, Y., Copeland, N.G., Gilbert, D.J., Jenkins, N.A., Chisaka, O., Takeichi, M., and Uemura, T. (2002). Differential expression of the seven-pass transmembrane cadherin genes Celsr1-3 and distribution of the Celsr2 protein during mouse development. Dev. Dyn. *223*, 321–332.

Shin, W.S., Maeng, Y.S., Jung, J.W., Min, J.K., Kwon, Y.G., and Lee, S.T. (2008). Soluble PTK7 inhibits tube formation, migration, and invasion of endothelial cells and angiogenesis. Biochem. Biophys. Res. Commun. *371*, 793–798.

Shnitsar, I., and Borchers, A. (2008). PTK7 recruits dsh to regulate neural crest migration. Development *135*, 4015–4024.

Shum, A.S.W., Poon, L.L.M., Tang, W.W.T., Koide, T., Chan, B.W.H., Leung, Y.C.G., Shiroishi, T., and Copp, A.J. (1999). Retinoic acid induces down-regulation of Wnt-3a, apoptosis and diversion of tail bud cells to a neural fate in the mouse embryo. Mech. Dev. *84*, 17–30.

Sienknecht, U.J., Anderson, B.K., Parodi, R.M., Fantetti, K.N., and Fekete, D.M. (2011). Non-cell-autonomous planar cell polarity propagation in the auditory sensory epithelium of

vertebrates. Dev. Biol. *352*, 27–39.

Silva, J., and Smith, A. (2008). Capturing Pluripotency. Cell *132*, 532–536.

Silva, J., Barrandon, O., Nichols, J., Kawaguchi, J., Theunissen, T.W., and Smith, A. (2008). Promotion of reprogramming to ground state pluripotency by signal inhibition. PLoS Biol. *6*, 2237–2247.

Smith, R., and McLaren, A. (1977). Factors affecting the time of formation of the mouse blastocoele. J. Embryol. Exp. Morphol. *41*, 79–92.

Smith, A.G., Heath, J.K., Donaldson, D.D., Wong, G.G., Moreau, J., Stahl, M., and Rogers, D. (1988). Inhibition of pluripotential embryonic stem cell differentiation by purified polypeptides. Nature *336*, 688–690.

Smith, J.L., Gesteland, K.M., and Schoenwolf, G.C. (1994). Prospective fate map of the mouse primitive streak at 7.5 days of gestation. Dev. Dyn. *201*, 279–289.

Song, H., Hu, J., Chen, W., Elliott, G., Andre, P., Gao, B., and Yang, Y. (2010). Planar cell polarity breaks bilateral symmetry by controlling ciliary positioning. Nature *466*, 378–382.

Stower, M.J., and Srinivas, S. (2014). Heading forwards: anterior visceral endoderm migration in patterning the mouse embryo. Philos. Trans. R. Soc. B Biol. Sci. *369*, 20130546–20130546.

Struhl, G., Casal, J., and Lawrence, P. a (2012). Dissecting the molecular bridges that mediate the function of Frizzled in planar cell polarity. Development *139*, 3665–3674.

Strutt, D., and Strutt, H. (2007). Differential activities of the core planar polarity proteins during Drosophila wing patterning. Dev. Biol. *302*, 181–194.

Strutt, H., and Strutt, D. (2008). Differential Stability of Flamingo Protein Complexes Underlies the Establishment of Planar Polarity. Curr. Biol. *18*, 1555–1564.

Strutt, H., and Strutt, D. (2009). Asymmetric localisation of planar polarity proteins: Mechanisms and consequences. Semin. Cell Dev. Biol. *20*, 957–963.

Sulik, K., Dehart, D.B., Inagaki, T., Carson, J.L., Vrablic, T., Gesteland, K., and Schoenwolf, G.C. (1994). Morphogenesis of the murine node and notochordal plate. Dev. Dyn. *201*, 260–278.

Sun, X., Meyers, E.N., Lewandoski, M., and Martin, G.R. (1999). Targeted disruption of Fgf8 causes failure of cell migration in the gastrulating mouse embryo. Genes Dev. *1*, 1834–1846.

Tada, M., and Smith, J.C. (2000). Xwnt11 is a target of Xenopus Brachyury: regulation of gastrulation movements via Dishevelled, but not through the canonical Wnt pathway. Development *127*, 2227–2238.

Takada, S., Stark, K.L., Shea, M.J., Vassileva, G., McMahon, J.A., and McMahon, A.P. (1994a). Wnt-3a regulates somites and tailbud formation in the mouse embryo. Genes Dev. *8*, 174–189.

Takada, S., Stark, K.L., Shea, M.J., Vassileva, G., McMahon, J.A., and McMahon, A.P. (1994b). Wnt-3a regulates somite and tailbud formation in the mouse embryo. Genes Dev. *8*, 174–189.

Takemoto, T., Uchikawa, M., Kamachi, Y., and Kondoh, H. (2005). Convergence of Wnt and FGF signals in the genesis of posterior neural plate through activation of the Sox2 enhancer N-1. Development *133*, 297–306.

Takeuchi, S., Takeda, K., Oishi, I., Nomi, M., Ikeya, M., Itoh, K., Tamura, S., Ueda, T., Hatta, T., Otani, H., et al. (2000). Mouse Ror2 receptor tyrosine kinase is required for the heart development and limb formation. Genes to Cells *5*, 71–78.

Tam, P.P.L., and Behringer, R.R. (1997). Mouse gastrulation: The formation of a mammalian body plan. Mech. Dev. *68*, 3–25.

Tao, H., Inoue, K. ichi, Kiyonari, H., Bassuk, A.G., Axelrod, J.D., Sasaki, H., Aizawa, S., and Ueno, N. (2012). Nuclear localization of Prickle2 is required to establish cell polarity during early mouse embryogenesis. Dev. Biol. *364*, 138–148.

Tarkowski, A.K., and Wróblewska, J. (1967). Development of blastomeres of mouse eggs isolated at the 4- and 8-cell stage. J. Embryol. Exp. Morphol. *18*, 155–180.

Tatin, F., Taddei, A., Weston, A., Fuchs, E., Devenport, D., Tissir, F., and Makinen, T. (2013). Planar cell polarity protein Celsr1 regulates endothelial adherens junctions and directed cell rearrangements during valve morphogenesis. Dev. Cell *26*, 31–44.

Tesar, P.J., Chenoweth, J.G., Brook, F.A., Davies, T.J., Evans, E.P., Mack, D.L., Gardner,

R.L., and Mckay, R.D.G. (2007). New cell lines from mouse epiblast share defining features with human embryonic stem cells. Nature *448*, 2–8.

Thomas, P., and Beddington, R. (1996). Anterior primitive endoderm may be responsible for patterning the anterior neural plate in the mouse embryo. Curr. Biol. *6*, 1487–1496.

Tissir, F., and Goffinet, A.M. (2006). Expression of planar cell polarity genes during development of the mouse CNS. Eur. J. Neurosci. *23*, 597–607.

Tissir, F., Qu, Y., Montcouquiol, M., Zhou, L., Komatsu, K., Shi, D., Fujimori, T., Labeau, J., Tyteca, D., Courtoy, P., et al. (2010). Lack of cadherins Celsr2 and Celsr3 impairs ependymal ciliogenesis, leading to fatal hydrocephalus. Nat. Neurosci. *13*, 700–707.

Topol, L., Jiang, X., Choi, H., Garrett-Beal, L., Carolan, P.J., and Yang, Y. (2003). Wnt-5a inhibits the canonical Wnt pathway by promoting GSK-3-independent β-catenin degradation. J. Cell Biol. *162*, 899–908.

Torban, E., Wang, H.J., Groulx, N., and Gros, P. (2004). Independent mutations in mouse Vangl2 that cause neural tube defects in Looptail mice impair interaction with members of the Dishevelled family. J. Biol. Chem. *279*, 52703–52713.

Torban, E., Wang, H.J., Patenaude, A.M., Riccomagno, M., Daniels, E., Epstein, D., and Gros, P. (2007). Tissue, cellular and sub-cellular localization of the Vangl2 protein during embryonic development: Effect of the Lp mutation. Gene Expr. Patterns *7*, 346–354.

Torban, E., Patenaude, A.-M., Leclerc, S., Rakowiecki, S., Gauthier, S., Andelfinger, G., Epstein, D.J., and Gros, P. (2008). Genetic interaction between members of the Vangl family causes neural tube defects in mice. Proc. Natl. Acad. Sci. *105*, 3449–3454.

Tree, D.R.P., Shulman, J.M., Scott, M.P., Gubb, D., and Axelrod, J.D. (2002). Prickle Mediates Feedback Amplification to Generate Asymmetric Planar Cell Polarity Signaling. Cell *109*, 371–381.

Tsakiridis, A., and Wilson, V. (2015). Assessing the bipotency of in vitro-derived neuromesodermal progenitors. F1000Research *4*, 100.

Tsakiridis, A., Huang, Y., Blin, G., Skylaki, S., Wymeersch, F., Osorno, R.R., Economou, C., Karagianni, E., Zhao, S., Lowell, S., et al. (2014). Distinct Wnt-driven primitive streak-like populations reflect in vivo lineage precursors. Development *141*, 1209–1221.

Turco, M.Y., Furia, L., Dietze, A., Diaz, L.F., Ronzoni, S., Sciullo, A., Simeone, A., Constam, D., Faretta, M., and Lanfrancone, L. (2012). Cellular heterogeneity during embryonic stem cell differentiation to epiblast stem cells is revealed by the ShcD/RaLP adaptor protein. Stem Cells *30*, 2423–2436.

Turner, D. a, Hayward, P.C., Baillie-Johnson, P., Rué, P., Broome, R., Faunes, F., and Martinez Arias, A. (2014). Wnt/β-catenin and FGF signalling direct the specification and maintenance of a neuromesodermal axial progenitor in ensembles of mouse embryonic stem cells. Development *141*, 4243–4253.

Tzouanacou, E., Wegener, A., Wymeersch, F.J., Wilson, V., and Nicolas, J.F. (2009). Redefining the Progression of Lineage Segregations during Mammalian Embryogenesis by Clonal Analysis. Dev. Cell *17*, 365–376.

Usui, T., Shima, Y., Shimada, Y., Hirano, S., Burgess, R.W., Schwarz, T.L., Takeichi, M., and Uemura, T. (1999). Flamingo, a seven-pass transmembrane cadherin, regulates planar cell polarity under the control of Frizzled. Cell *98*, 585–595.

vandenBerg, A.L., and Sassoon, D.A. (2009). Non-canonical Wnt signaling regulates cell polarity in female reproductive tract development via van gogh-like 2. Development *136*, 1559–1570.

Veeman, M.T., Axelrod, J.D., and Moon, R.T. (2003). A second canon: Functions and mechanisms of β-catenin-independent Wnt signaling. Dev. Cell *5*, 367–377.

Verhey van Wijk, N., Witte, F., Feike, A.C., Schambony, A., Birchmeier, W., Mundlos, S., and Stricker, S. (2009). The LIM domain protein Wtip interacts with the receptor tyrosine kinase Ror2 and inhibits canonical Wnt signalling. Biochem. Biophys. Res. Commun. *390*, 211–216.

Wallingford, J.B. (2012). Planar Cell Polarity and the Developmental Control of Cell Behavior in Vertebrate Embryos. Annu. Rev. Cell Dev. Biol. *28*, 627–653.

Wallingford, J.B., and Habas, R. (2005a). The developmental biology of Dishevelled: an enigmatic protein governingcell fate and cell polarity. Development *132*, 4421–4436.

Wallingford, J.B., and Habas, R. (2005b). The developmental biology of Dishevelled: an enigmatic protein governing cell fate and cell polarity. Development *132*, 4421–4436.

Wang, J., Mark, S., Zhang, X., Qian, D., Yoo, S.-J., Radde-Gallwitz, K., Zhang, Y., Lin, X., Collazo, A., Wynshaw-Boris, A., et al. (2005). Regulation of polarized extension and planar cell polarity in the cochlea by the vertebrate PCP pathway. Nat. Genet. *37*, 980–985.

Wang, M., De Marco, P., Merello, E., Drapeau, P., Capra, V., and Kibar, Z. (2015). Role of the planar cell polarity gene Protein tyrosine kinase 7 in neural tube defects in humans. Birth Defects Res. Part A - Clin. Mol. Teratol. *103*, 1021–1027.

Wang, Y., Guo, N., and Nathans, J. (2006). The Role of Frizzled3 and Frizzled6 in Neural Tube Closure and in the Planar Polarity of Inner-Ear Sensory Hair Cells. J. Neurosci. *26*, 2147–2156.

Wang, Y., Chang, H., Rattner, A., and Nathans, J. (2016). Frizzled Receptors in Development and Disease (Elsevier Inc.).

Wehner, P., Shnitsar, I., Urlaub, H., and Borchers, A. (2011). RACK1 is a novel interaction partner of PTK7 that is required for neural tube closure. Development *138*, 1321–1327.

Wharton, K. a, Zimmermann, G., Rousset, R., and Scott, M.P. (2001). Vertebrate proteins related to Drosophila Naked Cuticle bind Dishevelled and antagonize Wnt signaling. Dev. Biol. *234*, 93–106.

Wilkinson, D.G., Bhatt, S., and Herrmann, B.G. (1990). Expression pattern of the mouse T gene and its role in mesoderm formation. Nature *343*, 657–659.

Williams, B.B., Cantrell, V. a., Mundell, N. a., Bennett, a. C., Quick, R.E., and Jessen, J.R. (2012). VANGL2 regulates membrane trafficking of MMP14 to control cell polarity and migration. J. Cell Sci. *125*, 2141–2147.

Williams, M., Yen, W., Lu, X., and Sutherland, A. (2014). Distinct apical and basolateral mechanisms drive planar cell polarity-dependent convergent extension of the mouse neural plate. Dev. Cell *29*, 34–46.

Wilson, V., and Beddington, R. (1997). Expression of T protein in the primitive streak is necessary and sufficient for posterior mesoderm movement and somite differentiation. Dev. Biol. *192*, 45–58.

Wilson, V., and Beddington, R.S.P. (1996). Cell fate and morphogenetic movement in the late mouse primitive streak. Mech. Dev. *55*, 79–89.

Wilson, V., Manson, L., Skarnes, W.C., and Beddington, R.S. (1995). The T gene is necessary for normal mesodermal morphogenetic cell movements during gastrulation. Development *121*, 877–886.

Wilson, V., Olivera-Martinez, I., and Storey, K.G. (2009). Stem cells, signals and vertebrate body axis extension. Development *136*, 2133–2133.

Winnier G, Blessing M, Labosky P, H.B. (1995). Bone morphogenetic protein-4 Is required for mesoderm formation and patterning in the mouse. Genes Dev. 2105–2116.

Wong, H.C., Bourdelas, A., Krauss, A., Lee, H.J., Shao, Y., Wu, D., Mlodzik, M., Shi, D.L., and Zheng, J. (2003). Direct binding of the PDZ domain of Dishevelled to a conserved internal sequence in the C-terminal region of Frizzled. Mol. Cell *12*, 1251–1260.

Wood, H.B., and Episkopou, V. (1999). Comparative expression of the mouse Sox1, Sox2 and Sox3 genes from pre-gastrulation to early somite stages. Mech. Dev. *86*, 197–201.

Wu, J., and Mlodzik, M. (2008). The Frizzled Extracellular Domain Is a Ligand for Van Gogh/Stbm during Nonautonomous Planar Cell Polarity Signaling. Dev. Cell *15*, 462–469.

Wu, J., and Mlodzik, M. (2009). A quest for the mechanism regulating global planar cell polarity of tissues. Trends Cell Biol. *19*, 295–305.

Wu, J., Klein, T.J., and Mlodzik, M. (2004). Subcellular localization of frizzled receptors, mediated by their cytoplasmic tails, regulates signaling pathway specificity. PLoS Biol. *2*, 1004–1014.

Wymeersch, F.J., Huang, Y., Blin, G., Cambray, N., Wilkie, R., Wong, F.C.K., and Wilson, V. (2016). Position-dependent plasticity of distinct progenitor types in the primitive streak. Elife *5*, 1–28.

Xu, B., Washington, A.M., Domeniconi, R.F., Ferreira Souza, A.C., Lu, X., Sutherland, A., and Hinton, B.T. (2016). Protein tyrosine kinase 7 is essential for tubular morphogenesis of the Wolffian duct. Dev. Biol. *412*, 219–233.

Yamada, M., Udagawa, J., Matsumoto, A., Hashimoto, R., Hatta, T., Nishita, M., Minami, Y., and Otani, H. (2010). Ror2 is required for midgut elongation during mouse development. Dev. Dyn. *239*, 941–953.

Yamaguchi, T.P., Harpal, K., Henkemeyer, M., Rossant, J., Hospital, M.S., and Mg, C. (1994). fgfr-1 is required for embryonic growth and mesodermal patterning during mouse gastrulation. Genes Dev. *8*, 3032–3044.

Yamaguchi, T.P., Takada, S., Yoshikawa, Y., Wu, N., and McMahon, A.P. (1999a). T (Brachyury) is a direct target of Wnt3a during paraxial mesoderm specification. Genes Dev. *13*, 3185–3190.

Yamaguchi, T.P., Bradley, a, McMahon, a P., and Jones, S. (1999b). A Wnt5a pathway underlies outgrowth of multiple structures in the vertebrate embryo. Development *126*, 1211–1223.

Yan, D., Wallingford, J.B., Sun, T.Q., Nelson, A.M., Sakanaka, C., Reinhard, C., Harland, R.M., Fantl, W.J., and Williams, L.T. (2001). Cell autonomous regulation of multiple Dishevelled-dependent pathways by mammalian Nkd. Proc. Natl. Acad. Sci. U. S. A. *98*, 3802–3807.

Yanagisawa, K.O., Fujimoto, H., and Urushihara, H. (1981). Effects of the Brachyury (T) mutation on morphogenetic movement in the mouse embryo. Dev. Biol. *87*, 242–248.

Yang, Y., and Mlodzik, M. (2015). Wnt-Frizzled/Planar Cell Polarity Signaling: Cellular Orientation by Facing the Wind (Wnt). Annu. Rev. Cell Dev. Biol. *31*, 623–646.

Yang, T., Bassuk, A.G., and Fritzsch, B. (2013). Prickle1 stunts limb growth through alteration of cell polarity and gene expression. *242*, 1293–1306.

Yao, R., Natsume, Y., and Noda, T. (2004). MAGI-3 is involved in the regulation of the JNK signaling pathway as a scaffold protein for frizzled and Ltap. Oncogene *23*, 6023–6030.

Yen, W.W., Williams, M., Periasamy, A., Conaway, M., Burdsal, C., Keller, R., Lu, X., and Sutherland, A. (2009). PTK7 is essential for polarized cell motility and convergent extension during mouse gastrulation. Development *136*, 2039–2048.

Yin, H., Copley, C.O., Goodrich, L. V., and Deans, M.R. (2012). Comparison of phenotypes between different vangl2 mutants demonstrates dominant effects of the looptail mutation during hair cell development. PLoS One *7*.

Ying, Q.L., and Smith, A.G. (2003). Defined Conditions for Neural Commitment and Differentiation. Methods Enzymol. *365*, 327–341.

Yoshida, M., Uchikawa, M., Rizzoti, K., Lovell-Badge, R., Takemoto, T., and Kondoh, H. (2014). Regulation of mesodermal precursor production by low-level expression of B1 Sox genes in the caudal lateral epiblast. Mech. Dev. *132*, 59–68.

Yoshikawa, Y., Fujimori, T., McMahon, a P., and Takada, S. (1997). Evidence that absence of Wnt-3a signaling promotes neuralization instead of paraxial mesoderm development in the mouse. Dev. Biol. *183*, 234–242.

Yu, H., Smallwood, P., Wang, Y., Vidaltamayo, R., Reed, R., and Nathans, J. (2010). Frizzled 1 and frizzled 2 genes function in palate, ventricular septum and neural tube closure: general implications for tissue fusion processes. Development *137*, 3707–3717.

Yu, H., Ye, X., Guo, N., and Nathans, J. (2012). Frizzled 2 and frizzled 7 function redundantly in convergent extension and closure of the ventricular septum and palate: evidence for a network of interacting genes. Development *139*, 4383–4394.

Zhang, H., Gayen, S., Xiong, J., Zhou, B., Shanmugam, A.K., Sun, Y., Karatas, H., Liu, L., Rao, R.C., Wang, S., et al. (2016). MLL1 Inhibition Reprograms Epiblast Stem Cells to Naive Pluripotency. Cell Stem Cell *18*, 481–494.

Zhou, L., Bar, I., Achouri, Y., Campbell, K., Backer, O. De, Hebert, J.M., Jones, K., Kessaris, N., Rouvroit, C.L. De, Leary, D.O., et al. (2008). Early Forebrain Wiring : Genetic Dissection Using Conditional Celsr3 Mutant Mice. Science (80-.). *320*, 946–949.

Appendix

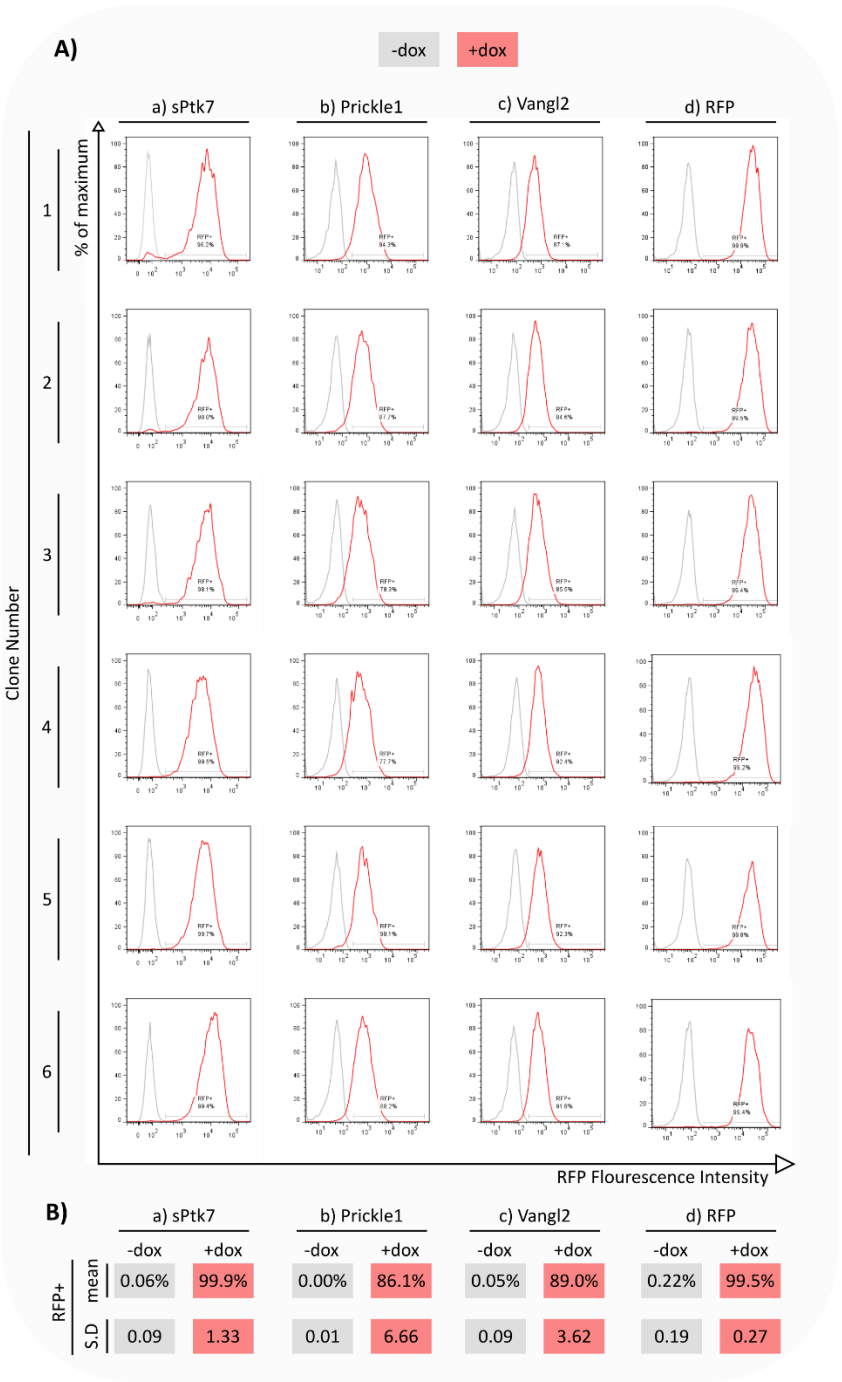

S-Fig. 5.1 – Flow cytometry analysis of sPtk7, Prickle1, Vangl2 and RFP inducible clones.
(A) Flow cytometry analysis of (a) sPtk7, (b) Prickle1, (c) Vangl2, and (d) RFP inducible clones, under 2i/LIF culture conditions with dox (+dox – red) and without dox (-dox – grey), plotted for 6 separate clones for each cell line. Threshold of RFP positivity was added based on flow analysis of wildtype 2i/LIF conditions to determine number of RFP positive cells (RFP+), shown as a percentage. For all graphs, RFP positivity is plotted against percentage maximum for each sample. (B) Calculated averages, and standard deviations (s.d) of RFP+ percentages between clones of the same cell line.

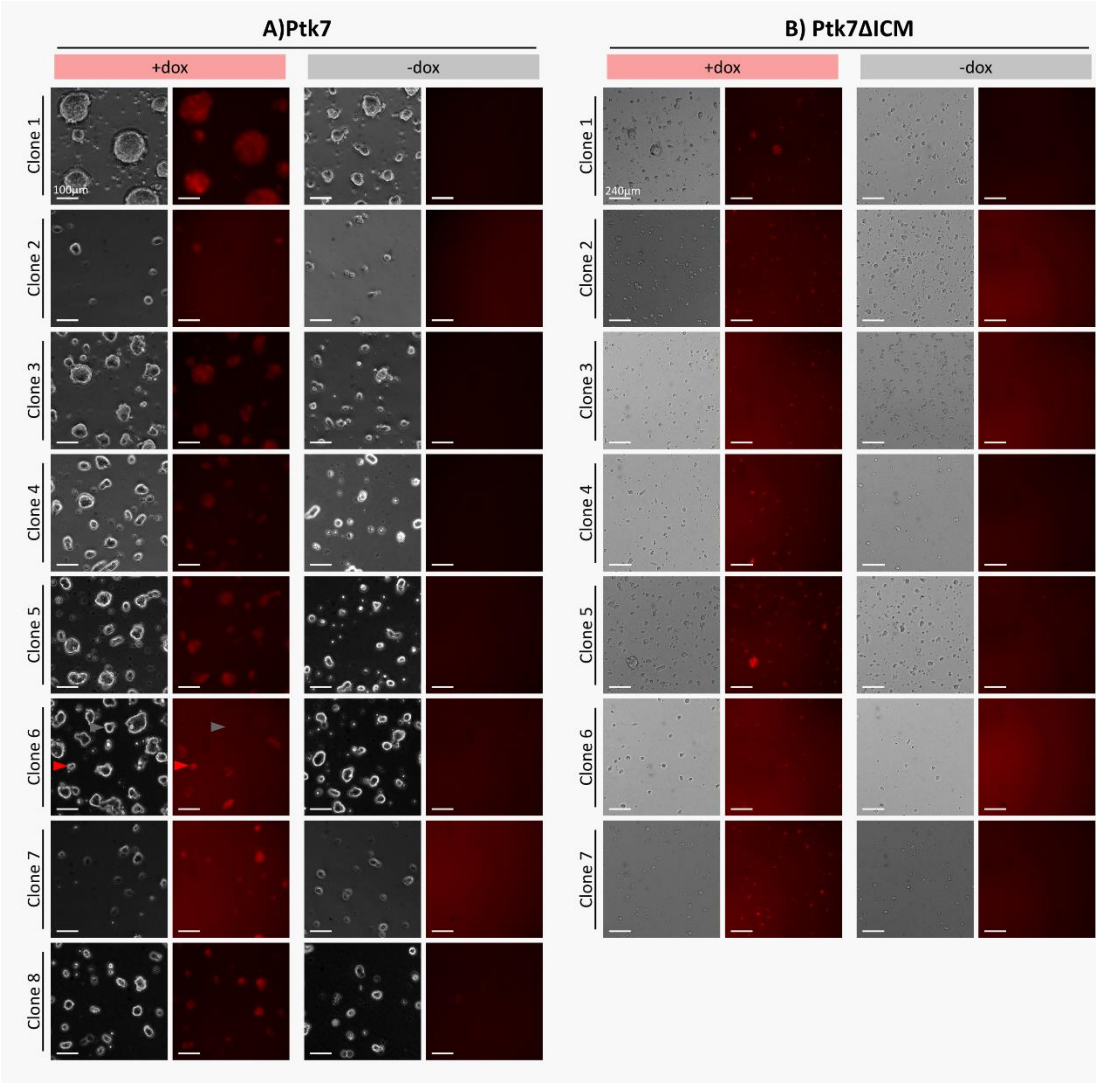

S-Fig. 5.2 – All clones picked for Ptk7 and Ptk7ΔICM cell lines were inducible.
Brightfield and RFP live images taken of generated (A) Ptk7 and (B) PtkΔICM inducible cell lines, in the presence (+dox) and absence (-dox) of dox in 2i/LIF culture conditions. All cells shows homogenous for RFP induction, except for Ptk7 clone 6 in which some colonies were negative (grey arrow) and some were positive (red arrow). RFP was never found in cells not treated with dox.

Examining polarity in *in vivo* using PickCells 3D image analysis Software

Following visual analysis of polarity *in vivo* during axial elongation using golgi and nuclear envelope markers *(3.2.4)*, it remained unknown if this could be quantified to examine the presence of planar cell polarity. High quality staining was needed for both the nuclear envelope and organelle staining for this to be possible. As further optimisation of LaminB1 was not possible *(3.2.4.1)*, analysis was limited to early stage embryos in which laminB1 penetrance was adequate to identify individual cells. Triple immunohistochemistry and imaging was performed on early somitogenesis embryos, using LaminB1(nuclear envelope), γ-tubulin and T(Bra) antibodies and high resolution 3D confocal microscopy *(S-Fig. 3.1A)*. γ-tubulin, a key player in centrosome and cytoskeleton regulation (O'Toole et al., 2012) was chosen as a replacement of GM13), golgi antibody previously described *(3.2.4.1)*. This antibody detected protein in more distinct and compact spots compared with the elongated golgi staining *(S-Fig. 3.1Ac/d)*, which was advantageous when using the software detection.

Images were processed in a similar manner to those for *in vitro* analysis *(6.2.1)*. Nuclei were segmented using NESSY software, and Centrosomes identified from γ-tubulin staining using Spot finder function *(S-Fig.3.1B)*. Despite thorough optimisation of segmentation settings many mis-segmented cells remained in the final segmentation result, and were most common in the CLE region *(S-Fig. 3.1Ba)*. These included missing cells (false negative - red arrow) and false positive cells (white surround arrow). The CLE was particularly hard to segment as the cells are bundled very close together, and unfortunately due to the time needed to correct this segmentation this was not possible in the scope of this thesis. Centrosome identification using Spot finder was very successful at identifying Centrosomes in the CLE regardless of γ-tubulin spots being very closely localised between nuclei (red arrow) *(S-Fig. 3.1Bb)*.

Despite imperfect segmentation results, to explore the capabilities of the software and general polarity further, assignment of Centrosomes to nuclei was performed regardless. First nuclei and Centrosomes residing the CLE were separated from all data before assignment was performed. This was performed to prevent nuclei in the CLE

being assigned incorrectly to Centrosomes lying in adjacent pre-somitic mesoderm and streak (blue arrow) *(S-Fig. 3.1Bb).*

Nuclei and Centrosomes inhabiting the CLE were isolated by creating a region of interest using a PickCells function, and associating objects to it *(S-Fig. 3.2Aa)*. T(Bra) was used as a landmark to place the CLE boundaries and avoid objects of the streak *(S-Fig. 3.2Ab)* and a 3D object of the CLE region was created *(S-Fig. 3.2Ac)*. Assignment was then carried out between the isolated CLE-nuclei and the CLE Centrosomes similarly to that described before for *in vitro (S-Fig. 3.2B).* This association showed clear apical-basal polarity of cells, with all polarity vectors pointed towards the cavity of the embryo. Unfortunately, no conclusion regarding PCP can be drawn from this association map as inaccurate segmentation, including missing cells (red arrow) may have propagated assignment mistakes to surrounding neighbours, making it impossible to determine if coordination of cells in areas is real PCP.

In summary, using PickCells software on 3D high resolution it was possible to generate polarity maps of areas containing NMPs. From these, strong apical basal polarity in NMPs was observed, however current limitations in segmentation prevented any conclusions about planar cell polarity in these areas.

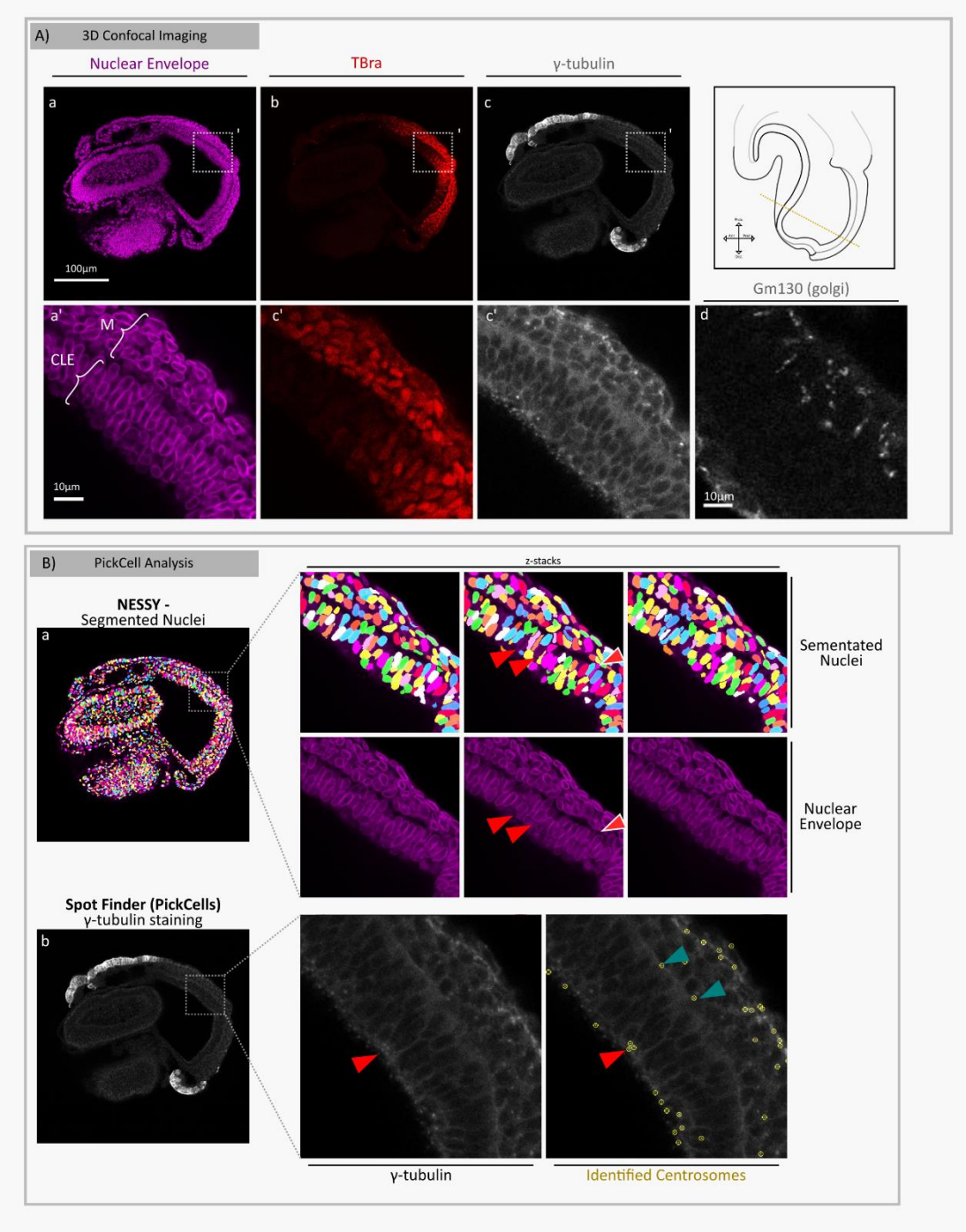

S-Fig. 3.1 – PickCell Analysis of polarity during early somitogenesis.
(A) High resolution 3D confocal images of early somitogenesis embryos immunostained with (a) LaminB1 (nuclear envelope)- magenta, (b) T(Bra)- red and (c)γ-tubulin (Centrosomes) - grey; dashed bounded box shows magnified area. d) shows immunohistochemistry using gm130 (Golgi) as described in (3.2.4). (B) a) segmentation result using PickCell software, magnification of dashed bounded box and z-stacks show mis-segmentation in the CLE (red arrows - false negative segmentation, white arrow - false positive segmentation). b) Spot finder identification (yellow circles) of γ-tubulin spots; red arrow- identification of near Centrosomes. Blue arrows- centrosomes of the PSM, which are close to NMPs of the CLE.

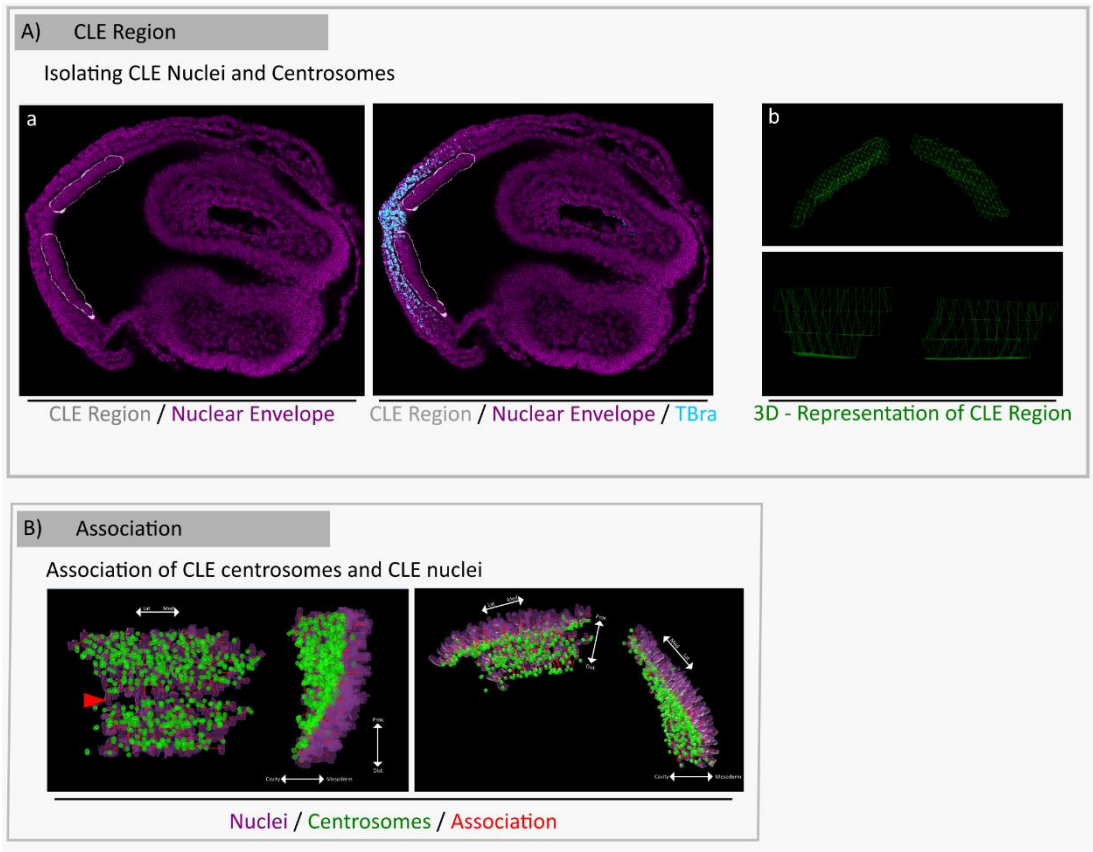

S-Fig 3.2 – Assignment of Polarity vectors in the CLE of early embryos.
(A) a) Creation of CLE region containing NMPs based on T(Bra) levels to avoid cells in the streak. b) CLE object created and represented in 3D (B) 3d view of polarity map. Centrosomes and nuclei assigned to CLE region object are then assigned to each other to create 3d polarity vectors. Centrosomes -green, nuclei- magenta, polarity vectors (red), red arrow shows gap in segmentation. Lat - lateral, med - medial, dis. - distal, prox. - proximal.

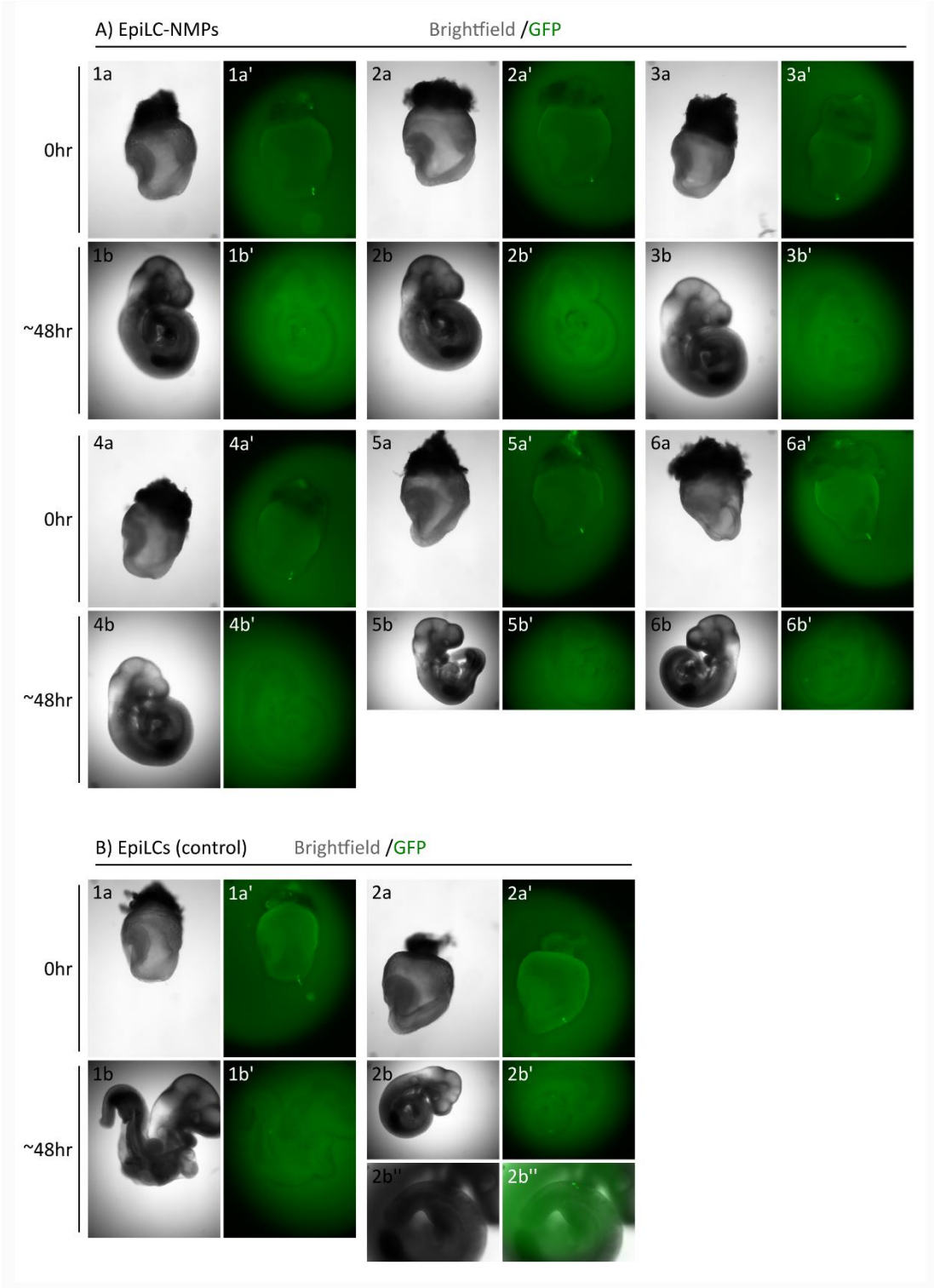

S-Fig 4.1 – Grafting of EpiLC-NMPs and EpiLCs using C2 GFP Cell Line.